



## **COLD SPRING CREEK DEBRIS FLOOD MITIGATION**

# **Cold Spring Creek Hazard Assessment**

**Final**  
**September 25, 2020**

**BGC Project No.: 1572005**

Prepared by BGC Engineering Inc. for:  
**Regional District of East Kootenay**



## TABLE OF REVISIONS

ISSUE	DATE	REV	REMARKS
DRAFT	August 12, 2020	0	Original issue
FINAL	September 25, 2020	1	Final issue

## LIMITATIONS

BGC Engineering Inc. (BGC) prepared this document for the account of the Regional District of East Kootenay. The material in it reflects the judgment of BGC staff in light of the information available to BGC at the time of document preparation. Any use which a third party makes of this document or any reliance on decisions to be based on it is the responsibility of such third parties. BGC accepts no responsibility for damages, if any, suffered by any third party as a result of decisions made or actions based on this document.

As a mutual protection to our client, the public, and ourselves, all documents and drawings are submitted for the confidential information of our client for a specific project. Authorization for any use and/or publication of this document or any data, statements, conclusions or abstracts from or regarding our documents and drawings, through any form of print or electronic media, including without limitation, posting or reproduction of same on any website, is reserved pending BGC's written approval. A record copy of this document is on file at BGC. That copy takes precedence over any other copy or reproduction of this document.

## SUMMARY

Debris-flow hazards and associated risks at Cold Spring Creek are substantially higher than previously understood.

The community of Fairmont Hot Springs is located on two fans that partially overlap: Cold Spring Creek and Fairmont Creek. A fan is a landform that develops at the location where a creek leaves the confines on the watershed and starts to spill water and sediment over its banks. These fans have developed over the course of some 10,000 years primarily by processes called debris floods and debris flows. Both are more destructive than normal floods. Debris flows can be life threatening in particular, and some 100 people in BC have lost their lives through debris flows. Worldwide, this number is much higher with over 78,000 fatalities resulting from debris flows between 1950 and 2011 (Dowling & Santi, 2014).

Most of the present community of Fairmont Hot Springs has been developed since 1975. This short habitation period means that, unlike for old villages and towns in the European Alps or Japan, there are few historical records of destructive debris flow or debris flood events. The July 2012 event on Fairmont Creek, however, gives a sense of how powerful such events can be. The lack of known extreme events in the historic record on Cold Spring Creek can give the perception to residents and regulators that the problem is manageable as only nuisance property flooding is expected. This is a severe and consequential misconception.

Debris floods are characterized by abnormally high rates of sediment movement with boulders, logs and other debris being transported downstream. Debris floods can clog culverts and bridges, jump out of the confines of the channel and erode its banks or road fills. Damage to buildings during debris floods can occur through bank undercutting and flooding, sometimes up to 30 cm deep on fans and deeper in depressions. BGC Engineering Inc. (BGC) concludes that such events have and will occur with annual likelihood of occurrence of 1 to 30% on Cold Spring Creek. The lower the annual likelihood of debris flood occurrence, the larger and more destructive the event will be. The latest (May 31, 2020) debris flood had an estimated return period of 5 to 10 years. Even at a 1% annual likelihood of occurrence, there is still about a 64% likelihood that it will occur in a person's lifetime (80 years).

Debris flows occur at a lower annual probability (< 1% likelihood). Debris flows are a landslide process and they are typically even more destructive than debris floods (see Figure E-1.). The forces associated with a wall of mud and boulders over 2 m (6 feet) in diameter, which can be found on Cold Spring Creek fan, is such that they can fully destroy homes, and people inside homes can and have died in the past in BC. Debris flows often come without warning. They can be triggered by intense rain, or a landslide damming the creek upstream of the community of Fairmont Hot Springs and then bursting the landslide dam. According to BGC's assessment and numerical debris flow modeling, should a debris flow occur on Cold Spring Creek there is a substantial chance that people will die and be injured. Figure E-1 provides an example of the kind of damage that can be expected given the flow depths and flow velocities modeled at Cold Spring Creek. Note that in the direct path of a debris flow, damage can be even more severe.



**Figure E-1-1. Home damaged by debris flow at Montecito, California in January of 2018. Photo by USGS (public domain), <https://www.usgs.gov/media/images/1s-post-fire-debris-flow>. This type of destruction is entirely possible and even likely at Cold Spring Creek in the future.**

Various effects of climate change are very likely to worsen the situation by creating more and potentially larger debris floods and debris flows in the future. The world has now entered temperatures not seen for 3 million years, long before humans existed. Three principle factors conspire: One is that in a warming climate more moisture can be held in the air and with more available energy, air masses are becoming more unstable. This means more frequent extreme rainfalls and higher intensity rainfalls, even when the total annual rainfall may be unchanged or even be reduced. In addition, in a rapidly warming world the trees in the Cold Spring Creek watershed will increasingly be stressed through drought and beetle infestation. That, in combination with a century of fire suppression has created substantial fuel loads, which means more, hotter and more severe wildfires. Debris flows can become particularly destructive after wildfires as the important buffer of trees and duff layer reestablishes. Finally, the upper watershed of Cold Spring Creek is likely underlain by permafrost which is continually frozen ground which thaws only superficially by a metre or so and then refreezes in the winter. In permafrost terrain, whenever water ingresses into rock cracks or soil voids it freezes and holds rock or soil together like glue. With a rapidly warming world, this “glue” disappears, and one can expect an increase in rockfall and other landsliding in the upper watershed. This process feeds the channel system with debris that is then ready for transport to the fan where people live.

In collaboration with McElhanney Ltd. and the Regional District of East Kootenay, a mitigation strategy is being developed to use available funds to reduce the risk of debris flows as much as possible at Cold Spring Creek. However, a residual risk will prevail as total risk reduction would be cost-prohibitive. Such risk could be further managed by provision of a real-time warning system and/or restrictive covenants for future developments on the fan of Cold Spring Creek.

## TECHNICAL SUMMARY

This report and its appendices provide a hydrogeomorphic hazard assessment of Cold Spring Creek, BC. This creek has been studied before by Clark Geoscience and Tetra Tech EBA. The present report is an update of their analysis and has included some of their data.

This report provides some geomorphological and hydrological background and details the analytical techniques applied to create scenario and composite hazard rating maps for the Cold Spring Creek fan. This work could be used as the foundation for future quantitative risk assessments which estimates the probability of loss of life of individuals and groups.

The present hazard assessment is intended to directly inform mitigation works on that creek that for which McElhanney Ltd. and BGC Engineering Inc. (BGC) authored a proposal on May 19, 2020.

To assess the hazards at Cold Spring Creek, multiple hazard scenarios were developed for specific event return period classes (3 to 10, 10 to 30, 30 to 100, 100 to 300, 300 to 1000 and 1000 to 3000 years). BGC differentiated between debris floods which are believed to be the key hydro-geomorphic hazard for return periods up to 100 years and debris flows, which are believed to be the dominant hydro-geomorphic hazard for return periods in excess of 100 years.

A variety of field and desktop analytical techniques were combined to achieve a credible frequency-magnitude relationship for debris flows. This includes consideration of climate change, a highly complex topic. Complex because of the different layers of climate change impact: These include predicted increases in both the frequency and magnitude of rare short-duration rainfall events (high confidence) as well as more and more severe wildfires (high confidence) and permafrost degradation and higher frequency of rock falls (moderate confidence).

Debris-flood and debris-flow frequency-magnitude relationships were developed through a model ensemble in which BGC compared different approaches relating to a regional frequency-magnitude approach, dendrochronological investigation, radiocarbon dating from organic materials found in test trenches, stratigraphic analysis of test trenches and natural exposures and a post-fire debris-flow magnitude analysis (shown in Table E-1), and summarized graphically in Figure E-2.

**Table E-1. Final frequency-magnitude numbers for debris floods and debris flows on Cold Spring Creek using a model ensemble.**

Return Period (years)	Process	Debris Volume Best Estimate (m <sup>3</sup> )	Peak Discharge (m <sup>3</sup> /s)
3 to 10	Debris Flood	4,400	2.4
10 to 30	Debris Flood	4,800	3.8
30 to 100	Debris Flood	5,200	5.2
100 to 300	Debris Flow	63,500	210
300 to 1000	Debris Flow	76,000	260
1000 to 3000	Debris Flow	96,000	320

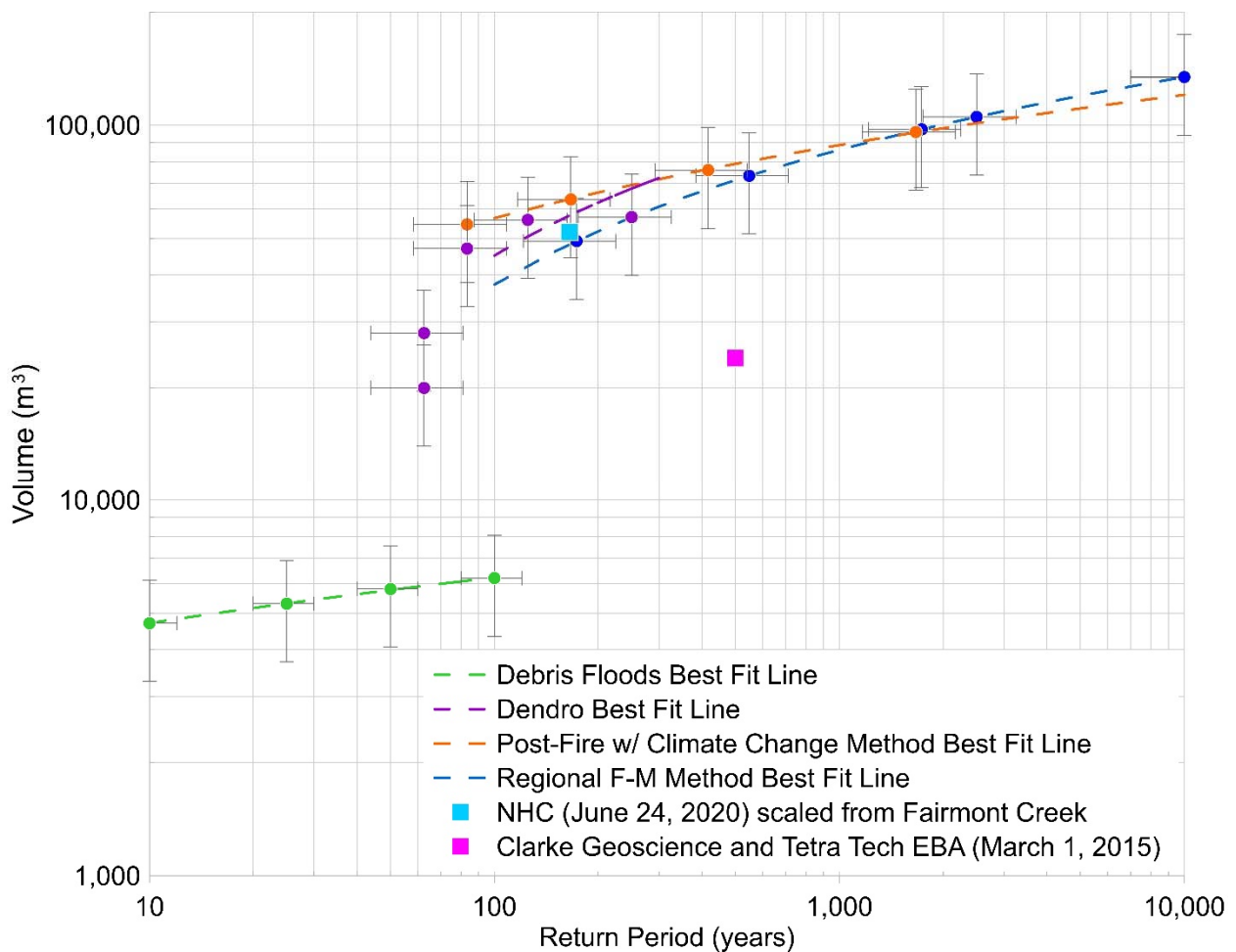


**Figure E-1-2. The frequency-volume methods considered reasonable for Cold Spring Creek. Best fit lines are trimmed at the 100-year return period as BGC considers debris flows below that return period are unlikely. The figure also shows the Clarke Geoscience and Tetra Tech EBA (March 1, 2015) F-M estimate as well as the recently updated (NHC, June 24, 2020) estimate for Fairmont Creek adjusted by watershed area. Error bars are based on judgement.**

A two-dimensional hydrodynamic model (FLO-2D) was employed to simulate debris-flood and debris-flow hazard scenarios on the fan. Bank erosion was not modeled as there are no properties in the immediate vicinity of the creek and because debris flows are the dominant (i.e., more destructive hazard at Cold Spring Creek). Debris flows tend to deposit, rather than scour, on fans such as Cold Spring Creek. Should a major channel avulsion occur, however, bank erosion is possible but difficult to predict given that the flow path of a future avulsion is highly uncertain and is influenced by existing homes and infrastructure. Table E-2. provides key observations derived from the numerical modelling.

**Table E-2. Key findings from numerical modeling of Cold Spring Creek debris floods and debris flows.**

Process	Key Observations
Debris-flood inundation (return periods from 3 to 100 years)	<ul style="list-style-type: none"> <li>• Debris floods are believed to avulse from the channel downstream of the water reservoir for return periods in excess of approximately 3 years.</li> <li>• Avulsions are likely to occur at all road crossings with avulsion probability increasing with return period.</li> <li>• The channel at return periods in excess of 30 years is likely to entirely fill with sediment and cause ubiquitous overflow on the southern fan, mostly south of Fairmont Resort Road</li> <li>• Access to the resort community from the south will largely be severed for most return periods modeled</li> <li>• Debris floods, while causing significant property damage are unlikely to lead to loss of life, though infrastructure damage can be in the millions of dollars for high return period debris floods</li> </ul>
Debris flow inundation (FLO 2D model results from 100 to 3000-year return periods)	<ul style="list-style-type: none"> <li>• All modeled debris flows will fill the water reservoir within minutes and then continue their path downstream</li> <li>• All modeled debris flows are very likely to avulse from the existing channel under current fan configuration towards the central portions of the fan north of the Fairmont Resort Road.</li> <li>• All modeled debris flows will cover portions of the upper and mid fan portions with flow velocities between 3 and 5 m/s and flow depths between 0.5 and 3 m.</li> <li>• The impact forces for all modeled debris flows will be of sufficient magnitude to results in property damage ranging from nuisance flooding away from the flow paths and in the distal fan portions to total building destruction along the main flow paths.</li> <li>• Though not quantified as part of this report, the potential of life loss on Cold Spring Creek fan is considered high to very high. If compared to risk tolerance thresholds adopted, for example for the District of North Vancouver, or the Town of Canmore life loss risk is likely unacceptable for numerous properties.</li> </ul>
Auxiliary Hazards	<ul style="list-style-type: none"> <li>• Most (if not all) properties on Cold Spring Creek fan heat with propane gas. Large gas tanks are omnipresent on the fan. Boulder impact to gas tanks is possible during debris flows and could lead to leakage and possible ignition of the highly flammable gas. Such explosions could substantially increase overall life loss and economic risk. While BGC did not inventory buried linear infrastructure, severe damage can be expected.</li> </ul>

The numerical modelling demonstrates that the key hazards and associated risks stem from debris flows. Those could result in widespread fan inundation, particularly on the upper and central fan and affect multiple properties with possibly severe consequences.

Model results are cartographically expressed in two ways: The individual hazard scenarios and a composite hazard rating map. The individual hazard scenarios (defined by return period and

avulsion scenarios) are captured by showing the impact force which combines flow velocity, flow depth and material density. Impact force is an index of destructiveness of an event and is suited for debris floods and debris flows alike. The individual hazard scenario maps are useful for hazard assessments of individual properties as part of the building permit process as well as to guide emergency response.

The composite hazard rating map combines all hazard scenarios into one map and incorporates the respective debris flood and debris flow frequencies. It provides a sense of the areas that could possibly be impacted by future events up to the highest modelled return period. The composite hazard rating map can serve to guide subdivision and other development permit approvals. It requires discussions and regulatory decisions on which of the hazard ratings is attributed to specific land use prescriptions, covenants, bylaws or other limiting clauses for both existing and proposed development. The categories range from low to very high hazard and are classified via the impact force intensity. The composite hazard rating map shows that the majority of the mid to proximal fan (everything upstream of Highway 93/95) is subject to high and very high hazards. The lower fan downstream of Highway 3A is subject to very high (near the outlet of Cold Spring Creek) to low hazards.

Some uncertainties persist in this study. As with all hazard assessments and corresponding maps, they constitute a snapshot in time. Re-assessment and/or re-modelling may be warranted due to significant alterations of the fan surface topography or infrastructure, such as future fan developments, debris flows, formation of landslides in the watershed, culvert re-design or alteration to any fan infrastructure. BGC's analysis does not include breaches of the constructed water reservoir. Furthermore, the assumptions made on climate changes will likely need to be updated occasionally as scientific understanding evolves.

All hazards contain some component of chaotic behaviour, meaning that it is not possible to adequately model every possible scenario or outcome. For example, unforeseen log jams may alter flow directions and create avulsions into areas not specifically considered in the individual hazard scenarios. Sediment deposition patterns cannot be predicted exactly and are expected to be somewhat random as buildings (sheared off their foundations or remaining in place), log jams and sequential stalled debris lobes can deflect sediment in various directions. Finally, debris-flow behaviour is affected by the triggering storm intensity and duration as well as tributary landslides or debris flows in the watershed.

Despite these limitations and uncertainties, a credible hazard assessment has been achieved on which land use decisions and mitigation strategies can be based.

## TABLE OF CONTENTS

<b>TABLE OF REVISIONS .....</b>	<b>i</b>
<b>LIMITATIONS .....</b>	<b>i</b>
<b>TABLE OF CONTENTS .....</b>	<b>ix</b>
<b>LIST OF TABLES .....</b>	<b>xi</b>
<b>LIST OF FIGURES .....</b>	<b>xii</b>
<b>LIST OF APPENDICES .....</b>	<b>xv</b>
<b>LIST OF DRAWINGS .....</b>	<b>xv</b>
<b>1. INTRODUCTION.....</b>	<b>1</b>
1.1. Scope of Work .....	1
1.2. Study Team .....	2
<b>2. STEEP CREEK HAZARDS .....</b>	<b>3</b>
2.1. Introduction .....	3
2.2. Debris Floods .....	3
2.3. Debris Flows .....	4
2.4. Comparing Steep Creek Processes .....	4
2.5. Avulsions .....	5
<b>3. STUDY AREA CHARACTERIZATION.....</b>	<b>7</b>
3.1. Previous Debris Floods on Cold Spring Creek .....	7
3.1.1. July 15, 2012 Event .....	7
3.1.2. June 20, 2013 Event .....	7
3.1.3. August 12, 2019 Event .....	9
3.1.4. May 31, 2020 Event .....	10
3.2. Site Visit .....	15
3.3. Physiography .....	15
3.4. Geology .....	15
3.4.1. Bedrock Geology .....	15
3.4.2. Watershed Surficial Geology and Geomorphology .....	15
3.4.3. Cold Spring Creek Fan .....	20
3.5. Existing Development.....	22
3.5.1. Cold Spring Water Reservoir .....	22
3.5.2. Culverts .....	23
3.5.3. Sediment End-Dump Location .....	26
3.6. Climate Change Impacts .....	27
3.6.1. Temperature, Precipitation and Runoff .....	27
3.6.2. Permafrost Changes .....	30
<b>4. PREVIOUS REPORTS .....</b>	<b>31</b>
<b>5. METHODS .....</b>	<b>33</b>
5.1. Frequency-Magnitude Relationships .....	35
5.2. Flood & Debris Flood Frequency-Discharge Relationship.....	35
5.2.1. Clearwater Peak Flow Estimation .....	35

5.2.2.	Climate Change Adjustment .....	36
5.2.3.	Discharge Bulking Method .....	36
5.2.4.	Debris Flood Sediment Volume Estimates from Empirical Rainfall-Sediment Transport Relations .....	39
5.2.5.	Application to Cold Spring Creek .....	40
<b>5.3.</b>	<b>Debris Flow Frequency Assessment .....</b>	<b>42</b>
5.3.1.	Air Photo Interpretation .....	42
5.3.2.	Post-Wildfire Debris-Flow Frequency .....	42
5.3.3.	Test Trenching and Radiocarbon Dating .....	44
<b>5.4.</b>	<b>Debris Flow Sediment Volume Estimates.....</b>	<b>44</b>
5.4.1.	Regional Fan-Debris Flow Frequency-Magnitude Analysis .....	45
5.4.2.	Empirical Estimates for Post-Wildfire Debris-Flow Volumes.....	46
5.4.3.	Debris-flow Volume Estimates from Dendrochronological Analysis .....	50
5.4.4.	Area-Volume Relationships .....	52
<b>5.5.</b>	<b>Magnitude Cumulative Frequency (MCF) Analysis.....</b>	<b>52</b>
<b>5.6.</b>	<b>Peak Discharge Estimates .....</b>	<b>53</b>
5.6.1.	Debris-Flood Peak Discharge Estimates for the May 31, 2020 Debris Flood.....	53
5.6.2.	Debris-Flow Peak Discharge .....	54
<b>5.7.</b>	<b>Numerical Debris Flood and Debris Flow Modelling .....</b>	<b>56</b>
5.7.1.	Basic Setup and Input Parameters .....	56
5.7.2.	Sediment Model Setup and Calibration .....	57
<b>5.8.</b>	<b>Hazard Mapping .....</b>	<b>57</b>
5.8.1.	Debris Flood and Debris Flow Model Result Maps.....	58
5.8.2.	Composite Hazard Rating Map.....	58
<b>6.</b>	<b>RESULTS .....</b>	<b>60</b>
<b>6.1.</b>	<b>Hydrogeomorphic Process Characterization .....</b>	<b>60</b>
<b>6.2.</b>	<b>Frequency Assessment.....</b>	<b>60</b>
6.2.1.	Air Photo Interpretation .....	60
6.2.2.	Dendrogeomorphic Interpretation .....	62
6.2.3.	Test Pit Logging and Radiocarbon Testing.....	65
6.2.4.	Summary .....	66
<b>6.3.</b>	<b>Frequency-Magnitude Relationships .....</b>	<b>67</b>
6.3.1.	Debris Flood Frequency-Magnitude.....	67
6.3.2.	Debris Flow Frequency-Magnitude .....	68
6.3.3.	Debris Flood and Debris Flow Frequency-Magnitude Values.....	70
6.3.3.1.	Debris-Flow Peak Discharge .....	71
6.3.3.2.	Frequency-Magnitude Model Check.....	72
<b>6.4.</b>	<b>Numerical Flood and Debris-Flow Modeling and Hazard Mapping .....</b>	<b>74</b>
6.4.1.	Results .....	74
6.4.2.	Numerical Model Check I: Area-Volume Relationship .....	79
6.4.3.	Numerical Model Check II: Boulder Size as Indicator of Flow Depth.....	80
<b>6.5.</b>	<b>Hazard Mapping .....</b>	<b>81</b>
<b>6.6.</b>	<b>Comparison to Previous Hazard Mapping.....</b>	<b>83</b>
<b>7.</b>	<b>SUMMARY AND RECOMMENDATIONS .....</b>	<b>84</b>
<b>7.1.</b>	<b>Summary .....</b>	<b>84</b>
7.1.1.	Hydrogeomorphic Process.....	84
7.1.2.	Air Photo Interpretation .....	84

7.1.3.	Frequency-Magnitude Relationship .....	84
7.1.4.	Numerical Modeling .....	86
7.1.5.	Hazard Mapping .....	86
<b>7.2.</b>	<b>Limitations and Uncertainties .....</b>	<b>86</b>
<b>7.3.</b>	<b>Concluding Remarks .....</b>	<b>87</b>
<b>8.</b>	<b>CLOSURE.....</b>	<b>89</b>

## LIST OF TABLES

Table E-1.	Final frequency-magnitude numbers for debris floods and debris flows on Cold Spring Creek using a model ensemble. ....	5
Table E-2.	Key findings from numerical modeling of Cold Spring Creek debris floods and debris flows. ....	7
Table 1-1.	Return period classes used for the hazard assessment on Cold Spring Creek. ....	2
Table 3-1.	Watershed characteristics of Cold Spring Creek.....	16
Table 3-2.	Estimated dimensions of culvert crossings on Cold Spring Creek fan, heading downstream.....	24
Table 3-3.	Projected change (RCP 8.5, 2050) from historical (1961 to 1990) conditions for the Cold Spring Creek watershed (Wang et. al, 2016, and Prein et al., 2016). ....	28
Table 4-1.	Previous reports and documents on Cold Spring Creek. ....	31
Table 5-1.	Rheological parameters for FLO-2D modeling.....	57
Table 6-1.	Summary of observed changes in the air photo record (1949-2000). ....	61
Table 6-2.	Summary of Cold Spring Creek events interpreted from dendrogeomorphic samples.....	63
Table 6-3.	Delineated areas and debris-flow volume results from the dendrogeomorphology analysis. ....	65
Table 6-4.	Radiocarbon dates from test pits across the fan.....	66
Table 6-5.	Flood frequency analysis on Cold Spring Creek. ....	67
Table 6-6.	Rainfall and sediment volume summary for debris floods on Cold Spring Creek.....	68
Table 6-7.	Post-fire debris-flow frequency-magnitude relationships adjusted for climate-change effects. The volume ranges come from the assumption of two-thirds of the watershed being burned.....	69
Table 6-8.	Final frequency-magnitude numbers for debris floods and debris flows on Cold Spring Creek using a model ensemble. ....	70
Table 6-9.	Estimated peak discharges at cross sections measured during field traverse. Historical debris flows are bolded.....	71
Table 6-10.	Total volume of fan sediments as the integral of the frequency-magnitude curve. ....	73

Table 6-11. Summary of modeling results. ....	75
Table 6-12. Key differences in hazard mapping between Clarke Geoscience and Tetra Tech EBA (March 1, 2015) and this report.....	83
Table 7-1. Summary of climate change effects on debris flood and debris flow F-M relationships. ....	85
Table 7-2. Cold Spring Creek best estimate debris flood and debris flow frequency-volume relationship including the effects of climate change. Peak discharge is referenced to the fan apex. Debris volume is referenced to volumes passing the fan apex. All figures are best estimates using a combination of data. ....	85

## LIST OF FIGURES

Figure E-1-1. Home damaged by debris flow at Montecito, California in January of 2018. Photo by USGS (public domain), <a href="https://www.usgs.gov/media/images/lr-post-fire-debris-flow">https://www.usgs.gov/media/images/lr-post-fire-debris-flow</a> . This type of destruction is entirely possible and even likely at Cold Spring Creek in the future. ....	3
Figure E-1-2. The frequency-volume methods considered reasonable for Cold Spring Creek. Best fit lines are trimmed at the 100-year return period as BGC considers debris flows below that return period are unlikely. ....	5
Figure 2-1. Illustration of steep creek hazards.....	3
Figure 2-2. Continuum of steep creek hazards.....	3
Figure 2-3. Conceptual steep creek channel cross-section showing peak discharge levels for different events. Note that for some outburst floods or debris flows the discharge may exceed what is shown here.....	5
Figure 2-4. Schematic of a steep creek channel with avulsions downstream of the fan apex. Artwork by BGC.....	6
Figure 3-1. View upstream (east) on Fairmont Resort Road at approximately the crossing with Hot Springs Road showing muddy water and debris from an avulsion at the uppermost culvert beneath Fairmont Resort Road. RDEK photograph of June 20, 2013 7:00 AM. ....	8
Figure 3-2. Avulsions associated with the debris flood of June 20, 2013. Debris is seen to flow past the old Barn towards Highway 95. RDEK photograph of June 20, 2013 2:15 PM.....	8
Figure 3-3. Lower sedimentation basin at Glen Eagle Drive looking North. RDEK photograph of June 20, 2013 9:00 AM.....	9
Figure 3-4. Cold Spring Reservoir shortly after the August 12, 2020 debris flood showing the reservoir full of sediment. Photo: RDEK.....	10
Figure 3-5. Destroyed path across Cold Spring Creek at an elevation of approximately 1285 m, looking downstream (west). The structure likely failed through outflanking on the left (south) which subsequently eroded the foundation of the lock blocks and leading to their toppling downstream. Photo: BGC July 14, 2020. ....	12

Figure 3-6. RDEK photograph of the reconstruction of the FHSR after the 2012 debris flood (photo date unknown). This is the same location as in the previous photograph. .... 12

Figure 3-7. Sediment removal after the May 31, 2020 debris flood on Cold Spring Creek. Photo: NHC, June 1 or 2, 2020. .... 13

Figure 3-8. RDEK image of the Cold Spring Creek reservoir dam entirely filled with sediment. Note that debris also overtopped to the right of the structure which is shielding the spillway from view. June 1, 2020..... 13

Figure 3-9. RDEK image of Cold Spring Creek at Fairview Drive downstream of Highway 95. The culvert is not visible to the left of the road and water is flowing down Fairview Drive. May 31, 2020, 3:45 PM. .... 14

Figure 3-10. Extensive talus slopes in the upper watershed of Cold Spring Creek at an elevation of 2000 to 2300 m facing South. Permafrost is possible on north-facing slopes in this elevation band. Google Earth. .... 17

Figure 3-11. Oblique view of the “Cold Spring Landslide” delineated in red with the potential source zone rock slide shown in yellow. View is towards the East. Google Earth imagery (date 8/4/2019)..... 18

Figure 3-12. Example of an undercut slope on the mid-reaches of Cold Spring Creek at an elevation of approximately 1270 m. Photo: BGC, June 23, 2020..... 19

Figure 3-13. Tendency of creeks to produce floods, debris floods and debris flows, as a function of Melton Ratio and stream length (data from Holm et al., 2016 and Lau, 2017). See Section 3.4.2 for Cold Spring Creek watershed data..... 22

Figure 3-14. Images of the Cold Spring Creek Dam and Reservoir looking upstream, across the dam and from downstream of the dam..... 23

Figure 3-15. Cold Spring Creek culverts: A) Fairmont Resort Road outlet, B) Hot Spring Road inlet, C) Fairway Drive inlet, D) Highway 93/95 inlet, E) Riverview Road inlet, and F) Golf course culvert inlet. BGC photos taken June 2020..... 25

Figure 3-16. Sedimentation pond upstream of golf course culvert on Cold Spring Creek, looking upstream. BGC photo taken June 2020..... 26

Figure 3-17. Insert map from Drawing 01, showing the location of sediment end-dumping from a switch back of the Fairmont Ski Area access road. .... 27

Figure 3-18. Projected change (RCP 8.5, 2050) from historical (1961 to 1990) monthly average temperature and precipitation for the Cold Spring Creek watershed. ... 29

Figure 3-19. Approximate permafrost distribution in the Cold Spring and Fairmont Creek watersheds (mapping from Gruber, 2012). The mapping indicates that permafrost is possible in favourable location but will be shallow and “warm”, meaning near zero degree Celsius and thus particularly sensitive to climate change. .... 30

Figure 5-1. Flood and debris flow prone steep creeks workflow used for developing frequency-magnitude relationships, modeling, and preparing hazard maps..... 34

Figure 5-2. Debris flood bulking method logic chart for Cold Spring Creek. Only Type 1 and Type 2 debris floods were considered for Cold Spring Creek as the return period for Type 3 events is unknown..... 38

Figure 5-3. Log transformed sediment ( $V_S$ ) and available water ( $V_R$ ) data from the Swiss and Bow Valley datasets compiled by Rickenmann and Koschni (2010) and BGC, respectively..... 41

Figure 5-4. Cut-out image of historic natural fire regime in the Cold Spring Creek watershed circled in black (Blackwell, Grey, & Compass, 2003). ..... 43

Figure 5-5. Regional debris flow frequency-magnitude data normalized by fan area for seven detailed studies in the Bow Valley, AB. From Jakob et al. (2020). ..... 45

Figure 5-6. Relative changes in the exceedance probability of the 99.95th percentile of hourly precipitation intensities for June, July and August in large portions of North America (Prein et al., 2017)..... 49

Figure 5-7. Hourly extreme precipitation for June, July and August expressed as relative changes for 100 x 100 km grid boxes. Dots indicate statistically significant changes. The approximate changes for the area of interest is between 21 and 35% (Prein et al., 2017)..... 50

Figure 5-8. Impact scars on a spruce tree near Fergusson Creek in southwest BC showing an example of scars that can be dated precisely. The red arrow points at a scar, and the blue arrow points at the center of the tree (from Jakob, 1996)..... 51

Figure 5-9. Cross-section at approximately 1350 m across the Coldspring Creek channel looking upstream. .... 54

Figure 5-10. Bovis and Jakob (1999) relationship between peak discharge and volume for British Columbia, with comparison regressions computed by Mizuyama et al. (1992). .... 55

Figure 5-11. Simplified geohazard impact intensity frequency matrix. .... 59

Figure 6-1. Air photos of Cold Spring Creek fan from A) 1949, B) 1964, C) 1975, and D) 2000 showing development on the fan. Air photos have been manually georeferenced by BGC..... 62

Figure 6-2. Cutout of 1975 air photograph BC 7818, No. 17 (approximate scale: 1:20,000). The channel alignment of Cold Spring Creek is unclear at this time. Fairmont Close and Falcon Drive and Wills Road appear to just have been built..... 64

Figure 6-3. The frequency-volume methods considered reasonable for Cold Spring Creek. Best fit lines are trimmed at the 100-year return period as BGC considers debris flows below that return period are unlikely. .... 69

Figure 6-4. Different models for fan volume reconstruction using the SLBL model..... 74

Figure 6-5. Modeled event volumes for Cold Spring Creek (red) in comparison to typical non-volcanic debris flow dataset (black) developed by Griswold and Iverson (2008). The Fairmont Creek 2012 event (green) is shown for comparison..... 79

Figure 6-6. Modeled flow depth vs. calculated flow depth using boulder size as a proxy for flow depth. The plot includes an estimated 30% error for both the numerical modeling flow depth and the calculated flow depth..... 81

## **LIST OF APPENDICES**

- APPENDIX A TEST PIT LOGS
- APPENDIX B RADIOCARBON SAMPLE RESULTS
- APPENDIX C DENDROGEOMORPHOLOGY ANALYSIS RESULTS

## **LIST OF DRAWINGS**

- DRAWING 01 FAN AND WATERSHED OVERVIEW
- DRAWING 02 CREEK PROFILE
- DRAWING 03 INDIVIDUAL MODELING RESULTS
- DRAWING 04 COMPOSITE HAZARD MAP

## 1. INTRODUCTION

### 1.1. Scope of Work

The Regional District of East Kootenay (RDEK, the District) retained BGC Engineering Inc. (BGC) and McElhanney Ltd. (McElhanney) to complete design and construction of debris flood mitigation measures on Cold Spring Creek in Fairmont Hot Springs, BC. Within the design and construction work, BGC proposed to update the hazard assessment for Cold Spring Creek before McElhanney and BGC move forward with detailed design.

This report documents the approach used by BGC to conduct a steep creek geohazards assessment for Cold Spring Creek (Drawing 01). Cold Spring Creek is a steep mountain creek that runs through the community of Fairmont Hot Springs, and discharges into the Columbia River. The creek has a frequent history of debris floods and geomorphic indicators of debris flows which have led to flooding in the community. On nearby Fairmont Creek, a damaging debris flow occurred in July of 2012 that deposited an estimated 65,000 m<sup>3</sup> onto the fan (Clarke Geoscience Ltd. & Golder Associates, January 11, 2013). Debris flows and debris flooding on Cold Spring Creek have been previously assessed, most recently by Northwest Hydraulic Consultants (NHC) (NHC, October 20, 2019). The recent NHC report also provided conceptual-level designs for mitigation measures to reduce the impacts of debris flooding on the community of Fairmont Hot Springs and an existing Irrigation Pond located at the fan apex.

The aim of this project is to mitigate debris flooding issues and concerns on Cold Spring Creek as effectively as possible within the available project budget. An updated hazard assessment is required to adequately define a design event and associated flows, velocities, and impact forces. The second component of the work is a mitigation review and the design and construction of mitigation works at Cold Spring Creek. This report only focuses on the first aspect of the project, which entailed:

- Field study to assist in the geohazard characterization (i.e., test pitting, channel hikes, dendrochronology, boulder measurements and other surface investigation)
- Frequency-magnitude analysis
- Numerical modeling
- Hazard mapping.

The scope of work considers the “return period ranges” and “representative return periods” outlined in Table 1-1. The representative return periods fall close to the mean of each range<sup>1</sup>. Given uncertainties, they generally represent the spectrum of event magnitudes within the return period ranges which are similar to those listed in the Engineers and Geoscientists British Columbia (EGBC) Guidelines for Legislated Flood Assessments in a Changing Climate (2018), though amended to reflect the fact that both debris floods and debris flows are acting on Cold Spring Creek.

---

<sup>1</sup> The 5-, 50- and 500-year events do not precisely fall at the mean of the return period ranges shown in Table 1-1 but were chosen as round figures due to uncertainties and because these return periods have a long tradition of use in BC.

BGC assessed Cold Spring Creek for the 5-, 20-, 50-, 200-, and 500 and 2000-year return periods. As precision is not warranted for these types of assessments, BGC chose to work with return period classes, namely the 3 to 10-, 10 to 30-, 30 to 100-, 100 to 300-, 300 to 1000- and 1000 to 3000-year return periods. While there is no mandate in BC to examine such return period classes for existing residential development, the in-progress update of the EGBC Guidelines for Landslide Assessments (to be published in 2021) encourages practitioners to apply the current guidance provided in the Guidelines for Legislated Flood Assessments in a Changing Climate (EBGC, 2018). Appendix D in those guidelines stipulate that for developments of 100 homes or greater up to the 2500-year return period should be considered. This is the case at Cold Spring Creek where approximately 240 homes are situated on the active fan.

**Table 1-1. Return period classes used for the hazard assessment on Cold Spring Creek.**

<b>Return Period Range (years)</b>	<b>Representative Return Period (years)</b>
3 to 10	5
10 to 30	20
30 to 100	50
100 to 300	200
300 to 1000	500
1000 to 3000	2000

## **1.2. Study Team**

This study was multidisciplinary, and contributors are listed below.

- Matthias Jakob, Ph.D., P.Geo., Principal Geoscientist (Technical Lead)
- Hamish Weatherly, M.Sc., P.Geo., Principal Hydrologist (Technical Reviewer)
- Beatrice Collier-Pandya, B.A.Sc., EIT, Geological Engineer (Project Engineer)
- Emily Moase, M.Sc., P.Eng., Geotechnical Engineer (Geotechnical/Mitigation)
- Patrick Grover, M.A.Sc., P.Eng. (AB, ON), Senior Hydrotechnical Engineer (Climate Change/Hydrology).

## 2. STEEP CREEK HAZARDS

### 2.1. Introduction

Steep creek or hydrogeomorphic hazards are natural hazards that involve a mixture of water and debris or sediment (Figure 2-1). These hazards typically occur on creeks and steep rivers with small watersheds (usually less than 100 km<sup>2</sup>) in mountainous terrain, usually after intense or long rainfall events, sometimes aided by snowmelt and worsened by forest fires.

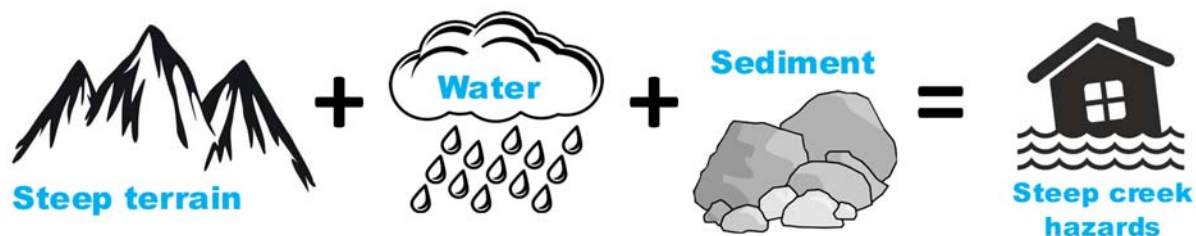


Figure 2-1. Illustration of steep creek hazards.

Steep creek hazards span a continuum of processes from clearwater floods (flood) to debris flows (Figure 2-2). Debris floods and debris flows are described further in the following sections.

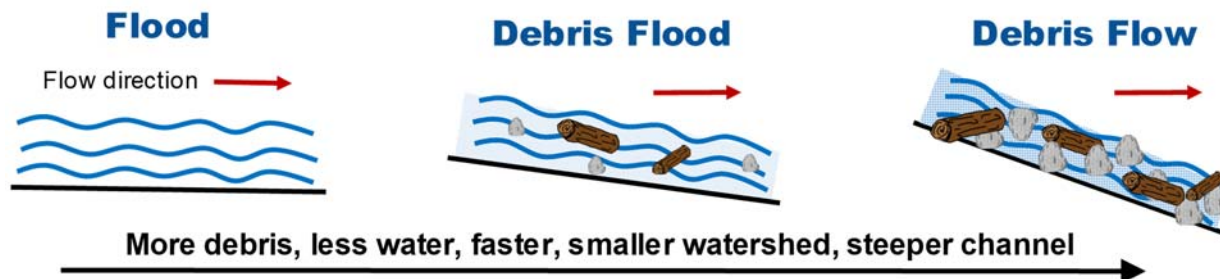


Figure 2-2. Continuum of steep creek hazards.

### 2.2. Debris Floods

Debris floods occur when large volumes of water in a creek or river entrain the gravel, cobbles and boulders on the channel bed; this is known as “full bed mobilization”. Debris floods can occur from different mechanisms. BGC has adopted the definitions of three different sub-types of debris floods per Church and Jakob (2020):

- Type 1 – Debris floods that are generated from rainfall or snowmelt runoff resulting in sufficient water depth to result in full bed mobilization.
- Type 2 – Debris floods that are generated from diluted debris flows (e.g., a debris flow that runs into a main channel in the upper watershed).
- Type 3 – Debris floods that are generated from natural (e.g., landslide dam, glacial lake outbursts, moraine dam outbursts) or artificial dam (e.g., water retention or tailings dam) breaches.

The process of sediment and woody debris getting entrained in the water of a flood leads to an increase in the volume of organic and mineral debris flowing down a channel with a commensurate increase in peak discharge. This is referred to as flow bulking. Imagine a bucket

of water filled with water. Then it is spilled down a children's slide. That's a clearwater flood. Refill the bucket with 10 litres of water and take a shovel of sand and some twigs and put it into the bucket. Now the water-sediment mixture occupies 12 litres worth of volume. It has bulked by a factor of 1.2. If one mixes it a bit and then spill it down the slide, one has a bulked debris flood with some 20% sediment concentration by volume. The experiment can be repeated with increasing volumes of sediment until it becomes a debris flow (see Section 2.3).

The effects of debris floods can range from relatively harmless to catastrophic depending on their magnitude and duration. Debris floods can be relatively harmless if of short duration and low magnitude. In contrast, they can be damaging when they cause bank erosion and channel change but do not jeopardize major infrastructure or threaten lives. A catastrophic level is reached when major infrastructure damage occurs in the form of riprap erosion, bridge foundation collapse of isolation, culverts becoming blocked or bypassed and road surfaces being eroded. Furthermore, homes are impacted beyond repair, and injuries and/or fatalities occur.

In the study area, debris floods occurred on Cold Spring Creek and Fairmont Creek on May 31, 2020, as described in the report by NHC, dated June 24, 2020.

### **2.3. Debris Flows**

Debris flows have higher sediment concentrations than debris floods and can approach consistencies similar to wet concrete. Using the example of a bucket again, if one adds sand to fill the bucket to the top, so that the fluid is half sand, half water, it is bulked by 100%, so a bulking factor of 2. Spilling it down the slide, one now has a debris flow that behaves more like liquid concrete than a fluid.

Debris flows are typically faster than debris floods and have substantially higher peak discharges and impact forces. They are particularly threatening to life and properties due to these characteristics.

### **2.4. Comparing Steep Creek Processes**

Individual steep creeks can be subject to a range of process types and experience different peak discharges depending on the process, even within the same return period class. Figure 2-3 demonstrates this concept with an example cross-section of a steep creek, including representative flood depths for the peak discharge of the following processes:

- $Q_2$ ; Clearwater flow with 2-year return period
- $Q_{200}$ ; Clearwater flow with 200-year return period (i.e., a clearwater flood)
- $Q_{\max}$  debris flood (full bed mobilization); Type 1 debris flood generated by full bed mobilization
- $Q_{\max}$  debris flood (outburst flood); Type 3 debris flood generated by an outburst flood
- $Q_{\max}$  debris flow; Debris flow.

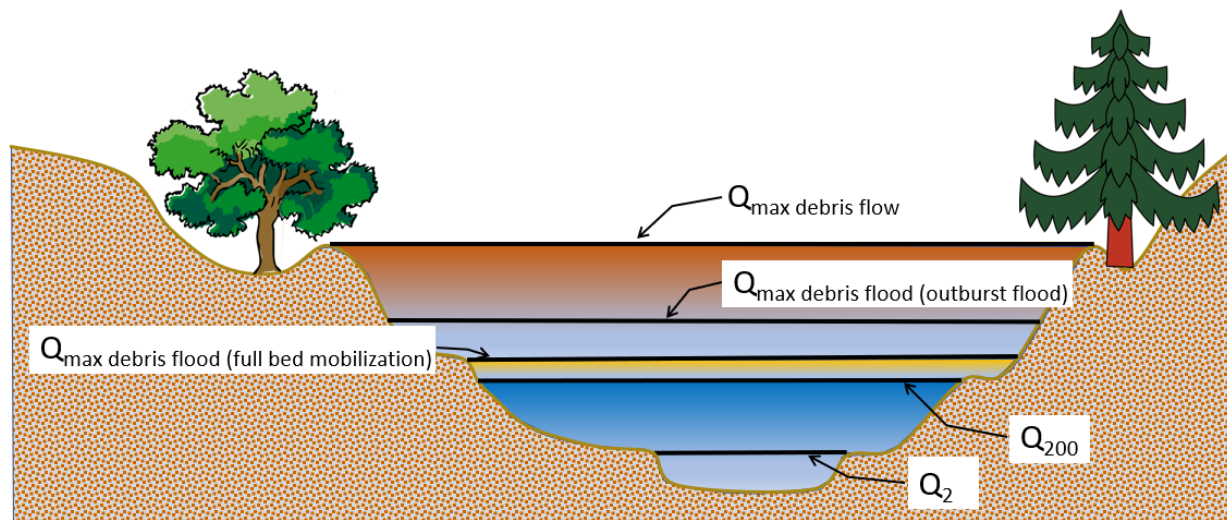


**Figure 2-3. Conceptual step creek channel cross-section showing peak discharge levels for different events. Note that for some outburst floods or debris flows the discharge may exceed what is shown here.**

This difference in peak discharge is one of the reasons that process-type identification is critical for steep creeks. For example, if a bridge is designed to accommodate a 200-year flood, but the creek experiences a debris flow with a much larger peak discharge, the bridge would likely be damaged or destroyed. For floods, a longer duration is more likely to saturate protective dikes, increasing the likelihood for piping and dike failure prior to, or instead of, the structure being overtopped. For debris floods, the duration of the event will also affect the total volume of sediment transported and the amount of bank erosion occurring.

## 2.5. Avulsions

An avulsion occurs when a watercourse jumps out of its main channel into a new course across its fan or floodplain. This can happen because the main channel cannot convey the flood discharge and simply overflows, or because the momentum of a flow allows overtopping on the outside of a channel bend. Finally, an avulsion can occur because a log jam or blocked bridge redirects flow away from the present channel. The channel an avulsion flow travels down is referred to as an avulsion channel. An avulsion channel can be a new flow path that forms during a flooding event or a channel that was previously occupied.

In Figure 2-4, a schematic of a steep creek and fan is shown where the creek avulses on either side of the main channel. The avulsion channels are shown as dashed blue lines as avulsions only occur during severe floods (i.e., rarely). On high resolution topographic maps generated from LiDAR, avulsion channels are generally visible and are tell-tale signs of past and potential future avulsions.

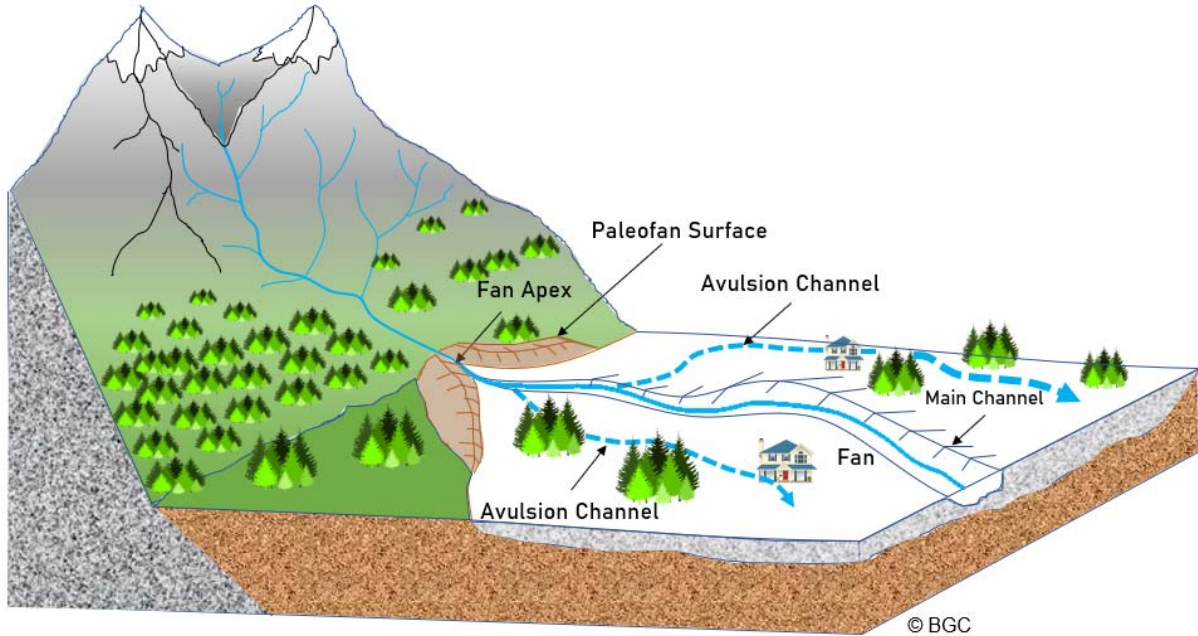


**Figure 2-4. Schematic of a steep creek channel with avulsions downstream of the fan apex. Artwork by BGC.**

### 3. STUDY AREA CHARACTERIZATION

#### 3.1. Previous Debris Floods on Cold Spring Creek

This section provides information on three debris floods that occurred on Cold Spring Creek in the last decade. According to Brian Funke, engineering manager of the RDEK, the 2013 event was the most significant in terms of damage, followed by the 2020 and 2012, events respectively.

##### 3.1.1. July 15, 2012 Event

The information here is extracted from Clarke Geoscience Ltd. and Golder Associates, (October 21, 2013) and NHC (June 24, 2020).

- On July 15, 2012 convective storms triggered debris flows in the upper basin of Fairmont Creek that transitioned to debris floods in the lower basin and resulted in 65,000 m<sup>3</sup> of sediment being deposited on the golf course and downstream fan.
- Gauges in the region showed a wide range of precipitation rates on July 15, 2012 and the maximum daily precipitation rate at any of the rain gauges in the region was 26 mm two days before the event at Fort Steele.
- The day before the event the Cranbrook Airport experienced 23 mm of rain.
- 8 mm/h of rain fell in the vicinity of the Fairmont and Cold Spring Creek basins as extracted from Doppler radar imagery from the Silver Star station. Note that such intensities are not as reliable as from measured rainfalls.
- 20-30% of the watershed was estimated to have been snow covered.
- Snow water equivalent at the start of the July 15, 2012 event was 30 mm at Floe Lake at 2090 m elevation but was snow free by the end of the event.
- The total amount of sediment mobilized on Fairmont Creek was 65,000 m<sup>3</sup>, compared to approximately 2000 to 3000 m<sup>3</sup> at Cold Spring Creek.

##### 3.1.2. June 20, 2013 Event

Clarke Geoscience Ltd. And Golder Associates (January 11, 2013) describes a debris flow event on Fairmont Creek and Clarke Geoscience Ltd. (October 21, 2013) describes a debris flood on Cold Spring Creek. The findings below are abstracted from both reports. Photos were provided by the RDEK.

- Emily Creek weather station (23 km to the southwest of Fairmont Hotspings at elevation 1190 m recorded 106 mm of rainfall between June 18 and June 21, 2013.
- The storm triggered floods on Fairmont, Cold Spring and Dutch creeks on June 20.
- A debris flow (6000 m<sup>3</sup>) occurred on Fairmont Creek and a debris flood (unquantified sediment volume) on Cold Spring Creek.
- A state of emergency was declared for the Fairmont Hotspings community
- Culverts were blocked (Figure 3-1), avulsions occurred down roads and overland through developed areas (Figure 3-2), and reservoirs and sediment traps were filled with sediment (Figure 3-3).
- A helicopter overview flight showed signs of recent debris flows and debris floods, sediment storage in channels, debris jams, landslides and large tension cracks.



**Figure 3-1.** View upstream (east) on Fairmont Resort Road at approximately the crossing with Hot Springs Road showing muddy water and debris from an avulsion at the uppermost culvert beneath Fairmont Resort Road. RDEK photograph of June 20, 2013 7:00 AM.



**Figure 3-2.** Avulsions associated with the debris flood of June 20, 2013. Debris is seen to flow past the old Barn towards Highway 95. RDEK photograph of June 20, 2013 2:15 PM.



**Figure 3-3. Lower sedimentation basin at Glen Eagle Drive looking North. RDEK photograph of June 20, 2013 9:00 AM.**

### 3.1.3. August 12, 2019 Event

This event has been chronicled by NHC (Oct. 20, 2019). It had the following characteristic:

- Filled in the Cold Spring Creek reservoir (Figure 3-4) and the sedimentation basin at Glen Eagle Drive.
- The ski hill intake pond was completely filled with sediment and the creek had avulsed over the left bank. Sediment was removed and stored on the left bank of the creek.
- According to NHC (2019), the culvert beneath Fairmont Resort Road was not clogged, but video footage from the event supplied by Kara Zandbergen (RDEK) showed that it overflowed the road.
- The larger (1200 mm) the adjacent smaller (900 mm) CSP culverts completely clogged during the August 12, 2019 event and the creek overflowed Fairview Drive.
- At the Hotsprings Drive crossing both existing culverts (800 mm and 900 mm) were likely clogged during the event and damaged by in-bending of the CSP culvert.
- The 1500 mm Highway 95 culvert was partially blocked by woody debris.
- The 1500 mm Riverview Road culvert was clogged.
- The Ogilvy Ave. 1100 to 2200 mm culvert was partially clogged leading to a backwater effect in the basin and fine sediment accumulation.



**Figure 3-4. Cold Spring Reservoir shortly after the August 12, 2020 debris flood showing the reservoir full of sediment. Photo: RDEK.**

#### 3.1.4. May 31, 2020 Event

This event has been documented in detail by NHC (June 24, 2020) who visited both Fairmont Creek and Cold Spring Creek shortly after the May 31 debris flood. Observations listed here are extracted largely from their report in bullet form. The reader is referred to NHC (June 24, 2020) for more detail. Based on field observations of high-water marks, BGC estimates the peak discharge for this event on Cold Spring Creek to be between 2 and 3 m<sup>3</sup>/s.

#### Hydroclimate Summary:

- A strong low-pressure cold front across the region leading to heavy rain, severe thunderstorms and low temperatures followed a period of hot weather.
- A climate station at 1480 m elevation showed no snow but recorded precipitation and temperature data.
- Approximately 60 mm of snowmelt occurred at nearby Morrissey Ridge on May 29 and 30, 2020 with a cumulative melt of 115 mm over the two days which is expected to be similar to the middle and upper Fairmont Creek watershed.

- The one-day melt values on May 30 and May 31, 2020 were in the 94<sup>th</sup> and 97<sup>th</sup> percentile for melt rates in the month of May. The two-day melt total on May 31, 2020 was within the 96<sup>th</sup> percentile for two-day melt totals in the month of May.
- 40-50% of the watershed was estimated to be snow-covered.
- Between May 25 and June 1, 2020, 33 mm of rain fell at the Fairmont Creek gauge.
- The amount of rain received at the Fairmont gauge was equivalent to a 10-year 6-hour storm at Cranbrook (78 km to the south) using Cranbrook's Intensity-Duration-Frequency (IDF) data.
- At Fairmont Creek, the discharge was estimated as 4 to 7 m<sup>3</sup>/s equaling approximately a 10 to 20-year flood.
- It was expected that the debris flood on Cold Spring Creek had a similar return period.

#### Effects to Cold Spring Creek Infrastructure, the Reservoir and Dam:

- Destroyed a lock-block supported access road and bridge in the watershed accessed via the Fairmont Hot Springs Resort Ski Area (Figure 3-5). Figure 3-6 shows the same location after the reconstruction of the weir at the FHSR in 2012.
- Completely filled with sediment, aggraded at an angle of 8.5% +/- 1% (Figure 3-7, Figure 3-8). The capacity of the reservoir is approximately 900 to 1600 m<sup>3</sup> for water (KWL, 2014) and a greater amount for debris given the debris storage angle.
- The total amount of sediment deposited was approximately 3300 m<sup>3</sup> at the Cold Spring Creek reservoir but it includes a smaller event that deposited approximately 1500 m<sup>3</sup> in the reservoir which implies that May 31 event added approximately 1800 m<sup>3</sup>. This compares to 20,000 m<sup>3</sup> at Fairmont Creek. Some 1000 to 2000 m<sup>3</sup> were also deposited in the lower debris basin at Glen Eagle Drive (Brian Funke, pers. comm., August 2020), increasing the total event volume from May 31 to 2800 to 3800 m<sup>3</sup>.
- On the downstream side of the dam, embankment fill was eroded on the right abutment.
- Water flowed over the abutments rather than solely over the spillway.

#### Downstream Consequences

- At Fairmont Resort Road, the culvert was overtopped and eroded the embankment on the downstream side. Sediment discharged downstream the road (Figure 3-9).
- All other downstream culverts were overtopped and the road embankments eroded on the downstream side. Some culverts were damaged.



**Figure 3-5. Destroyed path across Cold Spring Creek at an elevation of approximately 1285 m, looking downstream (west). The structure likely failed through outflanking on the left (south) which subsequently eroded the foundation of the lock blocks and leading to their toppling downstream. Photo: BGC July 14, 2020.**



**Figure 3-6. RDEK photograph of the reconstruction of the FHSR after the 2012 debris flood (photo date unknown). This is the same location as in the previous photograph.**



**Figure 3-7. Sediment removal after the May 31, 2020 debris flood on Cold Spring Creek. Photo: NHC, June 1 or 2, 2020.**



**Figure 3-8. RDEK image of the Cold Spring Creek reservoir dam entirely filled with sediment. Note that debris also overtopped to the right of the structure which is shielding the spillway from view. June 1, 2020.**



**Figure 3-9. RDEK image of Cold Spring Creek at Fairview Drive downstream of Highway 95. The culvert is not visible to the left of the road and water is flowing down Fairview Drive. May 31, 2020, 3:45 PM.**

### **3.2. Site Visit**

Fieldwork on Cold Spring Creek was conducted on June 23 and 24, 2020 by Beatrice Collier-Pandya, EIT and Dr. Matthias Jakob, P.Geo., of BGC. Dr. Jakob returned to the field on July 9 and 10. The initial field work included channel hikes across the fan, from the fan apex (elevation = 930 m) to 1 km upstream where a large landslide complex exists on the north side of creek (elevation = 1130 m), and a 1.3 km channel hike from the end of a small access road at elevation 1280 m to an elevation of 1560 m. Furthermore, BGC mapped and measured boulders distributed over the Cold Spring Creek fan and obtained 21 dendrochronological samples from trees within the channel and on the fan.

During Dr. Jakob's return visit, five test trenches in different parts of the fan were logged and organic materials extracted for radiocarbon dating. At the same time, an additional 15 dendrochronological samples were obtained.

### **3.3. Physiography**

The physiography of Cold Springs Creek fan has been described by Clarke Geoscience Ltd. and Tetra Tech EBA (March 1, 2015). That description is not repeated herein as it is not material to the results of this study.

### **3.4. Geology**

#### **3.4.1. Bedrock Geology**

The general bedrock geology has been described by Clarke Geoscience Ltd. and Tetra Tech EBA (March 1, 2015) and is not repeated herein.

#### **3.4.2. Watershed Surficial Geology and Geomorphology**

The Cold Spring Creek watershed is outlined in Drawing 01, which shows a shaded, bare earth<sup>2</sup> Digital Elevation Model (DEM) of those portions of the watershed covered by LiDAR as well as the fan, and surrounding terrain created from LiDAR data. The DEM was used to generate the contours shown on the report drawings. Watershed characteristics are provided in Table 3-1.

A reconnaissance-level terrain map is available that includes the Cold Spring Creek watershed (Ryder and Rollerson, 1977), but is of insufficient detail for site-specific interpretations. The geomorphology of the watershed has been characterized by Clarke Geoscience and Tetra Tech EBA (March 1, 2015) and is supplemented by BGC mapping of landslides from LiDAR (see Drawing 01). Clarke Geoscience and Tetra Tech EBA (March 1, 2015) describe that the lower to mid watershed as underlain by thick (10-20 m thick) sequences of glaciofluvial sediments. Clarke Geoscience and Tetra Tech EBA (March 1, 2015) describe the lower to mid watershed as underlain by thick (10-20 m thick) sequences of glaciofluvial sediments. BGC did not encounter glaciofluvial sediments during BGC's fieldwork but noted glaciolacustrine units up to an elevation of approximately 1060 +/- 10 m, overlain by till and underlain by phyllitic bedrock. BGC hiked the channel up to the Cold Spring Landslide and noted till at the escarpment.

---

<sup>2</sup> Vegetation and buildings removed.

**Table 3-1. Watershed characteristics of Cold Spring Creek.**

Characteristic	Value
Watershed area (km <sup>2</sup> )	7.7
Fan area (km <sup>2</sup> )	1.0
Maximum watershed elevation (m)	2,608
Minimum watershed elevation (m)	936
Watershed relief (m)	1,672
Melton Ratio (km/km) <sup>1</sup>	0.6
Average channel gradient of mainstem above fan apex (%)	57
Average channel gradient on fan (%)	8.8
Average fan gradient (%)	10.8

Note:

1. Melton ratio is an indicator of the relative susceptibility of a watershed to debris flows, debris floods or floods. Melton ratio is the ratio of elevation range to the square root of watershed area.

Approximately 70% (540 ha) of the watershed is presently forested, and there is no record of significant timber harvesting activity (FLNRORD, 2019b). BGC reviewed the provincial wildfire hazard database (FLNRORD, 2019a) and noted that there are no recorded wildfires at Cold Spring Creek since the record began in 1917 (over 100 years of record).

Abundant colluvium exists in the upper watershed which has, in some cases, created vast talus slopes, especially in the eastern sub-watersheds. Those talus slopes are a primary source of debris for transport in debris floods and debris flows (Figure 3-10).

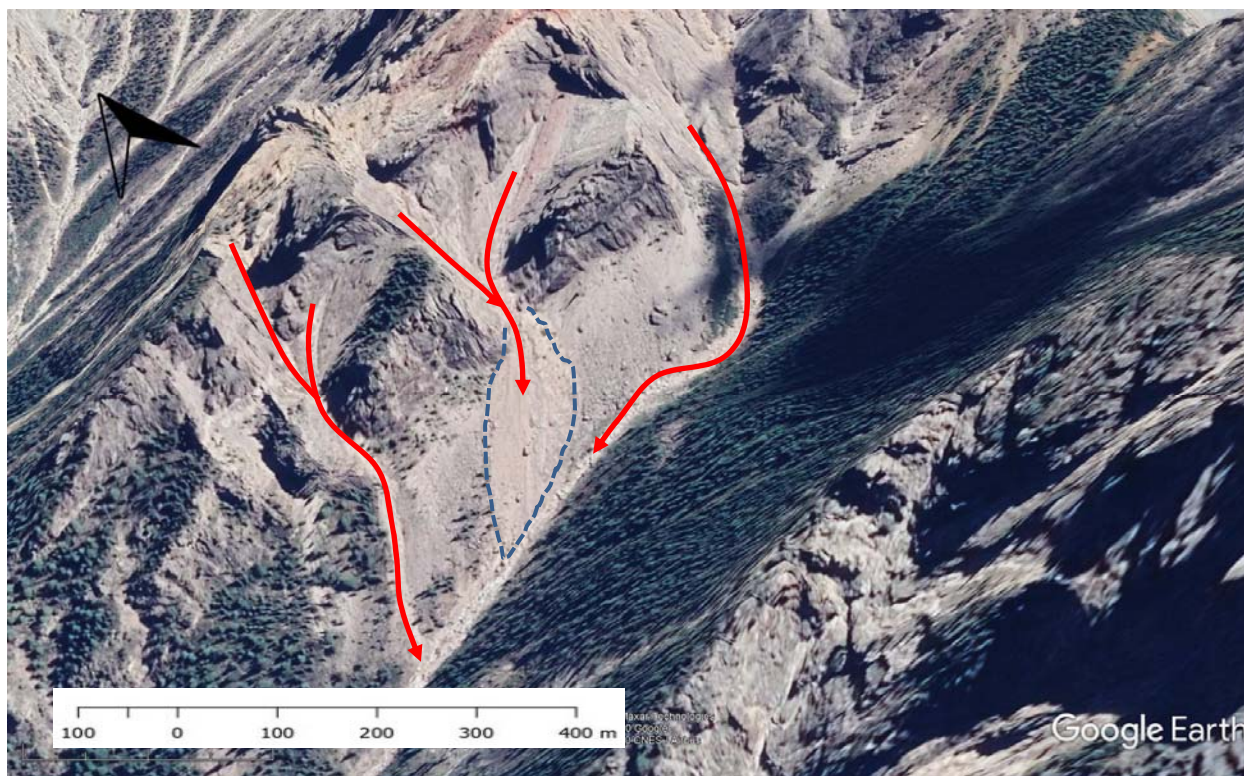


**Figure 3-10. Extensive talus slopes in the upper watershed of Cold Spring Creek at an elevation of 2000 to 2300 m facing South. Permafrost is possible on north-facing slopes in this elevation band. Google Earth.**

The primary importance of the surficial geology from a geohazard perspective is that it provides debris for channel side slope landslides. This occurs in situations where either the landslides consist entirely of surficial sediments or where they are overlying instable bedrock and contributing to landsliding where bedrock is undercut by fluvial erosion. Alternatively, overlying surficial sediments are being rafted on top of slow-moving bedrock-controlled landslides. Those materials ravel into the creek during high runoff events. Given the friable bedrock and the abundance of surficial late-Pleistocene sediments, the watershed can be classified as quasi-supply limited. This implies that there is always an abundance of surficial sediments readily available for erosion and conveyance to the fluvial system.

BGC identified numerous landslides in the lower watershed which were mapped on LiDAR imagery (Drawing 01). This includes a very large landslide (0.43 km<sup>2</sup> surface area) on the south side of the valley originating at an elevation of approximately 1870 m. Assuming an average depth range of 30 to 50 m, this landslide has an estimated volume of 16 to 27 million m<sup>3</sup>. It has, in the past, very likely dammed Cold Spring Creek up to a height of approximately 50 m as confirmed by LiDAR and BGC's field observations (Drawing 01). This landslide is informally referred to as the Cold Spring Landslide in this report. Its failure kinematics are unknown and detailed investigation is beyond the scope of this study. It is, however, speculated that a large rock slope failure from the rock slopes northeast of the landslide scarp loaded late Pleistocene sediments (presumably primarily till) leading to a surging earthflow that reached and dammed Cold Spring Creek. The rationale for this interpretation is that extensive talus slopes can be identified on the

northern portions of the upper landslide (see Figure 3-11). An alternative explanation could be a failure along low friction angle bedding planes of the Proterozoic or Paleozoic sedimentary bedrock.

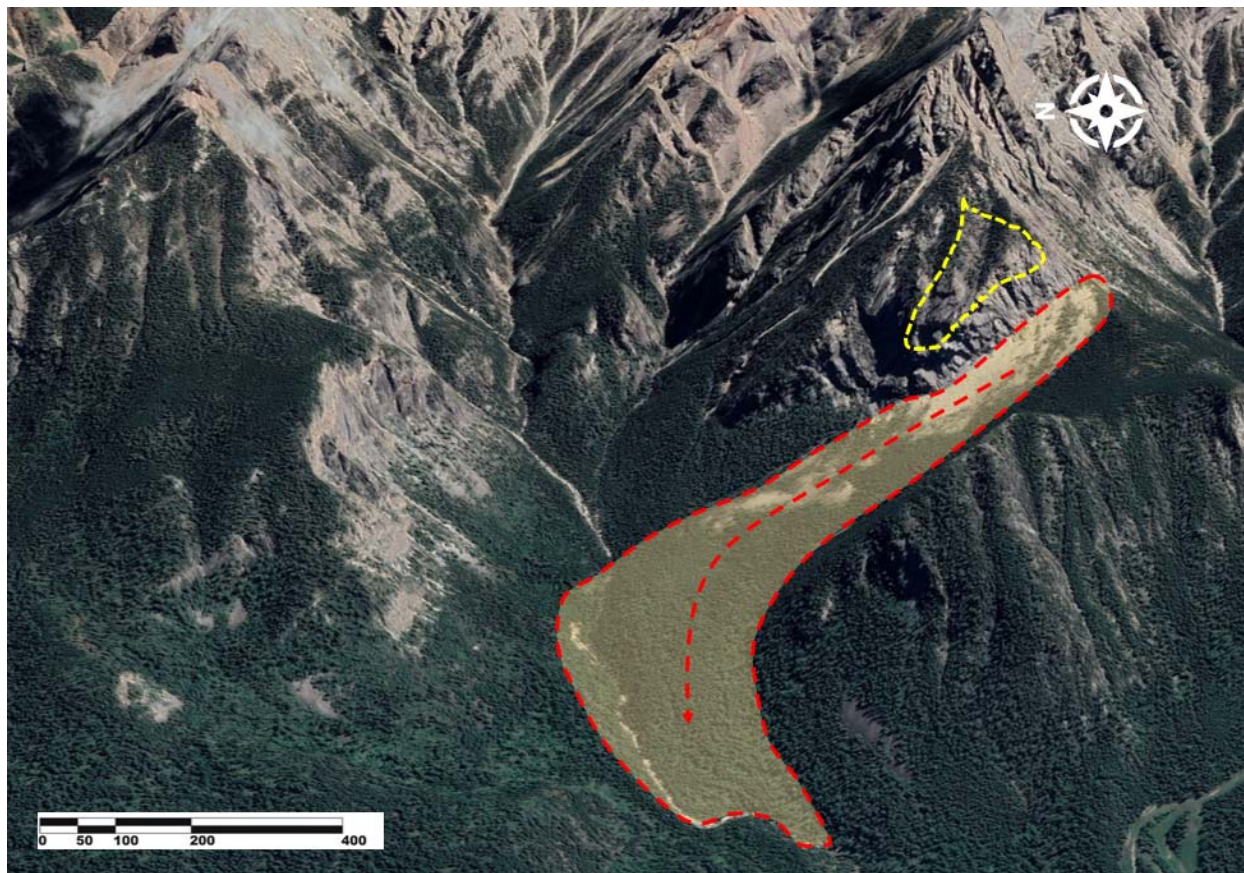


**Figure 3-11. Oblique view of the “Cold Spring Landslide” delineated in red with the potential source zone rock slide shown in yellow. View is towards the East. Google Earth imagery (date 8/4/2019).**

Numerous smaller landslides flank the lower section of Cold Spring Creek. They consist partially of brittle phyllitic rock with very low rock mass strength, till, and interbedded glaciolacustrine sediments as observed during BGC’s channel traverse. It was outside BGC’s scope to provide a detailed characterization of such landslides. However, BGC hiked the toe of most mapped landslides and crossed over the Cold Spring Landslide as well as the large (108,000 m<sup>2</sup> surface area) landslide north of Cold Spring Creek between elevations 1020 m and 1130 m that Clarke Geoscience Ltd. and Tetra Tech EBA (March 1, 2015) refer to in their report. Clark Geoscience and Tetra Tech EBA (March 1, 2015) refer to as follows: “*The slide feature was inspected by Ministry of Forests Lands and Natural Resources Operations geomorphologists, Peter Jordan in 2012. At the time, the 30 m high headscarp, unvegetated due to the south-west aspect, showed no indications of recent movement and was judged to be unlikely to present a hazard of large-scale failure or creek blockage (pers. comm., 2014). Currently, there is no instability or bulging at the toe of the slope to suggest recent movement of the slope.*” BGC confirmed that neither the Cold Spring Landslide or the lower landslide as referenced above by Clarke Geoscience Ltd. and

Tetra Tech EBA (March 1, 2015) showed signs of active movement in the main landslide mass such as open tension cracks or tilted trees.

However, BGC identified and photographed several small failures on the lower landslide that were likely triggered by undercutting of the main landslide toes by fluvial erosion. An example is shown in Figure 3-12.



**Figure 3-12. Example of an undercut slope on the mid-reaches of Cold Spring Creek at an elevation of approximately 1270 m. Photo: BGC, June 23, 2020.**

The process of landslide undercutting and landsliding is important for two reasons: First, as soon as the toe of one landslide is undercut and a slump or slide occurs, it diverts the creek into the opposing side which, in many cases, is equally unstable. This then triggers shallow landsliding on the opposite side, pushing the creek back in its former bed. This process is exacerbated during high runoff events as stream power is high and thus erosive forces are also high. The undercutting introduces substantial volumes of debris to a debris flood and debris flow and could also reactivate some of the dormant landslides. Secondly, as the relatively small side slope landslides have high fines contents, they can add to the mobility of debris flows. This process was recently demonstrated by a series of debris flows from July 4 to July 17, 2020 on Willox Creek in the Regional District of Fraser Fort George. High fines content debris flows on Willox Creek achieved

flow velocities of 6 m/s in the confined channel sections and carried boulders of up to 1 m diameter (BGC, July 31, 2020).

The potential of any of the larger landslides surging or new landslides forming and damming Cold Spring Creek has not been investigated separately and is outside of BGC's scope. However, given the stratigraphic analysis conducted on the Cold Spring Creek fan as well as the regional frequency-magnitude approach, such past events are integrated in the frequency-magnitude relationship created by BGC (see Section 5.1).

### 3.4.3. Cold Spring Creek Fan

An overview of the Cold Spring Creek watershed and fan is shown in Drawing 01, which also shows geomorphic features. Locations referred to in the text below are labelled on this drawing. The fan areas delineated in the drawings have been interpreted by BGC based on LiDAR and field data.

Cold Spring Creek fan is a complex landform. It consists of a paleofan (i.e., a fan portion not affected by contemporary debris floods and debris flows) and an active fan portion. Within the fan perimeter there are remnants of glaciolacustrine terraces which have been spared by fan erosion. The northern paleofan and the glaciolacustrine terraces are not affected directly by modern floods, debris floods and debris flows. BGC has delineated three segments within the active fan. The upper fan is located between the former access road crossing (now severed by the May 31, 2020 debris flood) and the approximate elevation of 925 m which traces a line between the southern end of Mountain Top Drive and Fairmont Resort Road. The middle fan is located between this line and Highway 95A at an elevation of approximately 860 m. The lower fan extends from Highway 95A to the Columbia River floodplain at approximately elevation 810 m.

The paleofan on the north side of the fan may have different origins which cannot be confirmed in absence of detailed study which was not part of BGC's scope. Two competing hypotheses are:

1. In the early postglacial when Windermere and Columbia lakes were connected and at a much higher level (approximately elevation 1060 m), the baselevel (i.e., the base to which Cold Spring Creek is reporting) was at least 250 m higher than today. This means that the post-glacial fan started to form at higher elevation than today. After the glacially-dammed lake drained, the base level was lowered and the fan began to erode through the glaciolacustrine (glacial lake bed sediment) terraces. The base level change abandoned the northern paleofan and isolated remaining glaciolacustrine "islands", one of which is Fairmont's Evergreen Cemetery, incidentally one of the safest places on the fan complex. The southern paleofan was partially eroded by the advancing Fairmont Creek fan. Clark (1975) describes the Quaternary history of the southern Rocky Mountain Trench and notes that the final recession of the trunk glacier in the valley occurred prior to 10,000 years AD. He also reports that in the latter stages of deglaciation, lacustrine sediments were deposited primarily from tributary creeks which were ice-free much earlier than the main valley. Those sediments can still be identified in the watershed today.
2. At an unknown time in the Holocene era (last 11,000 years), the Cold Spring Landslide occurred and created a 50 m high landslide dam impounding water. Either the landslide directly evolved into a debris flow, or an outbreak flood occurred which caused massive

aggradation on the fan that later incised by fluvial erosion and redistribution of fan deposits.

On the balance of probabilities BGC believes that the first hypothesis is more credible given how much higher the paleofan fan surfaces are above the modern ones.

The fan of Cold Spring Creek is on average 11% steep. It was probably formed by both debris floods and debris flows. One obvious expression of past debris flow occurrence is the over 140 boulders with a diameter greater than 0.5 m that were recorded by BGC on the fan (Drawing 01). Those boulders are a combination of surface boulders and boulders excavated during basement excavations that were placed ornamentally near the home or used as non-engineered retaining walls. The boulders are generally sub-rounded to subangular and are sourced from the watershed. The sub-rounded nature of some of the boulders suggests transport over a distance of several kilometers from rockfall in the upper watershed. This transport tends to round sharp edges of boulders originating from rock fall. Some boulders may also be till from undercutting side slopes. Till boulders are typically sub-rounded.

No distinct boulder levees (a characteristic surficial landform of debris flows) were encountered on the mid or upper fan which is attributed to the fact that the entire fan surface has been altered by construction of the current development and should thus not be interpreted as indicating the absence of debris flows. However, boulder levees were observed along lower reaches of the channel above the fan apex. Debris lobes were also visible on the lower fan though muted by vegetation and human fan surface alterations.

The test trenching (Section 5.3.3) indicates that most events that have affected the fan sectors that have been trenched were debris flows. This is indicated by units that are matrix-supported (i.e., individual particles rarely touch each other) and unsorted and lack stratification (meaning there is no layering within a deposit that indicates fluvial deposition). They are, however, interspersed with debris flood deposits that show some stratification, are mostly clast-supported and show some imbrication (boulder shingling) (Church & Jakob, 2020). This also verifies the earlier assumption that Cold Spring Creek fan is subject to both debris flows and debris floods.

Cold Spring Creek has changed its course numerous times in the past which is typical for any active fan. This observation is derived from air photograph analysis, dendrochronology and test pitting which all suggest an actively moving channel system. Additional details are provided in Section 5.

Steep creek process type can also be assessed based on the Melton Ratio as described above. In comparison with a large dataset of steep creeks in B.C. and Alberta, Cold Spring Creek plots in the data cluster prone to debris floods and debris flows (Figure 3-13). This result is consistent with BGC's field observations.

Debris floods can be subdivided into three types, those triggered by the exceedance of a critical bed shear stress threshold (Type 1), those through transitions from debris flows (Type 2), and those triggered from outbreak floods (Type 3) (Church & Jakob, 2020). This differentiation is not included in Figure 3-13 as such nuances are unknown for the data included above; however, it is included in this detailed assessment.

BGC interprets debris floods to be the dominant hydrogeomorphic process at Cold Spring Creek for the 5-year to 100-year return periods, while debris flows dominate at the higher return periods. This rationalization is discussed further in Section 5.

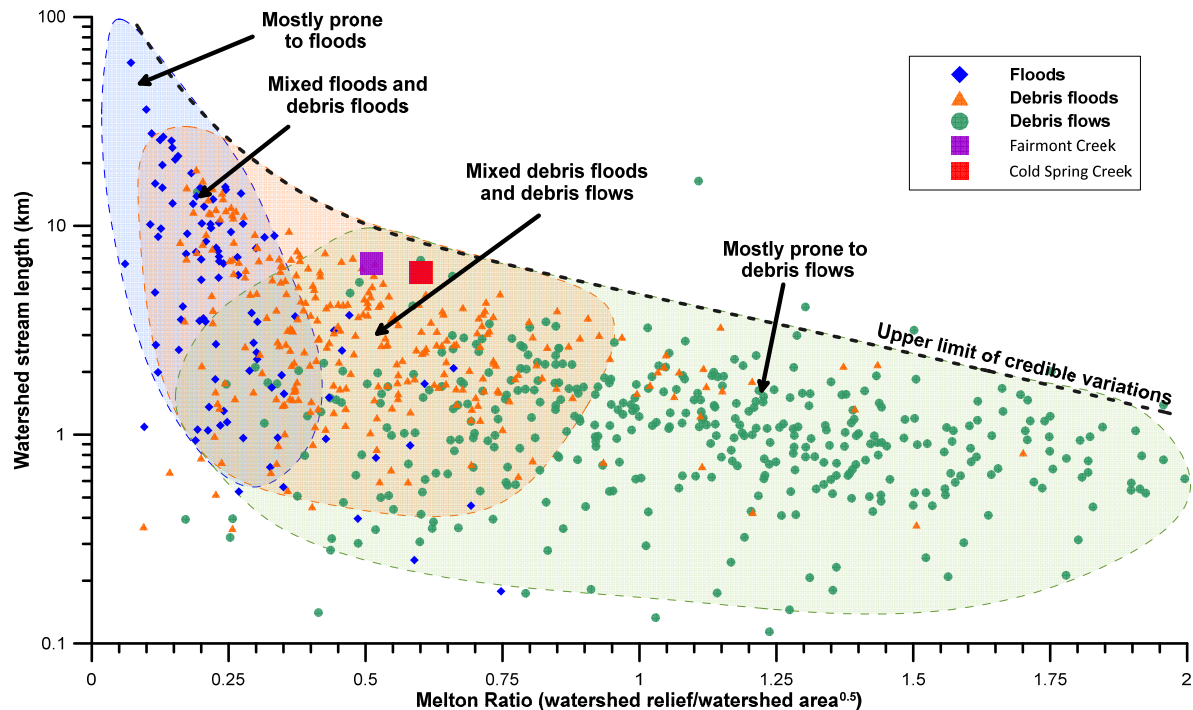


**Figure 3-13. Tendency of creeks to produce floods, debris floods and debris flows, as a function of Melton Ratio and stream length (data from Holm et al., 2016 and Lau, 2017). See Section 3.4.2 for Cold Spring Creek watershed data.**

### 3.5. Existing Development

The existing development extends upstream of Highway 95A and downstream to the Columbia River floodplain. The assessed value of all buildings within the fan footprint is approximately \$121 million (pers. comm. Shaun Thompson, July 2020). Not all buildings on the fan are subject to debris flow hazards.

#### 3.5.1. Cold Spring Water Reservoir

The Cold Spring Water reservoir has been described previously by various workers. A more detailed assessment is available from Kerr Wood Leidal Associates Ltd. (KWL) (December 29, 2014) who conducted a consequence assessment for the dam. The reservoir was constructed in 1980 and is located at the fan apex (Drawing 01).

KWL characterizes the dam and reservoir as: a concrete gravity structure 22 m long and 4.6 m high from the structure crest to the river bed of the creek at the downstream outside limit of the dam. The reservoir volume at full supply level (FSL) is estimated to be 1600 m<sup>3</sup> at an elevation of 943.4 m (Stepanek, 2013). Discharge through the outlet is controlled by a free Ogee spillway and a gated 0.9 m diameter pipe outlet (Figure 3-14).

KWL conducted a dam break failure analysis for a “sunny day” and “flood induced” failure and concluded that that sunny day failure would lead to 15 m<sup>3</sup>/s discharge. For the “flood induced” failure, peak discharge was estimated for the 100-year, 1000-year and probable maximum flood (PMF) scenarios. Those were estimated to 15, 21 and 40 m<sup>3</sup>/s, respectively, and are thus a multiple of a 100-year return period flood, estimated by KWL as 1.5 m<sup>3</sup>/s, immediately downstream of the barrier.



**Figure 3-14. Images of the Cold Spring Creek Dam and Reservoir looking upstream, across the dam and from downstream of the dam. BGC photographs of July 14, 2020.**

KWL modeled the outbreak floods and concluded that even with a 15 m<sup>3</sup>/s discharge there would be little damage other than to roads. KWL (December 29, 2014) reports that “avulsions may be possible; however, in our opinion, these would be minor and generally redirected towards the creek; if there were implications from escaped water beyond the modeling extents, it would be of low severity”. This contrasts BGC’s findings as later explained in Section 6.4. If BGC’s modeling results are more realistic (they are based on 2018 LiDAR which was unavailable to KWL at the time, and BGC used a very small grid size), then the main conclusions of a dam failure not resulting in damage to homes may need to be revisited.

A dam failure during a debris flow would aggravate the problem, however, given the peak flow of a debris flow being an order of magnitude higher than the outbreak flood, the incremental hazard increase is believed to be low.

### 3.5.2. Culverts

Culvert locations are shown in Drawings 01 and 02, and culvert dimensions are provided in Table 3-2.

Moving downstream from the fan apex, the first culvert on Cold Spring Creek is the Fairmont Resort Road culvert (Figure 3-15A), followed 180 m downstream by the Fairway Drive culvert (Figure 3-15B). On the mid-fan, the creek passes through the Hot Springs Road culvert (Figure 3-15C) 300 m downstream of Fairway Drive, then goes through the Highway 93/95 culvert (Figure 3-15D). On the distal fan there are two more culverts, the Riverview Road culvert (Figure 3-15E), 160 m downstream of the highway, and the golf course culvert, 530 m downstream of Riverview Road (Figure 3-15F). Just upstream of the golf course culvert, Cold Spring Creek passes through a sedimentation pond that is approximately 100 m long and 20 m wide (Figure 3-16).

**Table 3-2. Estimated dimensions of culvert crossings on Cold Spring Creek fan, heading downstream.**

<b>Culvert</b>	<b>Diameter (mm)</b>	<b>Notes</b>
Fairmont Resort Road	1200	Corrugated steel pipe
Fairway Drive	900, 1200	Corrugated steel pipes, damaged from recent event
Hot Springs Road	800, 900	Corrugated steel pipes, damaged from recent event and one-third full of sediment. Swale infrastructure in place over road.
Highway 93/95	1600	Corrugated steel pipe, significant grade under highway
Riverview Road	1460	Corrugated steel pipe
Golf course culvert	1600	Corrugated steel pipe, partially crushed under golf course

Note: The culvert dimensions were obtained in the field.



**A) Fairmont Resort Road outlet**



**B) Fairway Drive inlet**



**C) Hot Spring Road inlet**



**D) Highway 93/95 inlet**



**E) Riverview Road inlet**



**F) Golf course culvert inlet**

**Figure 3-15. Cold Spring Creek culverts: A) Fairmont Resort Road outlet, B) Hot Spring Road inlet, C) Fairway Drive inlet, D) Highway 93/95 inlet, E) Riverview Road inlet, and F) Golf course culvert inlet. BGC photos taken June 2020.**



**Figure 3-16. Sedimentation pond upstream of golf course culvert on Cold Spring Creek, looking upstream. BGC photo taken June 2020.**

### 3.5.3. Sediment End-Dump Location

During BGC's field visit on July 10, 2020, it was noted that sediment removed from the Cold Spring Creek reservoir was being deposited at the second switchback to the Fairmont ski area at an elevation of 1030 m (Figure 3-17). The end dump location is partially on a presumably presently inactive landslide. Loading it with debris, in conjunction with continued undercutting by Cold Spring Creek, may reactive this landslide or increase its movement rates. If the movement is slow, it will lead to continued sediment loading to Cold Spring Creek. If the movement is rapid, it could lead to a blockage of Cold Spring Creek, followed by an outbreak flood. For this reason, RDEK should either monitor movement rates of the landslide or discontinue end-dumping sediment at this location.

BGC did not evaluate the stability of the end dump. BGC also recommends that the stability of the waste rock should be investigated. Specifically, the possibility of it developing into a flow slide with runout to Cold Spring Creek ought to be assessed.

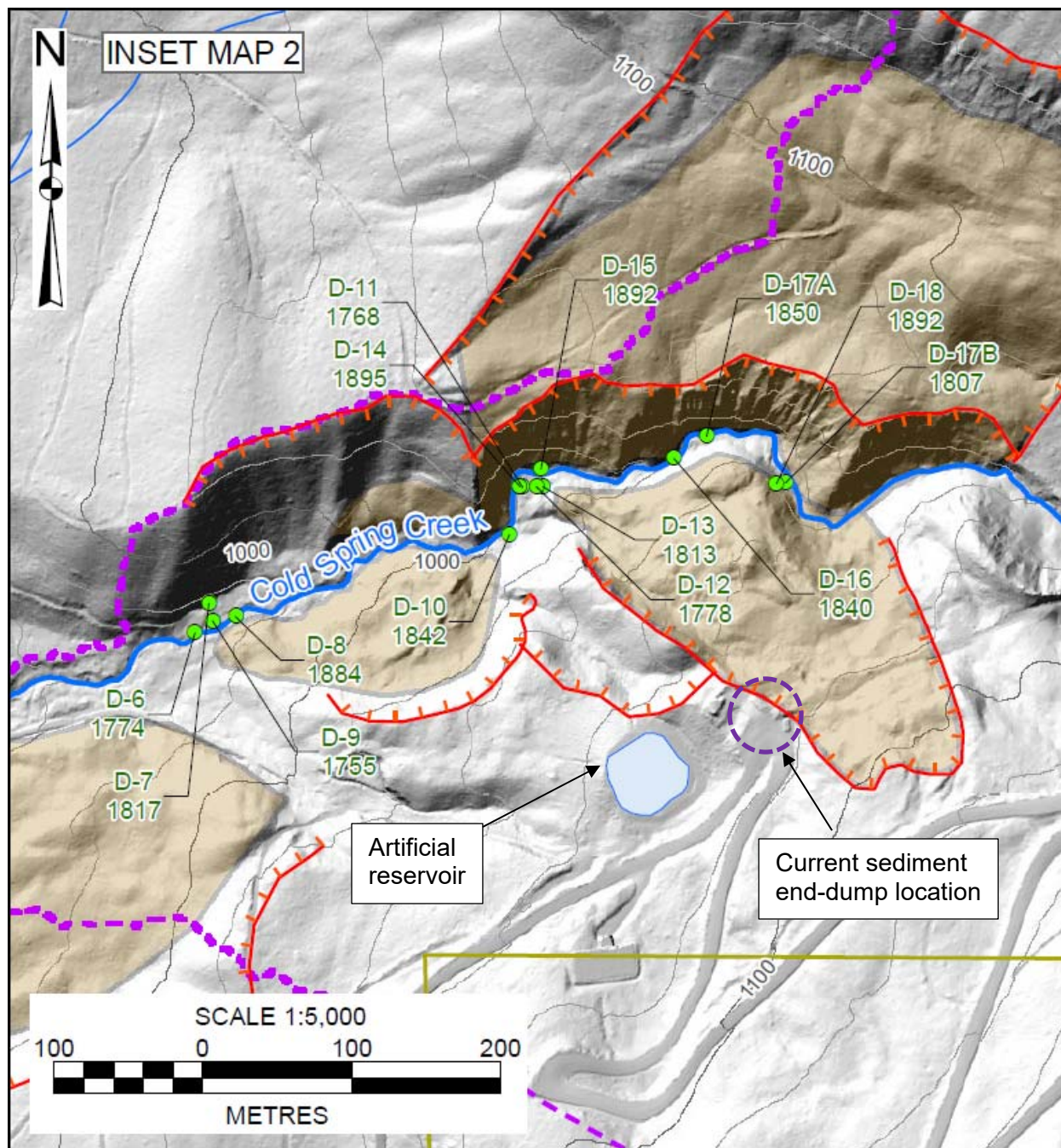


Figure 3-17. Inset map from Drawing 01, showing the location of sediment end-dumping from a switch back of the Fairmont Ski Area access road.

### 3.6. Climate Change Impacts

#### 3.6.1. Temperature, Precipitation and Runoff

The watershed falls within the western slopes of the Kootenay Ranges which within the southern section of the Rocky Mountains of the Western Cordillera ecoregion. Streamflows within this region exhibit a glacial-nival regime (e.g., snowmelt and glacier melt dominated) with the peak flows are dominated by the spring freshet followed by a gradual decrease in flows during the late

summer and fall with the lowest streamflows occurring during the winter (Schnorbus et al., 2014). The effects of climate change on streamflow differ throughout the Upper Columbia but the region is expected to retain a nival flow regime. Snowpack is expected to decline at lower elevations however, higher elevation regions are projected to experience increases in snowpack (Loukas & Quick, 1999; Schnorbus et al., 2014). This will likely result in higher discharges during the winter, an earlier freshet and lower average discharges during the summer months. Note that this does not imply that discharge extremes will be lower. Statistical analysis of historical freshet peak flows in rivers by Rood et al. (2016) found a general decreasing trends particularly for basins flowing north or northeast. The trends were likely a reflection of warmer winters with increasing rain and decreasing snow and melt and the advancement of the timing of the spring melt which extends the melt interval.

The Climate NA model provides downscaled climate projections for future conditions (Wang et al., 2016). The projections based on the Representative Concentration Pathway (RCP) 8.5<sup>3</sup> indicate that the mean annual temperature (MAT) in the Cold Spring Creek watershed is projected to increase from 1.0°C (historical period 1961 to 1990) to 6.6°C by 2050 (average for projected period 2041 to 2070). The mean annual precipitation (MAP) is projected to increase from 829 mm to 896 mm while the precipitation falling as snow (PAS) is projected to decrease from 425 mm to 155 mm by 2050 (Table 3-3). Figure 3-18 shows the historical and projected change (RCP 8.5, 2050) in the monthly average temperatures and precipitation. For the monthly average temperature, a uniform positive change can be observed in the monthly average temperatures. For the monthly precipitation, there is an overall increase in the precipitation during the Spring, Fall and Winter months and a decrease in precipitation during the summer months.

**Table 3-3. Projected change (RCP 8.5, 2050) from historical (1961 to 1990) conditions for the Cold Spring Creek watershed (Wang et. al, 2016, and Prein et al., 2016).**

Climate Variable	Projected Change
Mean Annual Temperature (MAT)	+6 °C
Mean Annual Precipitation (MAP)	+68 mm
Precipitation as Snow (PAS)	-151 mm
% increase in the frequency of hourly rainfall extremes	50 to 150
% increase in the magnitude hourly rainfall extremes	20 to 30%

Aside from changes in average temperature, precipitation and snow, changes in precipitation extremes are very important for the understanding of steep creek response to climate change. Prein et al. (2017) provides expected changes in the frequency and magnitude of high intensity rainfall for the USA and the southern portions of Canada. Those are also summarized in Table 3-3. These data suggest that both the frequency and magnitude of intensive rainfall will increase with the frequency roughly doubling and the magnitude increasing by as much as one third. The consequence of this change will be more, and possibly larger, debris floods and debris

<sup>3</sup> This implies an 8.5 Watt/m<sup>2</sup> increase in radiation due to greenhouse gas emissions.

flows in watersheds with little or no sediment supply limitations which is the case for Cold Spring Creek.

The changes as listed in Table 3-3 are profound and, in terms of temperature, unprecedented since humans changed from nomadic or settling behaviour. Hence, there are no modern precedents to orient oneself for the future. The very strong expected temperature increases will imply degradation of mountain permafrost which implies loss of the cohesive bond afforded by ground ice and more and possibly larger rock fall and rock slides events. It will also lead to more tree mortality by insect infestations, wildfires and droughts. These secondary and tertiary effects of climate change will invariably lead to more available sediment and a drastic change of the interaction of hillslope processes with channel changes. Cycles of heavy sediment input and scour can be expected, all of which will challenge existing and future mitigation measures.

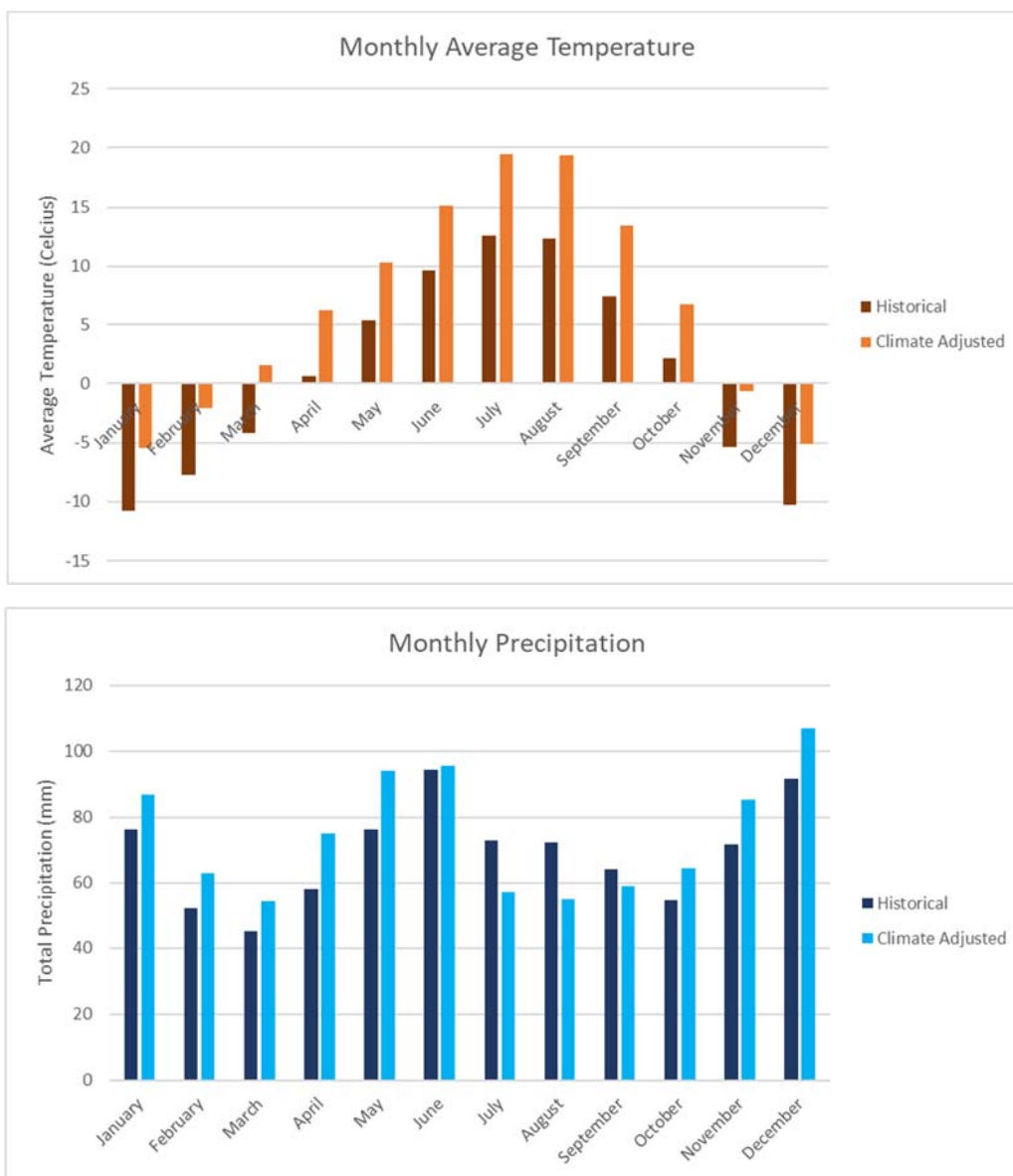


Figure 3-18. Projected change (RCP 8.5, 2050) from historical (1961 to 1990) monthly average temperature and precipitation for the Cold Spring Creek watershed.

### 3.6.2. Permafrost Changes

The upper watershed of Cold Spring Creek is likely underlain by permafrost which is continually frozen ground which thaws only superficially by a metre or so and then refreezes in the winter. This was confirmed by a global permafrost model (Gruber, 2012) which is shown for the study area in Figure 3-19.

Permafrost-underlain watersheds, particularly those at or near 0°C, are particularly sensitive to warming as changes in ground thermal status will alter most components of the hydrological cycle due to increases in subsurface storage for liquid water and reduction in surficial runoff as the ground temperatures increase and the active layer thickens.

In permafrost terrain, whenever water ingresses into rock cracks or soil voids it freezes and holds rock or soil together like glue. With a rapidly warming world, this “glue” disappears, and one can expect an increase in rockfall and other landsliding in the upper watershed. This process feeds the channel system with debris that is then ready for transport to the fan where people live. A summary of periglacial processes acting in mountainous terrain has recently been provided by Jakob (2020).

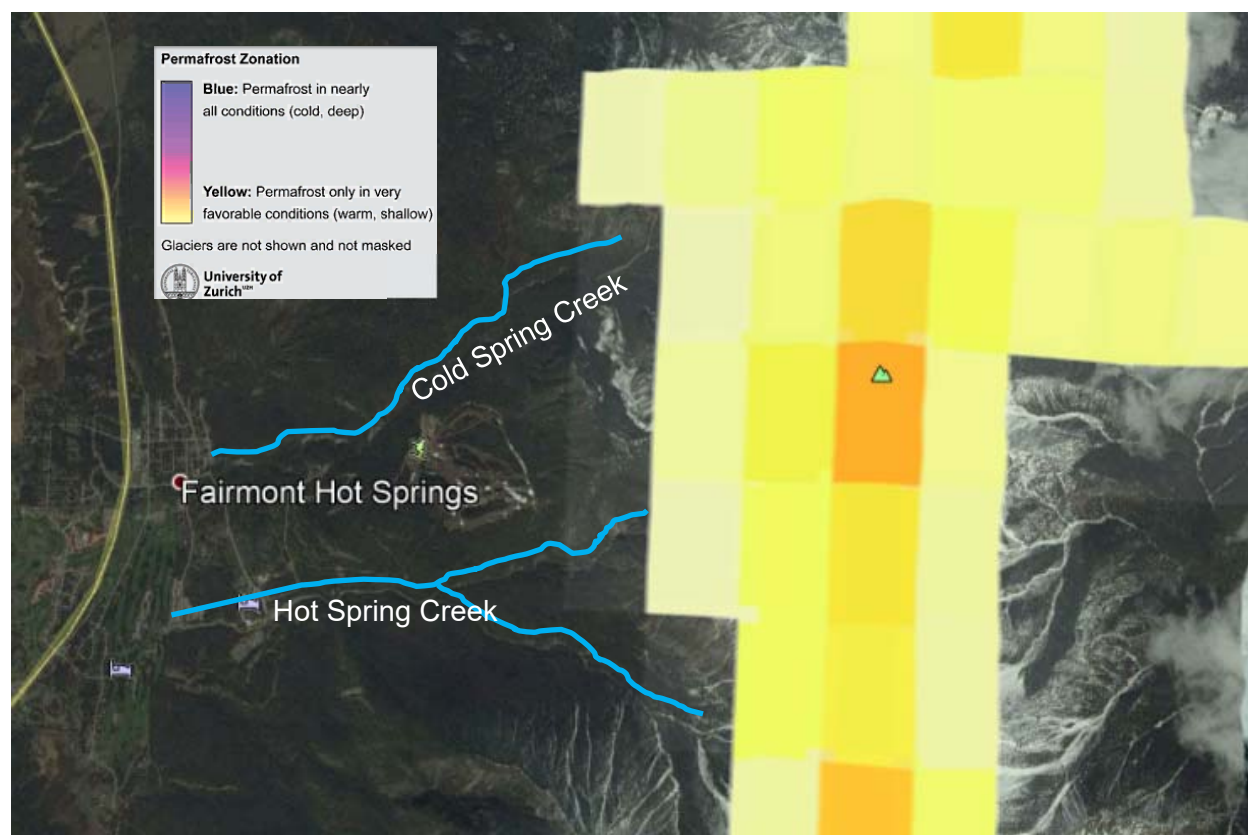


**Figure 3-19. Approximate permafrost distribution in the Cold Spring and Fairmont Creek watersheds (mapping from Gruber, 2012). The mapping indicates that permafrost is possible in favourable location but will be shallow and “warm”, meaning near zero degree Celsius and thus particularly sensitive to climate change.**

## 4. PREVIOUS REPORTS

In developing a flood, mitigation, and development history for Cold Spring Creek, BGC briefly reviewed several documents and provides key findings as summarized in Table 4-1. BGC's current work supersedes the hazard findings in the reports listed below.

**Table 4-1. Previous reports and documents on Cold Spring Creek.**

Year	Assessment Author	Purpose	Key Findings
1989	Dwain Boyer, Water Management Branch	Debris torrent concerns on Cold Spring and Fairmont Creeks	<ul style="list-style-type: none"> <li>Recognition that Cold Spring and Fairmont Creeks are subject to debris flow hazards.</li> <li>Placement of a restricted covenant on the area, requiring inspection of future development by a Professional Engineer.</li> </ul>
1994	Reid Crowther & Partners Ltd	Resort area terrain hazards assessment	<ul style="list-style-type: none"> <li>Terrain assessment indicating that Cold Spring Creek is subject to debris flows.</li> <li>Conceptual mitigation suggestions including debris retention structures and berms to maintain the flow within the channel.</li> </ul>
1995	Reid Crowther & Partners Ltd.	Cold Spring Creek – Highway 93 crossing comments	Comments on the potential blockage of Highway 93 from debris flows on Cold Spring Creek. Suggests that most of the risk is managed by the Cold Springs Creek Dam, and is mostly concerned with debris flows that generate between the reservoir and the highway.
1998	Klohn Crippen	Terrain stability inventory, alluvial and debris torrent fan mapping in the Kootenay region	Characterization and mapping of numerous alluvial fans and steep creek processes. For Cold Spring Creek, Klohn Crippen notes potential avulsion points and that the Cold Spring Creek reservoir decreases the overall sediment load. The watershed was characterized as being permeable being able to retain significant rainfall or snowmelt.
1999	J.E. Farrell & Associates Inc.	Letter to the Province on behalf of Fairmont Hot Springs Resort (FHSR)	<p>This letter is a response to February 25, 1999 letter from Mr. Boyer at the Ministry of Environment, Lands and Parks to Fairmont Hotsprings Resort (FHSR), which was not made available to BGC. Key pieces of information:</p> <ul style="list-style-type: none"> <li>FHSR was committed to complete channel improvements between the Highway and the concrete dam as development proceeds in the area.</li> <li>Mr. Boyer was concerned about the potential for avulsion above the concrete dam. Mr. Farrell noted that Cochrane Engineering Ltd. had completed an assessment and not identified this concern.</li> </ul>
2013	Clarke Geoscience Ltd.	Overview-level hazard assessment	<ul style="list-style-type: none"> <li>Description of the watershed, fan and June 2013 event impacts</li> <li>Sediment supply on Cold Spring Creek is similar to Fairmont Creek, and is sufficient to generate debris flows that are comparable to the 2012 Fairmont Creek event.</li> </ul>

Year	Assessment Author	Purpose	Key Findings
2014	Kerr Wood Leidal Associates Ltd. (KWL)	Dam Consequence Assessment	<ul style="list-style-type: none"> <li>Recommended changing the consequence classification of the Cold Spring Creek Dam from “Very High” to “Significant”</li> <li>If approved by the Provincial Regional Dam Safety Officer, the classification change would result in reduced site surveillance</li> <li>Modeling of a 15 m<sup>3</sup>/s outbreak flood did not show any significant avulsions.</li> </ul>
2015	Clarke Geoscience Ltd. and Tetra Tech EBA	Debris flow hazard and risk assessment	<ul style="list-style-type: none"> <li>Early air photos (1945 to 1964) indicate that Cold Spring Creek is not well confined across the fan, and multiple flow paths are possible.</li> <li>Field indicators of debris flows were observed, including levees and large boulders</li> <li>Possible debris flow volume estimated at 24,000 m<sup>3</sup> from channel yield calculations</li> <li>Obtained a radiocarbon date of 1200 BP from a paleosol at 0.7 m depth at the fan apex.</li> </ul> <p><u>Interpretations</u></p> <ul style="list-style-type: none"> <li>Debris flows in excess of 20,000 m<sup>3</sup> were assigned a minimum return period of 500 years.</li> <li>A small area of the fan, near the fan apex, is considered high risk. Two houses at the corner of Mountain View and Mountain Top Drives are on the edge of the high risk zone.</li> <li>The remainder of the fan is subject to moderate risk, low risk or no risk, where moderate risk is defined as at least a 0.2% annual probability of a property damaging debris flow and transported material could include a range from mud to gravel, cobbles and smaller woody debris.</li> </ul>
2019	NHC	Mitigation concepts	<ul style="list-style-type: none"> <li>Recommends conceptual mitigation measures, including construction of: <ol style="list-style-type: none"> <li>A sediment retention basin adjacent to the existing Cold Spring Creek dam</li> <li>24 check dams or grade control structures on the fan</li> <li>Trash racks and small sediment basins upstream of culverts</li> </ol> </li> <li>Estimated cost of all measures is about \$1 million CAD</li> </ul>

## **5. METHODS**

This section summarizes the overall workflow adopted by BGC and Figure 5-1 shows the workflow to develop hazard maps for individual return periods and a composite hazard map, both of which inform the design event basis for mitigation efforts. They can also be used to develop a quantitative risk assessment for life loss and economic losses should that be desired.

The principal components of the workflow consist of developing a frequency-magnitude (F-M) relationship for Cold Spring Creek. The F-M relation is of fundamental importance as it specifies how often the respective events occur and how much sediment they carry. A significant error in the F-M relationship implies that the numerical modeling is incorrect, any risk assessment is erroneous and mitigation is either over- or under-designed, both of which are undesirable outcomes.

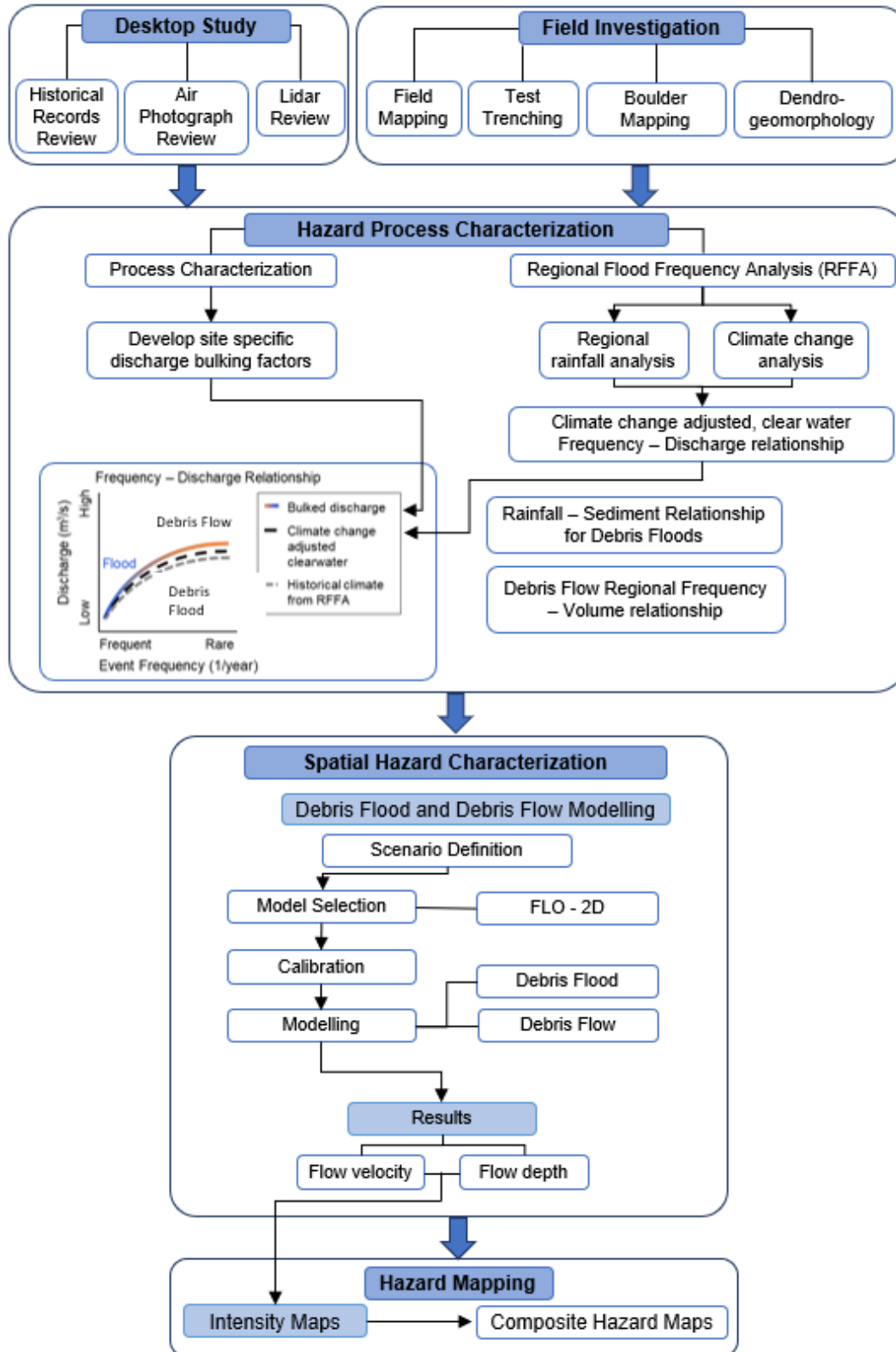


Figure 5-1. Flood and debris flow prone steep creeks workflow used for developing frequency-magnitude relationships, modeling, and preparing hazard maps.

## 5.1. Frequency-Magnitude Relationships

An F-M relationship answers the question “how often (frequency) and how big (magnitude) can steep creek hazards events become?”. The ultimate objective of an F-M analysis is to develop a graph that relates the frequency of the hazard to its magnitude. For this assessment, frequency is expressed using return periods<sup>4</sup>. Both peak discharge (for clearwater flows, debris floods and debris flows) and volume (only for debris flows) are used as measures of magnitude.

Because BGC assessed Cold Spring Creek to be subject to both debris floods and debris flows, F-M relationships have to be developed for the individual processes. Mixing the two data populations is not desirable as they are characterized by very different flow physics, F-M relationships and distinct hazard potential with debris flows being substantially more dangerous (higher impact forces and higher damage potential) compared to debris floods. The following subsections describe the methods employed by BGC to develop F-M relationships for debris floods and debris flows on Cold Spring Creek.

## 5.2. Flood & Debris Flood Frequency-Discharge Relationship

Peak flows for clearwater floods were estimated from Water Survey of Canada (WSC) streamflow records, using several gauges on creeks with watersheds <20 km<sup>2</sup> in the area, and then adjusted to account for climate change. These flows were then bulked to estimate debris-flood discharges (sediment and water), as described in the following sections.

### 5.2.1. Clearwater Peak Flow Estimation

Cold Spring Creek is an ungauged watercourse in that it does not have streamflow records from which to directly estimate the peak flows for the flood quantiles (i.e., 2-, 5-,10-year floods)<sup>3</sup>. Therefore, the peak discharge were estimated using a regional frequency analysis (Regional FFA). Regional FFA involves via transferring information from gauged watercourses to the ungauged site. The Regional FFA was performed using the flood quantile regression method. Flood quantile regression uses a transfer function to find a direct relationship between at-site flood quantiles (outputs) and physio-meteorological variables (predictors or inputs). For this study, BGC’s River Network Tools™ (RNT) was used. RNT uses a relationship between the flood quantiles and the catchment area:

$$Q_T = \alpha CA^\beta$$

where  $Q_T$  is the peak flow for the  $T^{\text{th}}$  quantile,  $CA$  is the catchment area and  $\alpha$  and  $\beta$  are parameters. The equation is linearized<sup>5</sup> by taking the log of both sides:

$$\log(Q_T) = \beta \log(CA) + \delta$$

where  $\gamma = \log(\alpha)$ . RNT uses ordinary least squares to estimate the parameters  $\beta$  and  $\gamma$ .

<sup>4</sup> Except for periods of  $T < 1$ , the return period (T) is the inverse number of frequency F (i.e.,  $T = 1/F$ ).

<sup>5</sup> A skew in the distribution violates the statistical assumption of a regression equation, hence the linearization.

RNT was used to select and rank candidate streamflow gauges from the Water Survey of Canada (WSC) based on their proximity to Cold Spring Creek, period of record and hydrological similarity. The peak flows for the flood quantiles of the gauged watercourses are modeled in RNT using the Generalized Extreme Value (GEV) distribution based on the observed instantaneous maximum peak flows. The list of candidate gauges produced by RNT was manually refined to select the top ranked gauges with catchment areas  $< 20 \text{ km}^2$ . The final list of gauges was used to estimate the regression parameters,  $\beta$  and  $\gamma$  which in-turn were used to determine the peak flows for the flood quantiles for Cold Spring Creek.

### 5.2.2. Climate Change Adjustment

It is now an undeniable scientific fact that global temperatures have been increasing for the past 60 years or so due entirely to human greenhouse gas emissions and this trend will continue until humans have largely replaced fossil fuels with alternative sources of energy (IPCC, 2014). Temperature increases unleash a myriad of feedback mechanisms in the atmosphere and biosphere. With every linkage, predictive uncertainty increases. This does not mean that climate change should be ignored in studies that pertain to higher order effects of global warming, rather, the uncertainty should be described and, if possible, quantified. In this sense, the reader of this report is reminded that all results presented here including the modeling are forward looking as they assume that climate will continue to change over the next century and beyond. Anecdotal information is emerging that extreme runoff events on Cold Spring and Fairmont creeks are increasing as evidenced by damaging events in 2012, 2013 and 2020.

EGBC (2018) offer guidelines that include procedures to account for climate change when flood magnitudes for protective works or mitigation procedures are required. BGC recently conducted a regional study for RDCK (BGC, March 31, 2020) using both statistical and process-based methods to estimate the change in the peak flows by 2050 (2041 to 2070). The results of this study found that the projected peak flows were difficult to synthesise as they were inconsistent. The results of the statistical flood frequency modeling generally project a small decrease in the flood magnitudes, while the results of the process-based methods generally show an increase with a wide range in magnitude. As a result, peak discharge estimates were adjusted upwards by 20% to account for the uncertainty in the impacts of climate change.

Note that this conclusion does not reflect the expected substantial increases in the frequency of extreme short-duration precipitation as postulated by Prein et al. (2017) and others.

### 5.2.3. Discharge Bulking Method

Clearwater floods and debris floods as defined by Church and Jakob (2020) are related as both are classified as Newtonian processes, which implies no yield strength resisting motion. However, debris floods have been characterized especially by their higher sediment concentrations and propensity to erode banks, scour and avulse (Hungry et al., 2014). While some measurements of sediment concentration exist from steep creeks, especially near volcanic centres and downstream of recently deactivated dams (Magirl et al., 2015; Mosbrucker and Major, 2019), systematic bedload and suspended sediment measurements in steep channels during extreme flows are rare.

Sediment concentration is important from the point of view of bulking a known discharge, but also because higher suspended sediment concentration can transport larger stones. The mobilization of large particles implies full bed mobilization (MacKenzie, Eaton, & Church, 2018; Church and Jakob, 2020), the characteristics of a Type 1 debris flood (Section 1.3). This necessitated specification of bulking factors based on geomorphological indicators in the watershed. The following text explains the rationale used to assign bulking factors. In absence of direct observations of sediment loads for different return periods and specifically for the creeks that were studied by BGC, geomorphological proxies were used. These bulking factors should not be interpreted as precise.

Figure 5-2 introduces the concept and logic inherent in determining the bulking coefficient of debris floods for small (<100 km<sup>2</sup>) watersheds.

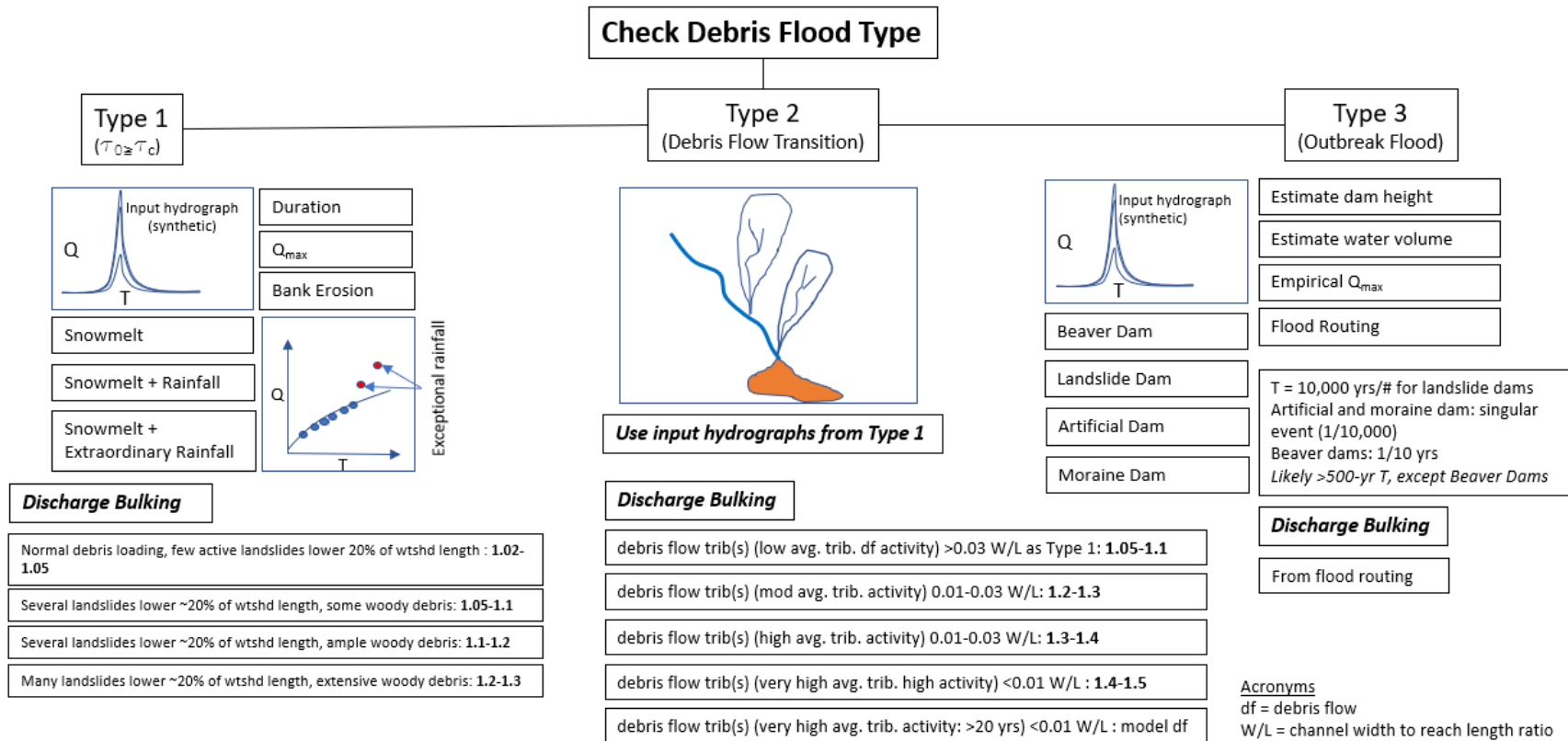


Figure 5-2. Debris flood bulking method logic chart for Cold Spring Creek. Only Type 1 and Type 2 debris floods were considered for Cold Spring Creek as the return period for Type 3 events is unknown.

The first step entailed identifying which debris-flood type (Type 1, 2 or 3 per Figure 5-2) is likely and at what return period, as debris flood types may change with the return period of the hydroclimatic events triggering it. At Cold Spring Creek all three types exist, albeit at different return periods. It was beyond BGC's scope to quantify the peak flows and frequencies of all three hazard types. Moreover, the greatest damages would result from debris flows, hence the emphasis of this report is placed on that process.

For this reason, BGC focused on quantifying the peak flows of Type 1 debris floods, which appear to occur most often on Cold Spring Creek.

#### 5.2.4. Debris Flood Sediment Volume Estimates from Empirical Rainfall-Sediment Transport Relations

Prediction of bedload transport can be important for hazard assessments and engineering applications although knowledge on sediment transport is still limited, particularly from a modeling perspective. Furthermore, few sediment transport studies have been completed for steep (> 5%) mountain creeks, and as noted by Hassan et al. (2005), sediment transport in such channels may be quite different from low-gradient channels. Hillslope processes are linked to channel processes with some channels being supply-limited while others being supply-unlimited (Jakob & Bovis, 1996; Rickenmann, 2005). As pointed out by Church and Zimmermann (2007), steep mountain creeks can display a multitude of grain sizes, variable sediment sources, and rough and structured stream beds with a step-pool morphology. Large boulders (keystones), woody debris and occasional bedrock sections further create significant variation in channel geometry, flow velocity and roughness, all of which render theoretical or flume-derived sediment transport equations questionable (Gomi and Sidle, 2003). These channel characteristics apply to Cold Spring Creek.

During August 21 to 23, 2005 severe flooding occurred in a large area of northern Switzerland with significant morphological changes in stream channels (Jäggi, 2007). This event was associated with more than 200 mm of rain within three days with corresponding return periods exceeding 100 years. As many mountain creek hazards have been mitigated by catchment basins, the sediment volumes could be determined.

A database was subsequently created with 33 debris flows and 39 fluvial sediment transport events, details of which are reported in Rickenmann and Koschni (2010). These authors used a variety of transport movement equations to compare modeled and predicted sediment transport volumes including those by Rickenmann (2001), Rickenmann and McArdell (2007), Hunziker and Jäggi (2002), Recking et al. (2008), and D'Agostino et al. (1996). Rickenmann and Koschni (2010) found reasonable agreements between modeled and measured sediment volumes for channels with less than 5% gradient using the Meyer-Peter and Müller equations. In contrast, for steeper channels, the observed sediment volumes transported by fluvial processes are over-predicted by bedload equations developed for steep channels.

Given the value of the Rickenmann and Koschni (2010) database, BGC analyzed the data further. First, BGC separated the debris-flow events from the mostly fluvial transport data. Watersheds with very large areas and correspondingly low gradients (< 1%) were also deleted from the dataset. These deletions provided a final dataset of 36 cases. Multivariate regression analysis

was then applied to the log-transformed dataset to determine sediment volumes based on catchment area, rainfall volume, runoff coefficient, surface runoff and channel gradient. This analysis yielded the two following formulae:

$$\log V_S = 0.753 \log V_R - 0.553, R^2 = 0.79 \quad [\text{Eq. 5-1}]$$

$$\log V_S = -1.55 + 0.877 \log V_R + 0.019S, R^2 = 0.81 \quad [\text{Eq. 5-2}]$$

where  $V_S$  is the total sediment volume displaced and  $V_R$  is the total rainfall. The difference between the two formulae is the inclusion of channel slope  $S$  in Equation 5-2. However, since the increase in variance is very small (2%), the effect of slope appears small. Neglecting slope would not be appropriate had the entire dataset been used as that also includes debris flows. Therefore, the formula presented above is only appropriate for debris floods with channel gradients from approximately 2 to 24%.

In addition to the Swiss dataset, BGC created a dataset with 14 creeks in the Bow Valley<sup>6</sup> that experienced debris floods during a June 2013 storm (i.e., BGC, October 31, 2014). Sediment volumes for these events were estimated by comparing 2008 or 2009 LiDAR to 2013 LiDAR (pre- and post-event LiDAR).

Both the Swiss and Bow Valley data were log transformed and a linear regression was applied to the combined data which resulted in Equation 5-3, which shows very little difference from the Swiss dataset regression. This combined regression was used in further analyses.

$$\log V_S = 0.740 \log V_R - 0.4624, R^2 = 0.78 \quad [\text{Eq. 5-3}]$$

where  $V_S$  is the total sediment volume displaced and  $V_R$  is the rainfall volume. The regression analysis of the combined data is shown in Figure 5-3 below. For the Bow Valley dataset a snowmelt contribution was added to the rainfall volume (i.e., rainfall + snowmelt = available water), as a shallow snowpack was present in mid to upper reaches of the watersheds.

As illustrated by Figure 5-3, the rainfall-sediment relation observed in the Bow Valley correlates well with the Swiss dataset. This observation suggests that a relationship between runoff and sediment mobilized is location independent (as long as a quasi-unlimited sediment supply is present), as similar results were seen in the Rocky Mountains as in the Alps. While this relation appears to be location independent, it has not been verified for temporal independence. It is still unknown as to whether this relation holds for different storms of different magnitudes for individual creeks.

### 5.2.5. Application to Cold Spring Creek

BGC estimated debris-flood volumes with the following workflow:

1. Using the nearest (Cranbrook Airport) Intensity-Duration-Frequency (IDF) curves, the 24-hour rainstorm volumes were extracted. A 24-hour storm was considered to be a reasonably proxy for a major storm. Extreme high intensity rainfall is likely to trigger a

---

<sup>6</sup> This analysis was restricted to the general vicinity of Canmore and Exshaw.

debris flow, while a longer duration moderate intensity storm is considered more likely to trigger a debris flood.

2. The 24-hour precipitation values were then multiplied with the watershed area of Cold Spring Creek (approx. 8 km<sup>2</sup>) to arrive at a total volume of rain falling onto the Cold Spring Creek watershed in a 24-hour period.
3. To allow for snowmelt contribution, BGC added 40% water equivalent over half of the watershed. This value can vary depending on the timing of a given storm (i.e., if there is still much snow left, at what elevation and at what water equivalent) and snow water equivalent (i.e., how wet the snow is at the time of the rainstorm). The 40% estimate is considered to be somewhat conservative, but appears warranted as for example, elevation-related increases in rainfall intensity due to the orographic effect (air masses being forced upwards) are not accounted for.
4. The final step was to use Equation 5-3 to estimate the debris flood sediment volumes for each return period class.

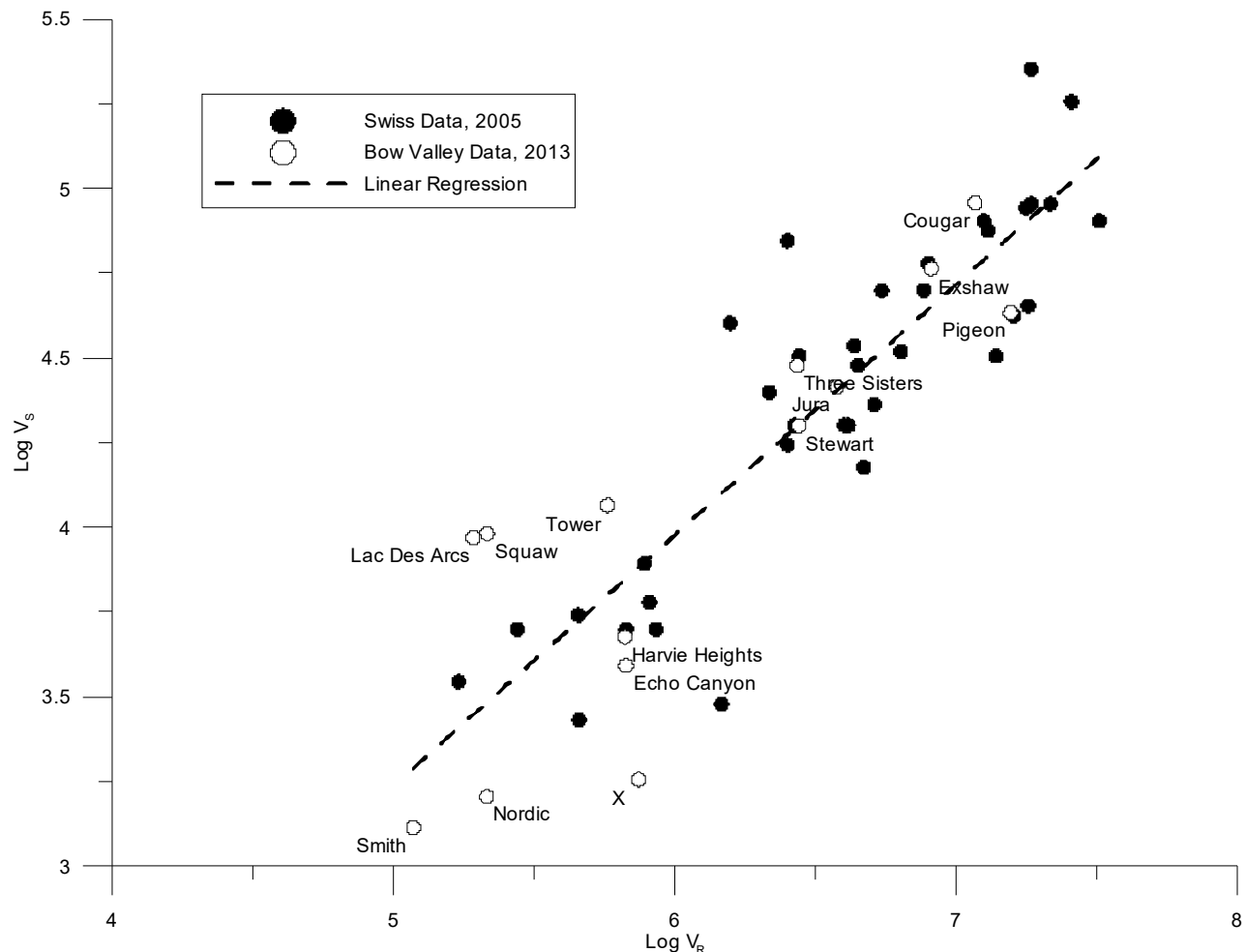


**Figure 5-3. Log transformed sediment (V<sub>S</sub>) and available water (V<sub>R</sub>) data from the Swiss and Bow Valley datasets compiled by Rickenmann and Koschni (2010) and BGC, respectively.**

### 5.3. Debris Flow Frequency Assessment

This section discusses the methods employed to estimate debris flow frequency.

#### 5.3.1. Air Photo Interpretation

Air photos dated between 1945 and 2017 were examined for evidence of past major transport events on Cold Spring Creek. Events were identified from the appearance of bright areas and disturbed vegetation relative to previous air photos that is indicative of debris-flow deposits. Smaller events that did not deposit sediment outside the channel or significantly change the course of the channel are not captured in this analysis. Similarly, events that occurred during large gaps between air photos or successive events that overlap may also not be identified by this approach. Air photo interpretation was supplemented by historical records of past events (Section 4).

#### 5.3.2. Post-Wildfire Debris-Flow Frequency

There have been no recorded wildfires in the Cold Spring Creek watershed since 1917 (FLNRORD, 2019a). This contrasts the estimated fire frequency of 35 to 100 years for the Cold Spring Creek watershed as reported by Blackwell, Grey and Compass (2003), (Figure 5-4). The discrepancy could be attributable to either wildfire suppression or an erroneous fire frequency as per Blackwell et al. (2003). Irrespective, the fact that there has not been a wildfire for at least 103 years implies significant fuel loading in the watershed.

Evidence of post-wildfire erosion and sediment transport was identified during BGC excavations on Cold Spring Creek fan, where BGC identified abundant charcoal interbedded in debris-flow units. Post-wildfire debris flows are a common occurrence in the dry areas of southern and south-western BC (Jordan and Covert, 2009; Jordan, 2013).

Post-wildfire debris-flow frequencies can be estimated by combining the probability of a wildfire occurring with that of a potential debris flow-triggering storm occurring in the critical post-wildfire period, which is about 2 years (Cannon & Gartner, 2005). For example, in a region with a 100-year fire frequency, the post-wildfire debris flow probability of a watershed impacted by a storm with a 10-year return period within the first two years after the fire would be 0.002 (which is equivalent to a 500-year return period). This means that, for example, if a 2-year return period wildfire of given extent and severity were to occur within 2 years of the fire, a comparatively small debris flow would result. However, if within the 2 years of a significant wildfire a 50-year return period storm were to affect the watershed, a very large debris flow could be expected to the high runoff volumes and intensities which can mobilized correspondingly higher sediment volumes.

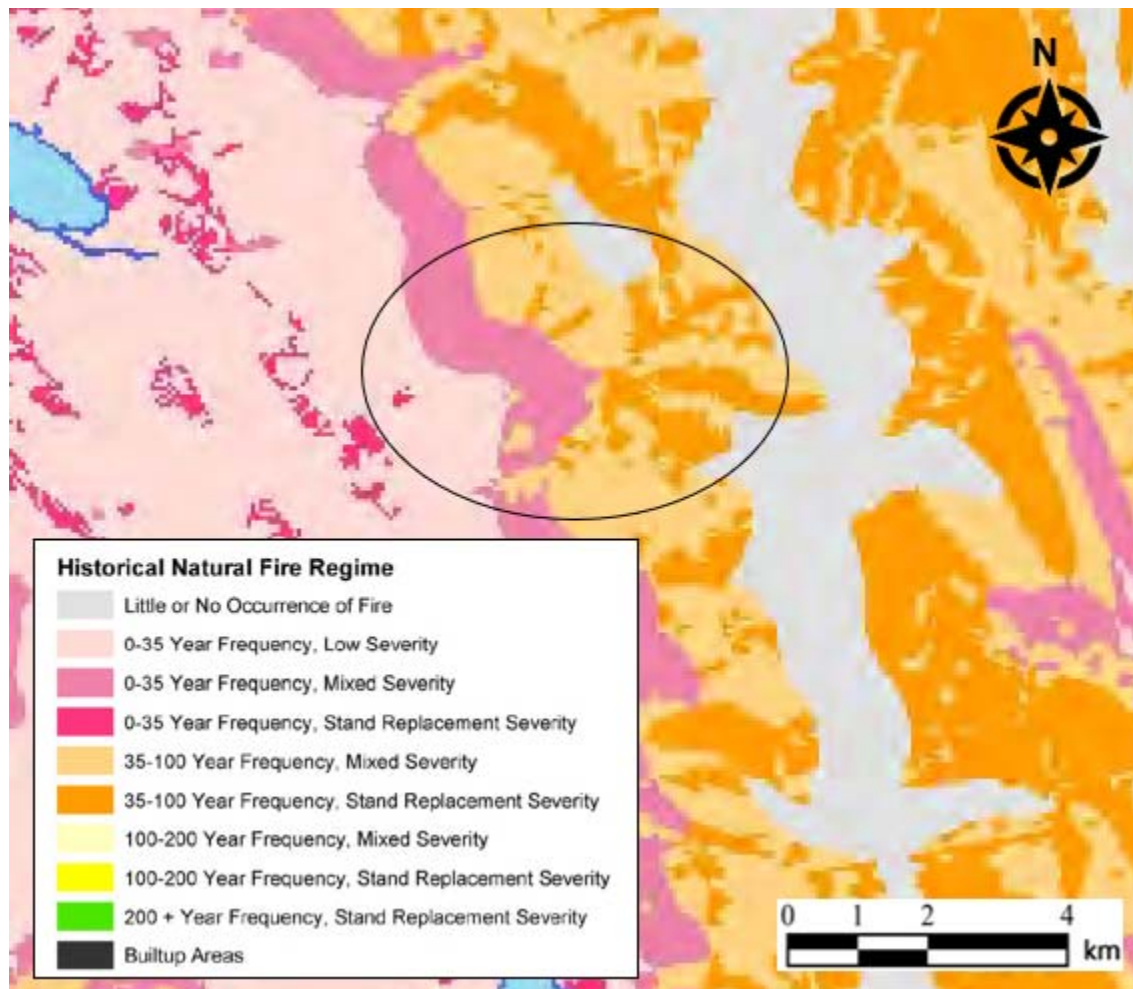


**Figure 5-4. Cut-out image of historic natural fire regime in the Cold Spring Creek watershed circled in black (Blackwell, Grey, & Compass, 2003).**

Previous research in California and Colorado has demonstrated that even a 2-year return period storm, which has a 50% chance of occurring in any given year, can trigger a debris flow (Cannon et al., 2008; Staley et al., 2020). It is not clear if this is the case in southeastern BC (Jordan, pers. comm. 2020) as there is a pronounced general decrease in rainfall intensity from California to BC for all rainfall durations. The 2-year return period, 15-minute rainfall from Cranbrook (a nearby ECCC station with rainfall intensity-duration-frequency data [IDF]) exceeds the rainfall thresholds for debris-flow initiation defined for Colorado and California within the first year after a fire (Cannon et al., 2008; Cannon et al., 2011). This suggests that even relatively frequent (2-year) storm events are likely to be of sufficient magnitude to trigger post-wildfire debris flows at Cold Spring Creek if all other factors (soil composition and fire alteration, burn severity, and geomorphology) were similar.

Using the combination of fire frequency and return period of potentially post-fire debris-flow triggering storms, BGC estimated the frequency of post-fire debris flows.

### 5.3.3. Test Trenching and Radiocarbon Dating

Excavator-assisted test trenching allows estimation of the thickness of past debris flows/debris floods, which are typically distinct from overlying and underlying deposits. It also permits for sampling of datable organic materials found in paleosols (old soil layers) and embedded within the debris flow deposits. An approximate age can then be assigned to the deposit.

Radiocarbon dating involves measuring the amount of the radio isotope  $^{14}\text{C}$  preserved in organic materials and using the rate of radioactive decay to calculate the age of a sample. This method requires the deposition and preservation of organic materials within the sedimentary stratigraphy of the fan. The age range of this method is from approximately 45,000 years to several decades. As such, the method is applicable to the time scale of post-glacial fan formation in western Canada.

Five test pits were excavated by backhoe on Cold Springs Creek fan on July 9 and 10, 2020. Test pit BGC-TP-01 filled with water to a depth of approximately 0.5 m. The other four test pits were dug typically to about 3 m deep, the pit walls were logged, and photos taken at each location. Test pit locations are on Drawing 01 and detailed test pit logs are in Appendix A.

Unit contacts and buried soils were examined for organic carbon for radiocarbon dating. Test pits and exposures were photographed. Radiocarbon samples were collected in plastic bags, air-dried, and then sent to Beta Analytic labs in Florida for age determination by Accelerator Mass Spectrometry (AMS). Ten samples were collected and submitted for radiocarbon dating. Detailed results of the radiocarbon dating are in Appendix B.

Results from the radiocarbon were reviewed to identify unique events and corroborate the frequency of events on Cold Spring Creek fan. An insufficient number of test pits were dug due to permissions by landowners and budget constraints to allow a more complete assessment of flows with similar ages. This could have allowed the reconstruction of events spatially as was done via dendrochronology on the fan.

### 5.4. Debris Flow Sediment Volume Estimates

Estimating debris-flow sediment volumes is key for two reasons: One is that it provides an important input to numerical modeling as larger debris flows will travel further, have thicker flow depth and are more destructive. The other is that any mitigation measures aiming to contain debris need to be based on estimates of debris volumes for different return periods so that such measures can be sized appropriately.

BGC employed a range of methods to decipher debris-flow volumes. These are:

- An empirical method relating fan area to debris-flow F-M.
- An empirical method relating precipitation in the aftermath of wildfires to debris-flows volumes.
- An analytical approach that uses debris-flow damaged trees and their distribution on the fan via thickness-area relationships to debris-flow volumes.

- An analytical approach that uses sedimentary stratigraphy in test trenches and the thickness of overlying units to test and verify the above methods, and to estimate the onset of the debris flood-debris flow transition.

#### 5.4.1. Regional Fan-Debris Flow Frequency-Magnitude Analysis

In areas where comprehensive studies on debris flow or debris flood frequencies and magnitude have been conducted, a normalization procedure based on fan area or fan volume can be applied to generate an approximate F-M at other sites without the need for in-depth field investigation.

This methodology was first applied by Jakob et al. (2016), who compiled nine detailed debris-flow hazard and risk assessments completed by BGC and Cordilleran Geoscience over a period of approximately 15 years in southwest BC and later updated with data from the Bow Valley near Canmore (Jakob et al., 2020) (Figure 5-5). For each of these projects, an F-M curve had been established using a variety of methods. Jakob et al. (2020) normalized the individual F-M curves by fan area and plotted them on the same graph. A best-fit line was plotted, and a predictive equation extracted.

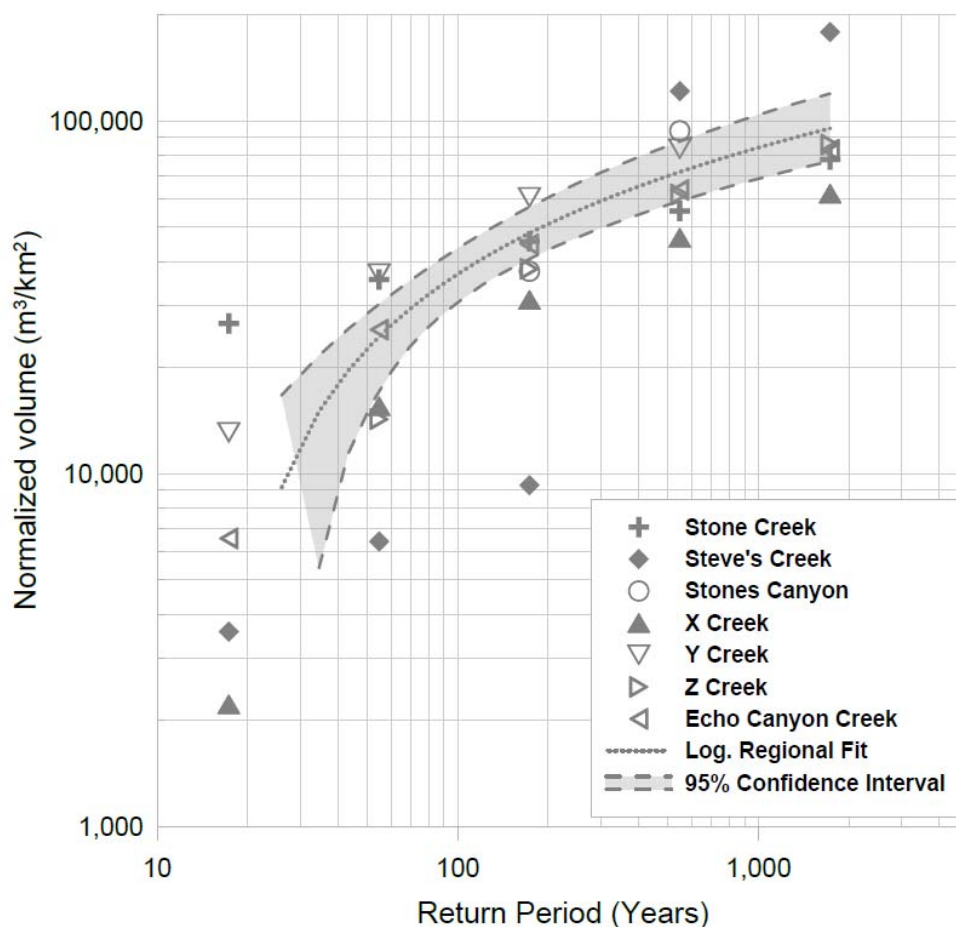


Figure 5-5. Regional debris flow frequency-magnitude data normalized by fan area for seven detailed studies in the Bow Valley, AB. From Jakob et al. (2020).

BGC used the F-M equation for the southwestern Albertan debris-flow creeks for application to Cold Spring Creek. Creek selection was based on:

- Similar geology and climate (The Bow Valley sites are only about 90 km east of Cold Spring Creek and local geology is dominated by sedimentary rocks in both regions. Mean annual precipitation at 2300 m elevation is approximately 1100 mm at Cold Spring Creek, while at similar elevation in the Bow Valley it is between 850 and 1000 mm).
- Similar process type (debris flow).
- Similar fan geomorphology (In both the Bow Valley and at Cold Spring Creek, the fans have incised through late Pleistocene sediments whose remnants are still visible. At both sites fans are also interfingering with floodplain deposits of the Bow River and Columbia River, respectively).

Equation 5-4 shows the resulting regional, fan-normalized F-M relationship.

$$V_{NAf} = 20,524 \ln(T) + 57,753 \quad [\text{Eq. 5-4}]$$

where  $V_{NAf}$  is the normalized sediment volumes associated with fan areas and watershed areas, respectively.  $T$  is the return period. The coefficient of determination ( $R^2$ ) is 0.67. A value of 1.0 implies a perfect model fit, while a value of 0 implies no predictive capability. The prediction is statistically significant.

Equation 5-4 allows the user to choose any return period ( $T$ ) and calculate the corresponding debris-flow volume. For example, for a return period of 100 years, the corresponding (rounded) debris-flow volume is 37,000 m<sup>3</sup> given a fan area of 1 km<sup>2</sup>.

In this study, the fan area used to develop the F-M relationship is the active fan area noted in Section 3.4 (1.024 km<sup>2</sup>) and excludes the paleosurfaces surrounding and within the fan.

#### 5.4.2. Empirical Estimates for Post-Wildfire Debris-Flow Volumes

Empirical models for predicting post-wildfire debris-flow volumes (e.g., Cannon et al., 2010; Gartner et al., 2014) can be used to assess hazards posed by debris flows following wildfires. These models predict volumes of material that may flow past a given point along a debris flow channel. The Gartner et al. (2014) model is currently used by the U.S. Geological Survey (USGS) for emergency assessments of post-wildfire debris-flow hazards (available online at [https://landslides.usgs.gov/hazards/postfire\\_debrisflow/](https://landslides.usgs.gov/hazards/postfire_debrisflow/)). The inputs for the model include the contributing watershed area burned at moderate and high severity<sup>7</sup>, the relief of the contributing watershed area, and the storm rainfall intensity measured over a 15-minute duration. The model is applicable for up to two years following the wildfire, after which plant re-growth and/or source area sediment depletion render it less reliable.

The Gartner et al. (2014) model was developed using data from southern California and had, to date, not been tested in southeastern BC. To affirm that the general methodology of the model is

<sup>7</sup> Burn severity describes the degree of vegetative loss in a burned area and is considered a proxy for the hydrologic changes to the soil due to the wildfire.

valid in southern BC, a comparative analysis was conducted by BGC in which the predicted and observed debris-flow volumes were compared. This comparative analysis involved the following steps:

1. A database on post-wildfire debris flows in southeastern BC compiled by Jordan (2015) was accessed and relevant data for estimating debris flow volumes using the Gartner et al. (2014) model were extracted.
2. The Jordan (2015) dataset did not contain reliable short-duration rainfall data from nearby rain gauges that are needed to implement the Gartner et al. (2014) model. Therefore, BGC used IDF data from the Cranbrook climate station to approximate the rainfall conditions. The rainfall data used included the 15-minute rainfall intensity for the 2-, 5-, 10- and 25-year return periods, with this range capturing the parameter uncertainty.
3. The observed debris-flow volumes reported in Jordan (2015) were compared to volumes predicted by the Gartner et al. (2014) model using watershed data from Jordan (2015) and rainfall IDF data from the Cranbrook climate station. The ratios between the observed and predicted volumes were also calculated.

The calculated ratios between the observed and predicted volumes that the Gartner et al. (2014) model overpredicts the available debris-flow dataset in southeastern BC by at least a factor of 2. This may be due to the fact that California has not been glaciated during the Quaternary period (the last 2.4 million years) and thus has deeper and more weathered soils. Those deposits may have less cohesion and be more prone to entrainment in subsequent rainstorms. Given the lack of glaciation history, the drainage density of California basins may also be higher, though this has not been verified through independent research. The above discussion and findings imply that the debris-flow volumes obtained from the Gartner et al. (2014) model need to be at least halved to be applicable to the setting in southeastern B.C.

For this assessment, the “emergency assessment model” in Gartner et al. (2014) was used to estimate post-wildfire debris flow volumes at the fan apex of Cold Spring Creek. BGC estimated the debris-flow volume for Cold Spring Creek assuming that a wildfire affects a range of the watershed proportions affected by moderate to high burn severity. Error bars were plotted around the assumption of one half of the treed watershed burning for the assumption of one third to 90% of the forested watershed burning to understand the variability inherent in the estimates.

The “emergency assessment model” from Gartner et al. (2014) is applicable for two years after a wildfire, after which time vegetation regeneration leads to progressive recovery from the effects of wildfire. Consequently, debris flows become quickly less likely. In that two-year period, BGC investigated what debris-flow volumes would be generated from rainfall events with intensities corresponding to 2-year to 100-year return periods (annual probabilities ranging from 0.5 to 0.01). Rainfall intensities were obtained from the IDF curves for Cranbrook, located approximately 90 km south of Cold Spring Creek.

In addition, BGC estimated the effects of climate change on the post-wildfire debris flow frequency-magnitude analysis. Two variables that factor into the Gartner et al. (2014) equation will likely change substantially with climate change: First, the frequency of wildfires will change and secondly, the rainfall intensity will change. Changes in wildfire frequency are an

under-researched subject in BC. Bruce Blackwell of BA Blackwell & Associates (pers. comm, July 2020) estimates that fire frequencies could increase by as much as 30 to 50% by late century in the BC southern interior accompanied by substantial increases in fire severity. Therefore, BGC increased the fire frequency estimates for the Gartner et al. (2014) model by 50%. Fire severity was not changed as it was already assumed that the burn will result in moderate to high burn severity.

Changes in rainfall intensities were estimated based on work by Prein et al. (2017) whose research group used advanced modeling techniques to quantify changes in extreme (defined as the 99.95<sup>th</sup> exceedance probability) hourly rainfall in terms of frequency (Figure 5-6) and magnitude (Figure 5-7).

The following steps led to the estimate of a post-fire debris flow volumes and peak discharges and, in combination with the frequency analysis produce an F-M relationship:

1. Use the 15-minute peak rainfall intensity and adjust it by the expected increase for the end of the century (25% increase as per Prein et al., 2017). Adjust this value to account for the orographic effect (20%).
2. Use a range of total treed watershed area (one third, one half, two thirds and 90%).
3. Use the Gartner et al. (2014) model to estimate climate change and elevation-adjusted debris flow volumes.
4. Use an empirical relationship between volume and peak discharge to estimate debris flow peak discharge which is described in Section 5.6.2.

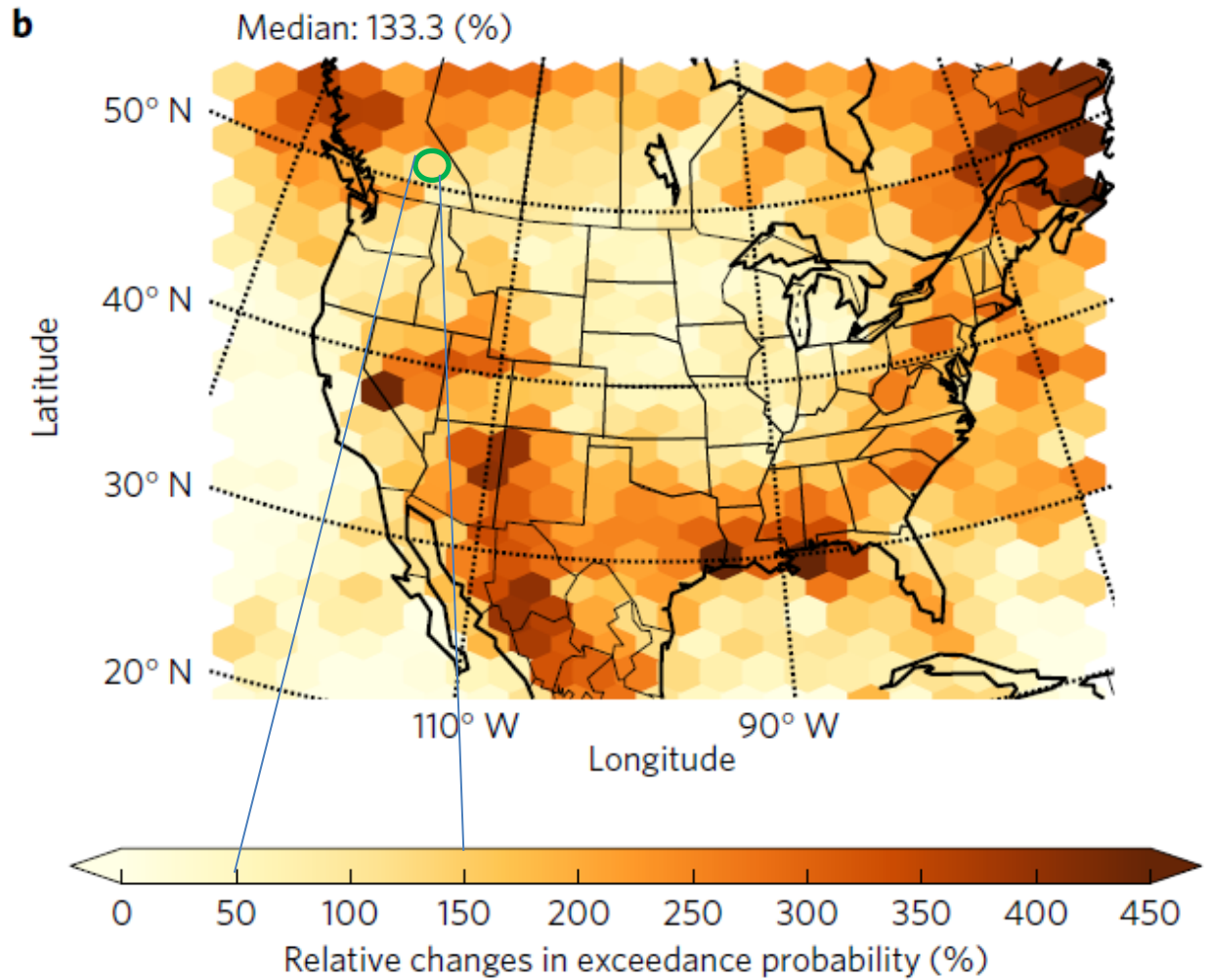


**Figure 5-6.** Relative changes in the exceedance probability of the 99.95th percentile of hourly precipitation intensities for June, July and August in large portions of North America (Prein et al., 2017). The rainfall intensity changes are estimated between 100 to 150%. A 100% increase implies a halving of the rainfall intensity return period. The approximate study site is circled in green.

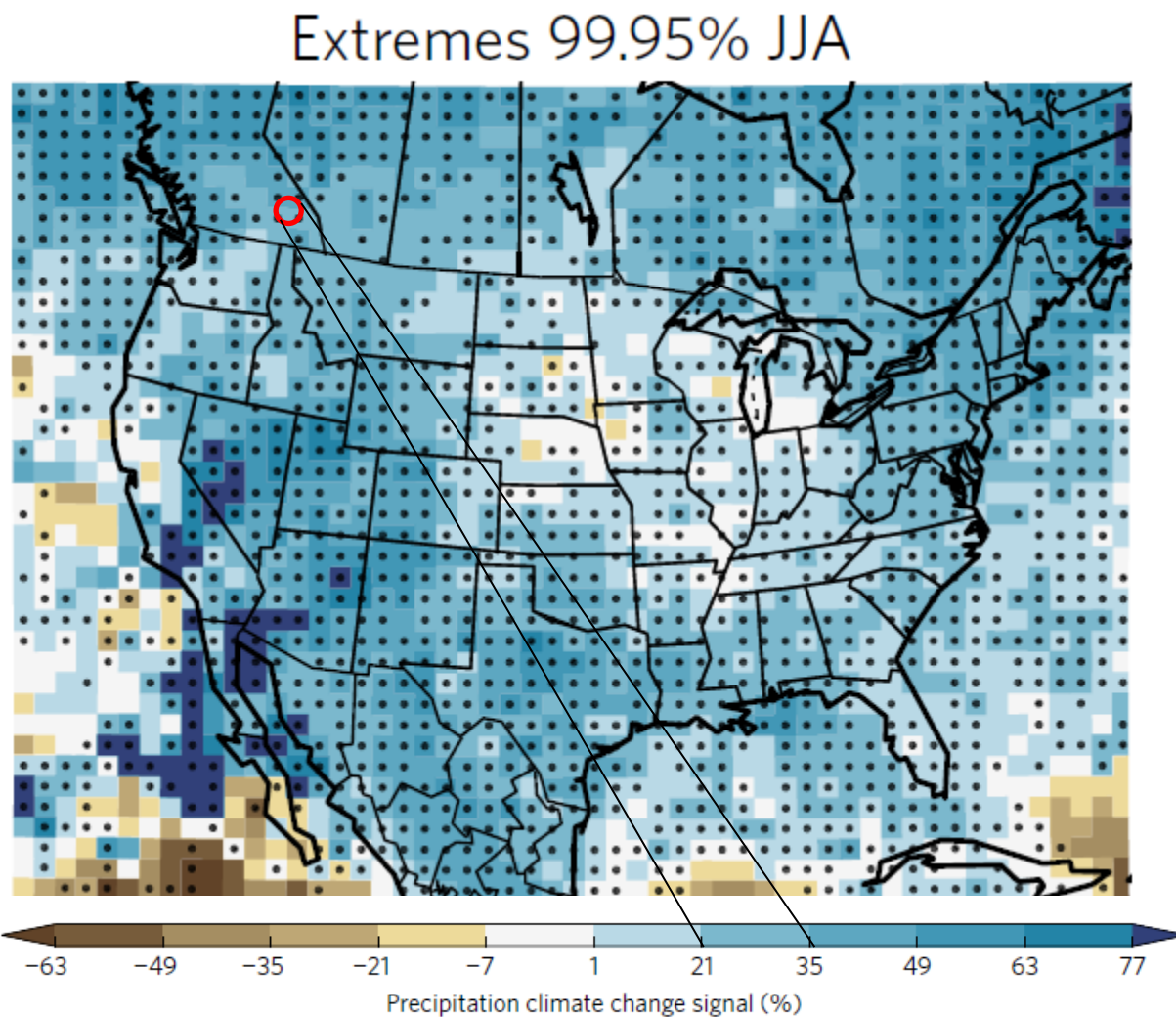


**Figure 5-7.** Hourly extreme precipitation for June, July and August expressed as relative changes for 100 x 100 km grid boxes. Dots indicate statistically significant changes. The approximate changes for the area of interest is between 21 and 35% (Prein et al., 2017).

#### 5.4.3. Debris-flow Volume Estimates from Dendrochronological Analysis

Dendrogeomorphology is a subdiscipline of dendrochronology, in which tree rings and tree growth are used to analyze historic landslide activity. Thirty-six conifers were sampled as part of the field program. The locations of the samples are shown on Drawing 01.

Dendrogeomorphology analysis is based on two main characteristics of tree ring samples:

1. Tree age: the age of the tree determines the “minimum establishment date”: in other words, the approximate time when the tree started growing.
  - If several trees in one area all started growing around the same time, that may indicate that a stand-destroying event occurred recently, which cleared the original trees and left space for new trees to establish.
  - The date is a minimum, because tree rings indicate the minimum age of the tree at the height where the coring was collected. Cores are usually collected at about

chest height (1.2 m), so it may have taken the tree a few years to grow 1.2 m. In addition, several years may pass for a tree seed to establish on a freshly disturbed surface.

2. **Special features (in conifers only):** Features in the wood that may suggest landslide activity include scars, traumatic resin ducts, reaction wood and growth disturbances.
  - Scars occur when a landslide or avalanche damages the bark or wood of a tree, but don't kill the tree. Figure 5-8 shows an example of a debris-flow scarred tree.
  - Traumatic resin ducts (TRDs) are small circles that appear within the wood, which indicate that the tree sustained damage during that year (similar to scar tissue).
  - Reaction wood appears when a tree has been knocked or tipped over by a landslide. Denser wood grows on the downslope side, to correct the growth of the tree and ensure that it continues to grow vertically.
  - Growth disturbances occur when a landslide changes the conditions around the tree, such as the availability of light, water or nutrients. These changes may cause the tree to grow noticeably faster or slower.

Tree cores were extracted from living trees using a 5 mm increment borer. In the office, the samples were glued onto wooden mounting boards and sanded to facilitate ring and feature identification. Analysis was completed using a specialized scanner and WinDENDRO software (Regent Instruments Inc., 2012). WinDENDRO is a semi-automatic image analysis program, which identifies tree rings and measures the width of the yearly growth. Once the tree ages were confirmed, the growth rings were analyzed to identify anomalies that may be associated with debris-flood, debris-flow or avalanche events. It can be difficult to differentiate between steep creek and avalanche processes, although sometimes, the location of the TRDs within the ring can indicate whether the damage occurred in the dormant period (winter) or the growing season (spring and summer).

The results of the tree ring analysis are presented in Section 6.2.2.

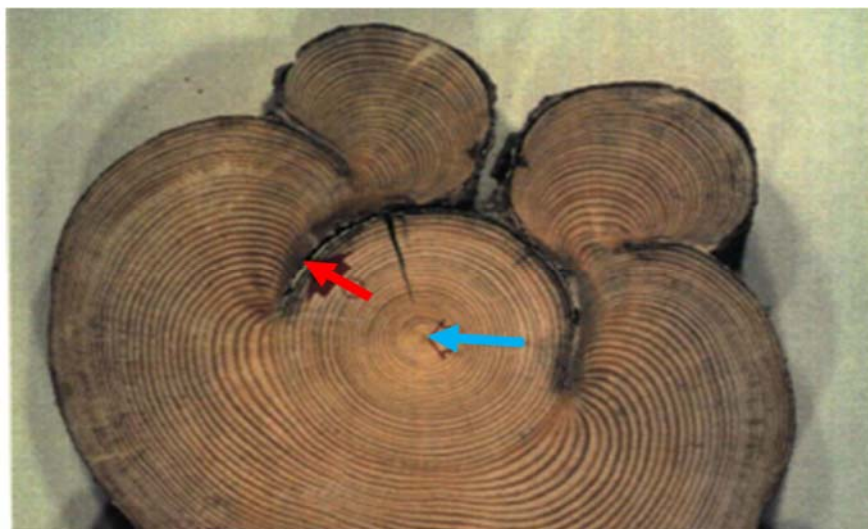


**Figure 5-8. Impact scars on a spruce tree near Fergusson Creek in southwest BC showing an example of scars that can be dated precisely. The red arrow points at a scar, and the blue arrow points at the center of the tree (from Jakob, 1996).**

Results of the dendrogeomorphologic analysis can be used to estimate both the frequency and inundation area of past hydrogeomorphic events, and in some cases establish a high-water cross-section.

#### 5.4.4. Area-Volume Relationships

Several of the hazard assessment methods described can be used to estimate the inundation area of debris flows or debris floods, but hazard analysis depends on knowing the event volume, not just the event area. Two methods that can be used to estimate debris-flow volumes given the deposit area via area-volume relationships.

The first method uses dendrochronological data to estimate the extent of past debris flows. This is a very generalized method as deposit depths can vary from process to process and from sector to sector on the fan. Hence, two different methods are compared to come up with a volume range.

The second method involves using empirical area-volume formulae, which relate the area of a debris-flow or debris-flood deposit with its estimated volume. The debris-flow formula in Equation 5-5 was developed from a global dataset collected by Iverson et al. (1998), while the debris-flood relationship in Equation 5-6 was developed by BGC using known event volumes (from detailed LiDAR change detection) and areas in the Bow Valley near Canmore, Alberta.

$$V = \frac{1}{200} A^{1.5} \quad [\text{Eq. 5-5}]$$

$$V = \frac{1}{95} A^{1.5} \quad [\text{Eq. 5-6}]$$

where V is sediment volume (m<sup>3</sup>) and A is deposit area (m<sup>2</sup>).

For Cold Spring Creek, the “muddy”, Iverson et al. (1998) debris-flow area-volume relationship provided the most realistic results and was applied to estimate the total event volume. The area-volume formulae were also used to estimate the volume of five historical events, which were identified through dendrogeomorphological analysis. The use of the “muddy” equation is also consistent with the use of the “muddy” debris-flow volume-peak discharge relationship discussed in Section 5.4.

#### 5.5. Magnitude Cumulative Frequency (MCF) Analysis

Once data pairs of the frequency and magnitude have been established, they need to be processed in a way that allows the construction of an F-M curve. Standard hydrological methods do not apply as they require at least annual peak observations.

Seismology has been the precursor to the use of regional magnitude-cumulative frequency curves (MCF) (Gutenberg and Richter, 1954). An inventory of sediment volumes of known dates in a given time interval T<sub>i</sub> is ranked from largest to smallest. The incremental debris-flood frequency of rank i is determined as 1/T<sub>i</sub> and the MCF then states the cumulative incremental frequencies as:

$$F_i = \sum_{i=1}^n f_i \quad [\text{Eq. 5-7}]$$

where  $f_i$  is the incremental frequency of an event of rank  $i$  and  $F_i$  is the annual debris-flood frequency of an event of greater than volume  $V_i$ . The MCF curve is then produced by plotting  $F_i$  against  $V_i$ .

The use of MCF assumes that all events are known, and volumes can be combined in reasonable volume classes, or that the dataset is stratified into classes where confidence exists that all such events have been included. The latter is believed to be the case at Cold Spring Creek, where return period classes are believed to span ranges of respective volumes. Furthermore, the selection of different plotting methods (cumulative vs. non-cumulative, linear and logarithmic binning, different bin sizes and choice of trend lines for extrapolations) can bias the results (Brardinoni and Church, 2004). The MCF technique is very sensitive to the number of events, as adding events will invariably decrease the individual return periods for events smaller than those newly added.

On Cold Spring Creek, MCF analysis was used to estimate event frequency for the identified radiocarbon events. MCF analysis was applied to dendrogeomorphology techniques; however, not to the air photo record because insufficient magnitude information could be gleaned from the air photographs.

## 5.6. Peak Discharge Estimates

### 5.6.1. Debris-Flood Peak Discharge Estimates for the May 31, 2020 Debris Flood

The rainfall frequency analysis described in the previous section is the primary input for estimating peak discharges based on rainfall-runoff modeling. Calibration for such modeling can be provided by highwater marks in the channel. During the channel hike of Cold Spring Creek on June 23 and 24, BGC observed six cross-sections with high water marks that are associated with the May 31, 2020 debris flood. In addition, higher (larger) cross-sections from previous debris flows were extracted from LiDAR imagery and confirmed in the field. Cross-section locations are shown on Drawing 01. Bedrock-controlled cross-sections would have been desirable as they provide more reliable discharge estimates but none were encountered in the channel reaches (approximately 2.5 km) that were hiked by BGC.

Channel depth, width, and gradient were measured at each of the high-water marks. Discharge calculations also depend on the Manning's  $n$  value, which is a measure of stream bed roughness. Manning's  $n$  value was calculated using the formula from Jarrett (1985). Jarrett investigated roughness coefficients for steep cobble-boulder streams in Colorado with channel gradients up to 5%. Jarrett's formula is a function of channel slope and hydraulic radius:

$$n = 0.39s^{0.38}R^{-0.16} \quad \text{[Eq. 5-8]}$$

where  $s$  is channel gradient (ft/ft) and  $R$  is the hydraulic radius<sup>8</sup> (ft).

Jarrett's research focused on streams with channel gradients of less than 5%, while channel gradients at the measured cross-sections ranged from 18% to 45% and may thus not be readily applicable. Therefore, BGC also applied an additional discharge calculation method, Prochaska,

<sup>8</sup> The ratio of the cross-sectional area of the channel to the wetted perimeter

Santi, Higgins & Cannon (2008). Estimates from both methods are reported in the results sections.

### 5.6.2. Debris-Flow Peak Discharge

Debris-flow peak discharge was reconstituted in two ways: One was direct cross-section measurements during the field traverse of coarse boulder levees (i.e., levees that can be identified on at least one side of the channel). This was followed by back-calculating the flow velocity using empirical relationships introduced in the previous section. The other method was to use the estimated debris-flow volumes and then use an empirical method to back-calculate debris-flow peak discharge as explained below.

Given that much of the lower channel is flanked by landslides, many old levees have been eroded, though BGC found some evidence of older debris flow levees. A key cross-section was encountered in the eroded toe of the Cold Spring Landslide. Here, a series of levees allowed estimation of cross-sections of debris flows with unknown ages (Figure 5-9). Importantly, these levees demonstrate that major debris flows occur on Cold Spring Creek.

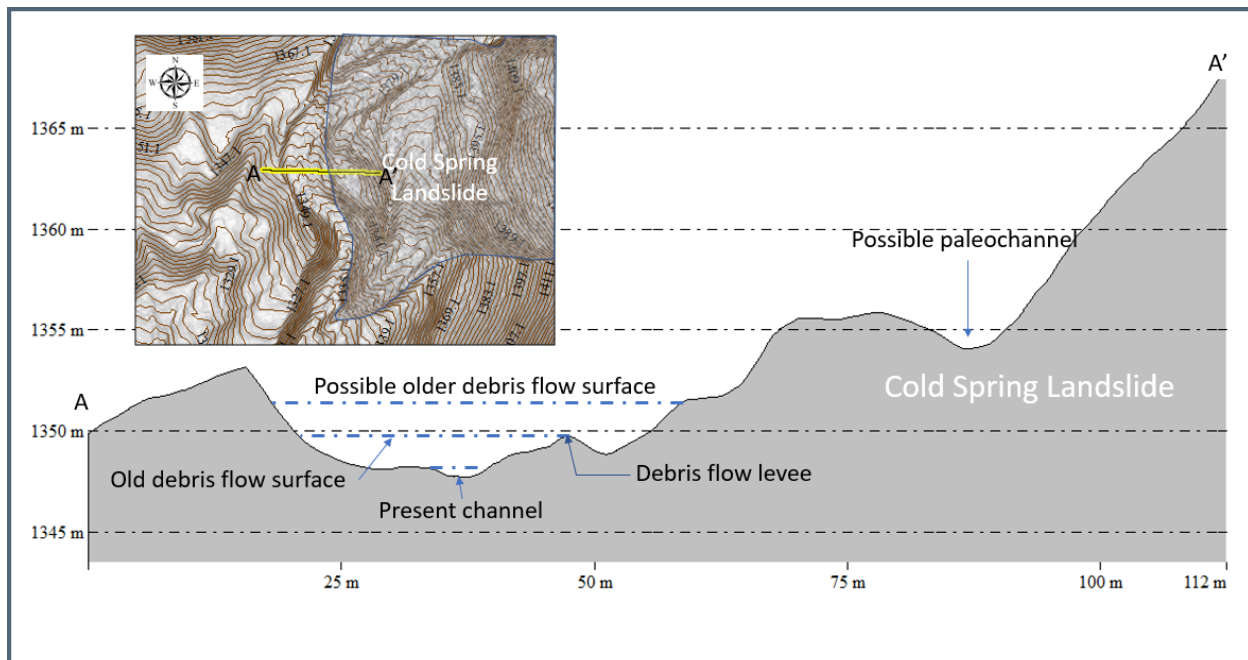


**Figure 5-9. Cross-section at approximately 1350 m across the Coldspring Creek channel looking upstream.**

The second method used by BGC to estimate debris flow peak discharge was developed by Bovis and Jakob (1999), who provide empirical correlations between peak discharge and debris-flow volume based on observations of 33 debris flow basins in southwestern British Columbia (Figure 5-10). This relationship was constructed for “muddy” debris flows and “granular” debris flows. Muddy debris flows are those with a relatively fine-grained matrix as found from volcanic source areas or fine-grained sedimentary rocks, while granular debris flows are those typical for granitic source areas with large clasts embedded in the flow which slow the flow through friction thus creating large surge fronts. For many (not all) post-wildfire debris flows, the initiation occurs

via progressive bulking of flows (Cannon and Gartner (2005) quote some 75% bulked by runoff-dominated erosion). This occurs via rilling and gullying in recently burned terrain and sometimes hydrophobic (water repellent) soils have developed preventing infiltration. The peak discharge of debris flows initiated by runoff-dominated erosion contrasts debris flows initiated by infiltration-triggered landslide mobilization. The latter results in comparatively higher peak flows.

Solving the muddy and granular equations in Figure 5-10 for Q, one obtains:

$$Q_{muddy} = (0.003 \cdot V)^{1.01} \quad [\text{Eq. 5-9}]$$

$$Q_{granular} = (0.04 \cdot V)^{0.9} \quad [\text{Eq. 5-10}]$$

As noted previously, Cold Spring Creek is a hybrid creek with debris floods and debris flows occurring at different return periods and debris flows in the upper watershed evolving into debris floods at lower elevation. Given that debris flows can and have diluted to debris floods, using Equation 5-10 would yield overly conservative results. This was independently checked with the 2012 debris flow on Fairmont Creek. This event had an estimated volume of 65,000 m<sup>3</sup> and an estimated peak discharge of 165 m<sup>3</sup>/s. Using Equation 5-9, the peak discharge (best estimate) is 206 m<sup>3</sup>/s, using Equation 5-10 it is approximately 1180 m<sup>3</sup>/s. Therefore, Equation 5-9 appears to be yield more realistic results.

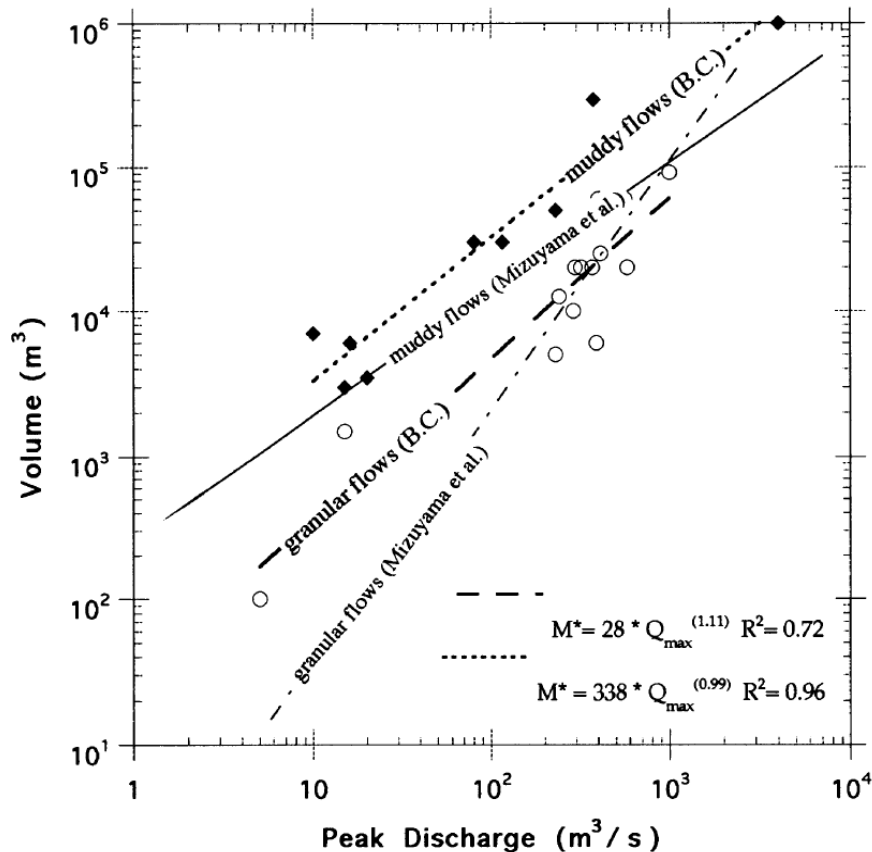


Figure 5-10. Bovis and Jakob (1999) relationship between peak discharge and volume for British Columbia, with comparison regressions computed by Mizuyama et al. (1992).

Using debris-flow volumes from the F-M curve (Section 5.4.2), the expected peak discharge is then calculated using Equation 5-9. Peak discharge and total debris flow volume is then input to the numerical model together with rheological parameters which is explained in the following section.

## 5.7. Numerical Debris Flood and Debris Flow Modelling

Hydrodynamic modeling was completed using FLO-2D Version 19.07.21, a two-dimensional, volume conservation hydrodynamic model. It is a Federal Emergency Management Agency (FEMA) approved model which lends additional legitimacy of the model. Comparisons between FLO-2D and other debris flow models (i.e., RAMMS or DAN 3D), have shown that it yields reasonable results once calibrated with known events (Cesca and D'Agostino, 2008; Moase, Strouth, & Mitchell, 2018).

In FLO-2D, flow progression is controlled by topography and flow resistance. The governing equations include the continuity equation and the two-dimensional equation of motion (dynamic wave momentum equation). The 2D representation of the motion equation is defined using a finite difference grid system and is solved by computing average flow velocity across a grid element boundary one direction at a time with eight potential flow directions. Pressure, friction, convective, and local accelerations components in the momentum equation are retained.

### 5.7.1. Basic Setup and Input Parameters

Models were run on a grid generated from a DEM constructed from the LiDAR-generated topography that was flown in 2018. An elevation is averaged for each cell from the DEM. BGC chose a cell size of 2 m to balance computational effort with necessary detail to capture topographic detail.

Appropriate boundaries and boundary conditions were selected to best show how the flows would interact with the topography and development. Individual buildings were not included, instead the model domain was designed to cover the main development on the fan. The model domain was set to include all the fan to allow for avulsions. Initial Manning's  $n$  values were input for all cells as FLO-2D overrides the specified Manning's  $n$  input value as required by the limiting Froude constraint (FLO-2D Software Inc., 2017). For all creeks a limiting Froude number of 1.0 for debris flood and 1.1 for debris flows was specified, as supercritical flow is rare for fan reaches with moderate gradients, especially for lower return period flows (Grant, 1997). A Manning's  $n$  value of 0.05 was chosen for the fan as the majority of the fan area is developed.

Infiltration parameters were not used in the analysis, as there was no known event to calibrate with and it is not possible to predict the antecedent moisture levels during an event. However, a significant portion of the Cold Spring Creek fan is sealed, either by homes or roads which precludes infiltration. Any road drainages are likely to become clogged during a debris flow.

In FLO-2D, inflow is defined using hydrographs, which can be assigned to grid cells at the fan apex. The peak discharge of the hydrograph is changed between model scenarios to model different event peak discharges; the volumes modeled are compared to the F-M relationship. Debris flood and debris flow hydrographs use a constant hydrograph shape that is varied by length

(i.e., time) to achieve the volumes specified from the F-M relationship. In general, debris flood hydrographs are on the order of 24 hours long due to low peak discharges, whereas debris flow hydrographs are very short (<10 minutes).

Cold Spring Creek debris floods were modeled for the 3 to 10-year, 10 to 30-year, and 30 to 100-year return period classes and debris flows were modeled for the 100 to 300-year, 300 to 1000-year, and 1000 to 3000-year return period classes.

### 5.7.2. Sediment Model Setup and Calibration

For debris-flow models, the “mud flow module” of FLO-2D is employed to represent the high sediment concentration of the flow. A constant sediment concentration of 50% was used for all debris flow scenarios. Debris-flow modeling also requires the definition of rheological parameters, which inform the flow behaviour of the water and debris slurry. In FLO-2D, the main rheological parameters are viscosity and yield stress. These parameters can be modified during model calibration in order to achieve the best possible match with the behaviour of known events. Neither variable is directly measured from observed events.

The 2012 event on Fairmont Creek was used for calibration. BGC used the event delineations and field observations from Clarke Geoscience Ltd. and Golder Associates (January 11, 2013) to calibrate the model. The rheology was estimated iteratively until the modeled debris-flow extent was similar to the observed runout and deposit depths as mapped in the field on Fairmont Creek. The resulting rheological parameters are presented in Table 5-1.

**Table 5-1. Rheological parameters for FLO-2D modeling.**

Viscosity Coefficient	Viscosity Exponent	Yield Stress Coefficient	Yield Stress Exponent
0.0075	14.39	2.6	17.48

These parameters are identical to those used by Dai et al. (1980).

### 5.8. Hazard Mapping

BGC prepared hazard maps based on the results from the numerical debris-flood and debris-flow modeling. Bank erosion on the fan was not considered for two reasons: First, banks are less susceptible to erosion during unconfined flow over the fan in case of avulsions. Second, the banks in the basin are armoured and will be protected by erosion once the basin fills and creates a depositional slope.

BGC prepared two types of steep creek hazard maps for Cold Spring Creek: debris flood and debris-flow model result maps and a composite hazard rating map. The model result maps support emergency planning and risk analyses, and the composite hazard rating map supports communication and policy implementation, as described further below.

### 5.8.1. Debris Flood and Debris Flow Model Result Maps

Model result maps display the hazard intensity (expressed as impact force) and extent of inundated areas from numerical modeling.

FLO-2D model outputs include grid cells showing the velocity, depth, and extent of debris-flood and debris-flow inundation. These variables describe the intensity of an event. Hazard quantification combines the intensity of potential events and their respective frequency. Sites with a low probability of being impacted and low intensities (for example, slow flowing ankle-deep muddy water) need to be differentiated from sites that are impacted frequently and at high intensities (such as water and rocks flowing at running speed). For the latter, the resulting geohazard risk is substantially higher and development must be more restrictive than the former.

### 5.8.2. Composite Hazard Rating Map

BGC prepared a “composite” hazard rating map that displays all modeled scenarios together on a single map. The composite hazard rating map is intended for hazard communication and decision making, where different zones on the map may be subject to specific land use prescriptions, covenants, bylaws or other limiting clauses for both existing and proposed development.

Given their application in policy, the composite map provided with this assessment is subject to further review and discussion with RDEK. Even where the underlying hazard scenarios do not change, cartographic choices (i.e., map colours and categories) can influence interpretation of the maps. BGC anticipates that discussions about hazard map application in policy will extend beyond final report delivery, and that these discussions may lead to further modifications of the composite hazard rating maps.

The composite hazard rating map is based on an impact force frequency (*IFF*) geohazard mapping procedure that consists of two principal components: the intensity expressed by an impact force and the frequency of the respective events. The underlying equation is:

$$IFF = v^2 \times \rho_f \times d_f \times P(H) \quad [\text{Eq. 5-11}]$$

where *v* is flow velocity (m/s), *d<sub>f</sub>* is the fluid’s flow depth (m), *ρ<sub>f</sub>* is the fluid density (kg/m<sup>3</sup>) to obtain a unit of force per metre flow width for the three left terms in Equation 5-11 and *P(H)* is the annual probability of the geohazard. The unit of *IFF* is then Newton or kilo Newton per metre per year (kN/m per yr).

Equation 5-11 can be translated into a matrix in which the impact force (*IF*) is on one axis and the return period (annual probability or *P(H)*) on the other. The matrix is then colour-coded to indicate the total hazard from yellow (low hazard) to dark red (extreme hazard) (Figure 5-11).

Return Period Range (years)	Geohazard Intensity				
	Very Low	Low	Moderate	High	Very High
1-3					
10-30					
30-100					
100-300					
300 - 1000					
1000 - 3000					

Figure 5-11. Simplified geohazard impact intensity frequency matrix.

The advantage of this mapping type is that a single map immediately codifies which areas are exposed to what hazard. Given that impact force is a surrogate for the destructiveness of a geohazard, *IFF* maps are relative proxies for risk assuming elements at risk are present in the specific hazard zones and the loss(es) associated with an event scale with impact force. For clarity, the values do not represent an absolute level of risk, which also depends on their vulnerability and their being present in the hazard area at the time of impact.

Interpreted hazard maps showing *IFF* values were developed for each return period class at all locations within the study area. For the individual hazard scenario maps that are added to the Cambio web application, the raw (no interpretation nor zone homogenization) impact force modeling results are presented. For the composite hazard rating map, the different intensities were interpreted by BGC to homogenize zones into easily identifiable polygons that are likely to fall into the range of intensity bins reported above. In some cases, individual properties may have been artificially raised and are thus less prone to debris flow impact. Such properties would need to be identified at a site-specific level of detail, for example, if the owner wishes to subdivide or renovate and ask for an exemption to existing bylaws.

## 6. RESULTS

### 6.1. Hydrogeomorphic Process Characterization

Figure 3-13 indicates that Cold Spring Creek is prone to debris flows and debris floods. This result is consistent with the following evidence:

- The creek produced debris floods in July 2012, June 2013, and May 2020.
- The average channel gradient above the fan apex is greater than 35% (Table 3-1), which allows sustained debris flow transport.
- The average fan gradient of 9% is typical of creeks prone to debris flows (Drawing 02).
- Test pits in various locations around the fan show sediments typical for debris flows (i.e., matrix supported, poorly sorted angular clasts).
- Boulders identified throughout the fan surface suggest debris flow transport as debris floods with lower sediment concentration and flow depths are likely insufficient to transport such boulders.
- Ample sediment supply from talus slopes and landslides in the entire watershed of Cold Spring Creek.

Together, this evidence indicates that Cold Spring Creek is subject to channel supply-unlimited debris flows for return periods greater than 100 years and debris floods at lower return periods. Different debris-flow triggering mechanisms are conceivable. Given the paucity of previous debris flows observed on air photos or historic accounts, rainstorm or rain-on-snow-triggered debris flows in absence of wildfires likely need to exceed a 100-year return period to initiate a debris flow. Second, post-wildfire debris flows would occur, likely with a combined probability of 1:100, a value that may change in the future due to increases in wildfire frequency and the frequency and severity of short-duration rainfall.

### 6.2. Frequency Assessment

#### 6.2.1. Air Photo Interpretation

Debris-flood and debris-flow frequency was assessed using historic air photos and historical accounts. BGC reviewed air photos from 1949 to 2000. Table 6-1 summarizes the observations that were made of the air photo record. Figure 6-1 shows air photos with significant development between them. BGC was not able to interpret deposition areas or characteristics of other hydrogeomorphic events in the air photo record. This observation may be attributable to: potential events may have been of relatively small magnitude with limited evidence of bank erosion, avulsion, or sediment deposition; the timing of the events relative to the next available air photo such that the evidence is no longer visible; or vegetation and residential development cover the affected areas.

**Table 6-1. Summary of observed changes in the air photo record (1949-2000).**

<b>Air Photo Year</b>	<b>Observations</b>
1949	Fan crossed by roads, similar to current day Hot Springs Road and lower Wills Road alignment. Few other small roads across the fan.
1960	Fairmont Resort Road built since last air photo (across Cold Spring Creek fan to Fairmont Creek).
1964	Highway 93/95 built since last air photo, beginning construction of Mountainside Golf Course.
1967	No significant changes since last air photo.
1975	Fairmont Hot Springs Resort Ski Area developed and start of residential development on fan since last air photo. Some businesses built up along highway. Road built up to dam and reservoir area.
1981	Continued residential development on fan.
1988	Start of construction of Riverside Golf Course, continued residential development on fan.
1995	Continued residential development, more businesses built along highway.
2000	Continued residential development, more businesses built along highway.

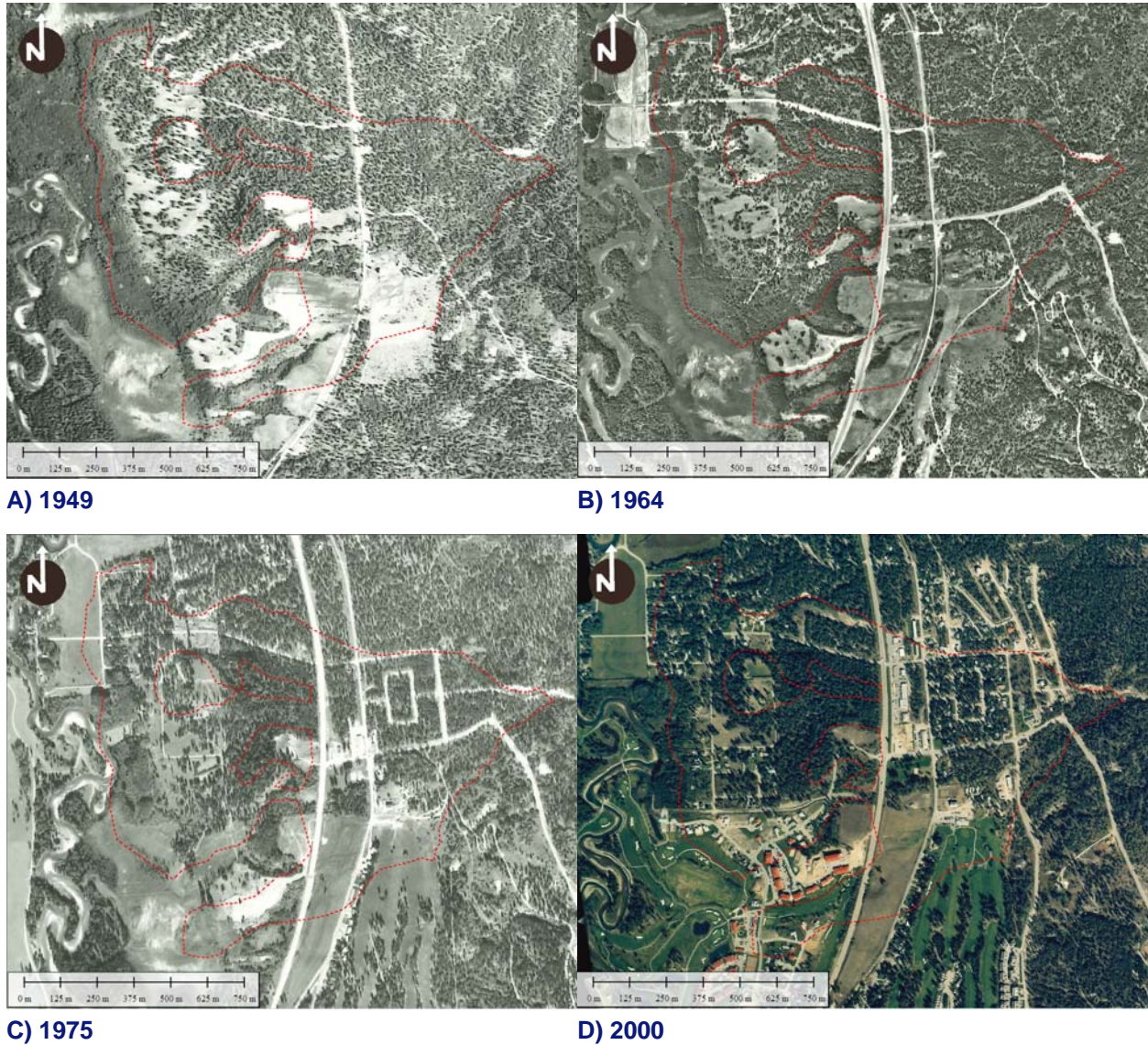


**Figure 6-1. Air photos of Cold Spring Creek fan from A) 1949, B) 1964, C) 1975, and D) 2000 showing development on the fan. Air photos have been manually georeferenced by BGC.**

### 6.2.2. Dendrogeomorphic Interpretation

A summary of the dendrogeomorphic analysis per sample is provided in Appendix C. Table 6-2 summarizes events interpreted from the features identified in the samples.

**Table 6-2. Summary of Cold Spring Creek events interpreted from dendrogeomorphic samples.**

Date	Confidence	Evidence
1770's	Moderate	6 establishment dates from 1768-1778, all samples hit near the pith, not core rot or scar
Late 1810's	Moderate	Scar and TRDs in 3 trees on fan
Early 1840's	Low	Scar, TRDs and growth reductions in 4 trees in watershed and on fan
Early 1870's	Low	Scar, TRDs and growth changes in 4 trees within 4 years, located in watershed and on fan
Late 1880's	Moderate	Scar, TRDs and growth changes in 7 trees within 6 years, 2 on fan
Mid 1950's	Moderate	Two scars, TRDs and growth acceleration in 7 trees within 3 years, located in watershed and on the fan
Late 1960's	Low	Scar, TRDs and growth changes in 7 trees within 5 years, 3 on fan
Mid 1980's	Low	Scar, TRDs and growth acceleration in 6 trees within 3 years, 3 on fan

The affected areas associated with the events outlined in Table 6-2 were delineated using tree locations, topography and professional judgement. The delineated areas were then used with the area-volume relationship as outlined in Section 5.4.4 and with the average test pit unit thicknesses (Section 6.2.3) to estimate event volumes. The results of the volume analysis are shown in Table 6-3 and were used in the F-M relationship. BGC used the average volume estimates as presented in the last column in Table 6-3.

This analysis shows that a debris flow between some 26,000 and 57,000 m<sup>3</sup> volume occurred on Cold Spring Creek in the late 1960s, large and intensive enough to injure trees. This provokes the question why such event is not visible on the 1975 air photographs. There are two explanations: One is that the event was of a long duration and the impact forces insufficient to fell trees and create a path of destruction. Then, in the aftermath of the event and prior to the 1975 air photograph the area re-vegetated and the evidence of the debris flow was no longer visible. Figure 6-2 shows an enlargement of the 1975 air photograph that does not show signs of a major debris flow. BGC also interviewed a local long-time resident (Mr. Lloyd Wilder) who had no recollection of such event.



**Figure 6-2. Cutout of 1975 air photograph BC 7818, No. 17 (approximate scale: 1:20,000). The channel alignment of Cold Spring Creek is unclear at this time. Fairmont Close and Falcon Drive and Willis Road appear to just have been built.**

The other explanation is that the event may have been of lesser magnitude than interpolated by dendrochronologic analysis and thus the volume reported for this event, as well as possibly the mid-1980s event, is lower than reported herein. Plotting the results of the dendrochronological analysis against both the post-fire debris-flow frequency magnitude data and the regional F-M data demonstrates that the dendrochronologic analysis results plot between the two distributions hence lending some credibility to the results.

**Table 6-3. Delineated areas and debris-flow volume results from the dendrogeomorphology analysis.**

Date	Delineated Area (m <sup>2</sup> )		Volume (m <sup>3</sup> )			
	Minimum or Best Estimate	Maximum	A-V Relationship		Test pit thicknesses	Average between methods
			Minimum or Best Estimate	Maximum		
1770's	128,900	399,600	16,000	89,000	64,000	56,000
Late 1810's	128,900	399,600	16,000	89,000	64,000	56,000
Early 1840's	128,900	399,600	16,000	89,000	64,000	56,000
Early 1870's	61,500	166,800	5,000	24,000	31,000	20,000
Late 1880's	129,300	308,500	16,000	61,000	65,000	47,000
Mid 1950's	147,700	-	20,000	-	74,000	47,000
Late 1960's	175,700	-	26,000	-	88,000	57,000
Mid 1980's	90,000	-	10,000	-	45,000	28,000

### 6.2.3. Test Pit Logging and Radiocarbon Testing

Radiocarbon sample dates and test pits logs were used to estimate minimum return periods and event deposit thicknesses (Table 6-4). The radiocarbon results showed a minimum event return period of 300 years for those areas in which test pits were dug. This number should be viewed as a minimum due to the limited number of test pits. No events could be delineated from the radiocarbon sample results as dates did not agree between test pit locations and an insufficient number of test pits were conducted due to budget limitations. Radiocarbon dates were used to determine the return period where debris floods transition to debris flows. Detailed results of the radiocarbon dating are provided in Appendix B.

**Table 6-4. Radiocarbon dates from test pits across the fan.**

Event Date (years BP1)	Sample	Depth (m)	# of units above	Minimum event return period (rounded) (years)
1280*	CG & TT EBA TP14-01 <sup>2</sup>	1.2	1	1300
Modern	CG & TT EBA TP14-02 <sup>2</sup>	1.7	-	-
Modern	CG & TT EBA TP14-04 <sup>2</sup>	3.0	-	-
1120	BGC20-TP-2A	1.0	1	1200
1227*	BGC20-TP-2B	1.5	2	700
364	BGC20-TP-3A	1.1	2	200
1795*	BGC20-TP-3B	2.0	4	500
3320**	BGC20-TP-3C	2.7	6	600
1835*	BGC20-TP-4A	1.3	3	600
3059	BGC20-TP-4B	2.2	4	800
2567	BGC20-TP-4C	3.1	5	500
1296*	BGC20-TP-5A	1.1	1	1400
3424**	BGC20-TP-5B	2.1	3	1200
2770	Grab 1 - Cutbank	2.5	5	600

Notes:

1. Radiocarbon results are expressed in years before present (BP), where present is taken to be the year 1950.
2. Samples from test pits dug and tested during Clarke Geoscience and Tetra Tech EBA (March 1, 2015)'s field investigation.
3. Radiocarbon dates marked with an asterisk are interpreted to be the same event.

Soil logging of the test pits identified event thicknesses ranging from 0.1 to 0.9 m, with a median thickness of 0.5 m (Appendix A). Given the size of Cold Spring Creek fan, it was impractical to dig enough trenches to allow a seamless extrapolation of deposits across the fan assuming that all deposits would have been datable. Instead, the median thickness of the deposits encountered in the test pits was used with events delineated from dendrogeomorphology to go into the F-M relationship (Table 6-3). Assuming that of the 12 dates obtained (one from Clarke Geoscience and Tetra Tech EBA (March 1, 2015)) 8 demark individual events over a period of approximately 3400 years, this yields an average debris-flow frequency of approximately 400 years. This does not imply that debris flows occur only every 400 years, but that debris flows occur *at least* every 400 years, on average, on Cold Spring Creek fan. There is no doubt that if a more extensive test pitting program would have been executed (this was not possible due to budget constraints and permitting), that more debris flows would have been encountered and dated.

#### 6.2.4. Summary

The above analyses indicate that Cold Spring Creek is a hybrid creek with floods, debris floods and debris flows all occurring but at different return periods and at different locations within the watershed. BGC's assessment suggests that with reference to the fan apex, debris floods with substantial bedload and organic debris transport (e.g., the May 2020 event) occur from approximately 1 in 5 years to 1 in 100 years. Debris flows occur at return periods in excess of

100 years. These values refer to the historical record. The effects of climate change are becoming increasingly prevalent. By the end of this century, the return periods of the respective events may at least half.

The most destructive and life-threatening hydrogeomorphic hazard at Cold Spring Creek is debris flow.

### 6.3. Frequency-Magnitude Relationships

This section provides the diagnostic reasoning for the compilation of various F-M approaches and F-M ensemble curves from which a best estimate is extracted. Several techniques were combined to estimate the F-M curve from the current data set.

#### 6.3.1. Debris Flood Frequency-Magnitude

A flood frequency analysis was conducted using a regional approach based on available hydrometric stations. Climate change and sediment bulking factor were then applied to the base clearwater discharges to estimate debris flood peak discharges. Table 6-5 shows results of the flood frequency analysis and bulked, climate change adjusted discharges used in debris flood numerical modeling. Bulking factors were estimated using the methods outlined in Section 5.2.3.

Associated sediment volumes are summarized in Table 6-6.

**Table 6-5. Flood frequency analysis on Cold Spring Creek.**

Return Period (years)	Base Discharge (m <sup>3</sup> /s)	Climate Change Adjusted Discharge (m <sup>3</sup> /s)	Bulking Factor	Bulked, Climate Change Adjusted Discharge <sup>1</sup> (m <sup>3</sup> /s)	Bulking Factor Comments
2	1.2	1.4	-	1.4	-
5	1.7	2.0	1.05	2.1	Normal debris loading, few active landslides
10	2.1	2.5	1.05	2.6	Normal debris loading, few active landslides
25	2.5	3.0	1.1	3.3	Several landslides in lower 20% of watershed length, some woody debris
50	2.6	3.1	1.1	3.4	Several landslides in lower 20% of watershed length, some woody debris
100	3.1	3.7	1.3	4.8	Many landslides in lower 20% of watershed, debris flow tributary highly active, diluted debris flows (Type 2 debris flood)
200	3.6	4.3	1.5	6.5	Many landslides in lower 20% of watershed, debris flow tributary very highly active, diluted debris flows (Type 2 debris flood)

Note:

1. Bulked, climate change adjusted discharges were used as the peak discharge for debris flood modeling.

**Table 6-6. Rainfall and sediment volume summary for debris floods on Cold Spring Creek.**

Return Period (years)	Rainfall (mm)	Snowmelt Contribution (mm)	Rainfall Volume (m <sup>3</sup> )	Total Available Water (m <sup>3</sup> )	Estimated Sediment Volume (m <sup>3</sup> )
2	25	40,000	200,000	240,000	3,300
5	34	54,000	270,000	324,000	4,100
10	40	64,000	320,000	384,000	4,700
25	48	76,000	380,000	456,000	5,300
50	53	86,000	430,000	516,000	5,800
100	59	94,000	470,000	564,000	6,200
200	65	104,000	520,000	624,000	6,700
May 2020		115,000	260,000	375,000	3,300 to 4,500

Note: \* The estimate of 3300 m<sup>3</sup> is from loads removed by excavator and truck, though Mr. Funke (engineering manager believes this might be an overestimate (email from Kara Zandbergen, personal communication, August 10, 2020). 1000 to 2000 m<sup>3</sup> were deposited in the lower basin.

The average estimate of the May 31, 2020 event was 4200 m<sup>3</sup>. According to BGC's analysis and including climate change consideration, an event of this debris volume would be associated in the future with a 5 to 10-year return period. This appears credible as, anecdotally, a debris flood in 2013 (only 7 years ago) was of higher magnitude than the May 31, 2020 event.

### 6.3.2. Debris Flow Frequency-Magnitude

Three distinct methods were used to create an F-M model ensemble for Cold Spring Creek: the regional fan area F-M relationship; the results of the dendrochronology analysis (Table 6-3); and the empirical model for post-wildfire debris flows.

Results for all three approaches are summarized in Figure 6-3, with tabulated results for the empirical model of post-wildlife debris flows results summarized in Table 6-7. The latter represents an approximation of F-M post-fire relationships for Cold Spring Creek considering climate change effects. However, given that there has not been a stand replacing fire over the period of the air photography or BC government forest fire records (since at least 1917), and hence no post-fire debris flow, these results cannot be verified independently. They are, however, used in conjunction with the other F-M models to achieve a consensus estimate.

**Table 6-7. Post-fire debris-flow frequency-magnitude relationships adjusted for climate-change effects. The volume ranges come from the assumption of two-thirds of the watershed being burned.**

Return Period (years)	Debris Flow Volume Best Estimate (m <sup>3</sup> )	Debris Flow Peak Discharge Best Estimate (m <sup>3</sup> /s)
30 to 100	54,500	180
100 to 300	63,500	210
300 to 1000	76,000	260
1000 to 3000	96,000	320

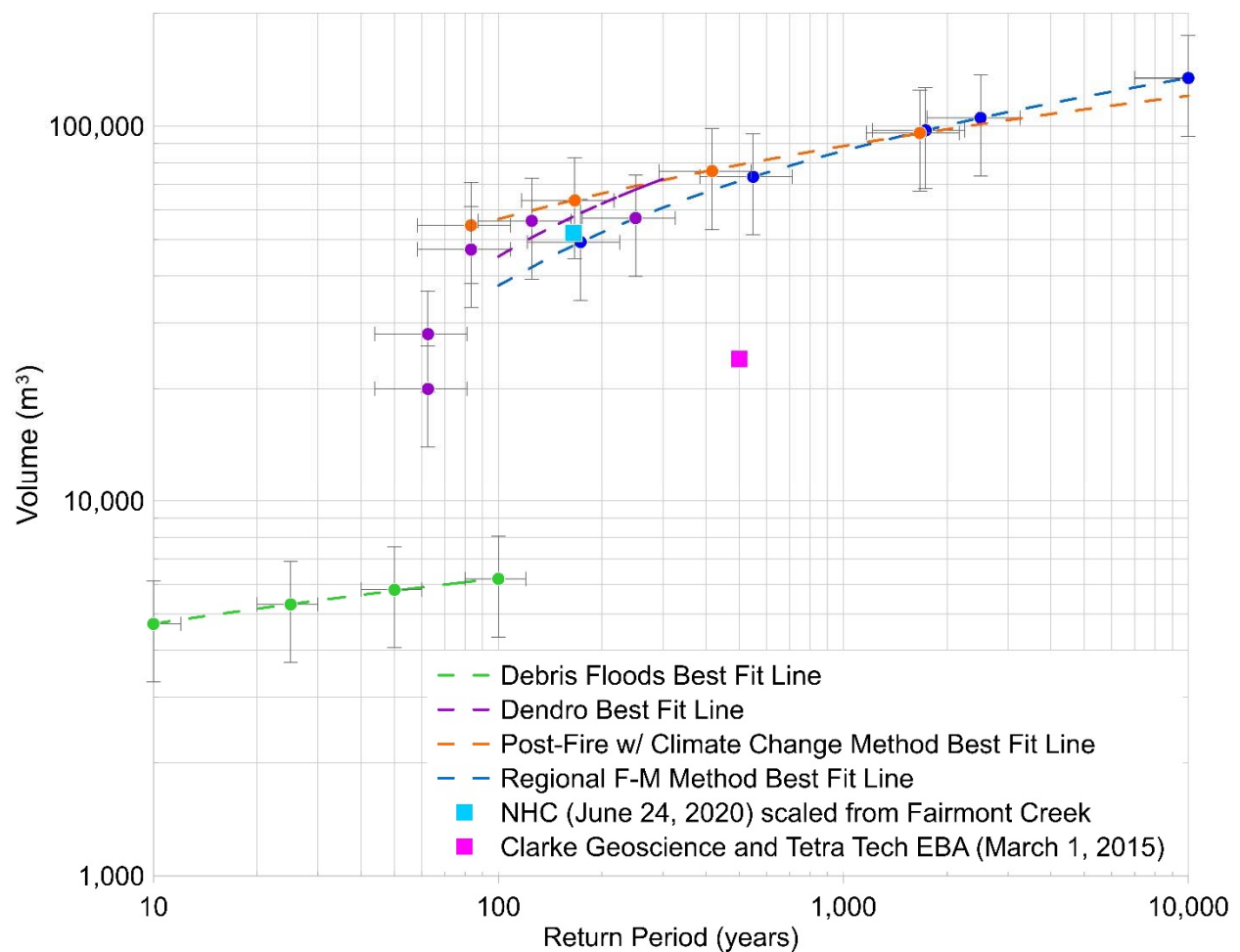


**Figure 6-3. The frequency-volume methods considered reasonable for Cold Spring Creek. Best fit lines are trimmed at the 100-year return period as BGC considers debris flows below that return period are unlikely. The figure also shows the Clarke Geoscience and Tetra Tech EBA (March 1, 2015) F-M estimate as well as the recently updated (NHC, June 24, 2020) estimate for Fairmont Creek adjusted by watershed area. Error bars are based on judgement.**

None of the three methods applied by BGC by themselves can produce precise results. However, model ensembles provide complimentary information providing increased credibility as long as the results are similar. Given the uncertainty associated with the effects of climate change, selecting conservative estimates is warranted due to the potential for life loss and major infrastructure damage at Cold Spring Creek.

For comparison, the recently updated frequency estimate for the 2012 debris flow on Fairmont Creek (NHC, 2020) was added, but adjusted by the watershed area (Cold Spring Creek is 8 km<sup>2</sup> compared to 10 km<sup>2</sup> for Fairmont Creek). In addition, the original F-M estimate by Clarke Geoscience and Tetra Tech EBA (March 1, 2015) was added for comparison.

The dendrochronological reconstruction of debris flow volumes is based on real data but assumes that all tree disturbances are reflective of debris flows. Moreover, the extent of debris flows is interpreted. These results were used for reliance for the 100 to 300-year return period class which BGC assessed is the lowest class subject to debris flows. It is encouraging to see how the F-M curve for this method is close to the one established for the other two methods discussed below.

The regional fan area method yields a somewhat lower F-M curve compared to the post-fire method up to a return period of approximately 1750 years. Beyond that return period, the regional fan area method rises above the post-fire method. This may be an artefact of the chosen fire severity and other assumptions that went into the development of the post-fire method. As both methods are empirical, it is very difficult to assign reliable error margins. The post-fire method results for return periods up to 1000 years and the regional analysis for return periods up to 3000 years were adopted by BGC. This approach is akin to multi-modeling ensemble predictions for hurricanes and other meteorological phenomena and includes a degree of professional judgement.

### 6.3.3. Debris Flood and Debris Flow Frequency-Magnitude Values

The final F-M estimates for all return period classes are summarized in Table 6-8. Peak discharges for debris flows are based on the Bovis and Jakob (1999) equation that relates peak discharge to total volume for muddy debris flows.

**Table 6-8. Final frequency-magnitude numbers for debris floods and debris flows on Cold Spring Creek using a model ensemble.**

Return Period (years)	Process	Debris Volume Best Estimate (m <sup>3</sup> )	Peak Discharge (m <sup>3</sup> /s)
3 to 10	Debris Flood	4,400	2.4
10 to 30	Debris Flood	4,800	3.8
30 to 100	Debris Flood	5,200	5.2
100 to 300	Debris Flow	63,500	210
300 to 1000	Debris Flow	76,000	260
1000 to 3000	Debris Flow	96,000	320

With respect to these results, the reader should note the following:

- The climate change impact assessment results were difficult to synthesize in order to select climate-adjusted peak discharges on a site-specific basis. Consequently, a 20% increase in peak discharge was adopted for debris flood peak discharges as per Section 5.2.2.
- The climate-adjusted and bulked discharge was used in the numerical modeling of debris floods.
- The debris-flow discharges were used in the debris flow modeling. Debris flow peak discharges are two orders of magnitude higher than those of clearwater floods and thus dictate hazards and risks (Jakob and Jordan, 2001).

### 6.3.3.1. Debris-Flow Peak Discharge

The peak discharges noted in Table 6-8 can be partially validated by comparison to field observations. Cross sections measured in the field at locations marked on Drawing 01 were analyzed using Jarrett (1984) and Prochaska et al. (2008) methods to estimate peak discharges. The cross sections collected during the channel hike represent both the most recent May 31, 2020 event and historical events based on debris flow levees observed. Table 6-9 summarizes the estimated discharges for each cross section.

**Table 6-9. Estimated peak discharges at cross sections measured during field traverse. Historical debris flows are bolded.**

Cross Section No.	Peak Discharge (m <sup>3</sup> /s)		Comments
	Jarrett (1984)	Prochaska (2008)	
1	10	30	May 31, 2020 event trimline
4a	15	50	May 31, 2020 event trimline
4b	100	170	Historical event between debris flow levees
5a	25	60	May 31, 2020 trimline on northern tributary
5b	120	180	Historical event between debris flow levees on northern tributary
6	30	70	May 31, 2020 trimline on southern tributary
7	2	10	May 31, 2020 trimline
8	2.5	15	May 31, 2020 trimline
11	10	25	May 31, 2020 trimline
Desktop Cross Section A	70	170	Cross section from 2018 Lidar, old debris flow surface from Figure 5-9.
Desktop Cross Section B	500	620	Cross section from 2018 Lidar, possible older debris flow surface from Figure 5-9.

Note: Cross sections 2, 3, 9 and 10 were rough cross sections for field estimates, not used in detailed analysis.

Estimates from higher in the watershed (cross sections 1 to 6) are much higher than cross sections at or near the fan apex (cross sections 7 to 11). This is attributable to most debris floods transitioning from debris flows as they dilute and their sediment concentration decreases. Some water may also be lost due to infiltration, though this is believed to be negligible prior to arriving on the fan surface. Of note is that the peak discharge estimates based on debris-flow levee trimlines are in excess of 100 m<sup>3</sup>/s, consistent with the peak discharge estimates of Table 6-8 for return period ranges in excess of 100 years. Desktop Cross Section B provides a peak discharge of up to approximately 600 m<sup>3</sup>/s which is more than 3 times higher than the next highest value of 180 m<sup>3</sup>/s. Reconstructing old cross-sections in alluvial channel reaches is fraught with difficulty as the amount of post-event erosion is unknown. Moreover, this cross-section may have been associated with the original Cold Spring Creek Landslide and thus not be representative of repeat events. Irrespective, it demonstrates that large, high discharge debris flows have occurred in the upper and mid watershed of Cold Spring Creek.

#### 6.3.3.2. Frequency-Magnitude Model Check

The F-M model ensemble has several components. On the one hand empirical methods to relate debris flood and debris flow magnitude to specific return periods. On the other hand, direct methods to determine debris flow frequency (air photograph analysis, dendrochronology, radiocarbon dating). The disadvantage of the latter method, unless carried out over the entire fan which is cost-prohibitive and not permissible due to private land ownership, is that it does not provide a continuous F-M relationship. Hence significant uncertainty remains. To check the validity of the F-M model, BGC developed an additional methodology. It compares the estimated alluvial fan volume with the integrated F-M curve. In short, summing all events over the past 10,000 years should approximate the fan volume given that debris floods and debris flows deposited their loads on the fan with only small-grained sediments discharging into the Columbia River floodplain.

Table 6-10 summarizes the results from this analysis. When summed, the total volume of debris having been transported onto the Cold Spring Creek fan from the Cold Spring Creek watershed is approximately 22 million m<sup>3</sup>. The annualized sediment volume is approximately 2200 m<sup>3</sup>.

**Table 6-10. Total volume of fan sediments as the integral of the frequency-magnitude curve.**

Event Type	Volume Class	From	To	Event Volume (m <sup>3</sup> )	Annual Probability of exactly 1 event in Volume Class	Annualized Volume (m <sup>3</sup> )
Debris Flood	1	3	10	4,400	0.23333	1,027
Debris Flood	2	10	30	4,800	0.06667	320
Debris Flood	3	30	100	5,200	0.02333	121
Debris Flow	4	100	300	62,000	0.00667	413
Debris Flow	5	300	1,000	83,000	0.00233	194
Debris Flow	6	1,000	3,000	100,000	0.00067	67
Debris Flow	7	3,000	10,000	130,000	0.00023	30
<b>Annualized Sediment Volume (m<sup>3</sup>):</b>						<b>2,200</b>
<b>Total Fan Sediment Volume (m<sup>3</sup>)</b>						<b>21,700,000</b>

BGC then estimated the fan volume via the Sloping Local Base Level (SLBL) tool. The SLBL is a geometrical approach to define a quadratic surface above which earth materials are considered to be erodible within a short period of time (i.e., 10,000 years; Jaboyedoff and Tacher, 2006). The approach was designed for landslide volume estimation and assumes that erosion by landsliding can affect only a limited thickness of a slope defined by the quadratic surface (Jaboyedoff et al., 2004a). The SLBL concept is similar to the geomorphological concept of “base level”, but SLBL surface is sloping (because landslide failure surfaces are sloping), as opposed to horizontal for the “base level”. Some points must be fixed for the computation of SLBL. Streams and crests can be considered as invariant (Jaboyedoff et al., 2004a). Alternatively, the invariant points defining the erodible area can be delineated by geomorphic mapping (e.g., tension cracks/linears, breaks in slope angle; Jaboyedoff et al., 2004b).

The SLBL method was adapted to estimate the volume of both Cold Spring Creek and Fairmont Creek fans. The quadratic surface generated by the software was calibrated to generate a “no-fan” topography, corresponding to the topography prior to the fan’s development. This approach assumes that the contours on the “no-fan” topography are approximately straight lines connecting the present-day contours outside of the fan boundaries (the topography outside of the fan boundaries having not been modified with the SLBL computation).

Three different pre-fan topographies were considered as summarized in Figure 6-4. Black contours show the present topography, while the blue contours show reconstructed surfaces. The left-hand panel is considered unlikely as fluvial erosion in the aftermath of the glacial lake drainage would have quickly created a valley pointing towards the modern fan apex. It is therefore considered to be an unlikely pre-fan topography. The middle and right-hand panels are considered more likely pre-event topographic reconstructions, though it is not possible to ascertain one being more likely than the other.

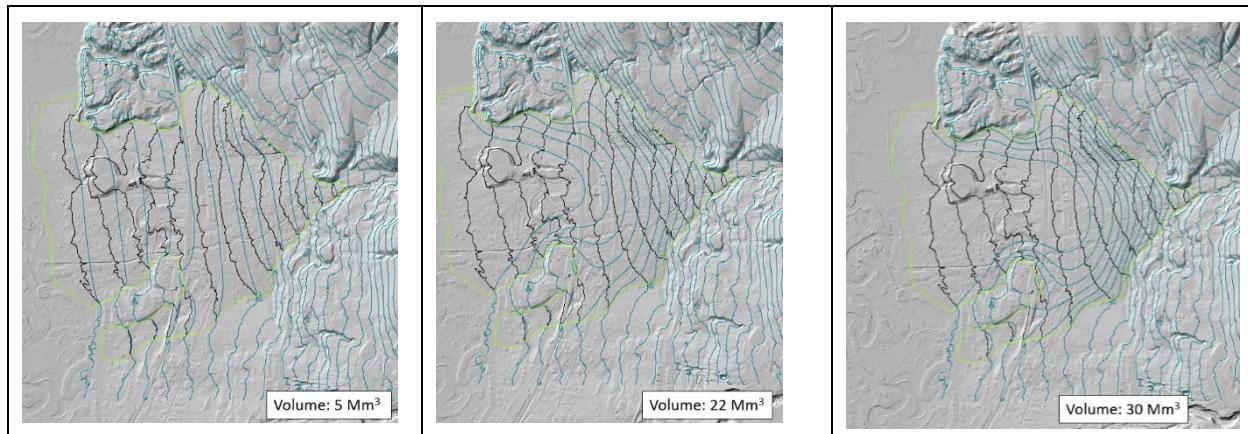


**Figure 6-4. Different models for fan volume reconstruction using the SLBL model.**

In summary, the integration (summation) of the debris flood and debris flow volumes, yields a volume of approximately 22 Mm<sup>3</sup>. Reconstructing the fan volume provides a model of somewhere between 22 Million m<sup>3</sup> and 30 Million m<sup>3</sup>. This affirms that the F-M analysis, while imperfect, is a close representation of the total fan volume which supports its validity.

A further check is provided by comparing the average fan thickness to the findings and dates from radiocarbon dating. Using the fan volumes as per Figure 6-4 and dividing it by the fan area provides average fan thicknesses which are 5, 21 and 29 m, respectively.

The test pitting and radiocarbon dating allows an extrapolation of fan thickness at the locations of the test pits assuming that aggradation rates remained linear throughout the Holocene. This can be achieved by calculating the aggradation rates of the deposits overlying a specific radiocarbon date and then extrapolating to 10,000 years which roughly demarks the time period of fan formation in the region (i.e. since deglaciation). The fan thicknesses calculated range from 8 m at TP 5 to 24 m at TP 3, and the average of the highest reconstituted fan thickness for each pit is 13 m which is approximately 60% of the centre model average fan thickness in Figure 6-4. This finding is somewhat inconclusive as there are an insufficient number of test pits, nor geophysical measurements to verify this result. The individual fan thickness extrapolations indicate that there may be as much as a 120% upward error. However, the results indicate that Cold Spring Creek fan is at least 13 m thick, on average, hence corroborating the F-M analysis.

## **6.4. Numerical Flood and Debris-Flow Modeling and Hazard Mapping**

### **6.4.1. Results**

A summary of the key observations from the debris flood and debris flow modeling is included in Table 6-11. Note that the results in the form of maps and description in Table 6-11 are based on numerical modeling which includes climate-change adjustment and are therefore forward looking.

**Table 6-11. Summary of modeling results.**

Return Period (years)	Process	Key Observations
3-10	<b>Debris Flood</b>	<ul style="list-style-type: none"> <li>• The debris flood is likely to stay confined through the channel upstream of the Cold Spring Creek reservoir.</li> <li>• The first upstream avulsion will occur at the Fairmont Resort Road due to an under-capacity culvert. The avulsion spills on either side of the east-west aligned Fairmont Resort Road and shallow (likely a few centimeter) water will affect adjacent properties.</li> <li>• At Hot Springs Road, the water will further fan out towards the north and south and reach Highway 95 where water will flow into the highway ditch except at the crossing of Fairmont Resort Road where water can travel across the highway and follow the road downstream until dissipating in the road ditches.</li> <li>• The culvert beneath Highway 95 is under-capacity and water is expected to run over the highway, overtop and north of the remnant glaciolacustrine terraces with some flood waters meeting the Riverview Road downstream.</li> <li>• Flood waters downstream of the Riverview Road culvert will continue down the road and into adjacent properties at shallow depth (&lt; 10 cm) until reaching the Columbia River floodplain.</li> <li>• Flood waters are likely to follow the Highway 95 ditch to the south and spill across Highway 95 north of Fox Place to then flow west towards the Columbia River through developed areas near Riverview Close.</li> <li>• Flow velocities in unconfined flow are low (&lt; 0.3 m/s), and may reach up to 2 m/s in the channel reaches on the fan.</li> </ul>
	Sedimentation	<ul style="list-style-type: none"> <li>• The modeled debris-flood sediment volume is well in excess of the capacity of the reservoir including the depositional angle (~ 1900 m<sup>3</sup>). Hence the Cold Spring Creek reservoir will fill up and overflow with sediment for this and all modeled debris-flood return periods.</li> </ul>
	Auxiliary Hazards	<ul style="list-style-type: none"> <li>• At all culvert crossings it can be expected that the culverts are overwhelmed and water run across the road surface to then erode the downstream side, possibly undermining the N-S aligned roads.</li> <li>• Downstream of Highway 95, flow across the glaciolacustrine terrace could (if of sufficient volume) erode into the downstream side of the terrace, creating a gully and sedimentation downstream.</li> </ul>

Return Period (years)	Process	Key Observations
10-30	<b>Debris Flood</b>	<ul style="list-style-type: none"> <li>As for the 3 to 10-year return period, insufficient capacity at the upper Fairmont Resort Road culvert can initiate avulsions.</li> <li>The debris flood stays largely within the wider creek corridor but has substantially more surface water flooding south towards Fairmont Creek. By the time the debris flood reaches Highway 95, the area wetted is over 400 m wide.</li> <li>Water will overflow Highway 95 in two main places: down Riverview Road which is the extension of Fairmont Resort Road on the lower fan and the area of Riverview Close and Riverview Crescent. These are also areas where several large boulders have been mapped.</li> <li>Some flow will continue down the main channel.</li> <li>Flow depth will remain shallow (centimeters to tens of centimeters in confined section).</li> </ul>
	Sedimentation	<ul style="list-style-type: none"> <li>Sedimentation is likely to be most significant in the Cold Spring Creek reservoir, and upstream due to the morphodynamic backwater effects (sediment piling up beyond the confines of the reservoir). Some sediment will escape over and past the dam as occurred in May 31, 2020.</li> <li>Thin (several centimeters) of sediment are expected throughout the area inundated as well as in closed depressions and highway ditches as well as in the sedimentation basin at Glen Eagle Drive which may fill to capacity for this event.</li> </ul>
	Auxiliary Hazards	<ul style="list-style-type: none"> <li>Given that all existing culverts will have their capacity exceeded, overtopping and downstream erosion may undercut existing road surfaces and lead to partial or full road surface collapse.</li> <li>Muddy water on Highway 95 as well as other flooded community roads may lead to aquaplaning and accidents before roads can be closed.</li> <li>Where flooding can ingress buildings through open or broken doors or windows, basements can entirely flood despite comparatively low flow depths.</li> <li>Knickpoint developments downstream of N-E trending highways with likely road undercutting by rushing water and partial loss of road surfaces.</li> </ul>
30-100	<b>Debris Flood</b>	<ul style="list-style-type: none"> <li>The event covers a more extensive area compared to the 10 to 30-year return period debris flood.</li> <li>Most of the southern fan (south of Fairmont Resort Road) is inundated with shallow water and debris</li> <li>Highway 95 is inundated over considerable length, mostly with water but also with some organic debris.</li> </ul>
	Sedimentation	<ul style="list-style-type: none"> <li>Sedimentation as for the 10 to 30-year event.</li> <li>Most of the stream channel will likely aggrade to the top and new channels will form throughout the southern fan</li> <li>Sediment will likely accumulate between a few centimeters to over a metre deep in depressions and upstream of homes.</li> </ul>
	Auxiliary Hazards	<ul style="list-style-type: none"> <li>Same as the 10 to 30-year event with more extensive damage.</li> </ul>

Return Period (years)	Process	Key Observations
100-300	<b>Debris Flow</b>	<ul style="list-style-type: none"> <li>• Unlike for the modeled debris-flood scenarios, a debris flow (due to a much higher peak discharge) will have a much higher flow depth upstream of the Cold Spring Creek reservoir and be at least 50 m wide at the fan apex.</li> <li>• Flows, due to higher momentum and discharge, will have two preferred flow paths. One down mid fan, between Falcon Drive and Wills Road, across Highway 95, further down Wills Road between the remnants of glaciolacustrine terraces and down to James Street where it will flow onto the Columbia River floodplain. The second major flow path is along Cold Spring Creek at similar extent as for the 10 to 30-year debris flood, however at substantially higher flow depth.</li> <li>• Flow depths on the upper fan to approximately Fairway Drive will be mostly between 0.8 and 1.5 m with some locations near the creek reaching up to 3 m. Flow velocities on the upper fan will range between around 3 m/s with more confined and deeper flow locally reaching up to 5 m/s. At those flow velocities and depths, major structural damage or building destruction is possible.</li> <li>• At mid fan, between Fairway Drive and Highway 95, flow covers most of the active fan with depths between 0.8 and 1.5 m including the channel of Cold Spring Creek. Flow velocities will be between 2 and 3 m/s. At those depths and velocities, major structural damage to buildings is possible.</li> <li>• On the lower fan, flow will become more narrowly confined and follow inactive channels and low points. Flow paths are similar to those observed for the 3 to 10-year return period debris flood. Flow depths will be mostly less than 0.8 m and flow velocities will be mostly less than 3 m/s, slowing to zero where the flow meets the Columbia River floodplain. At those velocities and flow depths, minor structural damage and nuisance flooding will likely prevail.</li> </ul>
	Sedimentation	<ul style="list-style-type: none"> <li>• Unlike for debris floods, sedimentation will be vast on the upper and mid fan. Sediment depths will be highly variable ranging from a few tens of centimeters to 2 m upstream of obstructions. Basements and first floors where debris ingresses through upstream-facing windows and doors will fill with dense debris.</li> <li>• On the lower fan sedimentation will be less and confined to the flow paths. All depressions within the flow paths will fill with sediment. All affected community roads and Highway 95 will be impassable. All culverts are likely to be filled entirely or partially be filled with sediment and be ineffective.</li> </ul>
	Auxiliary Hazards	<ul style="list-style-type: none"> <li>• Given the high impact forces associated with the debris flows and obstructions (buildings) in the flow paths, flow will be deflected into areas not entirely captured in the numerical modeling.</li> <li>• Most homes are heated or cook with propane gas. There are numerous gas containers across the fan. Should one of those containers be punctured or crushed and there is a source of flames or sparks from the boulder impact on the steel, such containers could explode greatly amplifying the damage by debris flows. BGC is unaware of cases where this has occurred, however, several cases of gas pipelines exploding due to debris flow impacts are known. The most recent one being in Montecito, California in January 2018.</li> </ul>

300-1000	<b>Debris Flow</b>	<ul style="list-style-type: none"> <li>Flow paths are similar to those for the 100 to 300-year return period. Flow width, especially on the lower fan in the vicinity of Wills Road will be wider with flow widths reaching over 100 m and occupying the entire width between the flanking glaciolacustrine terraces.</li> <li>Only a small triangle between Highway 95 and Falcon Drive is unlikely to be covered with debris.</li> <li>Flow velocities and flow depths will be marginally (perhaps 10-20%) higher for the 300 to 1000-year return period event compared to the 100 to 300-year return period event. The potential for property damage and destruction will be somewhat higher than the 100 to 300-year return period.</li> <li>Due to the higher flow proportion on the northern fan portions and the viscosity of debris flows, relatively little sediment is expected to pass Highway 95 on the southern fan portions. This could change, however, should there be a major flow blockage near the fan apex that may direct more flow towards the south. Such eventualities would have to be modeled if a quantitative risk assessment were desired.</li> </ul>
	Sedimentation	<ul style="list-style-type: none"> <li>Similar as for the 100 to 300-year return period debris flow with somewhat (~20%) higher amounts.</li> </ul>
	Auxiliary Hazards	<ul style="list-style-type: none"> <li>Same as described for the 100 to 300-year return period event</li> </ul>
1000-3000	<b>Debris Flow</b>	<ul style="list-style-type: none"> <li>Similar flow paths as for the 100 to 300 and 300 to 1000-year events, with an emphasis on the northern flow path. For this return period, the entire confinement between the glaciolacustrine terraces is occupied by flow.</li> <li>Flow depths for this event range reach up to 2 m for the northern flow path and can reach up to 5 m in the vicinity of the Cold Spring Creek reservoir. Flow velocities range from 1 to 3 m/s for much of the mid and lower fan up to perhaps 9 m/s near the fan apex where flow is still confined.</li> <li>The triangle between Highway 95 and Falcon Drive which is largely spared in the 300 to 1000-year return period event is beginning to be inundated by this event.</li> <li>At the flow depths and velocities modeled, major structural damage and destruction is conceivable for much of the upper fan and along the northern flow paths. The southern fan may be more subject to minor to major structural damage unless a blockage occurs on the upper fan directing the majority of debris and sediment towards the southern fan sector.</li> </ul>
	Sedimentation	<ul style="list-style-type: none"> <li>Sedimentation will be similar to the 300 to 1000-year event with somewhat (15-20%) higher amounts.</li> </ul>
	Auxiliary Hazards	<ul style="list-style-type: none"> <li>Same as described for the 100 to 300-year return period event.</li> </ul>

### 6.4.2. Numerical Model Check I: Area-Volume Relationship

Griswold and Iverson (2008) developed an empirical correlation between the planimetric area inundated by non-volcanic debris flows and the associated deposited volume. The chosen volumes for each return period (red triangles in Figure 6-5) for Cold Spring Creek plot somewhat lower than the expected range of typical non-volcanic debris flows based on the modeled surface inundation area. In other words, for the given debris-flow volume, the planimetric area is somewhat higher than expected. This can likely be attributed to the fact debris flows from sources of weak sedimentary rocks and low-grade metamorphic rocks contain more fines than typical granular debris flows. This means that given the Fairmont Creek back-calculated rheology, debris flows run out further and spread more readily than coarse granular debris flows, ultimately resulting in a larger planimetric area than expected for given non-volcanic debris-flow volumes. Interestingly, the Fairmont Creek area-volume plots in the centre of the distribution.

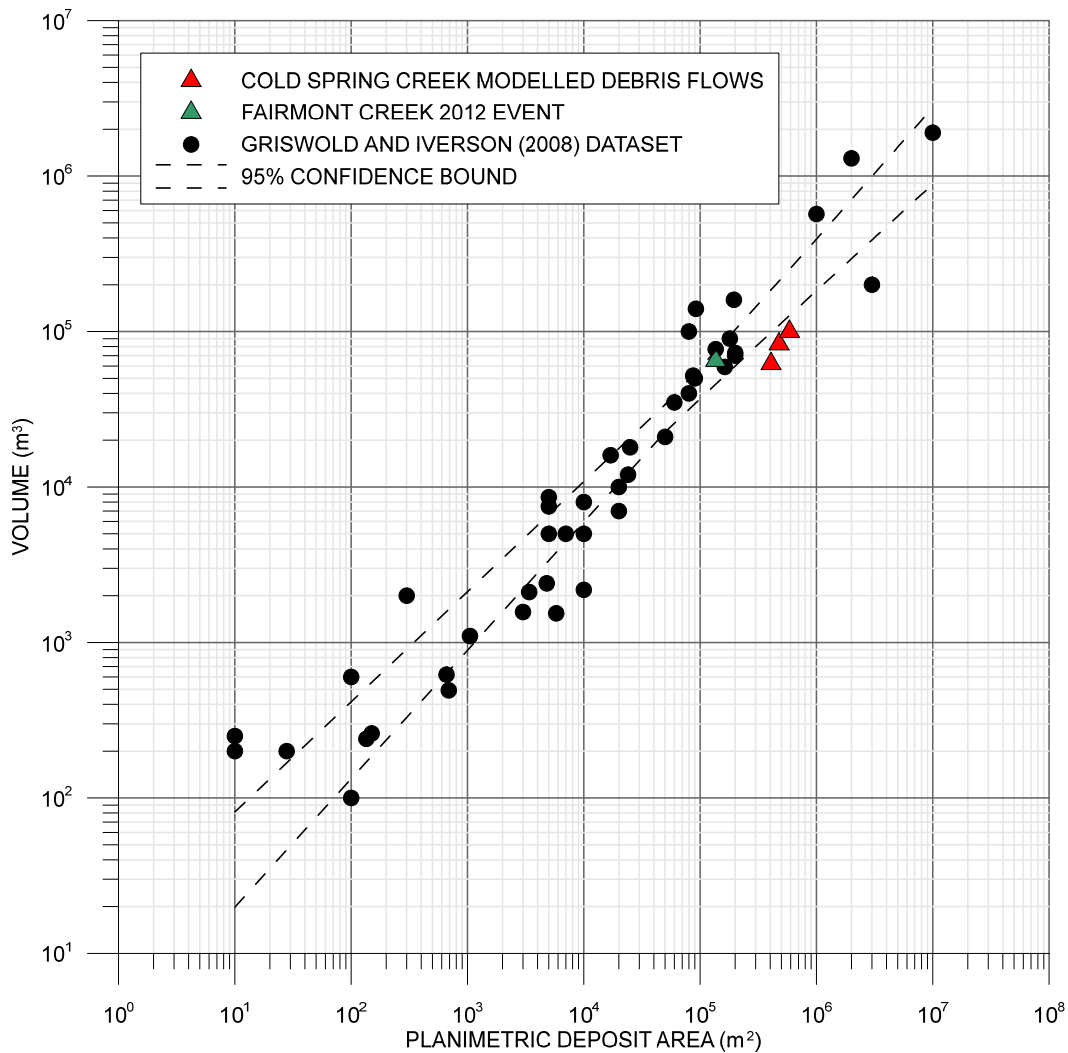


**Figure 6-5. Modeled event volumes for Cold Spring Creek (red) in comparison to typical non-volcanic debris flow dataset (black) developed by Griswold and Iverson (2008). The Fairmont Creek 2012 event (green) is shown for comparison.**

While the debris-flow volume and peak discharge estimates are derived indirectly, this independent check verifies that the debris-flow inundated area for the input volumes appears reasonable.

### 6.4.3. Numerical Model Check II: Boulder Size as Indicator of Flow Depth

BGC mapped approximately 140 surface boulders on the fan of Cold Spring Creek. Boulders were also measured along the A-, B- and C-axes. These boulders (sub-rounded to subangular) are believed to originate from debris flows in the Cold Spring Creek watershed. Some boulders are surface boulders, others have been excavated during foundation works and been used ornamentally in people's yards. The hypothesis is that the size boulders transported by debris flows is indicative of debris flow depth during motion and can thus be used to test the outcome of the numerical modeling and calibrate it if necessary. This can be achieved in two ways: The simplest is to assume that boulder size equals flow depth which can be seen in numerous YouTube and other amateur and professional movies showing debris flows in motion. However, these movies also show that, sometimes, boulders can be in excess of the flow depth front (<https://www.youtube.com/watch?v=Fsh5E9m3PrM>). At times boulders can be twice as large as the flow depth, however, mostly in confined channels where debris has little opportunity to bypass the boulder.

The other method is to use the well-known shear stress formula by Shields and solve it for  $D$ , the grain size, using a range of dimensionless Shields numbers to match the observed from the calculated boulder size.

Shear stress is made non-dimensional in the form of the Shields Number,

$$\tau_* = \tau / g(\rho_s - \rho_f)D \quad [\text{Eq. 6-1}]$$

in which  $\rho_s$  and  $\rho_f$  designate sediment and fluid density and  $\tau$  is shear stress. The Shields Number is the ratio of the grain mobilizing force over the resisting force, adopted simply as the submerged weight of the grain. While threshold values of  $\tau$  may be difficult to estimate for steep, ungauged channels, the much more conservative values of  $\tau_*$  might reasonably be estimated. Therefore, using  $\tau_{c50}$  as a scale we re-express the in terms of this frequently used metric of bed stability. Solving for  $D$ , yields

$$D = \tau_{c50} / (\rho_s - \rho_f) \tau_* \quad [\text{Eq. 6-2}]$$

The Shields number is then iteratively solved to match observed boulder size. The Shields number matching the observed boulder size in the five different fan segments then is 0.2.

To determine if the flow depth from the numerical model matches the flow depth ( $d$ ) required to move the mapped boulders, Equation 6-2 needs to be solved for  $d$ :

$$d = D \tau_* / (\rho_s - \rho_f) \tau_{c50} \quad [\text{Eq. 6-3}]$$

BGC then plotted the average flow depth derived from numerical modeling of the 100 to 300-year debris-flow event for the specific fan segments against the flow depth derived, independently, from the derivation of the Shields equation (Figure 6-6).

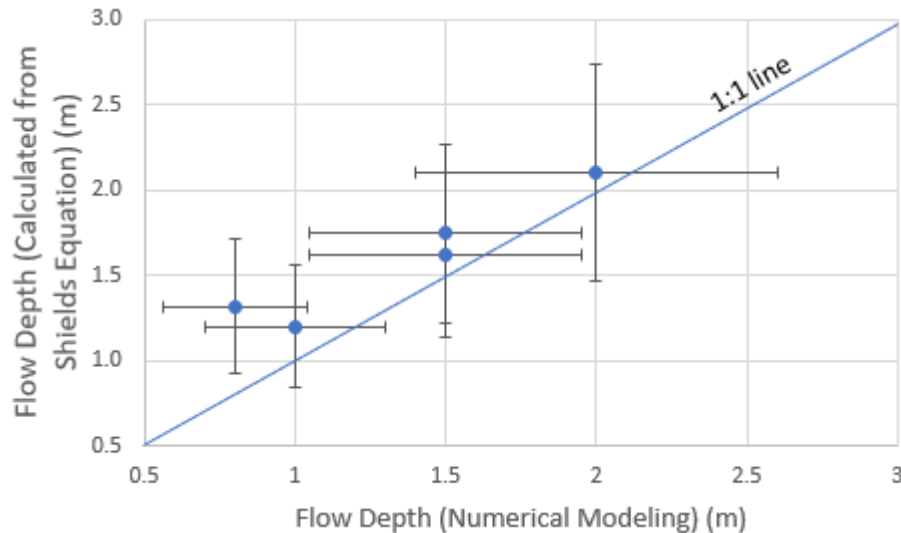


**Figure 6-6. Modeled flow depth vs. calculated flow depth using boulder size as a proxy for flow depth. The plot includes an estimated 30% error for both the numerical modeling flow depth and the calculated flow depth from the Shield’s equation.**

The analysis confirms that the modeled flow depth for debris flows using a nominal 100 to 300-year return period debris flow is similar to the estimated flow depth required to transport the caliber of boulders observed on Cold Spring Creek fan.

This finding supports that the numerical modeling adequately simulates debris flows in terms of flow depth and flow extent. Individual debris-flow units range between 0.4 and 1.1 m in thickness which is less than what is suggested by numerical modeling and the application of the Shield’s equation. It is expected as the maximum flow depth of a debris flow may be twice as high as the deposition final deposition depth (Major, pers. comm, 2020). This result is unsurprising given that during debris flows, the sediment concentration is 50% by volume.

### 6.5. Hazard Mapping

BGC produced six individual hazard maps for each of the return period classes. Blockage or avulsion scenarios were not simulated as the existing culverts are undersized for even small debris floods and because there are no obvious avulsion locations such as sharp channel bends. Moreover, the channel itself is poorly incised which implies that the channel has little bearing on debris flow trajectories. For each run, a raw hazard output was reviewed with respect to flow depths and flow velocity. Table 6-11 summarizes the findings from the individual hazard maps (Drawing 03). Drawing 04 is the composite hazard map that combines all findings as detailed in Section 5.6.

The individual hazard maps only show the impact force, which is a proxy of how vulnerable buildings and their inhabitants are should the modeled event occur. The composite hazard map combines impact forces and the event frequencies in one map that is suitable for land use decisions. It answers the question: How hazardous is a specific site on the fan given any of the modeled hazard events? The darker (warmer) the colour, the higher the hazard for the specific location.

A hazard map, when constructed prior to development, would guide the regulators towards which areas to permit, permit with restrictions or not permit at all in absence of mitigation. For example, a regulator may decide that a red (high) hazard zone be undevelopable, while an orange (moderate) hazard could only be developed with severe restrictions in the form of on-site mitigation, no habitable basements, wall reinforcement, no upstream facing windows and doors and a minimum flood construction level. Yellow (low) hazards zones would still have some, albeit lesser, restrictions than the orange hazard zones, while the remaining zones may have no restrictions at all. The composite hazard map for Cold Spring Creek (Drawing 04) indicates the following:

- The hazard increases with proximity to the fan apex and along existing active and inactive flow channels. The hazard is further modulated by topographic highs and lows which may increase the hazard should flow be constricted and thus accelerate. The following bullets summarize key findings of the new composite hazard map.
- The hazard is substantially higher than previously assumed (Clark Geoscience Ltd. and Tetra Tech EBA, March 1, 2015) and extends well beyond the previously incorrectly assumed fan limits.
- Hazards are dominated by the 100 to 300-year return period debris flow which is the lowest return period class that could lead to severe building damage and potential loss of life. For this reason, this event return period class is likely also associated with the highest relative risk and may, upon deliberation by the RDEK, become the design event.
- A high hazard zone extends with two prongs down from the fan apex. The north prong extends to Highway 95 in a swath approximately 100 to 200 m wide. The south prong follows the current channel south to Hot Springs Road in a swath approximately 50 to 150 m wide.
- A moderate hazard zone extends on the northern portion of the fan almost to the fan edge at Downey Avenue. Moderate hazard also persists for much of the upper fan upstream of Highway 95.
- The low hazard zone extends in places to the Columbia River floodplain and reaches entirely to south edge of the Cold Spring Creek fan, meeting the Fairmont Creek fan. Simultaneous events on both Cold Spring Creek and Fairmont Creek were not investigated in this scope but would probably interfinger around the fan boundaries.
- The centre of the fan is at slightly higher elevation and thus exposed to a somewhat lower hazard as it splits the main flows to either side.

The composite hazard map is a representation of the current hazard. It does not account for any major fan surface alterations by smaller debris flows or by construction. It also does not include the presence of homes and their effects on debris flows as it is unknown which buildings will survive a debris flow and how they could divert the flows. The hazard zones are not, and cannot, be precise and should not be interpreted as precise, as debris flows are to some extent chaotic processes and their exact behaviour cannot be predicted with precision. Any future mitigation measures will, depending on their scale, location and effectiveness, reduce the hazard. This requires re-modeling of debris floods and debris flows to determine the extent of hazard reduction.

## 6.6. Comparison to Previous Hazard Mapping

In this section BGC briefly describes hazard mapping efforts conducted by previous workers.

In 1998 Klohn Crippen provided a regional-scale mapping and characterization of steep creek hazards in the entire RDEK. The fan is described as having a history of debris flows, but currently has only limited activity. Klohn Crippen (1998) hand-mapped the main creek alignment as well as potential avulsion paths. A recently active fan polygon was provided, but this does not appear to exist in digital form for overlay. It also does not indicate the level of activity.

The KWL (2014) report focused on only modeling a Sunny-day dam outbreak at the Cold Spring Creek Reservoir that resulted in a peak discharge of 15 m<sup>3</sup>/s. The outbreak flood was modeled with the one-dimensional version of HEC RAS and showed no significant avulsions from the existing channel. Major avulsions are modeled for all return period modeled by BGC starting with 2.4 m<sup>3</sup>/s. The differences are likely attributable to BGC having a much more detailed topography available, using a 2-D model with 2-m grid size that more accurately reflects the current channel. This comparison shows that without the appropriate topography, one may obtain erroneous results as a 15 m<sup>3</sup>/s flood should spread substantially more than anticipated by KWL (December 29, 2014). The RDEK may wish to share this finding with Fairmont Resort. BGC's present findings may require a revision of the conclusions of the KWL (December 29, 2014) report.

The Clarke Geoscience and Tetra Tech EBA (March 1, 2015) report provides both hazard and risk maps. The key differences in hazard mapping between the 2015 report and the analysis herein are outlined in Table 6-12.

**Table 6-12. Key differences in hazard mapping between Clarke Geoscience and Tetra Tech EBA (March 1, 2015) and this report.**

Criteria	BGC (this report)	CG&EBA TT (2015)
Basis for Hazard Mapping	Impact force times hazard probability (numerical)	Debris flow volumes versus return period (matrix approach)
Total Hazard Extent	Covers much of the active fan of Coldspring Creek	Covers only a very small portion of the active fan
High Hazard Extent	Covers a substantial portion of the upper fan.	No High hazard
Moderate Hazard Extent	Covers most of the remaining upper fan and much of the middle and lower northern fan	Moderate hazard only extends along a narrow corridor along the current creek
Low Hazard Extent	Covers the remainder of the active fan	Narrow tongues of low hazard through upper fan

Table 6-12 demonstrates that compared to the present BGC report, Clarke Geoscience and Tetra Tech EBA (March 1, 2015) estimated a much lower debris-flow hazard and the associated risk on the active fan. Based on the additional evidence compiled in the assessment herein, BGC recommends that development and land use decisions going forward be based on BGC's composite hazard map.

## 7. SUMMARY AND RECOMMENDATIONS

### 7.1. Summary

#### 7.1.1. Hydrogeomorphic Process

Based on field observations and remote sensing data, Cold Spring Creek is subject to floods, debris floods and debris flows at different return periods. The return periods and hence the F-M relationships of the individual processes are expected to change fundamentally over time.

#### 7.1.2. Air Photo Interpretation

Air photos were interpreted to gain an understanding of watershed and channel changes on the fan and aid the development of an F-M relationship. No significant debris flow is visible in the air photo record back to 1949.

#### 7.1.3. Frequency-Magnitude Relationship

Frequency-volume relationships were constructed from combining an empirical approach relating fan area to F-M relationships, a statistical approach based on an expected increase in post-wildfire debris flow activity, radiocarbon dating and test trenching and dendrochronology with independent verification using the 71-year air photograph record.

Debris flood hazards were identified up to approximately a 100-year return period, based air photograph evidence, dendrogeomorphology, radiocarbon dating and professional judgement. The May 31, 2020 event had an approximate debris volume of 3300 to 4500 m<sup>3</sup> with a peak discharge of 2 to 3 m<sup>3</sup>/s. With that, BGC believes it was approximately a 5 to 10-year return period event. The 2013 debris flood appears to have been more extensive and damaging judged from helicopter and ground photographs and opinion by RDEK staff (Brian Funke, pers. comm., August 2020). This event may have a 10 to 30-year return period debris flood.

The first two approaches (regional F-M and postfire debris flow F-M) provide continuous F-M relationships once fitted to a statistical function. The other methods serve to test and verify the former two approaches. The regional F-M averages out climate over the past 10,000 years, while the post-fire debris-flow F-M explicitly allows for *predicted* climate change.

The effects of climate change are still very difficult to quantify as they are complex and intertwined (Jakob, 2020). However, the effects shown in Table 7-1 are considered likely to increase both the frequency and magnitude of debris floods and debris flows in the future. The estimate of confidence is based on literature review and judgement. A confidence of Very High symbolizes near certainty, while a confidence of Moderate indicates a roughly equal chance that the effect may occur.

**Table 7-1. Summary of climate change effects on debris flood and debris flow F-M relationships.**

Effect	F-M impact	Confidence
Increases in extreme rainfall frequency	Moves the F-M curve to the left	Very High
Increases in extreme rainfall intensity	Moves the F-M curve upwards	Very High
Increases in wildfire burn frequency due to drying and potential beetle infestation	Moves the F-M curve upward	High
Increase in wildfire burn severity	Not accounted for in the F-M curve	High
Degradation of mountain permafrost and attendant increases in rock fall/rock slide frequency	Accounted for by assuming that sediment supply will not be limited even if events occur more frequently	Moderate to High

In short, while informative and relevant in constructing a F-M relationship for the past, the future is unlikely to resemble the recent (hundreds or thousands of years), and a significant change in sediment delivery rates should be expected and accounted for in engineering design of risk reduction measures on Cold Spring Creek.

Peak discharges associated with debris floods and debris flows were estimated using a combination of techniques. Cross-sections were measured in the watershed, and velocities estimated with appropriate formulae. In addition, empirical relationships between assumed debris-flow volumes and peak discharges that were developed in southwestern BC were applied.

Peak discharges used for modeling the various return period events are also reported in Table 7-2.

**Table 7-2. Cold Spring Creek best estimate debris flood and debris flow frequency-volume relationship including the effects of climate change. Peak discharge is referenced to the fan apex. Debris volume is referenced to volumes passing the fan apex. All figures are best estimates using a combination of data.**

Return Period (years)	Process	Water Volume	Debris Volume Best Estimate (m <sup>3</sup> )	Peak Discharge Best Estimate (m <sup>3</sup> /s)
3 to 10	Debris Flood	210,000	4,400	2.4
10 to 30	Debris Flood	380,000	4,800	3.8
30 to 100	Debris Flood	520,000	5,200	5.2
100 to 300	Debris Flow	n/a	64,000	210
300 to 1000	Debris Flow	n/a	76,000	260
1000 to 3000	Debris Flow	n/a	96,000	320

#### 7.1.4. Numerical Modeling

Debris floods and debris flows of all return periods were modeled using FLO-2D software to simulate the chosen hazard scenarios on the Cold Spring Creek fan. Table 6-11 provides key observations derived from the numerical modeling.

The numerical modelling demonstrates that the key hazards at Cold Spring Creek stem from debris flows of the 100 to 300-year return period as those will be the lowest return periods at which substantial (structural) property damage can be expected.

#### 7.1.5. Hazard Mapping

Model results are cartographically expressed in two ways:

- The individual hazard scenarios are captured through an index of impact force that combines flow velocity, bulk density and flow depth (Drawing 03). These maps are useful for assessments of development proposals and emergency planning.
- A composite hazard rating map (impact force frequency map) that combines the debris flood and debris flow intensity (impact force) and frequency up to the 3000-year return period event. This map is useful to designate hazard zones (Drawing 04).

Both the individual scenario maps and the composite hazard rating map serve as decision-making tools to guide subdivision and other development permit approvals. Details on how to translate the hazard map into tangible land use decisions can be developed collaboratively between the RDEK, BGC and McElhanney.

## 7.2. Limitations and Uncertainties

While systematic scientific methods were applied in this study, some uncertainties prevail. As with all hazard assessment and concordant maps, the hazard maps prepared at Cold Spring Creek represent a snapshot in time. Future changes to the Cold Spring Creek watershed or fan including the following may warrant re-assessment and/or re-modeling:

- Future fan development and debris flow events
- Significant wildfires (defined as those affecting > 50% of the watershed at moderate or higher burn intensity)
- Mitigation work design and/or re-design including berms, basins, culvert replacements, debris nets and other measures.

The assumptions made on changes in debris flood and debris-flow frequency and magnitude due to climate change, while not unreasonable, are not infallible and will likely need to be updated occasionally as scientific understanding of such processes evolves.

BGC recognizes that all hazard processes display some chaotic behaviour and therefore not all hazards or hazard scenarios can be adequately modeled. For example, unforeseen log jams may alter flow directions and create avulsions into areas not specifically considered in the individual hazard scenarios. Despite these limitations and uncertainties, BGC believes that a credible hazard assessment has been achieved on which land use decisions can be made.

### 7.3. Concluding Remarks

Cold Spring Creek fan is subject to considerable hazard and risk. Given the now quantified hazards and the high development density in the high hazard zones, Cold Spring and Fairmont creek fans may be the highest risk fans within the RDEK. The watershed of Cold Spring Creek is still very geomorphologically active and produces large volumes of sediment through erosion and weathering.

Given the relatively recent (since about 1975) urban development on the fan, the general perception may be that it is subject only to minor floods and debris floods such as the one experienced in July 2012 or on May 31, 2020. During these events minor damage occurred to road crossings and culverts, but no substantial damage occurred to properties, nor did it lead to injury or loss of life. This perception is treacherous because infrequent larger debris flows have occurred on Cold Spring Creek fan and will, without doubt, occur again. When they occur, debris flows will, with virtual certainty, exit the existing channel and inundate the existing development where they can cause substantial damage and lead to injury and loss of life depending on occupancy at the time of the debris flow.

Some may argue that the tell-tale signs (large boulders, the radiocarbon dates and fan morphology) are a legacy of the deep past and are unlikely to re-occur. However, there is no evidence that would support such thinking. On the contrary, the effects of climate change will very likely increase both the frequency and magnitude of debris floods and debris flows on this fan: directly through increases in extreme rainfall frequency and magnitude, and indirectly by increasing wildfire frequency and severity as well as degradation of presumed remaining mountain permafrost which in turn increases the frequency of rock fall and rock slides in the upper watershed.

Previously published hazard extents and intensities are superseded by this work which demonstrates that most of the active fan of Cold Spring Creek is subject to debris-flow impact.

Mitigation works previously conceptualized by NHC (2019) could only reduce the impacts of debris floods, those that could be expected every few years to perhaps once in a century. They would be ineffective against debris-flow impacts.

Given the limited funds available for mitigation, the design of mitigation works ought to (a) maximize the debris retention and discharge reduction of debris flows prior to reaching the development and (b) allow for upgrades or additional structures so that if more funding becomes available further risk reduction can be achieved.

Severe losses on alluvial fans such as Cold Spring Creek will increase in both frequency and magnitude in coming decades due to continued development, increases in the frequency and magnitude severe weather events and through degradation of the watershed forest covers by beetle infestations and wildfires. Local governments should attempt to exert maximum pressures on the provincial government to:

- a. Provide economic and life loss risk tolerance standards as they exist in other nations.
- b. Carefully review the range of return periods that are being considered for steep creek hazard assessments which are unprecedented worldwide as this affects hazard zonation,

risk and risk tolerance. Currently, the guidance of considering up to the 10,000-year return period event for all life threatening landslide hazards is in stark contrast to the woefully inadequate available funding for steep creek processes, especially debris flows.

- c. Provide a fair and transparent funding scheme for steep creek mitigation projects for existing development that is slated to meet the risk tolerance standards as outlined in (a). This could be a funding formula in which a portion is paid for by the federal government, a portion by the provincial government and (depending on the tax income) by the local government (regional district or municipality). The ratio should be such that the project can be financed in full without jeopardizing the safety of downstream residents.
- d. Through working with EGBC, update and create new guidelines for steep creek hazard mapping and technical design guidance for the mitigation of steep creek hazards.
- e. Discourage new development on alluvial fans unless those who profit from such development are willing to pay for the design, construction and operation of mitigation works.

Local governments should consider to:

- a. Mandate that engineering or geoscience consultants follow EGBC guidance.
- b. Ask for third party reviews of consultant reports to assure the quality is appropriate.
- c. Discourage new development or development densification on alluvial fans unless the local government can guarantee that risk can be managed adequately.

## 8. CLOSURE

We trust the above satisfies your requirements at this time. Should you have any questions or comments, please do not hesitate to contact us.

Yours sincerely,

**BGC ENGINEERING INC.**

per:



Matthias Jakob, Ph.D., P.Ge. (BC/AB)  
Principal Geoscientist



Beatrice Collier-Pandya, B.A.Sc., EIT  
Geological Engineer

Reviewed by:

Hamish Weatherly, M.Sc., P.Ge. (BC/AB)  
Principal Hydrologist

MJ/HW/sf/mm

## REFERENCES

- BGC Engineering Inc. (BGC) (2014, October 31). *Three Sisters Creek debris-flood hazard assessment* [Report]. Prepared for the Town of Canmore.
- BGC Engineering Inc. (BGC). (2020, March 31). *RDCK Floodplain and Steep Creek Study - Steep Creek Assessment Methodology* [Report]. Prepared for Regional District of Central Kootenay.
- BGC Engineering Inc. (BGC). (2020, July 31). *Willox Creek Emergency Response Assessment: Post-Field Update* [Letter Report]. Prepared for Regional District of Fraser Fort George.
- Blackwell, B.A., Grey, R.W., & Compass Resource Management. (2003). *Historic Natural Fire Regime of south-central British Columbia*.
- Bovis, M., and Jakob, M. (1999). The role of debris supply conditions in predicting debris flow activity. *Earth Surface Processes and Landforms* 24(11), 1039-1054. [https://doi.org/10.1002/\(SICI\)1096-9837\(199910\)24:11<1039::AID-ESP29>3.0.CO;2-U](https://doi.org/10.1002/(SICI)1096-9837(199910)24:11<1039::AID-ESP29>3.0.CO;2-U)
- Boyer, D. (1989, March 8). *Debris Torrent Concerns Cold Spring and Fairmont Creeks*. Nelson, BC: Water Management Branch.
- Brardinoni, F., and Church, M. (2004). Representing the magnitude-frequency relation: Capilano river basin. *Earth Surface Processes and Landforms*, 29, 115-124.
- British Columbia Ministry of Forests, Lands, Natural Resource Operations and Rural Development (FLNRORD). (2019a, December 17). *Fire Perimeters - Historical* [GIS Data]. Retrieved from <https://catalogue.data.gov.bc.ca/dataset/fire-perimeters-historical>
- British Columbia Ministry of Forests, Lands, Natural Resource Operations and Rural Development (FLNRORD). (2019b, December 17). *Harvested areas of BC (Consolidated Cutblocks)* [GIS Data]. Retrieved from <https://catalogue.data.gov.bc.ca/dataset/harvested-areas-of-bc-consolidated-cutblocks->
- Cannon, S.H., and Gartner, J.E. (2005). Wildfire-related debris flow from a hazards perspective. In M. Jakob and O. Hungr (Eds.), *Debris-flow hazards and related phenomena* (pp. 363-385). Berlin, Heidelberg: Springer.
- Cannon, S.H., Gartner, J.E., Wilson, R.C., Bowers, J.C., & Laber, J.L. (2008). Storm rainfall conditions for floods and debris flows from recently burned areas in southwestern Colorado and southern California. *Geomorphology*, 96(3-4), 250-269. <https://doi.org/10.1016/j.geomorph.2007.03.019>
- Cannon, S.H., Gartner, J.E. Rupert, M.G., Michael, J.A., Rea, A.H., & Parrett, C. (2010). Predicting the probability and volume of post wildfire debris flows in the intermountain western United States. *Geological Society of America Bulletin*, 122(1-2), 127-144. <https://doi.org/10.1130/B26459.1>
- Cannon, S.H., Boldt, E.M., Laber, J.L., Kean, J.W., & Staley, D.M. (2011). Rainfall intensity-duration thresholds for post-fire debris-flow emergency response planning. *Natural Hazards*, 59, 209-236. <https://doi.org/10.1007/s11069-011-9747-2>

- Cesca, M., and D'Agostino, V. (2008). Comparison between FLO-2D and RAMMS in debris-flow modelling: a case study in the dolomite. *WIT Transaction on Engineering Sciences*, 60, 197-206. <https://doi.org/10.2495/DEB080201>
- Church, M., and Jakob, M. (2020). What is a debris flood? Accepted to *Water Resources Research*.
- Church, M., and Zimmermann, A. (2007). Form and stability of step-pool channels: research progress. *Water Resources Research*, 43(3), 1-21. <https://doi.org/10.1029/2006WR005037>
- Clark, J.J. (1975). Late Quaternary sediments and geomorphic history of the southern Rocky Mountain Trench, British Columbia. *Canadian Journal of Earth Sciences* 12: 595-605.
- Clarke Geoscience Ltd. (2013, October 21). *Overview-Level Hazard Assessment of Cold Spring Creek (2013)* [Letter Report]. Prepared for Regional District of Eastern Kootenay.
- Clarke Geoscience Ltd. and Golder Associates. (2013, January 11). *Fairmont Creek Debris Flow Hazard and Risk Assessment* [Report]. Prepared for Regional District of Eastern Kootenay.
- Clarke Geoscience Ltd. and Tetra Tech EBA. (2015, March 1). *Cold Spring Creek Debris Flow Hazard and Risk Assessment* [Report]. Prepared for Regional District of Eastern Kootenay.
- D'Agostino, V., Cerato, M., & Coali, R. (1996). Il trasporto solido di eventi estremi nei torrenti del Trentino Orientale. *Schutz des Lebensraumes vor Hochwasser, Muren, Massenbewegungen und Lawinen*, vol. 1, Interpraevent 1996, Tagungsband, Garmisch-Partenkirchen: Germany; 377–386 (in Italian).
- Dai, J., Chen, W., & Zhou, B. (1980). An experimental study of slurry transport in pipes. *Proceedings of International Symposium on River Sedimentation*, Beijing, China, 195–204.
- Dowling, C.A., Santi, P.M. Debris flows and their toll on human life: a global analysis of debris-flow fatalities from 1950 to 2011. *Nat Hazards* 71, 203–227 (2014). <https://doi.org/10.1007/s11069-013-0907-4>
- Engineers and Geoscientists BC (EGBC). (2018). *Professional Practice Guidelines - Legislated Flood Assessments in a Changing Climate in BC*. Version 2.1.
- Farrell, J.E. & Associates Inc. (1999, September 1). *Fairmont Flood Protection works* [Letter]. Prepared for Fairmont Hot Springs Resort Ltd.
- FLO-2D Software, Inc. (2017). FLO-2D Reference Manual. Build No. 16 January 2017.
- Gartner, J.E., Cannon, S.H., & Santi, P.M. (2014). Empirical models for predicting volumes of sediment deposited by debris flows and sediment-laden floods in the transverse ranges of southern California. *Engineering Geology*, 176(24), 45-56, <https://doi.org/10.1016/j.enggeo.2014.04.008>.
- Gomi, T., and Sidle, R. (2003). Bed load transport in managed steep-gradient headwater streams of southeastern Alaska. *Water Resources Research*, 39(12), <https://doi.org/10.1029/2003WR002440>

- Grant, G.E. (1997). Critical flow constrains flow hydraulics in mobile-bed streams: A new hypothesis. *Water Resources Research*, 33(2), 349-358. <https://doi.org/10.1029/96WR03134>
- Griswold, J.P., and Iverson, R.M. (2008). *Mobility statistics and automated hazard mapping for debris-flows and rock avalanches* (US Geological Survey Scientific Investigations Report 5276). Retrieved from: <https://pubs.usgs.gov/sir/2007/5276/sir2007-5276.pdf>
- Gruber, S. (2012), Derivation and analysis of a high-resolution estimate of global permafrost zonation. *The Cryosphere*, 6, 221-233. <https://doi.org/10.5194/tc-6-221-2012>.
- Gutenberg, B., and Richter, C.F. (1954). *Seismicity of the Earth (Second Edition)*. Princeton Press.
- Hassan, M., Church, M., Lisle, T., Brardinoni, F., Benda, L., & Grant, G. (2005). Sediment transport and channel morphology of small, forested streams. *Journal of the American Water Resources Association*, 41(4), 853-876.
- Holm, K., Jakob, M., Scordo, E., Strouth, A., Wang, R., & Adhikari, R. (2016). Identification, Prioritization, and Risk Reduction: Steep Creek Fans Crossed by Highways in Alberta. *GeoVancouver 2016*. Vancouver, Canada.
- Hungr, O., Leroueil, S., & Picarelli, L. (2014). The Varnes classification of landslide types, an update. *Landslides*, 11, 167-194. <https://doi.org/10.1007/s10346-013-0436-y>
- Hunziker, R.P., and Jäggi, M. (2002). Grain sorting processes. *Journal of Hydraulic Engineering*, 128, 1060- 1068. [https://doi.org/10.1061/\(ASCE\)0733-9429\(2002\)128:12\(1060\)](https://doi.org/10.1061/(ASCE)0733-9429(2002)128:12(1060))
- IPCC. (2014). *Climate Change 2014: Synthesis Report. Contribution of Working Groups I, II and III to the Fifth Assessment Report of the Intergovernmental Panel on Climate Change* [Core Writing Team, R.K. Pachauri and L.A. Meyer (eds.)]. IPCC, Geneva, Switzerland, 151 pp.
- Iverson, R., Schilling, S., & Vallance, J. (1998). Objective delineation of lahar-inundation hazard zones. *GSA Bulletin*, 110(8), 972-984.
- Jaboyedoff, M., and Tacher, L. (2006). Computation of landslides slip surfaces using DEM. *Sea to Sky Geotechnique 2006*, Vancouver, Canada.
- Jaboyedoff, M., Baillifard, F., Couture, R., Locat, J., & Locat, P. (2004a). Toward preliminary hazard assessment using DEM topographic analysis and simple mechanic modeling. In Lacerda, W.A., Ehrlich, M. Fontoura, A.B. and Sayo, A (Eds.), *Landslides Evaluation and Stabilization* (191-197). London: Taylor & Francis Group.
- Jaboyedoff, M., Couture, R., & Locat, J. (2004b). Structural analysis of Turtle Mountain (Alberta) using digital elevation model (DEM). *GeoQuebec 2004*.
- Jäggi, M. (2007). The flood of August 22-23, 2005, in Switzerland: some facts and challenges. *Developments in Earth Surface Processes*, 11, 587-603. [https://doi.org/10.1016/S0928-2025\(07\)11144-5](https://doi.org/10.1016/S0928-2025(07)11144-5)

- Jakob, M. (1996). *Morphometric and geotechnical controls of debris flow frequency and magnitude in southwestern British Columbia* (Ph.D. dissertation). Department of Geography, University of British Columbia, Vancouver, B.C.
- Jakob, M. (2020). Landslides in a changing climate. In T. Davies and N.J. Rosser (Eds.), *Landslides: Hazards, Risks and Disasters, 2nd edition*. Elsevier.
- Jakob, M., and Bovis, M.J. (1996). Morphometrical and geotechnical controls of debris flow activity, southern Coast Mountains, British Columbia, Canada. *Zeitschrift für Geomorphologie Supplementband, 104*, 13-26.
- Jakob, M., and Jordan, P. (2001). Design flood estimates in mountain streams: the need for a geomorphic approach. *Canadian Journal of Civil Engineering, 28*(3), 425-439.
- Jakob, M., Bale, S., McDougall, S., & Friele, P. (2016). Regional debris-flow and debris-flood frequency magnitude curves. In *GeoVancouver 2016, Proceedings of the 68th Canadian Geotechnical Conference*. Richmond, BC: Canadian Geotechnical Society.
- Jakob, M., Mark, E., McDougall, S., Friele, P., Lau, C.-A., & Bale, S. (2020). Regional debris-flow and debris-flood frequency-magnitude curves. Submitted to *Earth Surface Processes and Landforms*.
- Jarrett, R. (1984). Hydraulics of high-gradient streams. *Journal of Hydraulic Engineering, 110*(11). [https://doi.org/10.1061/\(ASCE\)0733-9429\(1984\)110:11\(1519\)](https://doi.org/10.1061/(ASCE)0733-9429(1984)110:11(1519))
- Jordan, P. (2013). Post wildfire debris-flows in southern British Columbia [Presentation Slides].
- Jordan, P. (2015) Post-wildfire debris flows in southern British Columbia, Canada. *International Journal of Wildland Fire*. <http://dx.doi.org/10.1071/WF14070>.
- Jordan, P., and Covert, S.A. (2009). Debris flows and floods following the 2003 wildfires in southern British Columbia. *Environmental and Engineering Geoscience, 15*(4), 217-234. <http://dx.doi.org/10.2113/gseegeosci.15.4.217>
- Kerr Wood Leidal Associates Ltd. (KWL). (2014, December 29). *Cold Spring Creek Consequence Assessment* [Report]. Prepared for Fairmont Hot Springs Resort Ltd.
- Klohn Crippen Consultants Ltd. (1998, February 23). *Terrain Stability Inventory: Alluvial and Debris Torrent Fans Kootenay Region* [Report]. Prepared for British Columbia Ministry of Environment, Lands and Parks.
- Lau, CA. (2017). *Channel scour on temperate alluvial fans in British Columbia* (Master's thesis). Simon Fraser University, Burnaby, BC. Retrieved from <http://summit.sfu.ca/item/17564>.
- Loukas, A., and Quick, M.C. (1999). The effect of climate change on floods in British Columbia. *Nordic Hydrology, 30*, 231-256.
- MacKenzie, L., Eaton, B.C., & Church, M. (2018). Breaking from the average: Why large grains matter in gravel-bed streams. *Earth Surface Processes and Landforms, 43*(15), 3190-3196. <https://doi.org/10.1002/esp.4465>

- Major, J.J. (personal communication, August 2020).
- Magirl, C.S., Hilldale, R.C., Curran, C.A., Duda, J.J., Straub, T.D., Domanski, M., ... Foreman, J.R. (2015). Large-scale dam removal on the Elwha River, Washington, USA: Fluvial sediment load. *Geomorphology*, 246, 669-686. <https://doi.org/10.1016/j.geomorph.2014.12.032>
- Mizuyama, T., Kobashi, S., & Ou, G. (1992). Prediction of debris flow peak discharge, Interpraevent. *International Symposium*, 4, 99-108.
- Moase, E., Strouth, A., & Mitchell, A. (2018, December). A comparison of different approaches for modelling a fine-grained debris flow at Seton Portage, British Columbia, Canada. *Second JTC1 Workshop on Triggering and Propagation of Rapid Flow-like Landslides*. Paper presented at the meeting of the Joint Technical Committee on Natural Slopes and Landslides of the Federation of International Geo-engineering Societies, Hong Kong.
- Mosbrucker, A.R., and Major, J.J. (2019) North Fork Toutle River debris flows initiated by atmospheric rivers. Paper presented at the joint Federal Interagency Sedimentation Conference and Federal Interagency Hydrologic Modeling Conference, Reno, NV. Retrieved from [https://www.sedhyd.org/2019/openconf/modules/request.php?module=oc\\_program&action=view.php&id=202&file=1/202.pdf](https://www.sedhyd.org/2019/openconf/modules/request.php?module=oc_program&action=view.php&id=202&file=1/202.pdf)
- Northwest Hydraulic Consultants Ltd. (NHC). (2020, June 24). *Fairmont Creek Debris Basins – May 31, 2020 Flood Assessment* [Report]. Prepared for Regional District of East Kootenay.
- Northwest Hydraulic Consultants Ltd. (NHC). (2019, October 20). *Cold Spring Creek 2019 Debris Flood Assessment and Mitigation Concept Design* [Letter Report]. Prepared for Regional District of Eastern Kootenay.
- Prein, A.F., Rasmussen, R.M., Ikeda, K., Liu, C., Clark, M.P., & Holland, G.J. (2017). The future intensification of hourly precipitation extremes. *Nature Climate Change*, 7, 48-52.
- Prochaska, A.B., Santi, P.M., Higgins, J. D., & Cannon, S.H. (2008). A study of methods to estimate debris flow velocity. *Landslides*, 5(4), 431-444. DOI: 10.1007/s10346-008-0137-0
- Recking, A., Frey, P., Paquier, A., Belleudy, P., & Champagne, J.Y. (2008). Feedback between bed load transport and flow resistance in gravel and cobble bed rivers. *Water Resource Research*, 44(5), <https://doi.org/10.1029/2007WR006219>
- Regent Instruments Inc. (2012). WinDENDRO [Computer software]. Canada.
- Reid Crowther & Partners Ltd. (1995, February 2). *Fairmont Hot Springs Resort Area Cold Spring Creek – Highway 93 Crossing* [Letter]. Prepared for Hot Springs Resort Ltd.
- Reid Crowther & Partners Ltd. (1994, October 7). *Fairmont Hot Springs Resort Area Terrain Hazard Assessment* [Report]. Prepared for Fairmont Hot Springs Resort Ltd.
- Rickenmann, D. (2001). Comparison of bed load transport in torrents and gravel bed streams. *Water Resources Research*, 37(2), 3295-3305. <https://doi.org/10.1029/2001WR000319>

- Rickenmann, D. (2005). Runout prediction methods. In M. Jakob & O. Hungr (Eds.), *Debris-flow hazards and related phenomena* (pp. 305-324). New York: Springer.
- Rickenmann, D., and Koschni, A. (2010). Sediment loads due to fluvial transport and debris flows during the 2005 flood events in Switzerland. *Hydrological Processes*, 24(8), 993-1007. <https://doi.org/10.1002/hyp.7536>
- Rickenmann, D., and McArdell, B.W. (2007). Continuous measurement of sediment transport in the Erlenbach stream using piezoelectric bedload impact sensors. *Earth Surface Processes and Landforms*, 32(9), 1362-1378. <https://doi.org/10.1002/esp.1478>
- Rood, S.B., Foster, S.G., Hillman, E.J., Luek, A., & Zanewich, K.P. (2016). Flood moderation: Declining peak flows along some Rocky Mountain rivers and the underlying mechanism. *Journal of Hydrology*, 536, 174-182. <https://doi.org/10.1016/j.jhydrol.2016.02.043>
- Ryder, J., and Rollerson, T. (1977). *Terrain Inventory Mapping – Mount Abruzzi, Fairmont Hot Springs, BC* [Map]. Scale 1:50,000, downloaded from iMap BC.
- Schnorbus, M., Werner, A., & Bennett, K. (2014). Impacts of climate change in three hydrologic regimes in British Columbia, Canada. *Hydrological Processes*, 28, 1170-1189. <https://doi.org/10.1002/hyp.9661>
- Staley, D.M., Kean, J.W., & Rengers, F.K. (2020). The recurrence interval of post-fire debris-flow generating rainfall in the southwestern United States. *Geomorphology*. In review.
- Stepanek, M. (2013). Letter regarding Cold Spring Dam 2012 Inspection, dated January 21, 2013.
- Wang, T., Hamann, A., Spittlehouse, D.L., & Carroll, C. (2016). Locally downscaled and spatially customizable climate data for historical and future periods for North America. *PLoS One* 11: e0156720. <https://doi.org/10.1371/journal.pone.0156720>

## **APPENDIX A TEST PIT LOGS**

Test Pit BGC-TP-01

Project: Cold Spring Creek Hazard Assessment Update

Location : Downey Avenue

Project No. : 1572005

Survey Method : GPS  
 Coordinates : 580,531.E, 5,577,091.N  
 Ground Elevation (m) :803  
 Datum : NAD83

Start Date : 09 Jul 20  
 Finish Date : 09 Jul 20  
 Final Depth of Pit (m) : 1.0  
 Logged by : MJ  
 Reviewed by : BCP

Depth (m)	Symbol	Sample Material for Dating	Sample Age	Lithologic Description
0				O-HORIZON Dark brown to black with root penetration.
				B-HORIZON Black to mottled with ocre-coloured, partially oxidized inclusions of clayey silt, low plasticity, sheen (mica-rich), some charcoal.
				Homogeneous, unstratified clayey silt to water table with no gravel inclusions, cohesive, some charcoal, no paleosol surfaces (likely frequent flooding from Columbia River), firm, near plastic limit.
1				END OF TEST PIT 1.0 m DUE TO GROUNDWATER LEVEL.
2				
3				
4				

RDEK (STRAT\_COOL) RDEK.GDL BGC.GDT 8/6/20

1 Unit Location Marker  
 A Grab Sample Marker



1. THIS FIGURE IS TO BE READ IN CONJUNCTION WITH THE REPORT ENTITLED "COLD SPRING CREEK HAZARD ASSESSMENT" AND DATED SEPTEMBER 2020.
2. UNLESS BGC AGREES OTHERWISE IN WRITING, THIS FIGURE SHALL NOT BE MODIFIED OR USED FOR ANY PURPOSE OTHER THAN THE PURPOSE FOR WHICH BGC GENERATED IT. BGC SHALL HAVE NO LIABILITY FOR ANY DAMAGES OR LOSS ARISING IN ANY WAY FROM ANY USE OR MODIFICATION OF THIS DOCUMENT NOT AUTHORIZED BY BGC. ANY USE OF OR RELIANCE UPON THIS DOCUMENT OR ITS CONTENT BY THIRD PARTIES SHALL BE AT SUCH THIRD PARTIES' SOLE RISK.

SCALE:	DATE: 09-2020	PREPARED BY: BCP	CHECKED BY: MJ	APPROVED BY: HW
		REPORT TITLE: COLD SPRING CREEK HAZARD ASSESSMENT		
		FIGURE TITLE: BGC-TP-01		
		PROJECT NO: 1572-005	FIGURE NO: A-1	

Test Pit BGC-TP-02

Project: Cold Spring Creek Hazard Assessment Update

Location : Wills Road

Project No. : 1572005

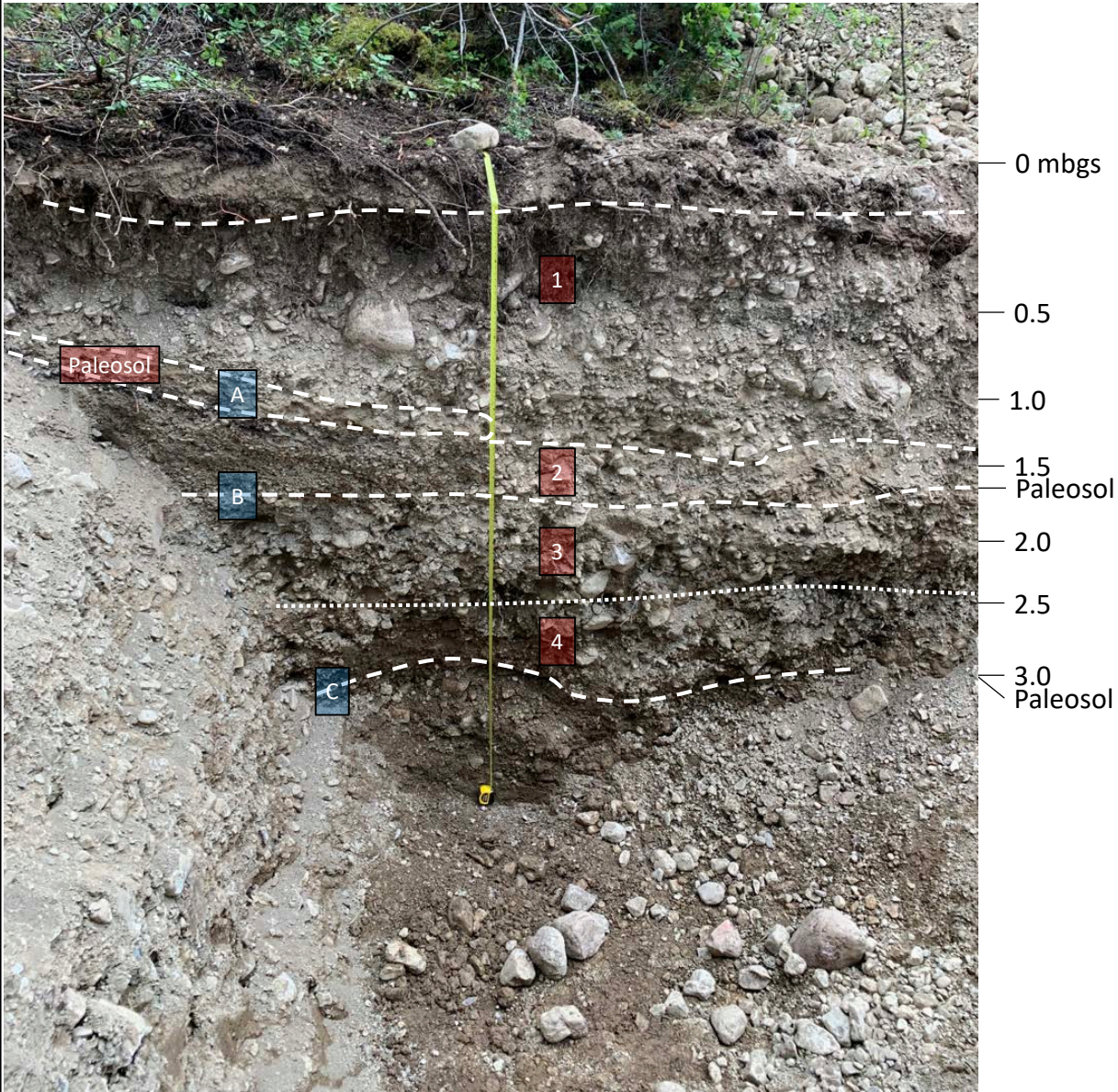
Survey Method : GPS  
 Coordinates : 581,099.E, 5,576,941.N  
 Ground Elevation (m) :835  
 Datum : NAD83

Start Date : 09 Jul 20  
 Finish Date : 09 Jul 20  
 Final Depth of Pit (m) : 3.1  
 Logged by : MJ  
 Reviewed by : BCP

Depth (m)	Symbol	Sample Material for Dating	Sample Age	Lithologic Description
0				O-HORIZON Organic, dark brown matter with abundant rootlets, some gravel.
				B-HORIZON Silty sand, trace gravel, non-cohesive, light brown.
				UNIT 1: DEBRIS FLOW DEPOSIT Gravel and boulder clasts, sandy matrix, poorly graded, compact to dense, subangular to subrounded clasts, light brown, dry, heterogeneous, no cementation, random clast orientation, matrix supported, contact to B-horizon above well defined, Dmax = 450 mm, Dmean = 50 mm.
1		A Charcoal (1.1 m)	1185 - 1055 cal BP	PALEOSOL Sand, silty, ocre-coloured with abundant charcoal, discontinuous, steepening uphill.
				UNIT 2: DEBRIS-FLOOD DEPOSIT Gravel, fine to medium grained, angular to subangular clasts, dry, no cementation, slight imbrication, poor stratification, debris flow-debris flood hybrid, clast supported, Dmax = 15 mm, Dmean = 3 mm.
2		B Charcoal (1.6 m)	1282 - 1172 cal BP	PALEOSOL Sand, silty, ocre-coloured with abundant overlying charcoal, discontinuous, steepening uphill.
				UNIT 3: DEBRIS-FLOW DEPOSIT Gravel and boulder clasts, sandy matrix, poorly graded, compact to dense, subangular to subrounded clasts, light brown, dry, heterogeneous, no cementation, apparent cohesion increasing with depth, random clast orientation, matrix supported, contact to Unit 4 below diffuse, could be one unit, Dmax = 350 mm, Dmean = 20 mm.
				UNIT 4: DEBRIS-FLOW DEPOSIT Gravel and boulder clasts, sandy matrix, poorly graded, compact to dense, subangular to subrounded clasts, light brown, dry, heterogeneous, no cementation, random clast orientation, matrix supported, contact to Unit 3 above diffuse, could be same unit.
3		C Paleosol (3.0 m)		PALEOSOL Sand, silty, discontinuous, steepening uphill at fan gradient.
				END OF TEST PIT 3.1 m
4				

RDEK (STRAT)\_COLL1\_RDEK.GDL BGC.GDT 8/6/20

- 1 Unit Location Marker
- A Grab Sample Marker



1. THIS FIGURE IS TO BE READ IN CONJUNCTION WITH THE REPORT ENTITLED "COLD SPRING CREEK HAZARD ASSESSMENT" AND DATED SEPTEMBER 2020.
2. UNLESS BGC AGREES OTHERWISE IN WRITING, THIS FIGURE SHALL NOT BE MODIFIED OR USED FOR ANY PURPOSE OTHER THAN THE PURPOSE FOR WHICH BGC GENERATED IT. BGC SHALL HAVE NO LIABILITY FOR ANY DAMAGES OR LOSS ARISING IN ANY WAY FROM ANY USE OR MODIFICATION OF THIS DOCUMENT NOT AUTHORIZED BY BGC. ANY USE OF OR RELIANCE UPON THIS DOCUMENT OR ITS CONTENT BY THIRD PARTIES SHALL BE AT SUCH THIRD PARTIES' SOLE RISK.

SCALE:	DATE: 09-2020	PREPARED BY: BCP	CHECKED BY: MJ	APPROVED BY: HW
		REPORT TITLE: COLD SPRING CREEK HAZARD ASSESSMENT		
		FIGURE TITLE: BGC-TP-02		
		PROJECT NO: 1572-005	FIGURE NO: A-2	

Test Pit BGC-TP-03

Project: Cold Spring Creek Hazard Assessment Update

Location : North of creek

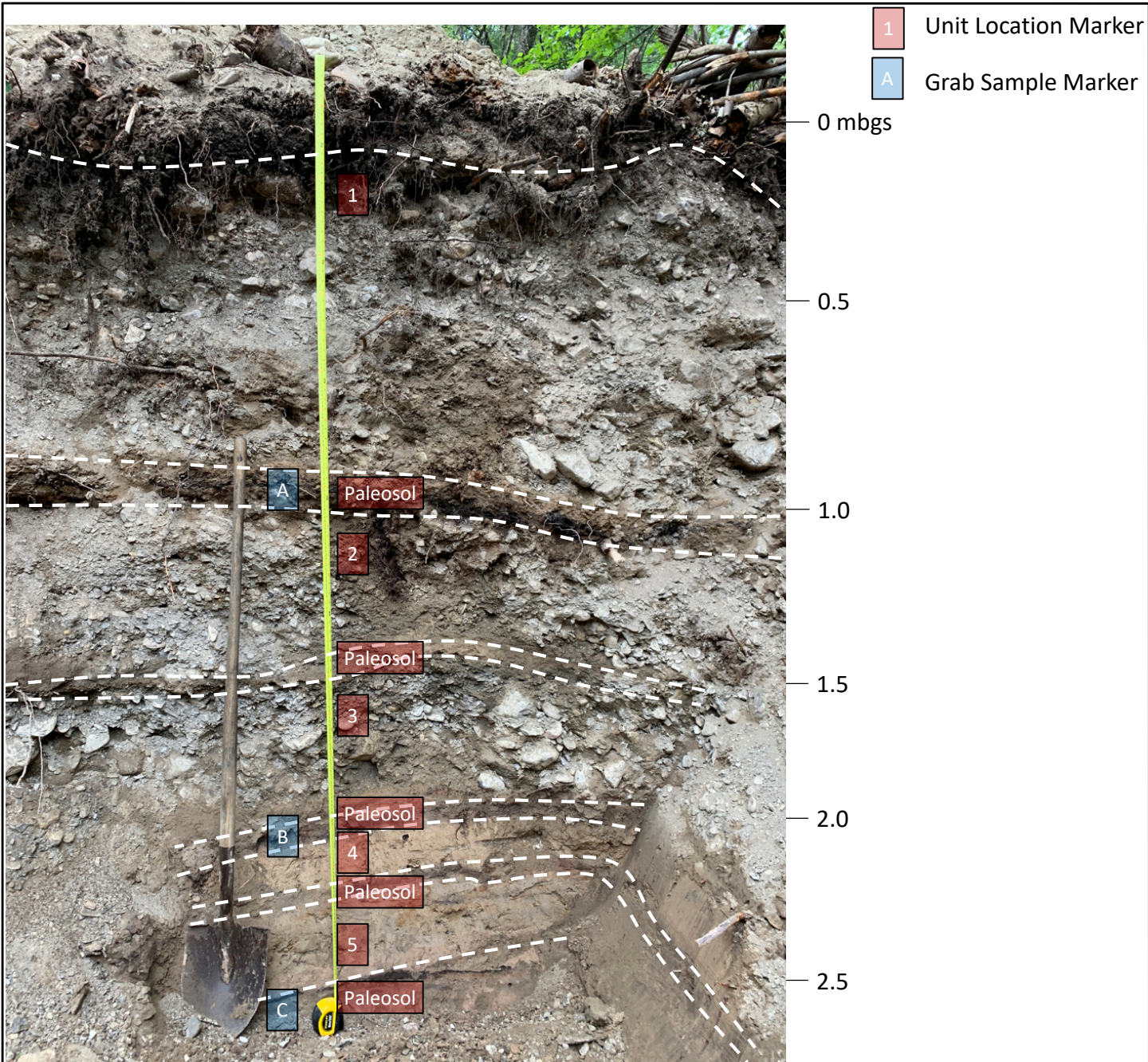
Project No. : 1572005

Survey Method : GPS  
 Coordinates : 581,219.E, 5,576,446.N  
 Ground Elevation (m) :838  
 Datum : NAD83

Start Date : 09 Jul 20  
 Finish Date : 09 Jul 20  
 Final Depth of Pit (m) : 2.8  
 Logged by : MJ  
 Reviewed by : BCP

Depth (m)	Symbol	Sample Material for Dating	Sample Age	Lithologic Description
0				O-HORIZON Black, abundant rootlets.
				UNIT 1: DEBRIS-FLOW DEPOSIT Gravel and boulder clasts, sandy matrix, some rootlets, poorly graded, compact to dense, subangular to subrounded clasts, light brown, dry, heterogenous, no cementation, random clast orientation, matrix supported, Dmax = 350 mm, Dmean = 50 mm.
				UNIT 2: DEBRIS-FLOW DEPOSIT Gravel and boulder clasts, sandy matrix, some rootlets, poorly graded, compact to dense, subangular to subrounded clasts, light brown, dry, heterogenous, no cementation, random clast orientation, matrix supported, Dmax = 250 mm, Dmean = 30 mm.
		A Paleosol w. charcoal (1.1 m)	412 - 315 cal BP	PALEOSOL Sand with abundant charcoal, some modern roots.
				UNIT 3: DEBRIS FLOW DEPOSIT Gravel and boulder clasts, sandy matrix, poorly graded, compact to dense, subangular to subrounded clasts, light brown, dry, heterogenous, no cementation, random clast orientation, matrix supported, bordering on debris flood process but no imbrication or stratification, Dmax = 150 mm, Dmean = 10 mm.
				PALEOSOL Fine sand, no charcoal.
				UNIT 4: DEBRIS-FLOW DEPOSIT Gravel and boulder clasts, sandy matrix, poorly graded, compact to dense, subangular to subrounded clasts, light brown, dry, heterogenous, no cementation, random clast orientation, matrix supported.
2		B Paleosol w. charcoal (2.0 m)	1870 - 1720 cal BP	PALEOSOL Fine to medium sand, some charcoal.
				UNIT 5: OVERBANK DEPOSIT Sand, fine grained, silty.
				PALEOSOL Sand, some charcoal.
				UNIT 6: OVERBANK DEPOSIT Sand, fine grained, silty, lower most 10 cm reddish (burned or oxidized).
		C Paleosol (2.7 m)	3399 - 3240 cal BP	PALEOSOL Sand, very well defined dark brown to black organic horizon.
3				END OF TEST PIT 2.8 m.
4				

RDEK (STRAT)\_COLL1.RDEK.GDL BGC.GDT 8/9/20



1. THIS FIGURE IS TO BE READ IN CONJUNCTION WITH THE REPORT ENTITLED "COLD SPRING CREEK HAZARD ASSESSMENT" AND DATED SEPTEMBER 2020.
2. UNLESS BGC AGREES OTHERWISE IN WRITING, THIS FIGURE SHALL NOT BE MODIFIED OR USED FOR ANY PURPOSE OTHER THAN THE PURPOSE FOR WHICH BGC GENERATED IT. BGC SHALL HAVE NO LIABILITY FOR ANY DAMAGES OR LOSS ARISING IN ANY WAY FROM ANY USE OR MODIFICATION OF THIS DOCUMENT NOT AUTHORIZED BY BGC. ANY USE OF OR RELIANCE UPON THIS DOCUMENT OR ITS CONTENT BY THIRD PARTIES SHALL BE AT SUCH THIRD PARTIES' SOLE RISK.

SCALE:	DATE: 09-2020	PREPARED BY: BCP	CHECKED BY: MJ	APPROVED BY: HW
		REPORT TITLE: COLD SPRING CREEK HAZARD ASSESSMENT		
		FIGURE TITLE: BGC-TP-03		
		PROJECT NO: 1572-005	FIGURE NO: A-3	

Test Pit BGC-TP-04

Project: Cold Spring Creek Hazard Assessment Update

Location : Riverview Road

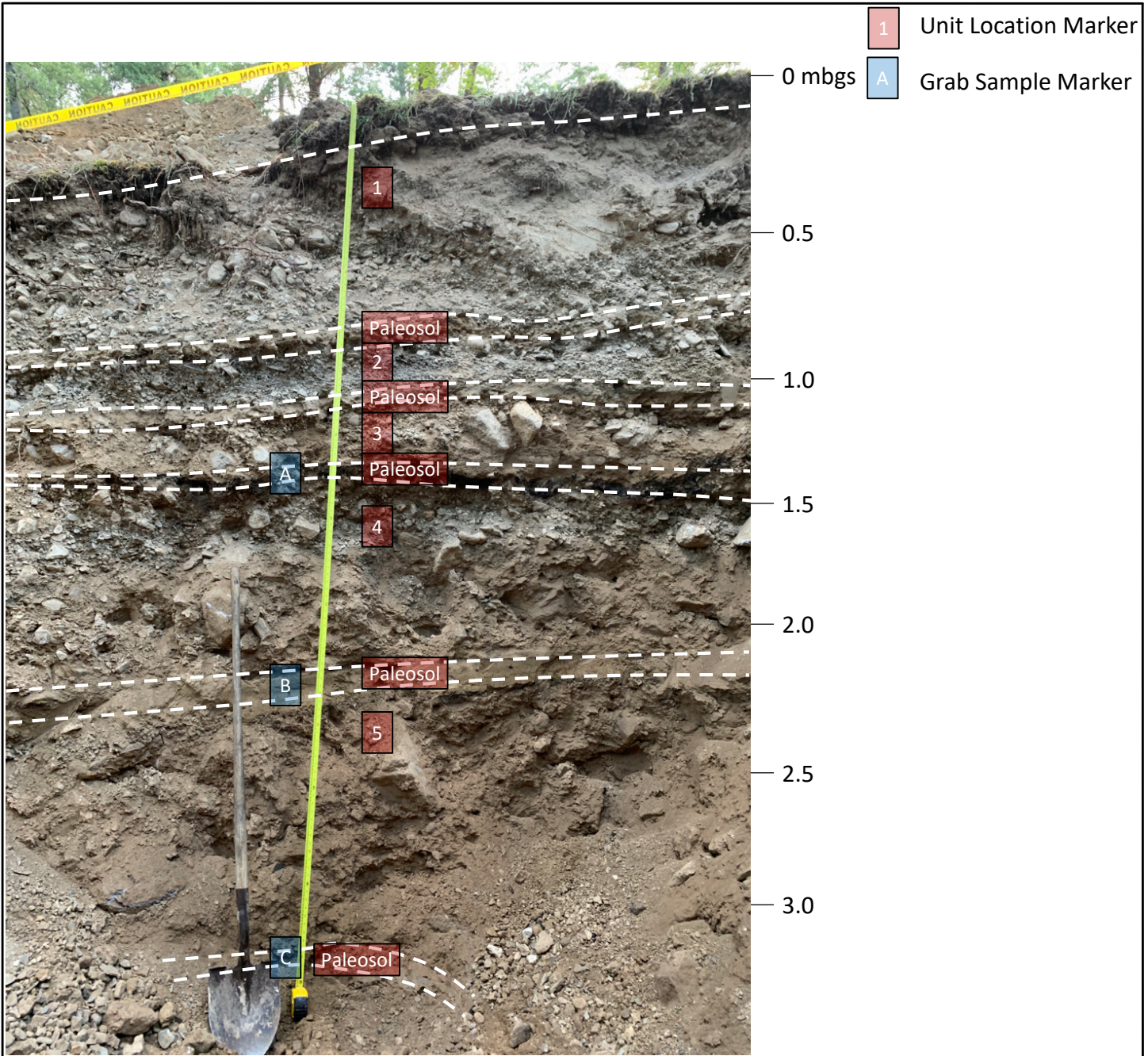
Project No. : 1572005

Survey Method : GPS  
 Coordinates : 581,088.E, 5,576,716.N  
 Ground Elevation (m) :834  
 Datum : NAD83

Start Date : 09 Jul 20  
 Finish Date : 09 Jul 20  
 Final Depth of Pit (m) : 3.2  
 Logged by : MJ  
 Reviewed by : BCP

Depth (m)	Symbol	Sample Material for Dating	Sample Age	Lithologic Description
0				O-HORIZON Abundant rootlets
0.5				UNIT 1: DEBRIS-FLOW DEPOSIT Gravel, coarse, some boulders, sandy matrix, poorly graded, compact to dense, subangular (larger clasts) to angular (smaller clasts), light brown, dry, heterogeneous, no cementation, random clast orientation, matrix supported, Dmax = 700 mm, Dmean = 60 mm.
0.8				PALEOSOL Sand, silty, poorly developed, dry, discontinuous, no charcoal or visible organics.
1.0				UNIT 2: DEBRIS-FLOOD DEPOSIT Gravel, fine, loose to compact, angular to subangular, grey, dry, imbricated, Dmax = 60 mm, Dmean = 10 mm.
1.2				PALEOSOL Sand, silty, dry, discontinuous, some fine-grained organics.
1.4		A Charcoal (1.4 m)	1900 - 1770 cal BP	
1.5				UNIT 3: DEBRIS-FLOW/FLOOD HYBRID DEPOSIT Gravel, fine, loose to compact, angular to subangular, grey, dry, imbricated, Dmax = 250 mm, Dmean = 15 mm.
1.8				PALEOSOL Complex paleosol sequence with 1 cm soil overlying B-horizon, then pronounced black organic-rich charcoal.
2.0				UNIT 4: DEBRIS-FLOW DEPOSIT Gravel, coarse, some boulders, sandy matrix, poorly graded, compact to dense, subangular (larger clasts) to angular (smaller clasts), light brown, dry, heterogeneous, no cementation, random clast orientation, matrix-supported, Dmax = 300 mm, Dmean = 40 mm.
2.3		B Organics (2.3 m)	3158 - 2960 cal BP	
2.5				PALEOSOL Complex paleosol sequence of 0.5 cm well-defined organic-rich layer, underlain by 20 cm silty sand, underlain by 1 cm thick organic-rich layer.
2.8				UNIT 5: DEBRIS-FLOW DEPOSIT Gravel, coarse, some boulders, sandy matrix, poorly graded, compact to dense, subangular (larger clasts) to angular (smaller clasts), dark grey, moist, heterogeneous, no cementation, random clast orientation, matrix supported, Dmax = 400 mm, Dmean = 50 mm.
3.1		C Organics and charcoal (3.1 m)	2643 - 2491 cal BP	
3.2				PALEOSOL Some organics and charcoal. END OF TEST PIT 3.2 m.
4				

RDEK (STRAT\_COOL) RDEK.GDL BGC.GDT 8/9/20



1 Unit Location Marker  
 A Grab Sample Marker

0 mbgs  
 0.5  
 1.0  
 1.5  
 2.0  
 2.5  
 3.0

1. THIS FIGURE IS TO BE READ IN CONJUNCTION WITH THE REPORT ENTITLED "COLD SPRING CREEK HAZARD ASSESSMENT" AND DATED SEPTEMBER 2020.
2. UNLESS BGC AGREES OTHERWISE IN WRITING, THIS FIGURE SHALL NOT BE MODIFIED OR USED FOR ANY PURPOSE OTHER THAN THE PURPOSE FOR WHICH BGC GENERATED IT. BGC SHALL HAVE NO LIABILITY FOR ANY DAMAGES OR LOSS ARISING IN ANY WAY FROM ANY USE OR MODIFICATION OF THIS DOCUMENT NOT AUTHORIZED BY BGC. ANY USE OF OR RELIANCE UPON THIS DOCUMENT OR ITS CONTENT BY THIRD PARTIES SHALL BE AT SUCH THIRD PARTIES' SOLE RISK.

SCALE:	DATE: 09-2020	PREPARED BY: BCP	CHECKED BY: MJ	APPROVED BY: HW
		REPORT TITLE: COLD SPRING CREEK HAZARD ASSESSMENT		
		FIGURE TITLE: BGC-TP-04		
		PROJECT NO: 1572-005	FIGURE NO: A-4	

0 5 10mm in ANSI A sized paper

Test Pit BGC-TP-05

Project: Cold Spring Creek Hazard Assessment Update

Location : Fairway Drive

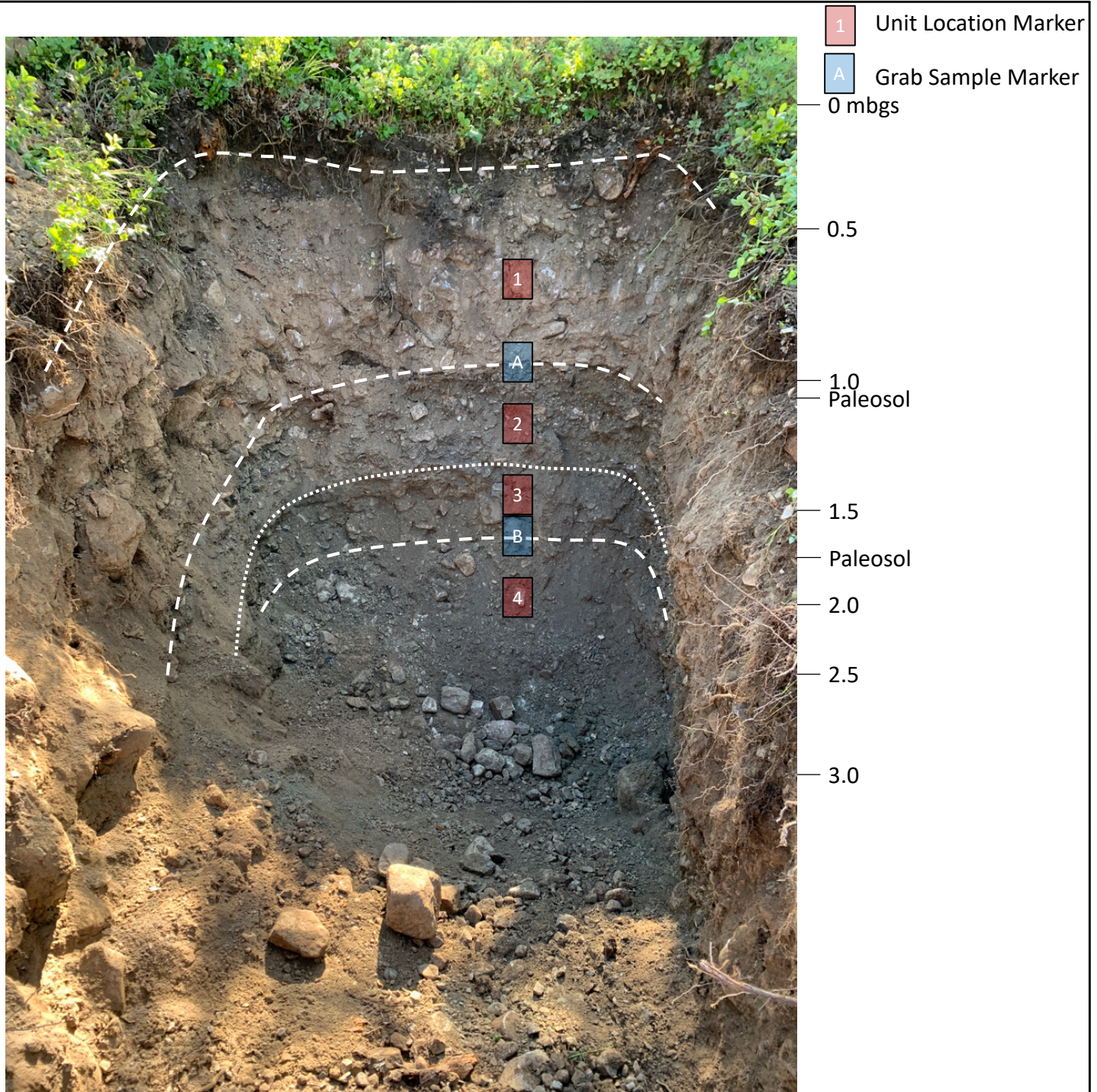
Project No. : 1572005

Survey Method : GPS  
 Coordinates : 581,801.E, 5,576,748.N  
 Ground Elevation (m) :898  
 Datum : NAD83

Start Date : 09 Jul 20  
 Finish Date : 09 Jul 20  
 Final Depth of Pit (m) : 2.9  
 Logged by : MJ  
 Reviewed by : BCP

Depth (m)	Symbol	Sample Material for Dating	Sample Age	Lithologic Description
0				O-HORIZON Dark brown to black organic soil, A-Horizon poorly distinguishable.
0.5				UNIT 1: DEBRIS-FLOW UNIT Cobble and boulder clasts, silty sand matrix, loose to compact, angular to subangular, light brown, moist, heterogeneous, no cementation, matrix supported, Dmax = 500 mm, Dmean = 200 mm.
1.1		A Charcoal (1.1 m)	1336 - 1256 cal BP	PALEOSOL Thin organic layer with some charcoal, continuous in pit, follows fan slope.
1.5				UNIT 2: DEBRIS-FLOW UNIT Cobble and boulder clasts, silty sand matrix, loose to compact, angular to subangular, light brown, moist, heterogeneous, no cementation, matrix supported, Dmax = 350 mm, Dmean = 40 mm.
2.0				UNIT 3: DEBRIS-FLOW UNIT Cobble and boulder clasts, silty sand matrix, loose, angular to subangular, light brown, moist, heterogeneous, no cementation, partially matrix supported, partially clast supported, Dmax = 350, Dmean = 40 mm.
2.2		B Organic (2.2 m)	3481 - 3367 cal BP	PALEOSOL Well-developed paleosol with distinct organic layer (1 cm) at base.
2.5				UNIT 4: DEBRIS-FLOW UNIT Cobble and boulder clasts, silty sand matrix, loose to compact, angular to subangular, light brown, moist, heterogeneous, no cementation, matrix-supported, Dmax = 500 mm, Dmean = 200 mm.
2.9				END OF TEST PIT 2.9 m.
3.0				
4.0				

RDEK ISTRAT\_COOL RDEK.GDL BGC.GDT 8/9/20



1. THIS FIGURE IS TO BE READ IN CONJUNCTION WITH THE REPORT ENTITLED "COLD SPRING CREEK HAZARD ASSESSMENT" AND DATED SEPTEMBER 2020.
2. UNLESS BGC AGREES OTHERWISE IN WRITING, THIS FIGURE SHALL NOT BE MODIFIED OR USED FOR ANY PURPOSE OTHER THAN THE PURPOSE FOR WHICH BGC GENERATED IT. BGC SHALL HAVE NO LIABILITY FOR ANY DAMAGES OR LOSS ARISING IN ANY WAY FROM ANY USE OR MODIFICATION OF THIS DOCUMENT NOT AUTHORIZED BY BGC. ANY USE OF OR RELIANCE UPON THIS DOCUMENT OR ITS CONTENT BY THIRD PARTIES SHALL BE AT SUCH THIRD PARTIES' SOLE RISK.

SCALE:	DATE: 09-2020	PREPARED BY: BCP	CHECKED BY: MJ	APPROVED BY: HW
		REPORT TITLE: COLD SPRING CREEK HAZARD ASSESSMENT		
		FIGURE TITLE: BGC-TP-05		
		PROJECT NO: 1572-005	FIGURE NO: A-5	

0 5 10mm in ANSI A sized paper

## **APPENDIX B RADIOCARBON SAMPLE RESULTS**



August 05, 2020

Ms. Emily Moase  
BGC Engineering  
500-980 Howe Street  
Vancouver, BC V6Z 0C8  
Canada

RE: Radiocarbon Dating Results

Dear Ms. Moase,

Enclosed are the radiocarbon dating results for ten samples recently sent to us. As usual, the method of analysis is listed on the report with the results and calibration data is provided where applicable. The Conventional Radiocarbon Ages have all been corrected for total fractionation effects and where applicable, calibration was performed using 2013 calibration databases (cited on the graph pages).

The web directory containing the table of results and PDF download also contains pictures, a cvs spreadsheet download option and a quality assurance report containing expected vs. measured values for 3-5 working standards analyzed simultaneously with your samples.

Reported results are accredited to ISO/IEC 17025:2005 Testing Accreditation PJLA #59423 standards and all chemistry was performed here in our laboratory and counted in our own accelerators here. Since Beta is not a teaching laboratory, only graduates trained to strict protocols of the ISO/IEC 17025:2005 Testing Accreditation PJLA #59423 program participated in the analyses.

As always Conventional Radiocarbon Ages and sigmas are rounded to the nearest 10 years per the conventions of the 1977 International Radiocarbon Conference. When counting statistics produce sigmas lower than +/- 30 years, a conservative +/- 30 BP is cited for the result. The reported  $\delta^{13}C$  values were measured separately in an IRMS (isotope ratio mass spectrometer). They are NOT the AMS  $\delta^{13}C$  which would include fractionation effects from natural, chemistry and AMS induced sources.

When interpreting the results, please consider any communications you may have had with us regarding the samples.

Thank you for prepaying the analyses. As always, if you have any questions or would like to discuss the results, don't hesitate to contact us.

Sincerely,

Digital signature on file

Chris Patrick  
Vice President of Laboratory Operations



ISO/IEC 17025:2005-Accredited Testing Laboratory

## REPORT OF RADIOCARBON DATING ANALYSES

Emily Moase

Report Date: August 05, 2020

BGC Engineering

Material Received: July 14, 2020

		Conventional Radiocarbon Age (BP) or Percent Modern Carbon (pMC) & Stable Isotopes
Laboratory Number	Sample Code Number	Calendar Calibrated Results: 95.4 % Probability High Probability Density Range Method (HPD)

<b>Beta - 563281</b>	<b>BGC20-TP2A</b>	<b>1200 +/- 30 BP</b>	<b>IRMS δ13C: -23.9 o/oo</b>
	<b>(87.9%) 765 - 895 cal AD</b>	<b>(1185 - 1055 cal BP)</b>	
	<b>( 6.1%) 714 - 744 cal AD</b>	<b>(1236 - 1206 cal BP)</b>	
	<b>( 1.5%) 928 - 940 cal AD</b>	<b>(1022 - 1010 cal BP)</b>	

Submitter Material: Organics  
 Pretreatment: (charred material) acid/alkali/acid  
 Analyzed Material: Charred material  
 Analysis Service: AMS-Standard delivery  
 Percent Modern Carbon: 86.12 +/- 0.32 pMC  
 Fraction Modern Carbon: 0.8612 +/- 0.0032  
 D14C: -138.76 +/- 3.22 o/oo  
 Δ14C: -146.02 +/- 3.22 o/oo (1950:2020)  
 Measured Radiocarbon Age: (without d13C correction): 1180 +/- 30 BP  
 Calibration: BetaCal3.21: HPD method: INTCAL13

Results are ISO/IEC-17025:2005 accredited. No sub-contracting or student labor was used in the analyses. All work was done at Beta in 4 in-house NEC accelerator mass spectrometers and 4 Thermo IRMSs. The "Conventional Radiocarbon Age" was calculated using the Libby half-life (5568 years), is corrected for total isotopic fraction and was used for calendar calibration where applicable. The Age is rounded to the nearest 10 years and is reported as radiocarbon years before present (BP), "present" = AD 1950. Results greater than the modern reference are reported as percent modern carbon (pMC). The modern reference standard was 95% the 14C signature of NIST SRM-4990C (oxalic acid). Quoted errors are 1 sigma counting statistics. Calculated sigmas less than 30 BP on the Conventional Radiocarbon Age are conservatively rounded up to 30. d13C values are on the material itself (not the AMS d13C). d13C and d15N values are relative to VPDB-1. References for calendar calibrations are cited at the bottom of calibration graph pages.



ISO/IEC 17025:2005-Accredited Testing Laboratory

## REPORT OF RADIOCARBON DATING ANALYSES

Emily Moase

Report Date: August 05, 2020

BGC Engineering

Material Received: July 14, 2020

		Conventional Radiocarbon Age (BP) or Percent Modern Carbon (pMC) & Stable Isotopes
Laboratory Number	Sample Code Number	Calendar Calibrated Results: 95.4 % Probability High Probability Density Range Method (HPD)

<b>Beta - 563282</b>	<b>BGC20-TP-2B</b>	<b>1260 +/- 30 BP</b>	<b>IRMS δ13C: -27.0 o/oo</b>
----------------------	--------------------	-----------------------	------------------------------

(85.1%)	<b>668 - 778 cal AD</b>	(1282 - 1172 cal BP)
( 6.0%)	<b>790 - 828 cal AD</b>	(1160 - 1122 cal BP)
( 4.3%)	<b>838 - 864 cal AD</b>	(1112 - 1086 cal BP)

Submitter Material: Charcoal  
 Pretreatment: (charred material) acid/alkali/acid  
 Analyzed Material: Charred material  
 Analysis Service: AMS-Standard delivery  
 Percent Modern Carbon: 85.48 +/- 0.32 pMC  
 Fraction Modern Carbon: 0.8548 +/- 0.0032  
 D14C: -145.17 +/- 3.19 o/oo  
 Δ14C: -152.38 +/- 3.19 o/oo (1950:2020)  
 Measured Radiocarbon Age: (without d13C correction): 1290 +/- 30 BP  
 Calibration: BetaCal3.21: HPD method: INTCAL13

Results are ISO/IEC-17025:2005 accredited. No sub-contracting or student labor was used in the analyses. All work was done at Beta in 4 in-house NEC accelerator mass spectrometers and 4 Thermo IRMSs. The "Conventional Radiocarbon Age" was calculated using the Libby half-life (5568 years), is corrected for total isotopic fraction and was used for calendar calibration where applicable. The Age is rounded to the nearest 10 years and is reported as radiocarbon years before present (BP), "present" = AD 1950. Results greater than the modern reference are reported as percent modern carbon (pMC). The modern reference standard was 95% the 14C signature of NIST SRM-4990C (oxalic acid). Quoted errors are 1 sigma counting statistics. Calculated sigmas less than 30 BP on the Conventional Radiocarbon Age are conservatively rounded up to 30. d13C values are on the material itself (not the AMS d13C). d13C and d15N values are relative to VPDB-1. References for calendar calibrations are cited at the bottom of calibration graph pages.



## REPORT OF RADIOCARBON DATING ANALYSES

Emily Moase

Report Date: August 05, 2020

BGC Engineering

Material Received: July 14, 2020

		Conventional Radiocarbon Age (BP) or Percent Modern Carbon (pMC) & Stable Isotopes
Laboratory Number	Sample Code Number	Calendar Calibrated Results: 95.4 % Probability High Probability Density Range Method (HPD)

<b>Beta - 563283</b>	<b>BGC20-TP-3A</b>	<b>350 +/- 30 BP</b>	<b>IRMS δ13C: -26.0 o/oo</b>
----------------------	--------------------	----------------------	------------------------------

(54.2%)	1538 - 1635 cal AD	(412 - 315 cal BP)
(41.2%)	1458 - 1530 cal AD	(492 - 420 cal BP)

Submitter Material: Charcoal  
 Pretreatment: (charred material) acid/alkali/acid  
 Analyzed Material: Charred material  
 Analysis Service: AMS-Standard delivery  
 Percent Modern Carbon: 95.74 +/- 0.36 pMC  
 Fraction Modern Carbon: 0.9574 +/- 0.0036  
 D14C: -42.64 +/- 3.58 o/oo  
 Δ14C: -50.71 +/- 3.58 o/oo (1950:2020)  
 Measured Radiocarbon Age: (without d13C correction): 370 +/- 30 BP  
 Calibration: BetaCal3.21: HPD method: INTCAL13

Results are ISO/IEC-17025:2005 accredited. No sub-contracting or student labor was used in the analyses. All work was done at Beta in 4 in-house NEC accelerator mass spectrometers and 4 Thermo IRMSs. The "Conventional Radiocarbon Age" was calculated using the Libby half-life (5568 years), is corrected for total isotopic fraction and was used for calendar calibration where applicable. The Age is rounded to the nearest 10 years and is reported as radiocarbon years before present (BP), "present" = AD 1950. Results greater than the modern reference are reported as percent modern carbon (pMC). The modern reference standard was 95% the 14C signature of NIST SRM-4990C (oxalic acid). Quoted errors are 1 sigma counting statistics. Calculated sigmas less than 30 BP on the Conventional Radiocarbon Age are conservatively rounded up to 30. d13C values are on the material itself (not the AMS d13C). d13C and d15N values are relative to VPDB-1. References for calendar calibrations are cited at the bottom of calibration graph pages.



## REPORT OF RADIOCARBON DATING ANALYSES

Emily Moase

Report Date: August 05, 2020

BGC Engineering

Material Received: July 14, 2020

Laboratory Number	Sample Code Number	Conventional Radiocarbon Age (BP) or Percent Modern Carbon (pMC) & Stable Isotopes	
		Calendar Calibrated Results: 95.4 % Probability High Probability Density Range Method (HPD)	

**Beta - 563284**

**BGC20-TP-3B**

**1860 +/- 30 BP**

**IRMS  $\delta^{13}C$ : -28.5 o/oo**

**(95.4%)**

**80 - 230 cal AD**

**(1870 - 1720 cal BP)**

Submitter Material: Charcoal

Pretreatment: (charred material) acid/alkali/acid

Analyzed Material: Charred material

Analysis Service: AMS-Standard delivery

Percent Modern Carbon: 79.33 +/- 0.30 pMC

Fraction Modern Carbon: 0.7933 +/- 0.0030

D14C: -206.69 +/- 2.96 o/oo

$\Delta^{14}C$ : -213.38 +/- 2.96 o/oo (1950:2020)

Measured Radiocarbon Age: (without  $\delta^{13}C$  correction): 1920 +/- 30 BP

Calibration: BetaCal3.21: HPD method: INTCAL13

Results are ISO/IEC-17025:2005 accredited. No sub-contracting or student labor was used in the analyses. All work was done at Beta in 4 in-house NEC accelerator mass spectrometers and 4 Thermo IRMSs. The "Conventional Radiocarbon Age" was calculated using the Libby half-life (5568 years), is corrected for total isotopic fraction and was used for calendar calibration where applicable. The Age is rounded to the nearest 10 years and is reported as radiocarbon years before present (BP), "present" = AD 1950. Results greater than the modern reference are reported as percent modern carbon (pMC). The modern reference standard was 95% the  $^{14}C$  signature of NIST SRM-4990C (oxalic acid). Quoted errors are 1 sigma counting statistics. Calculated sigmas less than 30 BP on the Conventional Radiocarbon Age are conservatively rounded up to 30.  $\delta^{13}C$  values are on the material itself (not the AMS  $\delta^{13}C$ ).  $\delta^{13}C$  and  $\delta^{15}N$  values are relative to VPDB-1. References for calendar calibrations are cited at the bottom of calibration graph pages.



## REPORT OF RADIOCARBON DATING ANALYSES

Emily Moase

Report Date: August 05, 2020

BGC Engineering

Material Received: July 14, 2020

Laboratory Number	Sample Code Number	Conventional Radiocarbon Age (BP) or Percent Modern Carbon (pMC) & Stable Isotopes	
		Calendar Calibrated Results: 95.4 % Probability High Probability Density Range Method (HPD)	

**Beta - 563285**

**BGC20-TP-3C**

**3120 +/- 30 BP**

**IRMS δ13C: -28.6 o/oo**

**(95.4%)**

**1450 - 1291 cal BC**

**(3399 - 3240 cal BP)**

Submitter Material: Charcoal

Pretreatment: (charred material) acid/alkali/acid

Analyzed Material: Charred material

Analysis Service: AMS-Standard delivery

Percent Modern Carbon: 67.81 +/- 0.25 pMC

Fraction Modern Carbon: 0.6781 +/- 0.0025

D14C: -321.86 +/- 2.53 o/oo

Δ14C: -327.58 +/- 2.53 o/oo (1950:2020)

Measured Radiocarbon Age: (without d13C correction): 3180 +/- 30 BP

Calibration: BetaCal3.21: HPD method: INTCAL13

Results are ISO/IEC-17025:2005 accredited. No sub-contracting or student labor was used in the analyses. All work was done at Beta in 4 in-house NEC accelerator mass spectrometers and 4 Thermo IRMSs. The "Conventional Radiocarbon Age" was calculated using the Libby half-life (5568 years), is corrected for total isotopic fraction and was used for calendar calibration where applicable. The Age is rounded to the nearest 10 years and is reported as radiocarbon years before present (BP), "present" = AD 1950. Results greater than the modern reference are reported as percent modern carbon (pMC). The modern reference standard was 95% the 14C signature of NIST SRM-4990C (oxalic acid). Quoted errors are 1 sigma counting statistics. Calculated sigmas less than 30 BP on the Conventional Radiocarbon Age are conservatively rounded up to 30. d13C values are on the material itself (not the AMS d13C). d13C and d15N values are relative to VPDB-1. References for calendar calibrations are cited at the bottom of calibration graph pages.



## REPORT OF RADIOCARBON DATING ANALYSES

Emily Moase

Report Date: August 05, 2020

BGC Engineering

Material Received: July 14, 2020

Laboratory Number	Sample Code Number	Conventional Radiocarbon Age (BP) or Percent Modern Carbon (pMC) & Stable Isotopes	
		Calendar Calibrated Results: 95.4 % Probability High Probability Density Range Method (HPD)	

<b>Beta - 563286</b>	<b>BGC20-TP-4A</b>	<b>1900 +/- 30 BP</b>	<b>IRMS δ13C: -22.5 o/oo</b>
----------------------	--------------------	-----------------------	------------------------------

<b>(88.4%)</b>	<b>50 - 180 cal AD</b>	<b>(1900 - 1770 cal BP)</b>
<b>( 5.1%)</b>	<b>186 - 214 cal AD</b>	<b>(1764 - 1736 cal BP)</b>
<b>( 1.9%)</b>	<b>28 - 39 cal AD</b>	<b>(1922 - 1911 cal BP)</b>

Submitter Material: Organics  
 Pretreatment: (charred material) acid/alkali/acid  
 Analyzed Material: Charred material  
 Analysis Service: AMS-Standard delivery  
 Percent Modern Carbon: 78.94 +/- 0.29 pMC  
 Fraction Modern Carbon: 0.7894 +/- 0.0029  
 D14C: -210.64 +/- 2.95 o/oo  
 Δ14C: -217.29 +/- 2.95 o/oo (1950:2020)  
 Measured Radiocarbon Age: (without d13C correction): 1860 +/- 30 BP  
 Calibration: BetaCal3.21: HPD method: INTCAL13

Results are ISO/IEC-17025:2005 accredited. No sub-contracting or student labor was used in the analyses. All work was done at Beta in 4 in-house NEC accelerator mass spectrometers and 4 Thermo IRMSs. The "Conventional Radiocarbon Age" was calculated using the Libby half-life (5568 years), is corrected for total isotopic fraction and was used for calendar calibration where applicable. The Age is rounded to the nearest 10 years and is reported as radiocarbon years before present (BP), "present" = AD 1950. Results greater than the modern reference are reported as percent modern carbon (pMC). The modern reference standard was 95% the 14C signature of NIST SRM-4990C (oxalic acid). Quoted errors are 1 sigma counting statistics. Calculated sigmas less than 30 BP on the Conventional Radiocarbon Age are conservatively rounded up to 30. d13C values are on the material itself (not the AMS d13C). d13C and d15N values are relative to VPDB-1. References for calendar calibrations are cited at the bottom of calibration graph pages.



## REPORT OF RADIOCARBON DATING ANALYSES

Emily Moase

Report Date: August 05, 2020

BGC Engineering

Material Received: July 14, 2020

Laboratory Number	Sample Code Number	Conventional Radiocarbon Age (BP) or Percent Modern Carbon (pMC) & Stable Isotopes	
		Calendar Calibrated Results: 95.4 % Probability High Probability Density Range Method (HPD)	

**Beta - 563287**

**BGC20-TP-4B**

**2910 +/- 30 BP**

**IRMS  $\delta^{13}C$ : -24.5 o/oo**

**(95.4%)**

**1209 - 1011 cal BC**

**(3158 - 2960 cal BP)**

Submitter Material: Organics

Pretreatment: (organic sediment) acid washes

Analyzed Material: Organic sediment

Analysis Service: AMS-Standard delivery

Percent Modern Carbon: 69.61 +/- 0.26 pMC

Fraction Modern Carbon: 0.6961 +/- 0.0026

D14C: -303.90 +/- 2.60 o/oo

$\Delta^{14}C$ : -309.77 +/- 2.60 o/oo (1950:2020)

Measured Radiocarbon Age: (without  $\delta^{13}C$  correction): 2900 +/- 30 BP

Calibration: BetaCal3.21: HPD method: INTCAL13

Results are ISO/IEC-17025:2005 accredited. No sub-contracting or student labor was used in the analyses. All work was done at Beta in 4 in-house NEC accelerator mass spectrometers and 4 Thermo IRMSs. The "Conventional Radiocarbon Age" was calculated using the Libby half-life (5568 years), is corrected for total isotopic fraction and was used for calendar calibration where applicable. The Age is rounded to the nearest 10 years and is reported as radiocarbon years before present (BP), "present" = AD 1950. Results greater than the modern reference are reported as percent modern carbon (pMC). The modern reference standard was 95% the  $^{14}C$  signature of NIST SRM-4990C (oxalic acid). Quoted errors are 1 sigma counting statistics. Calculated sigmas less than 30 BP on the Conventional Radiocarbon Age are conservatively rounded up to 30.  $\delta^{13}C$  values are on the material itself (not the AMS  $\delta^{13}C$ ).  $\delta^{13}C$  and  $\delta^{15}N$  values are relative to VPDB-1. References for calendar calibrations are cited at the bottom of calibration graph pages.



## REPORT OF RADIOCARBON DATING ANALYSES

Emily Moase

Report Date: August 05, 2020

BGC Engineering

Material Received: July 14, 2020

		Conventional Radiocarbon Age (BP) or Percent Modern Carbon (pMC) & Stable Isotopes
Laboratory Number	Sample Code Number	Calendar Calibrated Results: 95.4 % Probability High Probability Density Range Method (HPD)

<b>Beta - 563288</b>	<b>BGC20-TP-4C</b>	<b>2520 +/- 30 BP</b>	<b>IRMS δ13C: -24.3 o/oo</b>
----------------------	--------------------	-----------------------	------------------------------

(65.1%)	694 - 542 cal BC	(2643 - 2491 cal BP)
(29.2%)	795 - 728 cal BC	(2744 - 2677 cal BP)
( 1.1%)	717 - 707 cal BC	(2666 - 2656 cal BP)

Submitter Material: Charcoal  
 Pretreatment: (charred material) acid/alkali/acid  
 Analyzed Material: Charred material  
 Analysis Service: AMS-Standard delivery  
 Percent Modern Carbon: 73.07 +/- 0.27 pMC  
 Fraction Modern Carbon: 0.7307 +/- 0.0027  
 D14C: -269.27 +/- 2.73 o/oo  
 Δ14C: -275.43 +/- 2.73 o/oo (1950:2020)  
 Measured Radiocarbon Age: (without d13C correction): 2510 +/- 30 BP  
 Calibration: BetaCal3.21: HPD method: INTCAL13

Results are ISO/IEC-17025:2005 accredited. No sub-contracting or student labor was used in the analyses. All work was done at Beta in 4 in-house NEC accelerator mass spectrometers and 4 Thermo IRMSs. The "Conventional Radiocarbon Age" was calculated using the Libby half-life (5568 years), is corrected for total isotopic fraction and was used for calendar calibration where applicable. The Age is rounded to the nearest 10 years and is reported as radiocarbon years before present (BP), "present" = AD 1950. Results greater than the modern reference are reported as percent modern carbon (pMC). The modern reference standard was 95% the 14C signature of NIST SRM-4990C (oxalic acid). Quoted errors are 1 sigma counting statistics. Calculated sigmas less than 30 BP on the Conventional Radiocarbon Age are conservatively rounded up to 30. d13C values are on the material itself (not the AMS d13C). d13C and d15N values are relative to VPDB-1. References for calendar calibrations are cited at the bottom of calibration graph pages.



## REPORT OF RADIOCARBON DATING ANALYSES

Emily Moase

Report Date: August 05, 2020

BGC Engineering

Material Received: July 14, 2020

		Conventional Radiocarbon Age (BP) or Percent Modern Carbon (pMC) & Stable Isotopes
Laboratory Number	Sample Code Number	Calendar Calibrated Results: 95.4 % Probability High Probability Density Range Method (HPD)

<b>Beta - 563289</b>	<b>BGC20-TP-5A</b>	<b>1360 +/- 30 BP</b>	<b>IRMS δ13C: -23.9 o/oo</b>
----------------------	--------------------	-----------------------	------------------------------

(92.1%)	<b>614 - 694 cal AD</b>	<b>(1336 - 1256 cal BP)</b>
( 3.3%)	<b>747 - 763 cal AD</b>	<b>(1203 - 1187 cal BP)</b>

Submitter Material: Organics  
 Pretreatment: (organic sediment) acid washes  
 Analyzed Material: Organic sediment  
 Analysis Service: AMS-Standard delivery  
 Percent Modern Carbon: 84.43 +/- 0.32 pMC  
 Fraction Modern Carbon: 0.8443 +/- 0.0032  
 D14C: -155.75 +/- 3.15 o/oo  
 Δ14C: -162.87 +/- 3.15 o/oo (1950:2020)  
 Measured Radiocarbon Age: (without d13C correction): 1340 +/- 30 BP  
 Calibration: BetaCal3.21: HPD method: INTCAL13

Results are ISO/IEC-17025:2005 accredited. No sub-contracting or student labor was used in the analyses. All work was done at Beta in 4 in-house NEC accelerator mass spectrometers and 4 Thermo IRMSs. The "Conventional Radiocarbon Age" was calculated using the Libby half-life (5568 years), is corrected for total isotopic fraction and was used for calendar calibration where applicable. The Age is rounded to the nearest 10 years and is reported as radiocarbon years before present (BP), "present" = AD 1950. Results greater than the modern reference are reported as percent modern carbon (pMC). The modern reference standard was 95% the 14C signature of NIST SRM-4990C (oxalic acid). Quoted errors are 1 sigma counting statistics. Calculated sigmas less than 30 BP on the Conventional Radiocarbon Age are conservatively rounded up to 30. d13C values are on the material itself (not the AMS d13C). d13C and d15N values are relative to VPDB-1. References for calendar calibrations are cited at the bottom of calibration graph pages.



ISO/IEC 17025:2005-Accredited Testing Laboratory

## REPORT OF RADIOCARBON DATING ANALYSES

Emily Moase

Report Date: August 05, 2020

BGC Engineering

Material Received: July 14, 2020

Laboratory Number	Sample Code Number	Conventional Radiocarbon Age (BP) or Percent Modern Carbon (pMC) & Stable Isotopes	
		Calendar Calibrated Results: 95.4 % Probability High Probability Density Range Method (HPD)	

**Beta - 563290**

**BGC20-TP-5B**

**3210 +/- 30 BP**

**IRMS δ13C: -24.4 o/oo**

**(94.6%)                      1532 - 1418 cal BC                      (3481 - 3367 cal BP)**  
**( 0.8%)                      1595 - 1589 cal BC                      (3544 - 3538 cal BP)**

Submitter Material: Organics  
Pretreatment: (organic sediment) acid washes  
Analyzed Material: Organic sediment  
Analysis Service: AMS-Standard delivery  
Percent Modern Carbon: 67.06 +/- 0.25 pMC  
Fraction Modern Carbon: 0.6706 +/- 0.0025  
D14C: -329.42 +/- 2.50 o/oo  
Δ14C: -335.07 +/- 2.50 o/oo (1950:2020)  
Measured Radiocarbon Age: (without d13C correction): 3200 +/- 30 BP  
Calibration: BetaCal3.21: HPD method: INTCAL13

Results are ISO/IEC-17025:2005 accredited. No sub-contracting or student labor was used in the analyses. All work was done at Beta in 4 in-house NEC accelerator mass spectrometers and 4 Thermo IRMSs. The "Conventional Radiocarbon Age" was calculated using the Libby half-life (5568 years), is corrected for total isotopic fraction and was used for calendar calibration where applicable. The Age is rounded to the nearest 10 years and is reported as radiocarbon years before present (BP), "present" = AD 1950. Results greater than the modern reference are reported as percent modern carbon (pMC). The modern reference standard was 95% the 14C signature of NIST SRM-4990C (oxalic acid). Quoted errors are 1 sigma counting statistics. Calculated sigmas less than 30 BP on the Conventional Radiocarbon Age are conservatively rounded up to 30. d13C values are on the material itself (not the AMS d13C). d13C and d15N values are relative to VPDB-1. References for calendar calibrations are cited at the bottom of calibration graph pages.

# Calibration of Radiocarbon Age to Calendar Years

(High Probability Density Range Method (HPD): INTCAL13)

(Variables:  $\delta^{13}\text{C} = -23.9$  o/oo)

Laboratory number    **Beta-563281**

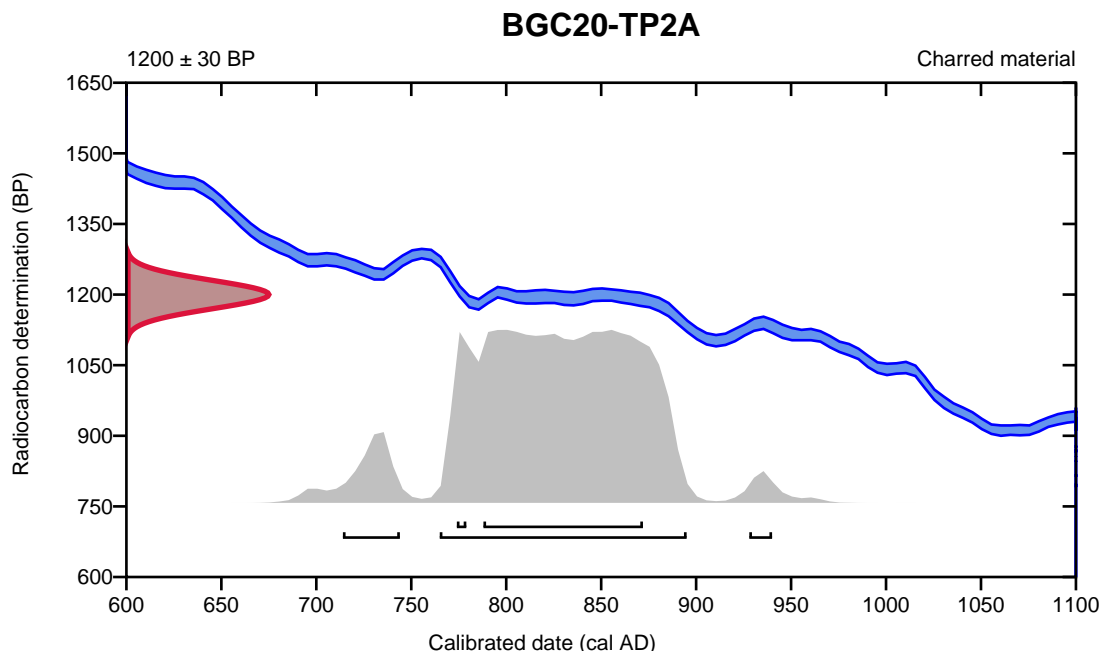
Conventional radiocarbon age    **1200 ± 30 BP**

95.4% probability

(87.9%)	765 - 895 cal AD	(1185 - 1055 cal BP)
(6.1%)	714 - 744 cal AD	(1236 - 1206 cal BP)
(1.5%)	928 - 940 cal AD	(1022 - 1010 cal BP)

68.2% probability

(64.8%)	788 - 872 cal AD	(1162 - 1078 cal BP)
(3.4%)	774 - 779 cal AD	(1176 - 1171 cal BP)



**Database used**  
INTCAL13

## References

### References to Probability Method

Bronk Ramsey, C. (2009). Bayesian analysis of radiocarbon dates. *Radiocarbon*, 51(1), 337-360.

### References to Database INTCAL13

Reimer, et.al., 2013, *Radiocarbon*55(4).

# Calibration of Radiocarbon Age to Calendar Years

(High Probability Density Range Method (HPD): INTCAL13)

(Variables:  $\delta^{13}\text{C} = -27.0$  o/oo)

**Laboratory number**      **Beta-563282**

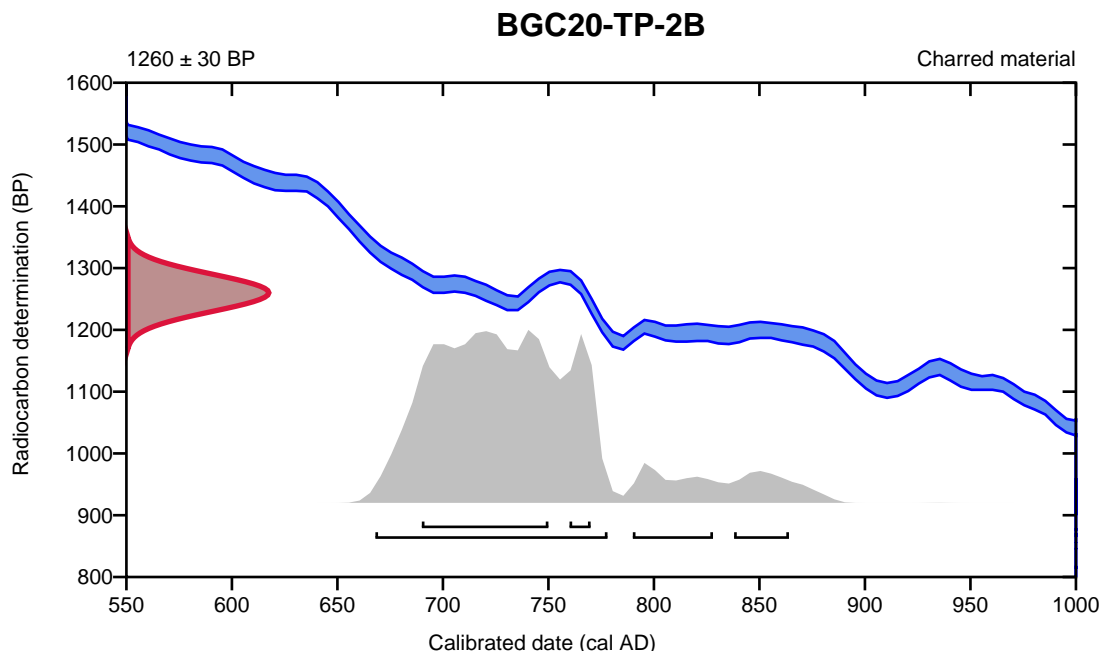
**Conventional radiocarbon age**      **1260 ± 30 BP**

95.4% probability

(85.1%)	668 - 778 cal AD	(1282 - 1172 cal BP)
(6%)	790 - 828 cal AD	(1160 - 1122 cal BP)
(4.3%)	838 - 864 cal AD	(1112 - 1086 cal BP)

68.2% probability

(59.3%)	690 - 750 cal AD	(1260 - 1200 cal BP)
(8.9%)	760 - 770 cal AD	(1190 - 1180 cal BP)



**Database used**  
INTCAL13

## References

### References to Probability Method

Bronk Ramsey, C. (2009). Bayesian analysis of radiocarbon dates. *Radiocarbon*, 51(1), 337-360.

### References to Database INTCAL13

Reimer, et.al., 2013, *Radiocarbon*55(4).

# Calibration of Radiocarbon Age to Calendar Years

(High Probability Density Range Method (HPD): INTCAL13)

(Variables:  $\delta^{13}\text{C} = -26.0$  o/oo)

**Laboratory number**      **Beta-563283**

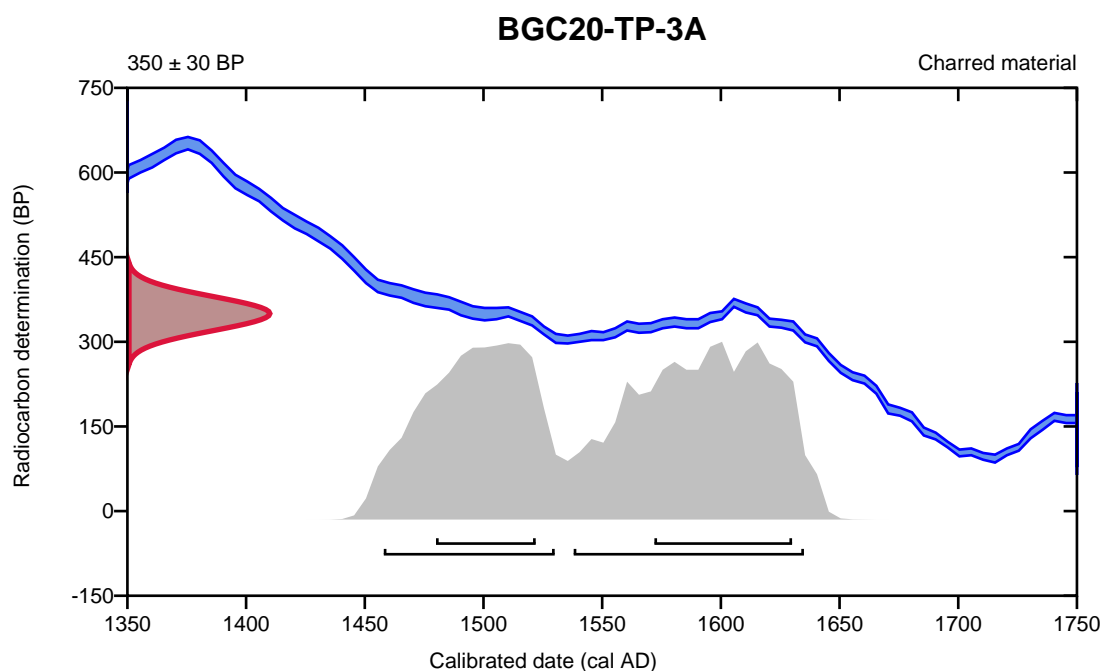
**Conventional radiocarbon age**      **350 ± 30 BP**

95.4% probability

(54.2%)	1538 - 1635 cal AD	(412 - 315 cal BP)
(41.2%)	1458 - 1530 cal AD	(492 - 420 cal BP)

68.2% probability

(38.8%)	1572 - 1630 cal AD	(378 - 320 cal BP)
(29.4%)	1480 - 1522 cal AD	(470 - 428 cal BP)



**Database used**  
INTCAL13

## References

### References to Probability Method

Bronk Ramsey, C. (2009). Bayesian analysis of radiocarbon dates. *Radiocarbon*, 51(1), 337-360.

### References to Database INTCAL13

Reimer, et.al., 2013, *Radiocarbon*55(4).

# Calibration of Radiocarbon Age to Calendar Years

(High Probability Density Range Method (HPD): INTCAL13)

(Variables:  $\delta^{13}C = -28.5$  o/oo)

**Laboratory number**      **Beta-563284**

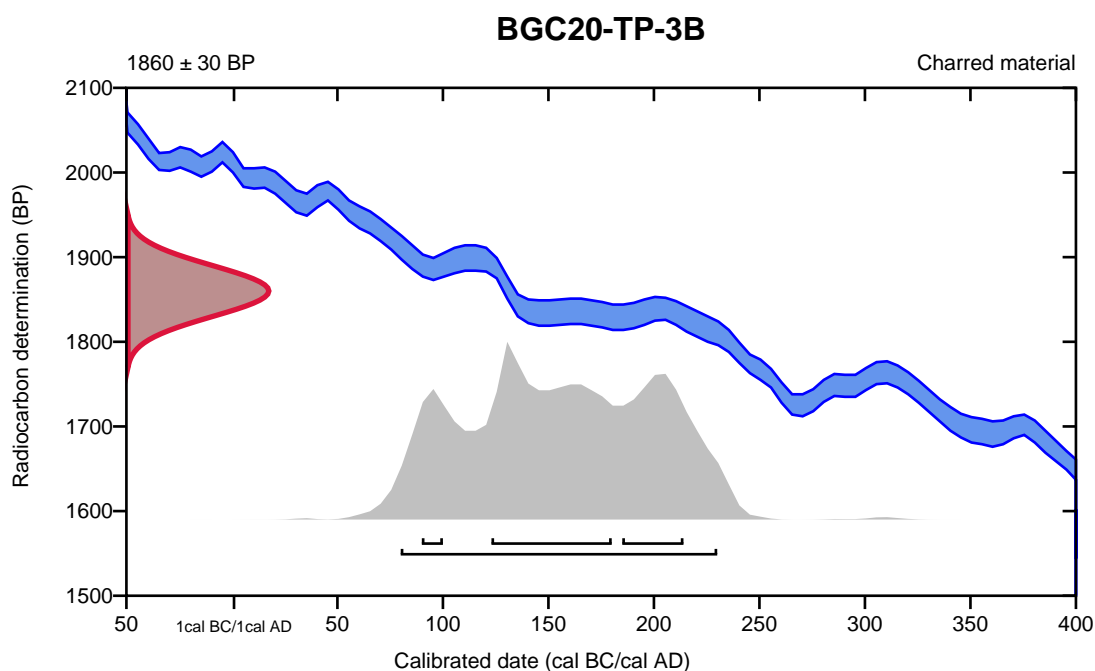
**Conventional radiocarbon age**      **1860  $\pm$  30 BP**

95.4% probability

(95.4%)    80 - 230 cal AD                      (1870 - 1720 cal BP)

68.2% probability

(41.4%)    123 - 180 cal AD                      (1827 - 1770 cal BP)  
(20%)       185 - 214 cal AD                      (1765 - 1736 cal BP)  
(6.9%)       90 - 100 cal AD                        (1860 - 1850 cal BP)



**Database used**  
INTCAL13

## References

### References to Probability Method

Bronk Ramsey, C. (2009). Bayesian analysis of radiocarbon dates. *Radiocarbon*, 51(1), 337-360.

### References to Database INTCAL13

Reimer, et.al., 2013, *Radiocarbon*55(4).

# Calibration of Radiocarbon Age to Calendar Years

(High Probability Density Range Method (HPD): INTCAL13)

(Variables:  $\delta^{13}\text{C} = -28.6$  o/oo)

**Laboratory number**      **Beta-563285**

**Conventional radiocarbon age**      **3120  $\pm$  30 BP**

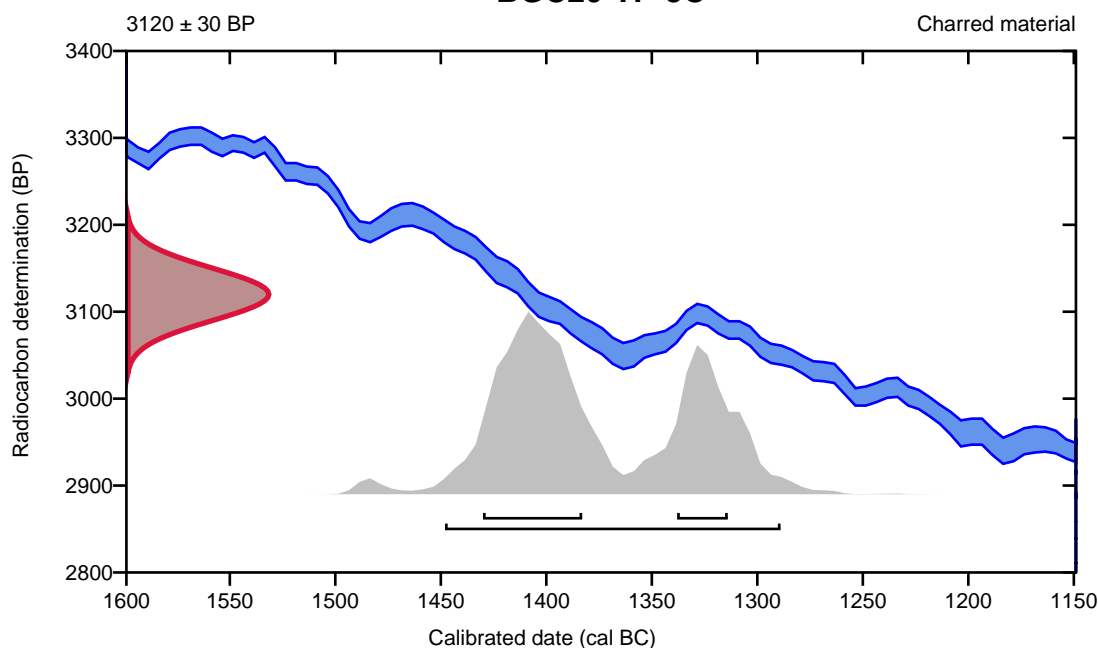
95.4% probability

(95.4%)    1450 - 1291 cal BC                      (3399 - 3240 cal BP)

68.2% probability

(47.5%)    1432 - 1385 cal BC                      (3381 - 3334 cal BP)  
(20.7%)    1340 - 1316 cal BC                      (3289 - 3265 cal BP)

## BGC20-TP-3C



**Database used**  
INTCAL13

### References

#### References to Probability Method

Bronk Ramsey, C. (2009). Bayesian analysis of radiocarbon dates. *Radiocarbon*, 51(1), 337-360.

#### References to Database INTCAL13

Reimer, et al., 2013, *Radiocarbon* 55(4).

# Calibration of Radiocarbon Age to Calendar Years

(High Probability Density Range Method (HPD): INTCAL13)

(Variables:  $\delta^{13}\text{C} = -22.5$  o/oo)

**Laboratory number**      **Beta-563286**

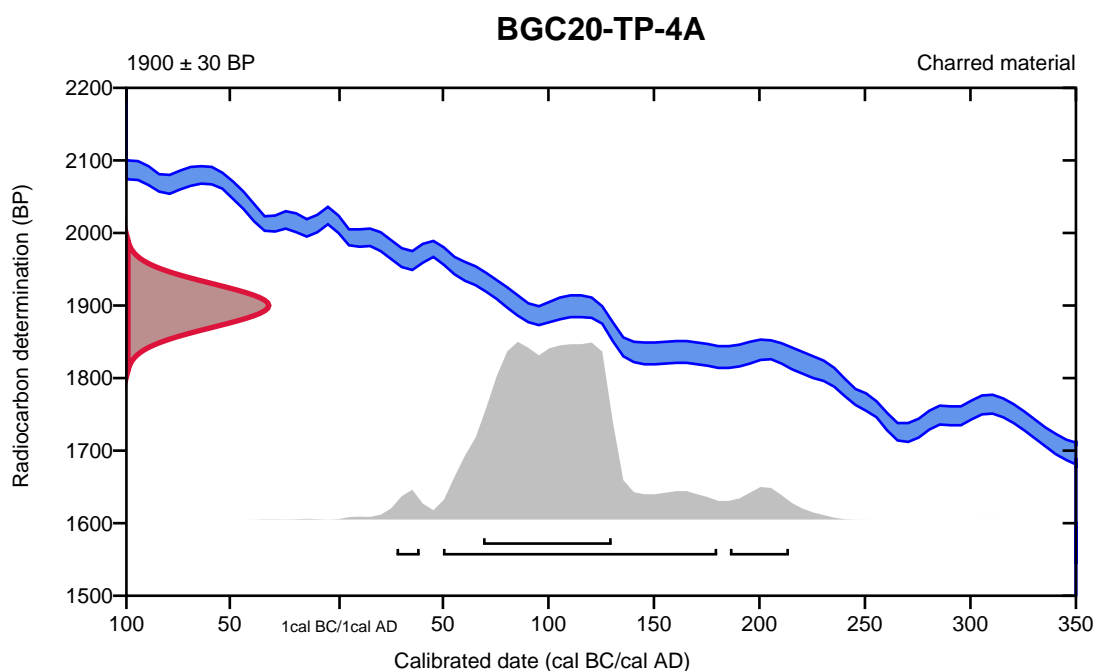
**Conventional radiocarbon age**      **1900  $\pm$  30 BP**

95.4% probability

(88.4%)	50 - 180 cal AD	(1900 - 1770 cal BP)
(5.1%)	186 - 214 cal AD	(1764 - 1736 cal BP)
(1.9%)	28 - 39 cal AD	(1922 - 1911 cal BP)

68.2% probability

(68.2%)	69 - 130 cal AD	(1881 - 1820 cal BP)
---------	-----------------	----------------------



**Database used**  
INTCAL13

## References

### References to Probability Method

Bronk Ramsey, C. (2009). Bayesian analysis of radiocarbon dates. *Radiocarbon*, 51(1), 337-360.

### References to Database INTCAL13

Reimer, et.al., 2013, *Radiocarbon*55(4).

# Calibration of Radiocarbon Age to Calendar Years

(High Probability Density Range Method (HPD): INTCAL13)

(Variables:  $\delta^{13}C = -24.5$  o/oo)

**Laboratory number**      **Beta-563287**

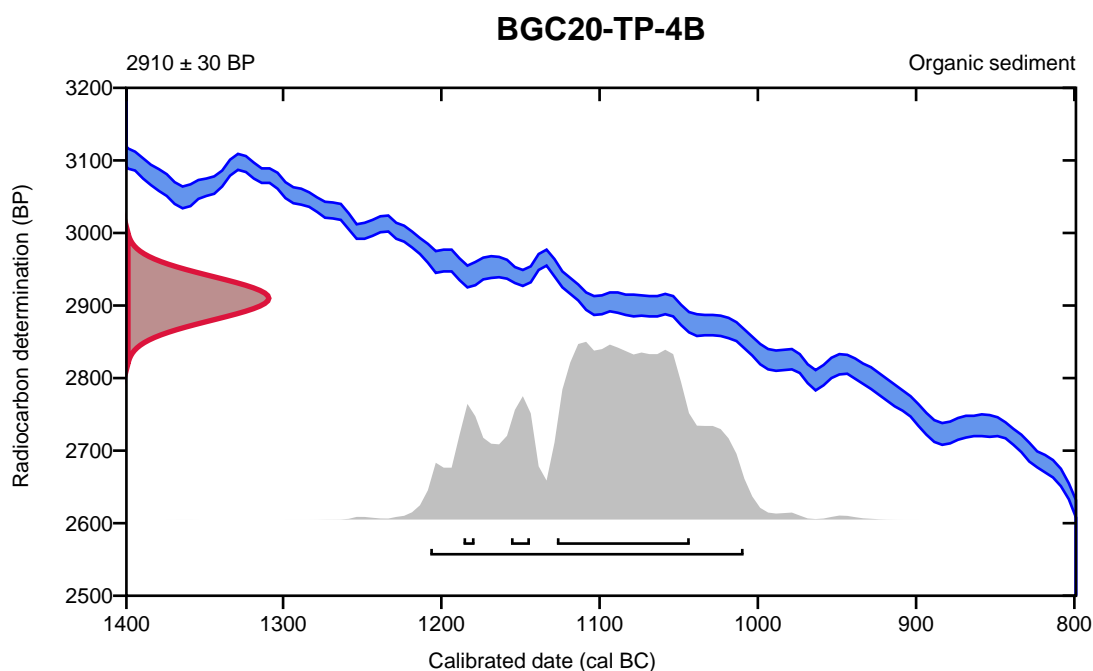
**Conventional radiocarbon age**      **2910  $\pm$  30 BP**

95.4% probability

(95.4%)      1209 - 1011 cal BC      (3158 - 2960 cal BP)

68.2% probability

(58.9%)      1129 - 1045 cal BC      (3078 - 2994 cal BP)  
(5.9%)      1158 - 1146 cal BC      (3107 - 3095 cal BP)  
(3.3%)      1188 - 1181 cal BC      (3137 - 3130 cal BP)



**Database used**  
INTCAL13

## References

### References to Probability Method

Bronk Ramsey, C. (2009). Bayesian analysis of radiocarbon dates. *Radiocarbon*, 51(1), 337-360.

### References to Database INTCAL13

Reimer, et.al., 2013, *Radiocarbon*55(4).

# Calibration of Radiocarbon Age to Calendar Years

(High Probability Density Range Method (HPD): INTCAL13)

(Variables:  $\delta^{13}\text{C} = -24.3$  o/oo)

**Laboratory number**      **Beta-563288**

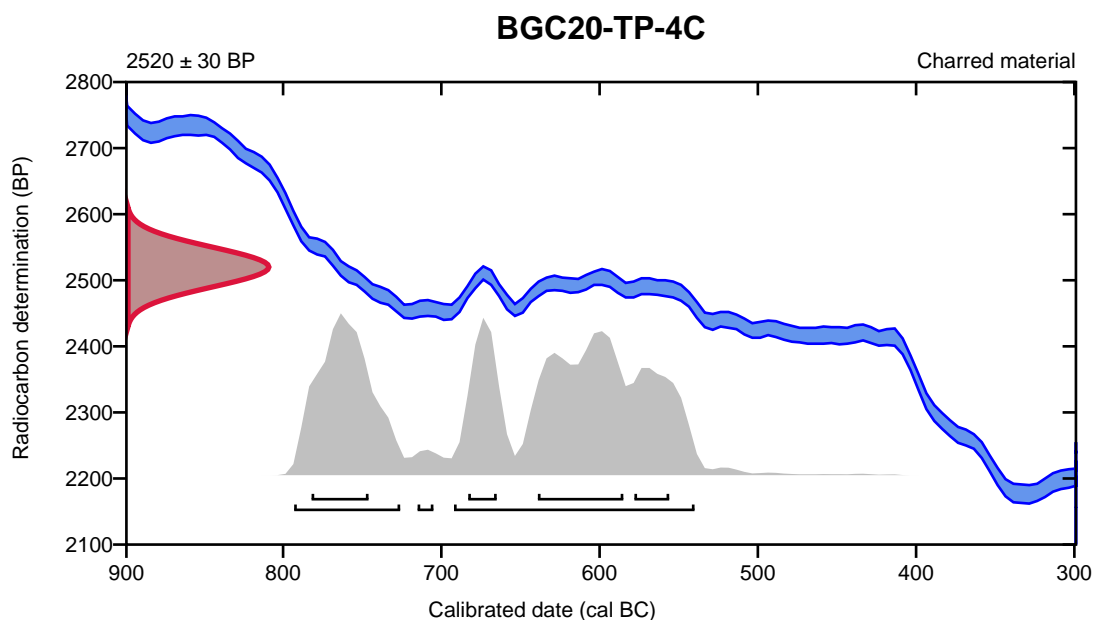
**Conventional radiocarbon age**      **2520  $\pm$  30 BP**

95.4% probability

(65.1%)	694 - 542 cal BC	(2643 - 2491 cal BP)
(29.2%)	795 - 728 cal BC	(2744 - 2677 cal BP)
(1.1%)	717 - 707 cal BC	(2666 - 2656 cal BP)

68.2% probability

(28.1%)	641 - 587 cal BC	(2590 - 2536 cal BP)
(20.3%)	784 - 748 cal BC	(2733 - 2697 cal BP)
(10.3%)	685 - 667 cal BC	(2634 - 2616 cal BP)
(9.6%)	580 - 558 cal BC	(2529 - 2507 cal BP)



**Database used**  
INTCAL13

## References

### References to Probability Method

Bronk Ramsey, C. (2009). Bayesian analysis of radiocarbon dates. *Radiocarbon*, 51(1), 337-360.

### References to Database INTCAL13

Reimer, et.al., 2013, *Radiocarbon*55(4).

# Calibration of Radiocarbon Age to Calendar Years

(High Probability Density Range Method (HPD): INTCAL13)

(Variables:  $\delta^{13}C = -23.9$  o/oo)

**Laboratory number**      **Beta-563289**

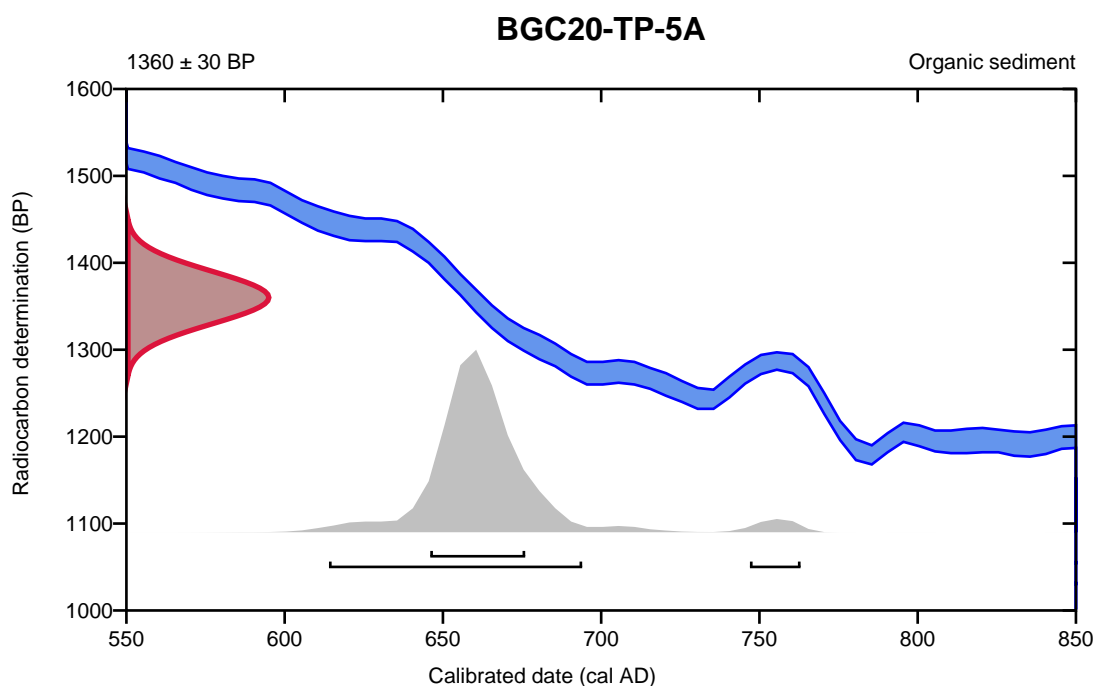
**Conventional radiocarbon age**      **1360 ± 30 BP**

95.4% probability

(92.1%)	614 - 694 cal AD	(1336 - 1256 cal BP)
(3.3%)	747 - 763 cal AD	(1203 - 1187 cal BP)

68.2% probability

(68.2%)	646 - 676 cal AD	(1304 - 1274 cal BP)
---------	------------------	----------------------



**Database used**  
INTCAL13

## References

### References to Probability Method

Bronk Ramsey, C. (2009). Bayesian analysis of radiocarbon dates. *Radiocarbon*, 51(1), 337-360.

### References to Database INTCAL13

Reimer, et.al., 2013, *Radiocarbon*55(4).

# Calibration of Radiocarbon Age to Calendar Years

(High Probability Density Range Method (HPD): INTCAL13)

(Variables:  $\delta^{13}\text{C} = -24.4$  o/oo)

**Laboratory number**      **Beta-563290**

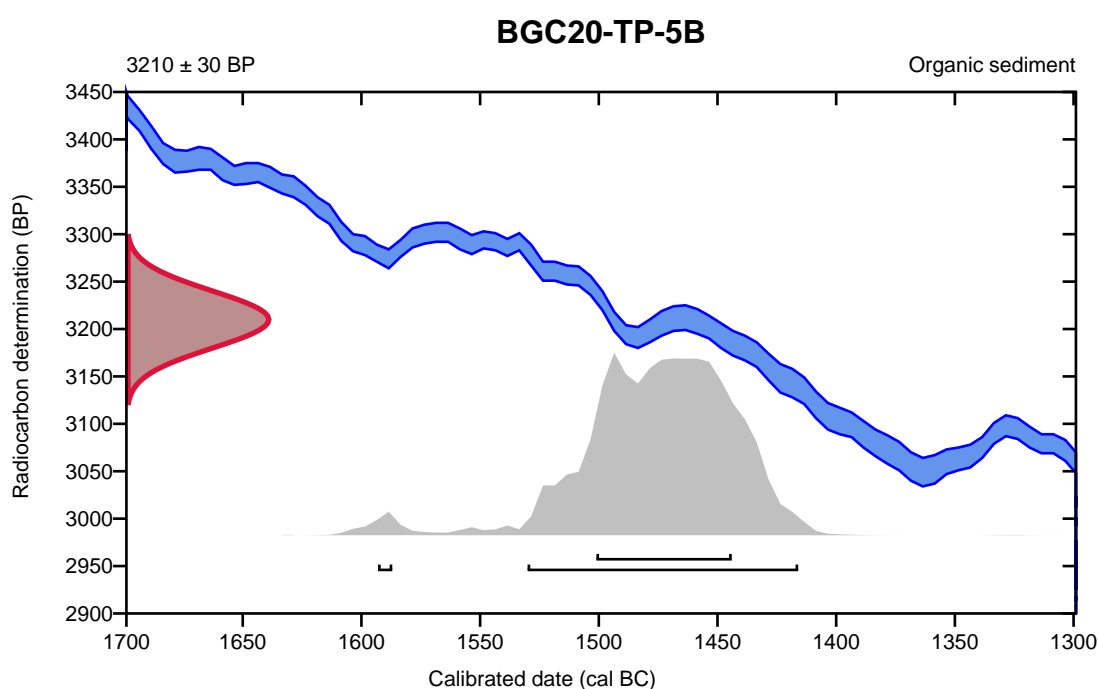
**Conventional radiocarbon age**      **3210  $\pm$  30 BP**

95.4% probability

(94.6%)	1532 - 1418 cal BC	(3481 - 3367 cal BP)
(0.8%)	1595 - 1589 cal BC	(3544 - 3538 cal BP)

68.2% probability

(68.2%)	1503 - 1446 cal BC	(3452 - 3395 cal BP)
---------	--------------------	----------------------



**Database used**  
INTCAL13

## References

### References to Probability Method

Bronk Ramsey, C. (2009). Bayesian analysis of radiocarbon dates. *Radiocarbon*, 51(1), 337-360.

### References to Database INTCAL13

Reimer, et.al., 2013, *Radiocarbon*55(4).



## Quality Assurance Report

This report provides the results of reference materials used to validate radiocarbon analyses prior to reporting. Known-value reference materials were analyzed quasi-simultaneously with the unknowns. Results are reported as expected values vs measured values. Reported values are calculated relative to NIST SRM-4990B and corrected for isotopic fractionation. Results are reported using the direct analytical measure percent modern carbon (pMC) with one relative standard deviation. Agreement between expected and measured values is taken as being within 2 sigma agreement (error x 2) to account for total laboratory error.

**Report Date:** August 05, 2020  
**Submitter:** Ms. Emily Moase

### QA MEASUREMENTS

#### Reference 1

Expected Value: 96.69 +/- 0.50 pMC

Measured Value: 97.15 +/- 0.29 pMC

Agreement: Accepted

#### Reference 2

Expected Value: 129.41 +/- 0.06 pMC

Measured Value: 129.37 +/- 0.35 pMC

Agreement: Accepted

#### Reference 3

Expected Value: 0.45 +/- 0.04 pMC

Measured Value: 0.44 +/- 0.03 pMC

Agreement: Accepted

**COMMENT:** All measurements passed acceptance tests.

**Validation:**

  
Digital signature on file

**Date:** August 05, 2020



July 13, 2020

Ms. Emily Moase  
BGC Engineering  
500-980 Howe Street  
Vancouver, BC V6Z 0C8  
Canada

RE: Radiocarbon Dating Results

Dear Ms. Moase,

Enclosed is the radiocarbon dating result for one sample recently sent to us. As usual, specifics of the analysis are listed on the report with the result and calibration data is provided where applicable. The Conventional Radiocarbon Age has been corrected for total fractionation effects and where applicable, calibration was performed using 2013 calibration databases (cited on the graph pages).

The web directory containing the table of results and PDF download also contains pictures, a cvs spreadsheet download option and a quality assurance report containing expected vs. measured values for 3-5 working standards analyzed simultaneously with your samples.

The reported result is accredited to ISO/IEC 17025:2005 Testing Accreditation PJLA #59423 standards and all pretreatments and chemistry were performed here in our laboratories and counted in our own accelerators here in Miami. Since Beta is not a teaching laboratory, only graduates trained to strict protocols of the ISO/IEC 17025:2005 Testing Accreditation PJLA #59423 program participated in the analysis.

As always Conventional Radiocarbon Ages and sigmas are rounded to the nearest 10 years per the conventions of the 1977 International Radiocarbon Conference. When counting statistics produce sigmas lower than +/- 30 years, a conservative +/- 30 BP is cited for the result. The reported d13C was measured separately in an IRMS (isotope ratio mass spectrometer). It is NOT the AMS d13C which would include fractionation effects from natural, chemistry and AMS induced sources.

When interpreting the result, please consider any communications you may have had with us regarding the sample. As always, your inquiries are most welcome. If you have any questions or would like further details of the analysis, please do not hesitate to contact us.

Thank you for prepaying the analyses. As always, if you have any questions or would like to discuss the results, don't hesitate to contact us.

Sincerely,



Digital signature on file

Chris Patrick  
Vice President of Laboratory Operations



## REPORT OF RADIOCARBON DATING ANALYSES

Emily Moase

Report Date: July 13, 2020

BGC Engineering

Material Received: June 30, 2020

Laboratory Number	Sample Code Number	Conventional Radiocarbon Age (BP) or Percent Modern Carbon (pMC) & Stable Isotopes	
		Calendar Calibrated Results: 95.4 % Probability High Probability Density Range Method (HPD)	

**Beta - 562124**

**1572-005 Grab 1**

**2650 +/- 30 BP**

**IRMS δ13C: -25.1 o/oo**

**(89.8%)  
( 5.6%)**

**850 - 791 cal BC  
895 - 870 cal BC**

**(2799 - 2740 cal BP)  
(2844 - 2819 cal BP)**

Submitter Material: Charcoal  
 Pretreatment: (charred material) acid/alkali/acid  
 Analyzed Material: Charred material  
 Analysis Service: AMS-Standard delivery  
 Percent Modern Carbon: 71.90 +/- 0.27 pMC  
 Fraction Modern Carbon: 0.7190 +/- 0.0027  
 D14C: -281.00 +/- 2.69 o/oo  
 Δ14C: -287.06 +/- 2.69 o/oo (1950:2020)  
 Measured Radiocarbon Age: (without d13C correction): 2650 +/- 30 BP  
 Calibration: BetaCal3.21: HPD method: INTCAL13

Results are ISO/IEC-17025:2005 accredited. No sub-contracting or student labor was used in the analyses. All work was done at Beta in 4 in-house NEC accelerator mass spectrometers and 4 Thermo IRMSs. The "Conventional Radiocarbon Age" was calculated using the Libby half-life (5568 years), is corrected for total isotopic fraction and was used for calendar calibration where applicable. The Age is rounded to the nearest 10 years and is reported as radiocarbon years before present (BP), "present" = AD 1950. Results greater than the modern reference are reported as percent modern carbon (pMC). The modern reference standard was 95% the 14C signature of NIST SRM-4990C (oxalic acid). Quoted errors are 1 sigma counting statistics. Calculated sigmas less than 30 BP on the Conventional Radiocarbon Age are conservatively rounded up to 30. d13C values are on the material itself (not the AMS d13C). d13C and d15N values are relative to VPDB-1. References for calendar calibrations are cited at the bottom of calibration graph pages.

# Calibration of Radiocarbon Age to Calendar Years

(High Probability Density Range Method (HPD): INTCAL13)

(Variables:  $\delta^{13}C = -25.1$  o/oo)

**Laboratory number**     **Beta-562124**

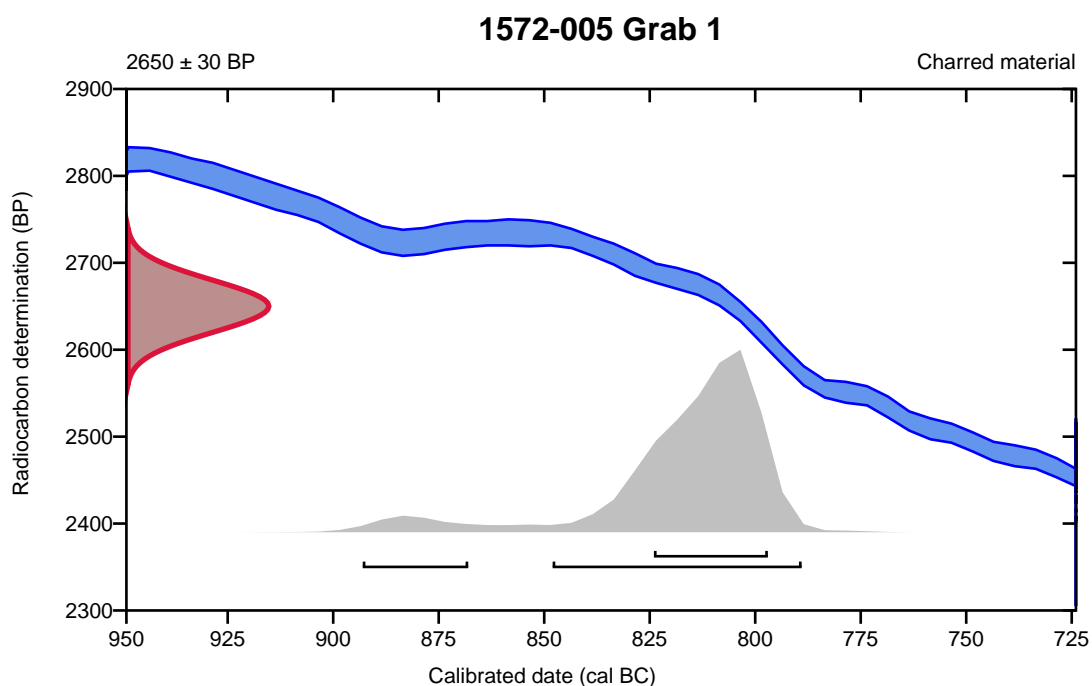
**Conventional radiocarbon age**     **2650  $\pm$  30 BP**

95.4% probability

(89.8%)	850 - 791 cal BC	(2799 - 2740 cal BP)
(5.6%)	895 - 870 cal BC	(2844 - 2819 cal BP)

68.2% probability

(68.2%)	826 - 799 cal BC	(2775 - 2748 cal BP)
---------	------------------	----------------------



**Database used**  
INTCAL13

## References

### References to Probability Method

Bronk Ramsey, C. (2009). Bayesian analysis of radiocarbon dates. *Radiocarbon*, 51(1), 337-360.

### References to Database INTCAL13

Reimer, et.al., 2013, *Radiocarbon*55(4).

## **APPENDIX C DENDROGEOMORPHOLOGY ANALYSIS RESULTS**

**Table C-1. Summary of Cold Spring Creek dendrogeomorphology sample features.**

Sample <sup>1</sup>	Tree type	Minimum establishment date (first ring) <sup>2</sup>	Features <sup>3</sup>
D-1A, D-1B	Spruce	1776	Moderate to strong TRDs in 1890, 1900, 1928, 1934, 2006 and 2014, sustained growth acceleration in 1876, 1964, 1993 and 2005, sustained growth reduction in 1917 and 1975
D-2	Spruce	1840	Scar in 1842, moderate TRDs in 1888, sustained growth acceleration in 1870, sustained growth reduction in 1858, 1920 and 2003
D-3A, D-3B	Spruce	1695	Sustained growth reduction in 1737 and 1813, sustained growth acceleration in 1765, 1875 and 1890.
D-4A, D-4B	Spruce	1911	Scars in 1985 and 2008, strong TRDs in 1916, 1917, 1918, 1919, 1920, 1934, 1940, 1946, 1951, 1988, 2006, 2012 and 2013, sustained growth acceleration in 1972
D-5	Spruce	1872	Scar in 1872, moderate to strong TRDs in 1874, 1876, 1912, 1985 and 1998
D-6	Douglas Fir	1774	Moderate to strong TRDs in 1886, 1890, 1930, 1944, 1972, 1974, 1994, 2000 and 2006, growth reduction in 1787, 1841 and 1982, growth acceleration in 1860
D-7	Douglas Fir	1817	Moderate to strong TRDs in 1869 and 1961
D-8	Douglas Fir	1884	Growth acceleration in 1981
D-9	Douglas Fir	1755	Moderate TRDs in 1979, sustained growth reduction in 1825 and 1837, sustained growth acceleration in 2009.
D-10	Spruce	1842	Sustained growth reduction in 1894 and 1935
D-11	Douglas Fir	1768	Sustained growth reduction in 1850 and 1957.
D-12	Douglas Fir	1778	Moderate TRDs in 2006, sustained growth acceleration in 1866
D-13	Douglas Fir	1813	Scar in 1968, sustained growth reduction in 1853, 1875 and 1925
D-14	Spruce	1895	Strong to moderate TRDs in 1908, 1911, 1948 and 2006, sustained growth reduction in 1951, growth acceleration in 1914
D-15	Spruce	1892	Strong to moderate TRDs in 1902, 1973, 2001 and 2002, growth acceleration in 1986 and 2004

**Table C-1. Summary of Cold Spring Creek dendrogeomorphology sample features.**

Sample <sup>1</sup>	Tree type	Minimum establishment date (first ring) <sup>2</sup>	Features <sup>3</sup>
D-16	Spruce	1840	Strong TRDs in 1902 and 1903, sustained growth reduction in 1868 and 1931, growth acceleration in 1903
D-17A	Douglas Fir	1850	Sustained growth acceleration in 1856 and 1964, growth reduction in 1943, 1949 and 1974
D-17B	Douglas Fir	1807	Moderate to strong TRDs in 1881, 1885, 1886, 1890, 1896, 1903, 1914 and 1916, sustained growth acceleration in 1859 and 1890, growth reduction in 1959
D-18	Spruce	1892	Scar in 1892, 1955 and 1979, moderate to strong TRDs in 1893, 1894, 1895, 1897, 1900, 1905, 1919 and 1987
D-19	Douglas Fir	1773	Strong TRDs in 1864, 1891, 1902, 1903, 1958, 1962, 1963, 1975, 1993 and 1994, growth acceleration in 1789, 1792, 1819, 1821 and 1916, sustained growth acceleration in 1805, 1898 and 2006, sustained growth reduction in 1970
D-20	Douglas Fir	1690	Scar in 1817, strong to moderate TRDs in 1899, 1911, 1912, 1987 and 2014, growth reduction in 1927 and 1929, sustained growth reduction in 1693 and 1984, growth acceleration in 1728 and 1732, sustained growth acceleration in 1715, 1742, 1755, 1783 and 1863
D-21	Douglas Fir	1776	Strong to moderate TRDs in 1814, 1817 and 1989, sustained growth reduction in 1793, 1818, 1841 and 1869, sustained growth acceleration in 1826
D-22	Douglas Fir	1880	Strong to moderate TRDs in 1952, 1956, 1971, 1972, 1975 and 1986
D-23	Douglas Fir	1867	Strong to moderate TRDs in 1868, 1870, 1886, 1898, 1916, 1924, 1934, 1936, 1939, 1943, 1950 and 1956, growth acceleration in 1869 and 1873, sustained growth acceleration in 1886, 1893, 1899, 1906 and 1936
D-24	Douglas Fir	1708	Scar in 1758, strong to moderate TRDs in 1727, 1760, 1782, 1904, 1968 and 1972, sustained growth reduction 1727, 1736 and 1866, growth acceleration 1734, 1759, 1788 and 1800, sustained growth acceleration 1837 and 2011
D-25	Douglas Fir	1785	Strong to moderate TRDs in 1791 and 1796, sustained growth acceleration 1808, growth acceleration 1836 and 1851, sustained growth reduction 1876, 1892 and 1948

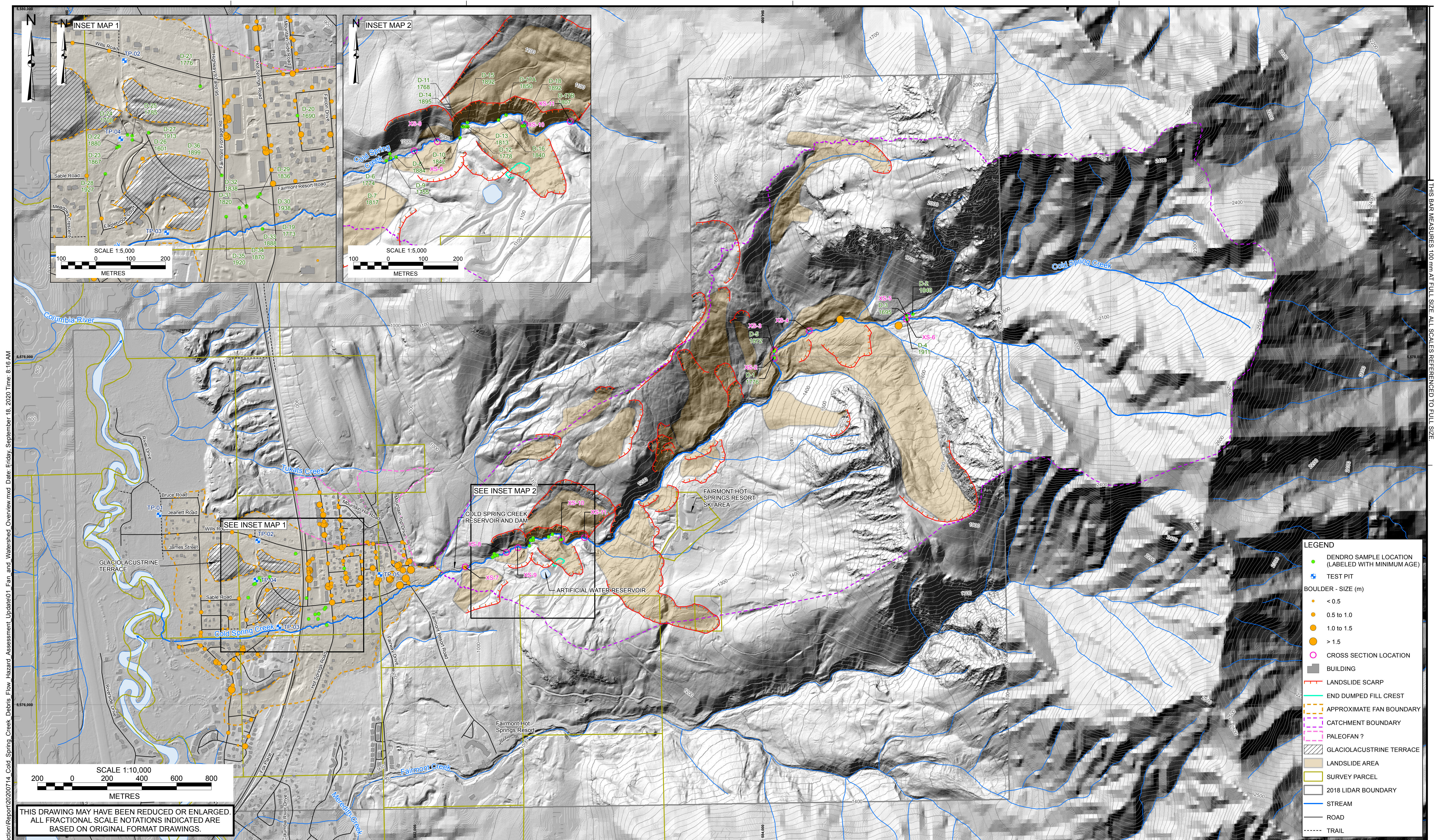
**Table C-1. Summary of Cold Spring Creek dendrogeomorphology sample features.**

Sample <sup>1</sup>	Tree type	Minimum establishment date (first ring) <sup>2</sup>	Features <sup>3</sup>
D-26	Douglas Fir	1601	Strong to moderate TRDs in 1622, 1783, 1792, 1831, 1852, 1862, 1863, 1864 and 1896, growth acceleration in 1623, sustained growth acceleration in 1745, 1757, 1832 and 1861, sustained growth reduction in 1638
D-27	Douglas Fir	1913	Growth acceleration in 1996, sustained growth acceleration 2006
D-28	Douglas Fir	1927	Strong to moderate TRDs in 1988, 1989, 1992, 1993, 1994, 1998, 2004 and 2005, growth acceleration in 1956, sustained growth acceleration in 1977
D-29	Douglas Fir	1836	Growth acceleration 1922, 1945 and 1999, sustained growth reduction in 1884 and 1976
D-30	Douglas Fir	1938	Strong TRDs in 1953, 1989 and 1991, growth reduction in 1967, sustained growth reduction in 1982 and 2002, growth acceleration in 1998 and 2000, sustained growth acceleration in 1969
D-31	Douglas Fir	1820	Moderate TRDs in 1992, sustained growth reduction in 1842, sustained growth acceleration in 1898, 1980 and 1990
D-32	Douglas Fir	1838	Scar in 1954, strong to moderate TRDs in 1842, 1844, 1845, 1848, 1864, 1866, 1914, 1956, 1971, 1974, 1983 and 1991, growth reduction in 1865, 1869, 1871, 1875 and 1999, growth acceleration in 1922, sustained growth acceleration in 1903, 1929, 1945 and 1989
D-33	Douglas Fir	1888	Strong to moderate TRDs in 1899, 1907, 1908, 1909, 1916 and 1920
D-34	Douglas Fir	1870	Sustained growth acceleration in 1991
D-35	Douglas Fir	1920	Sustained growth reduction in 1930 and 1976, growth acceleration in 1993 and 1997
D-36	Douglas Fir	1899	Strong to moderate TRDs in 1906, 1919, 1981, 1993 and 2014

Notes:

- 1 Sample locations are shown on Drawing 01.
- 2 Minimum establishment date refers to the oldest tree ring identified in the sample. The samples do not always hit the earliest tree rings so this year is taken as the minimum date the tree could have established itself.
- 3 Traumatic resin ducts (TRDs) are small circles that appear within the wood, which indicate that the tree sustained physical damage during that year (similar to scar tissue).

## **DRAWINGS**



X:\Projects\1572005\GIS\Production\Report\2020714\_Cold\_Spring\_Creek\_Debris\_Flow\_Hazard\_Assessment\_Update\01\_Fan\_and\_Watershed\_Overview.mxd Date: Friday, September 18, 2020 Time: 8:16 AM

THIS BAR MEASURES 100 mm AT FULL SIZE. ALL SCALES REFERENCED TO FULL SIZE.

THIS DRAWING MAY HAVE BEEN REDUCED OR ENLARGED.  
ALL FRACTIONAL SCALE NOTATIONS INDICATED ARE  
BASED ON ORIGINAL FORMAT DRAWINGS.

- NOTES:
1. ALL DIMENSIONS ARE IN METRES UNLESS OTHERWISE NOTED.
  2. THIS DRAWING MUST BE READ IN CONJUNCTION WITH BGC'S REPORT TITLED "COLD SPRING CREEK DEBRIS FLOW HAZARD ASSESSMENT UPDATE" DATED SEPTEMBER 2020.
  3. LIDAR DATA PROVIDED BY REGIONAL DISTRICT OF EAST KOOTENAY, PREPARED ON SEPTEMBER 12, 2018, AND CANADIAN DIGITAL ELEVATION MODEL (CDED). CONTOUR INTERVAL IS 10 m.
  4. ROADS, STREAM AND WATERBODY DATA FROM CANVEC, AND COLD SPRING CREEK DIGITIZED BASED ON LIDAR DATED SEPTEMBER, 2018. SURVEY PARCEL DATA FROM TANTALIS. BUILDING FOOTPRINT DATA FROM MICROSOFT BING, DOWNLOADED DECEMBER 2019.
  5. THE SURFACE TO THE NORTH OF COLD SPRING CREEK FAN HAS BEEN DELINEATED AS A PALEOFAN BUT REQUIRES MORE STUDY

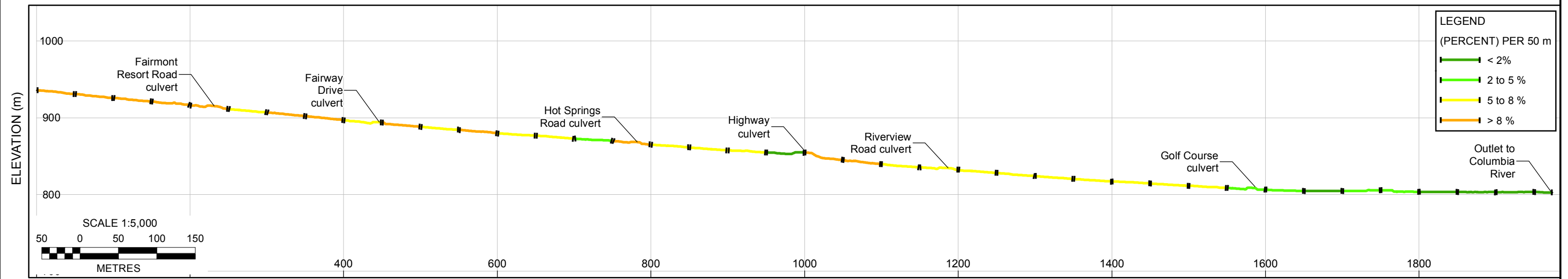
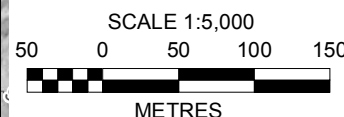
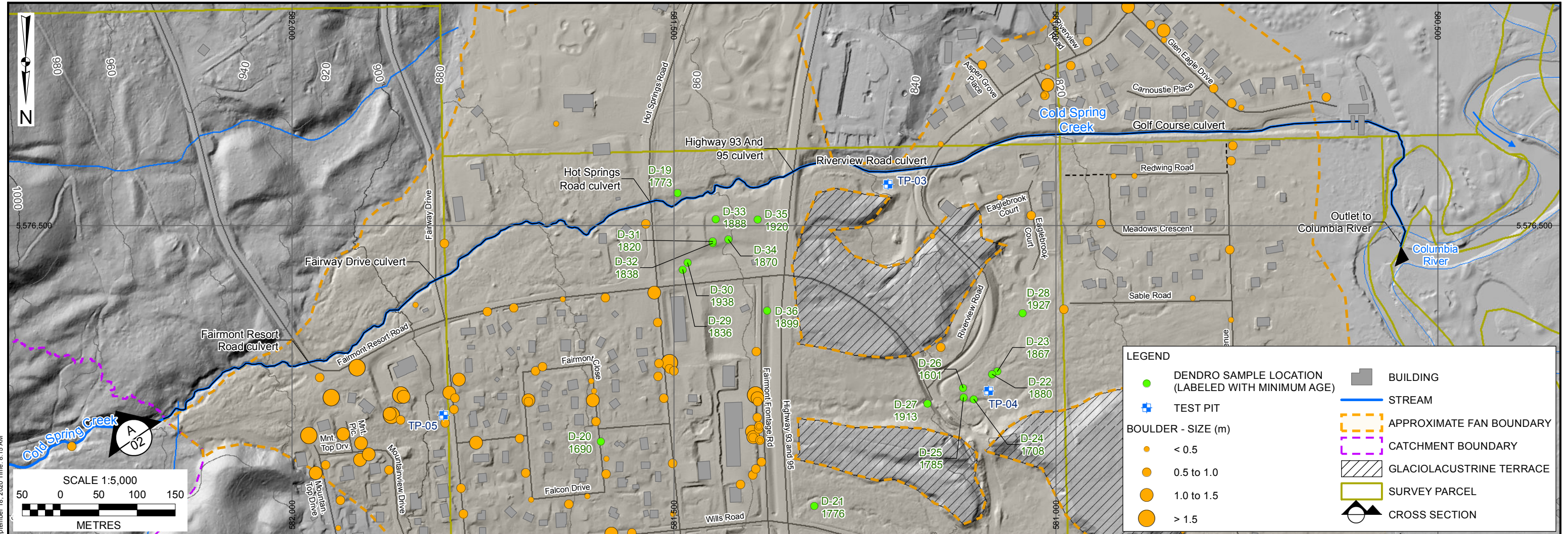
6. THE FAN BOUNDARY AS DRAWN IS APPROXIMATE AND DELINEATES THE LANDFORM BASED ON LIDAR DATED SEPTEMBER, 2018. THE BOUNDARY SHOULD NOT BE CONSTRUED AS A HAZARD MAP. NOR DOES IT SHOW THE SPATIAL EXTENT OF POTENTIAL FLOODING.
7. PROJECTION IS NAD 1983 UTM ZONE 11N. VERTICAL DATUM IS CGVD2013.
8. UNLESS BGC AGREES OTHERWISE IN WRITING, THIS DRAWING SHALL NOT BE MODIFIED OR USED FOR ANY PURPOSE OTHER THAN THE PURPOSE FOR WHICH BGC GENERATED IT. BGC SHALL HAVE NO LIABILITY FOR ANY DAMAGES OR LOSS ARISING IN ANY WAY FROM ANY USE OR MODIFICATION OF THIS DOCUMENT NOT AUTHORIZED BY BGC. ANY USE OF OR RELIANCE UPON THIS DOCUMENT OR ITS CONTENT BY THIRD PARTIES SHALL BE AT SUCH THIRD PARTIES' SOLE RISK.

SCALE:	1:10,000
DATE:	SEP 2020
DRAWN:	LL
REVIEW:	BCP
APPROVED:	MJ

CLIENT:




PROJECT: COLD SPRING CREEK DEBRIS FLOW HAZARD ASSESSMENT UPDATE	
TITLE: FAN AND WATERSHED OVERVIEW	
PROJECT No.: 1572 005	DWG No.: 01



DISTANCE (m)  
CROSS SECTION **A**/**02**

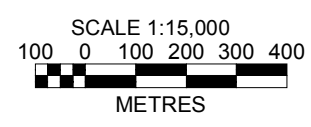
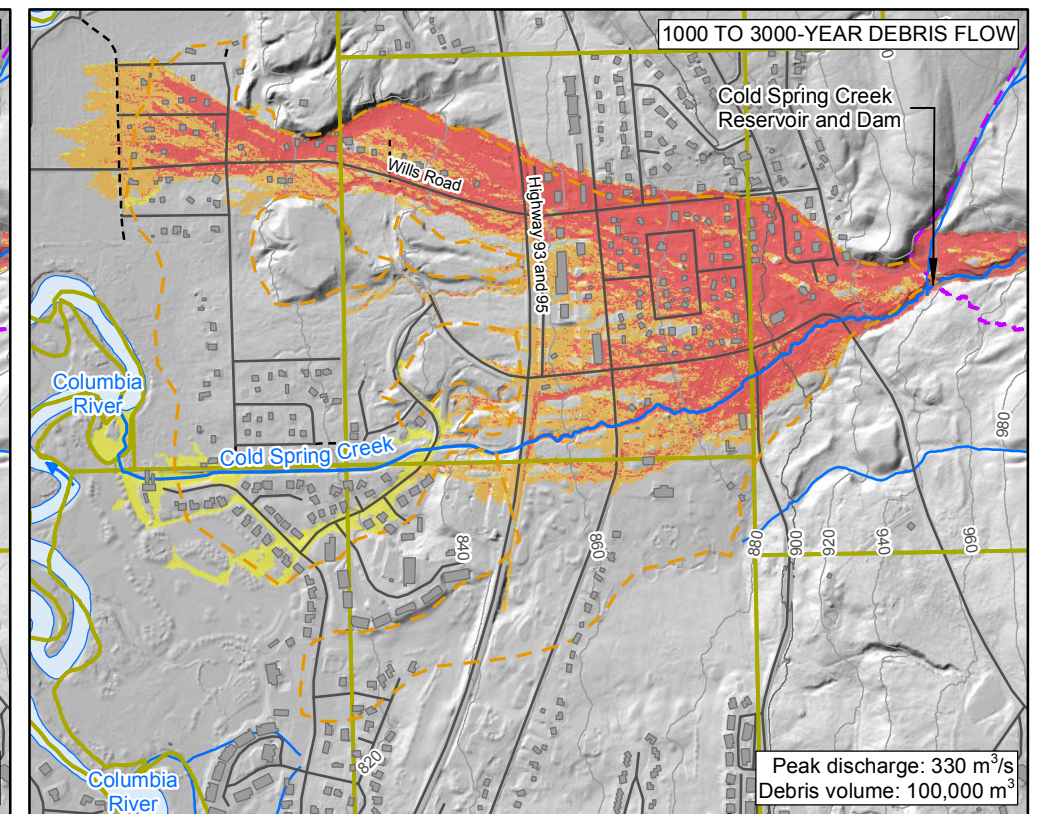
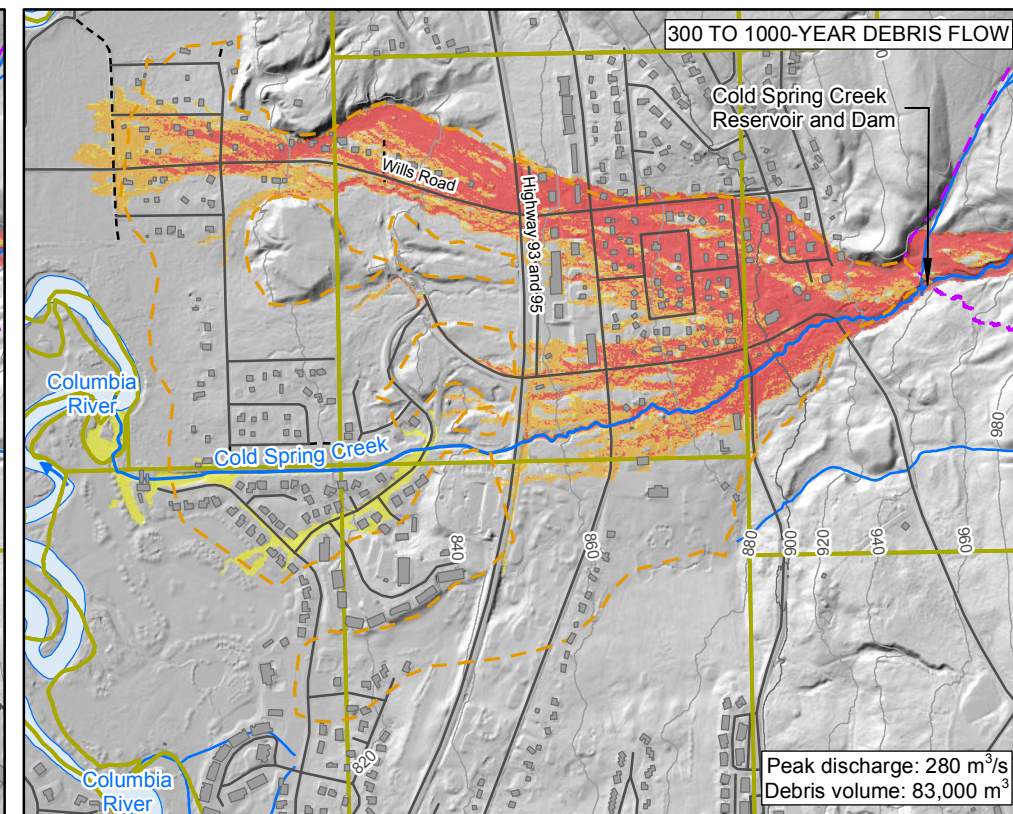
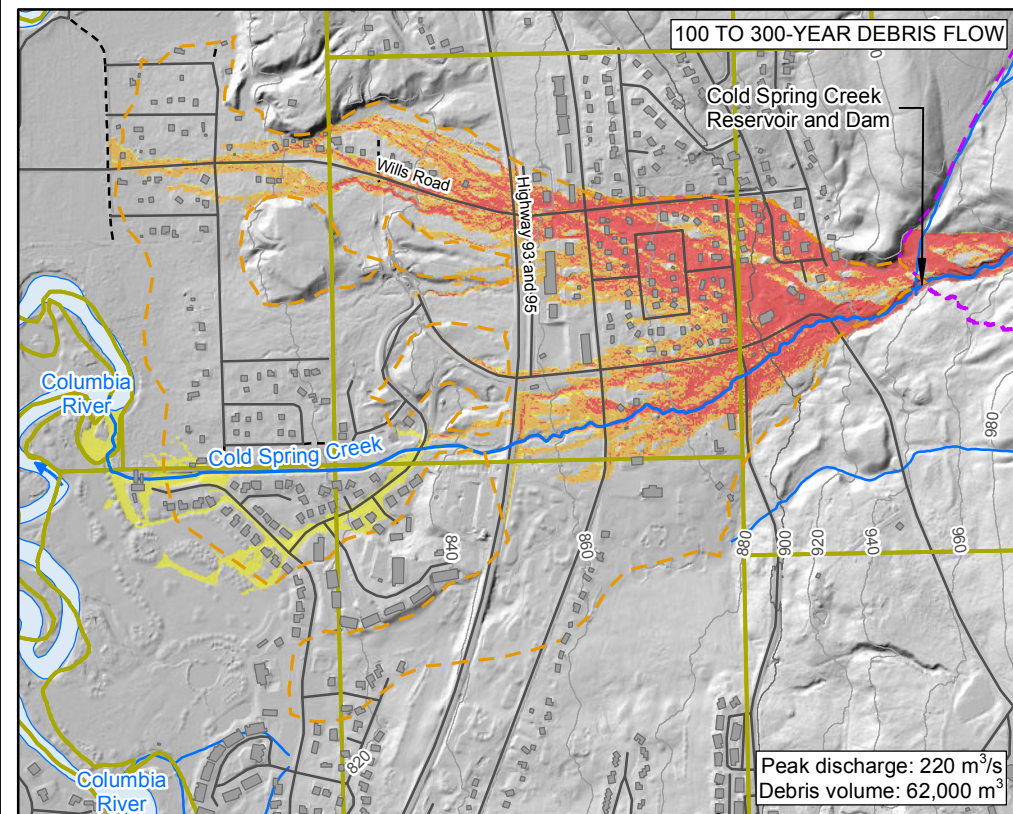
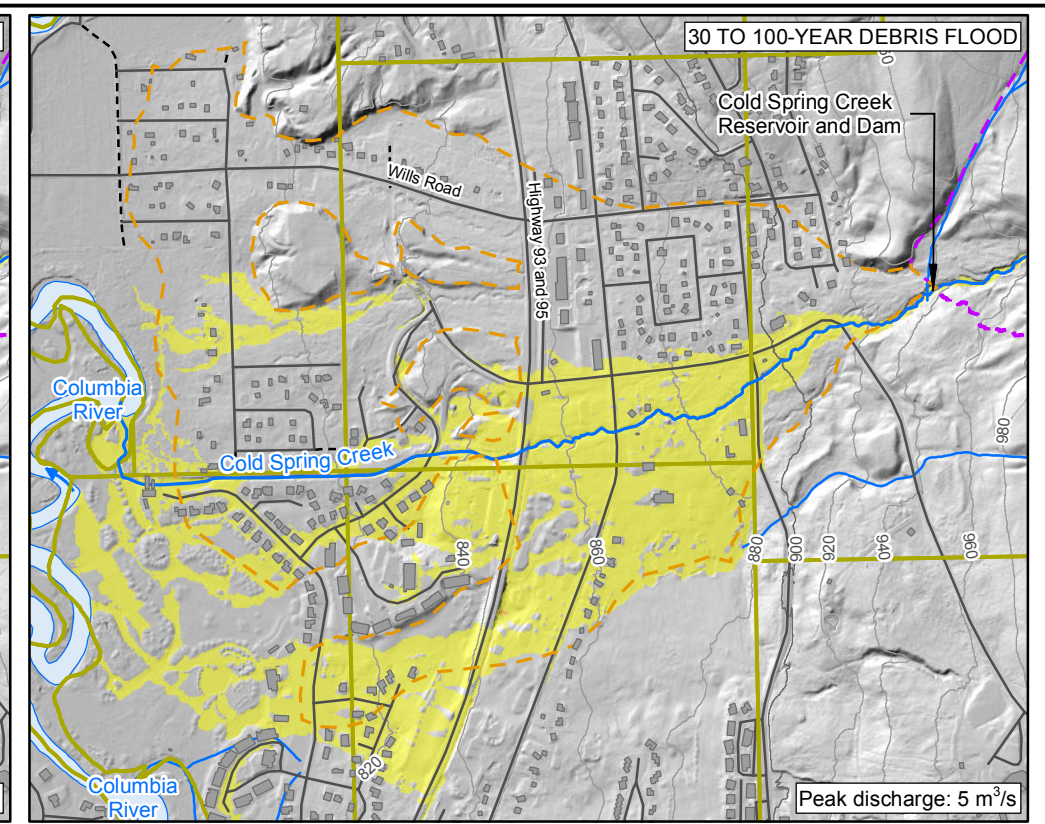
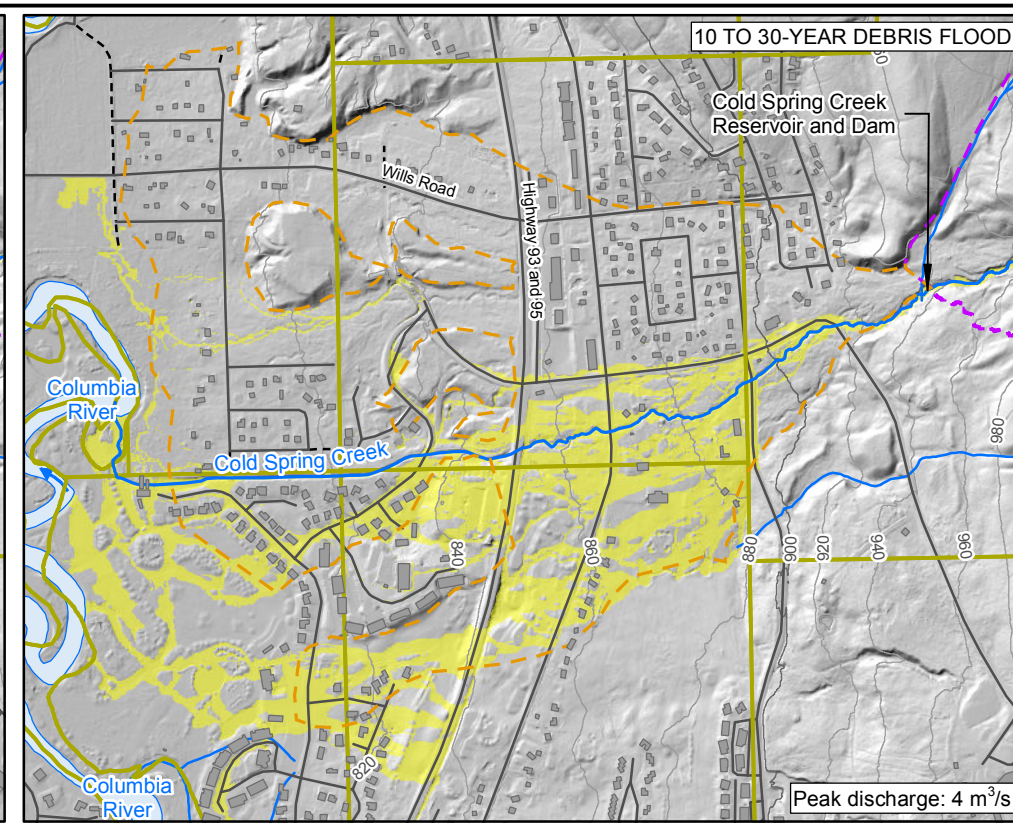
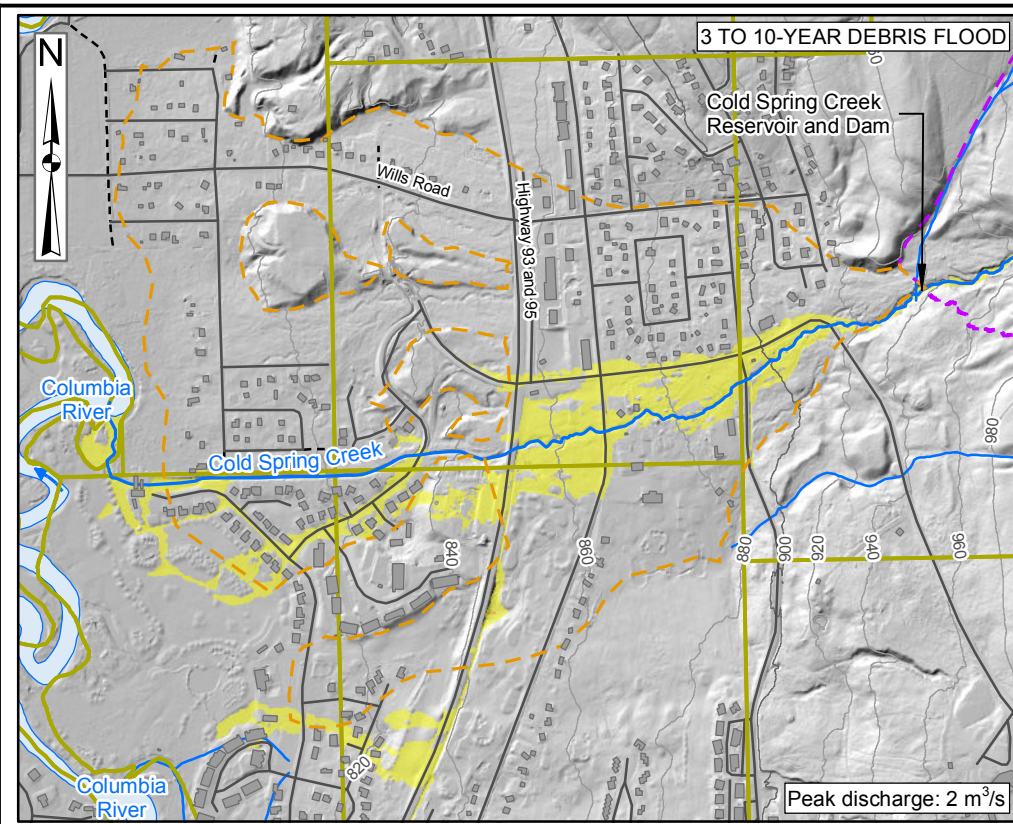
THIS DRAWING MAY HAVE BEEN REDUCED OR ENLARGED.  
ALL FRACTIONAL SCALE NOTATIONS INDICATED ARE  
BASED ON ORIGINAL FORMAT DRAWINGS.

NOTES:  
 1. ALL DIMENSIONS ARE IN METRES UNLESS OTHERWISE NOTED.  
 2. THIS DRAWING MUST BE READ IN CONJUNCTION WITH BGC'S REPORT TITLED "COLD SPRING CREEK DEBRIS FLOW HAZARD ASSESSMENT UPDATE" DATED SEPTEMBER 2020.  
 3. LIDAR DATA PROVIDED BY REGIONAL DISTRICT OF EAST KOOTENAY, PREPARED ON SEPTEMBER 12, 2018. CONTOUR INTERVAL IS 10 m.  
 4. ROADS, STREAM AND WATERBODY DATA FROM CANVEC, AND COLD SPRING CREEK DIGITIZED BASED ON LIDAR DATED SEPTEMBER, 2018. SURVEY PARCEL DATA FROM TANTALIS. BUILDING FOOTPRINT DATA FROM MICROSOFT BING, DOWNLOADED DECEMBER 2019.  
 5. THE FAN BOUNDARY AS DRAWN IS APPROXIMATE AND DELINEATES THE LANDFORM BASED ON LIDAR DATED SEPTEMBER, 2018. THE BOUNDARY SHOULD NOT BE CONSTRUED AS A HAZARD MAP, NOR DOES IT SHOW THE SPATIAL EXTENT OF POTENTIAL FLOODING.  
 6. PROJECTION IS NAD 1983 UTM ZONE 11N. VERTICAL DATUM IS CGVD2013.  
 7. UNLESS BGC AGREES OTHERWISE IN WRITING, THIS DRAWING SHALL NOT BE MODIFIED OR USED FOR ANY PURPOSE OTHER THAN THE PURPOSE FOR WHICH BGC GENERATED IT. BGC SHALL HAVE NO LIABILITY FOR ANY DAMAGES OR LOSS ARISING IN ANY WAY FROM ANY USE OR MODIFICATION OF THIS DOCUMENT NOT AUTHORIZED BY BGC. ANY USE OF OR RELIANCE UPON THIS DOCUMENT OR ITS CONTENT BY THIRD PARTIES SHALL BE AT SUCH THIRD PARTIES' SOLE RISK.

SCALE: 1:5,000	CLIENT: Regional District of East Kootenay	PROJECT: COLD SPRING CREEK DEBRIS FLOW HAZARD ASSESSMENT UPDATE
DATE: SEP 2020	 	TITLE: CREEK PROFILE
DRAWN: LL		PROJECT No.: 1572 005
REVIEW: BCP		DWG No: 02
APPROVED: MJ		

X:\Projects\1572005\GIS\Production\Report\20200714\_Cold\_Spring\_Creek\_Debriis\_Flow\_Hazard\_Assessment\_Update\02\_Creek\_Profile.mxd Date: Friday, September 18, 2020 Time: 8:15 AM

X:\Projects\1572005\GIS\Production\Report\20200714\_Cold\_Spring\_Creek\_Debbris\_Flow\_Hazard\_Assessment\_Update\03\_Individual\_Modelling\_Results.mxd Date: Friday, September 18, 2020 Time: 8:15 AM



THIS DRAWING MAY HAVE BEEN REDUCED OR ENLARGED. ALL FRACTIONAL SCALE NOTATIONS INDICATED ARE BASED ON ORIGINAL FORMAT DRAWINGS.

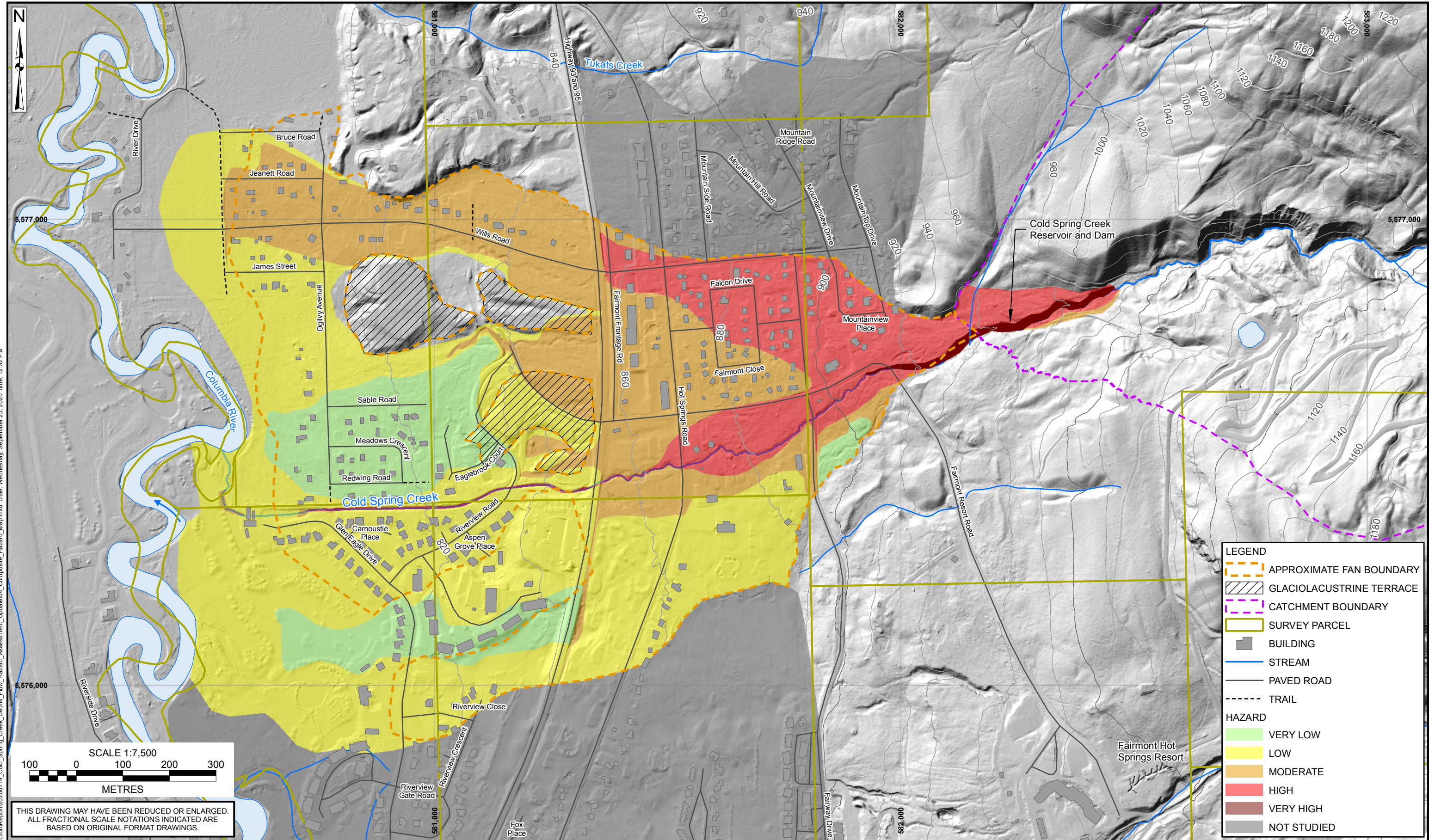
**LEGEND**

APPROXIMATE FAN BOUNDARY	SURVEY PARCEL	PAVED ROAD	IMPACT FORCE (kN/m) 10 – 100
CATCHMENT BOUNDARY	STREAM	TRAIL	< 1
BUILDING			100 – 1000
			1 – 10
			>1000

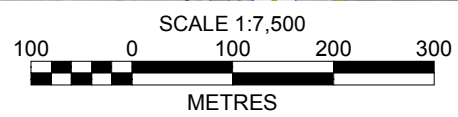
**NOTES:**

- ALL DIMENSIONS ARE IN METRES UNLESS OTHERWISE NOTED.
- THIS DRAWING MUST BE READ IN CONJUNCTION WITH BGC'S REPORT TITLED "COLD SPRING CREEK DEBRIS FLOW HAZARD ASSESSMENT UPDATE" DATED SEPTEMBER 2020.
- LIDAR DATA PROVIDED BY REGIONAL DISTRICT OF EAST KOOTENAY, PREPARED ON SEPTEMBER 12, 2018. CONTOUR INTERVAL IS 10 m.
- ROADS, STREAM AND WATERBODY DATA FROM CANVEC, AND COLD SPRING CREEK DIGITIZED BASED ON LIDAR DATED SEPTEMBER, 2018. SURVEY PARCEL DATA FROM TANTALIS. BUILDING FOOTPRINT DATA FROM MICROSOFT BING, DOWNLOADED DECEMBER 2019.
- THE FAN BOUNDARY AS DRAWN IS APPROXIMATE AND DELINEATES THE LANDFORM BASED ON LIDAR DATED SEPTEMBER, 2018. THE BOUNDARY SHOULD NOT BE CONSTRUED AS A HAZARD MAP, NOR DOES IT SHOW THE SPATIAL EXTENT OF POTENTIAL FLOODING.
- SCENARIO MAPS SHOW DEBRIS FLOOD OR DEBRIS FLOW IMPACT FORCE BASED ON FLO-2D MODEL RESULTS. MODEL RESULTS ARE INITIATED UPSTREAM OF THE FAN APEX. RESULTS ARE TRIMMED TO THE COLUMBIA RIVER AND DOWNSTREAM FAN BOUNDARY.
- THESE MAPS REPRESENT A SNAPSHOT IN TIME. FUTURE CHANGES (DEVELOPMENT, MITIGATION, GEOHAZARD EVENTS) MAY WARRANT THE RE-DRAWING OF CERTAIN AREAS.
- PROJECTION IS NAD 1983 UTM ZONE 11N. VERTICAL DATUM IS CGVD2013.
- UNLESS BGC AGREES OTHERWISE IN WRITING, THIS DRAWING SHALL NOT BE MODIFIED OR USED FOR ANY PURPOSE OTHER THAN THE PURPOSE FOR WHICH BGC GENERATED IT. BGC SHALL HAVE NO LIABILITY FOR ANY DAMAGES OR LOSS ARISING IN ANY WAY FROM ANY USE OR MODIFICATION OF THIS DOCUMENT NOT AUTHORIZED BY BGC. ANY USE OF OR RELIANCE UPON THIS DOCUMENT OR ITS CONTENT BY THIRD PARTIES SHALL BE AT SUCH THIRD PARTIES' SOLE RISK.

SCALE: 1:15,000	CLIENT: Regional District of East Kootenay	PROJECT: COLD SPRING CREEK DEBRIS FLOW HAZARD ASSESSMENT UPDATE	
DATE: SEP 2020		TITLE: INDIVIDUAL MODELLING RESULTS	
DRAWN: LL		PROJECT No.: 1572 005	DWG No.: 03
REVIEW: BCP			
APPROVED: MJ			



X:\Projects\1572005\GIS\Production\Report\20200714\_Cold\_Spring\_Creek\_Debbris\_Flow\_Hazard\_Assessment\_Update\04\_Composite\_Hazard\_Map.mxd Date: Wednesday, September 23, 2020 Time: 12:32 PM



THIS DRAWING MAY HAVE BEEN REDUCED OR ENLARGED.  
ALL FRACTIONAL SCALE NOTATIONS INDICATED ARE  
BASED ON ORIGINAL FORMAT DRAWINGS.

- NOTES:**
1. ALL DIMENSIONS ARE IN METRES UNLESS OTHERWISE NOTED.
  2. THIS DRAWING MUST BE READ IN CONJUNCTION WITH BGC'S REPORT TITLED "COLD SPRING CREEK DEBRIS FLOW HAZARD ASSESSMENT UPDATE" DATED SEPTEMBER 2020.
  3. LIDAR DATA PROVIDED BY REGIONAL DISTRICT OF EAST KOOTENAY, PREPARED ON SEPTEMBER 12, 2018. CONTOUR INTERVAL IS 10 m.
  4. ROADS, STREAM AND WATERBODY DATA FROM CANVEC, AND COLD SPRING CREEK DIGITIZED BASED ON LIDAR DATED SEPTEMBER, 2018. SURVEY PARCEL DATA FROM TANTALIS. BUILDING FOOTPRINT DATA FROM MICROSOFT BING, DOWNLOADED DECEMBER 2019.
  5. THE FAN BOUNDARY AS DRAWN IS APPROXIMATE AND DELINEATES THE LANDFORM BASED ON LIDAR DATED SEPTEMBER, 2018. THE BOUNDARY SHOULD NOT BE CONSTRUED AS A HAZARD MAP. NOR DOES IT SHOW THE SPATIAL EXTENT OF POTENTIAL FLOODING.
  6. THE DISTAL PORTIONS OF THE COLD SPRING CREEK DEBRIS FLOW FAN INTERFINGER WITH COLUMBIA RIVER FLOODPLAIN. COLUMBIA RIVER FLOODS WERE NOT MODELED AND ARE THUS NOT INDICATED ON THIS MAP.

7. AREAS DELINEATED AS NOT STUDIED MAY BE SUBJECT TO GEOHAZARDS FROM CREEKS OTHER THAN COLD SPRING CREEK AND WERE NOT INCLUDED IN THE SCOPE OF THIS STUDY.
8. THIS MAP REPRESENTS A SNAPSHOT IN TIME. FUTURE CHANGES (DEVELOPMENT, MITIGATION, GEOHAZARD EVENTS) MAY WARRANT THE RE-DRAWING OF CERTAIN AREAS.
9. PROJECTION IS NAD 1983 UTM ZONE 11N. VERTICAL DATUM IS CGVD2013.
10. UNLESS BGC AGREES OTHERWISE IN WRITING, THIS DRAWING SHALL NOT BE MODIFIED OR USED FOR ANY PURPOSE OTHER THAN THE PURPOSE FOR WHICH BGC GENERATED IT. BGC SHALL HAVE NO LIABILITY FOR ANY DAMAGES OR LOSS ARISING IN ANY WAY FROM ANY USE OR MODIFICATION OF THIS DOCUMENT NOT AUTHORIZED BY BGC. ANY USE OF OR RELIANCE UPON THIS DOCUMENT OR ITS CONTENT BY THIRD PARTIES SHALL BE AT SUCH THIRD PARTIES' SOLE RISK.

SCALE:	1:7,500
DATE:	SEP 2020
DRAWN:	LL
REVIEW:	BCP
APPROVED:	MJ

CLIENT:

**BGC**

PROJECT: COLD SPRING CREEK DEBRIS FLOW HAZARD ASSESSMENT UPDATE	
TITLE: COMPOSITE HAZARD MAP	
PROJECT No.: 1572 005	DWG No: 04